The Journal of Gemmology

Volume 36 / No. 8 / 2019

Sapphire Intaglio from Pompeii

Chinese Synthetic Diamonds

Trapiche Rubies from Vietnam

Renaissance Recipes for Artificial Pearls

SSEF Schweizerisches Gemmologisches Institut
Swiss Gemmological Institute
Institut Suisse de Gemmologie

Gem-A
The Gemmological Association of Great Britain

SSEF

SCHWEIZERISCHES GEMMOLOGISCHES INSTITUT
SWISS GEMMOLOGICAL INSTITUTE
INSTITUT SUISSE DE GEMMOLOGIE

ORIGIN DETERMINATION · TREATMENT DETECTION

DIAMOND GRADING · PEARL TESTING

EDUCATION · RESEARCH

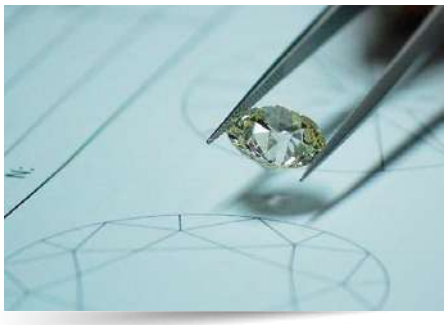

THE SCIENCE OF GEMSTONE TESTING™

Aeschengraben 26, 4051 Basel, Switzerland Tel. +41 61 262 06 40 Fax + 41 61 262 06 41 admin@ssef.ch www.ssef.ch

The Journal of Gemmology

Volume 36 / No. 8 / 2019

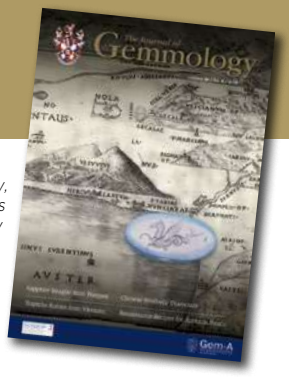

Cover photo: *An 11.62 ct intaglio excavated in 1986 from Pompeii, Italy, proved to be a basaltic-type sapphire (see article on pp. 710–725 of this issue) and therefore does not have a Sri Lankan origin as commonly described for Roman sapphires. The background map, from Italian Renaissance painter Girolamo Mocetto, shows the region near Mount Vesuvius, which erupted in 79 CE and buried Pompeii and the surrounding area under a thick layer of ash.*

COLUMNS

What's New 679

ABCD Pro-1 Gem Testing Set | D-Imaging Device | Raman Spectroscopy Application Notes | CIBJO Special Reports | 2019 GSA Annual Meeting Abstracts | Johnkoivulaite, a New Mineral | Market Research on Responsibly Sourced Diamonds | Santa Fe Symposium Proceedings 2019 | 2019 SSEF Presentations | Jewelry Journey Podcasts | Gemewizard Gem Color Academy

Gem Notes 682

Amethyst from Zimbabwe | Apatite from Durango, Mexico | Cobaltoan Calcite from Switzerland | Pyrite and Chromite Inclusion Assemblage in Emerald | Six-Rayed Star Enstatite from Madagascar | Yellowish Green Enstatite (and Star Enstatite) from Tanzania | Sunstone Labradorite-Bytownite from Ethiopia | Quartz from Brazil with Gormanite Inclusions | Quartz from Chile with Powellite and Molybdenite Inclusions | Quartz from Madagascar with Fuchsite Phantom Inclusions | Tourmaline from Sri Lanka with Transient Tenebrescence? | Diving for Natural Pearls off Bahrain | A Remarkably Large Natural Pearl from *Pinctada radiata* | Double Grafting in Peanut-Shaped Ming Cultured Pearls | Dyed Banded Agate from Madagascar

ARTICLES

Gemmological Analysis of a Roman Sapphire Intaglio and Its Possible Origin 710
By Michael S. Krzemnicki, Flavio Butini, Enrico Butini and Ernesto De Carolis

The Texture and Chemical Composition of Trapiche Ruby from Khoan Thong, Luc Yen Mining District, Northern Vietnam 726
By Isabella Pignatelli, Gaston Giuliani, Christophe Morlot and Pham Van Long

Current Status of Chinese Synthetic Diamonds 748
By Taijin Lu, Jie Ke, Yan Lan, Zhonghua Song, Jian Zhang, Shi Tang, Jun Su, Huiru Dai and Xuxu Wu

Renaissance Recipes for Making Artificial Pearls by Leonardo da Vinci and Others 758
By Annibale Mottana

Photo by Luciana Barbosa

Photo courtesy of The Met, New York

Conferences 766
36th International Gemmological Conference | Gem-A Conference

Gem-A Notices 776

New Media 790

Learning Opportunities 786

Literature of Interest 793

The Journal is published by Gem-A in collaboration with SSEF and with the support of AGL.

Gem-A THE GEMMOLOGICAL ASSOCIATION OF GREAT BRITAIN

SSEF SCHWEIZERISCHES GEMMOLOGISCHES INSTITUT SWISS GEMMOLOGICAL INSTITUTE INSTITUT SUISSE DE GEMMOLOGIE

AGL AMERICAN GEMOLOGICAL LABORATORIES

The Journal of Gemmology

CONTENT SUBMISSION

The Editor-in-Chief will consider original articles, news items, conference reports, announcements and calendar entries on subjects of gemmological interest for publication in *The Journal of Gemmology*. A guide to the various sections and the preparation of manuscripts is given at https://gem-a.com/index.php/news-publications/journal-of-gemmology/submissions, or contact the Editor-in-Chief.

SUBSCRIPTIONS

Gem-A members receive *The Journal* as part of their membership package, full details of which are given at https://gem-a.com/membership. Laboratories, libraries, museums and similar institutions may become direct subscribers to *The Journal*.

ADVERTISING

Enquiries about advertising in *The Journal* should be directed to advertising@gem-a.com.
For more information, see https://gem-a.com/news-publications/media-pack-2019.

DATABASE COVERAGE

The Journal of Gemmology is covered by the following abstracting and indexing services: Clarivate Analytics' (formerly Thomson Reuters/ISI) Science Citation Index Expanded (also known as SciSearch, in the Web of Science), *Journal Citation Reports (Science Edition)* and *Current Contents (Physical, Chemical and Earth Sciences)*; Elsevier's Scopus; Australian Research Council's Excellence in Research for Australia (ERA) Journal List; China National Knowledge Infrastructure (CNKI Scholar); EBSCO's Academic Search Ultimate; ProQuest (Cambridge Scientific Abstracts); GeoRef; CrossRef; Chemical Abstracts (CA Plus); Mineralogical Abstracts; Index Copernicus ICI Journals Master List; Gale Academic OneFile; British Library Document Supply Service; and Copyright Clearance Center's RightFind application.

Science Citation Index Expanded
Web of Science Clarivate Analytics

COPYRIGHT AND REPRINT PERMISSION

Design & production by Zest Design, www.zest-uk.com

Printed by DG3 Group (Holdings) Ltd

ISSN 1355-4565 (Print), ISSN 2632-1718 (Online)

Gem-A
THE GEMMOLOGICAL ASSOCIATION OF GREAT BRITAIN

21 Ely Place
London EC1N 6TD
UK
t: +44 (0)20 7404 3334
f: +44 (0)20 7404 8843
e: information@gem-a.com
w: https://gem-a.com

Registered Charity No. 1109555
A company limited by guarantee and registered in England No. 1945780
Registered office: Palladium House, 1–4 Argyll Street, London W1F 7LD

What's New

INSTRUMENTATION

ABCD Pro-1 Gem Testing Set

In November 2019, the Asian Gemmological Institute and Laboratory Ltd (AGIL) released an updated version of its ABCD Gem Testing Set. The 16-piece gemmological instrument kit includes a 10× loupe, incandescent Maglite torch with darkfield attachment, polariscope, prism spectroscope, long-wave UV source, conoscope, diffuser, stone holder, tweezers, and various adaptors and diffusers. New additions include a spectroscope stand and rotatable stage that can be used in conjunction with the spectroscope and the torch/UV source. Holders for the various instruments and filters permit convenient handling of the gem being examined for pleochroism, single/double refraction, inclusions and absorption/fluorescence spectra. Packaged in a convenient carrying case, the set weighs 0.78 kg and is designed for use by the travelling gemmologist. Visit http://eshop.agil.com.hk/index_eproduct_view.php?products_id=3.

Dr Dominic Mok FGA DGA (agil@agil.com.hk)
AGIL, Hong Kong

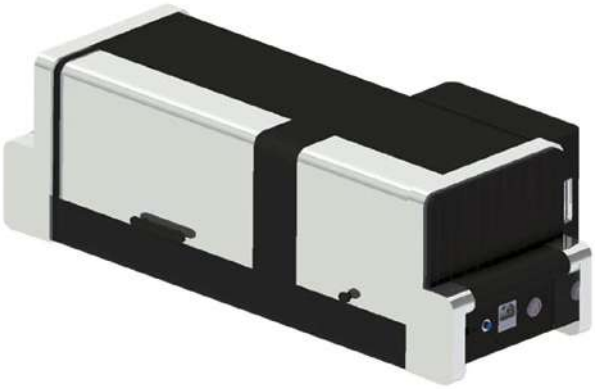

D-Imaging

DRC Techno (Gujarat, India) released the D-Imaging system in September 2019. The all-in-one unit is designed to produce a 360° image of a diamond that can display characteristics such as clarity, cut, colour, fluorescence and the 'hearts-and-arrows' optical effect. The system allows for enhanced representation of a diamond when it is not possible for a buyer to view the stone in person. The unit is 676 × 280 × 224 mm and weighs 10 kg. Visit www.drctechno.com/products/retail/d-imaging.

Raman Spectroscopy Application Notes

United ID RAMAN LAB

United ID Raman Laboratory (Taipei, Taiwan) has issued a series of application notes on Raman spectroscopy pertaining to gemmology. Topics include diamond, jadeite, nephrite, ruby, sapphire, amber, emerald, coral, pearl, chalcedony, opal and more. Some are freely available, while others are accessible only to United ID customers. Visit www.uid-ramanlab.com/gemstones.

NEWS AND PUBLICATIONS

CIBJO Special Reports

Reports prepared in advance of the 18–20 November 2019 CIBJO Congress are available for download at www.cibjo.org/congress2019/special-reports. They review issues for discussion by the various CIBJO commissions, with topics including Generation Z as a future consumer group (Marketing & Education Commission), corporate social responsibility principles for the jewellery industry (Responsible Sourcing Commission), market trends and supply chain integrity (Precious Metals Commission), natural vs. laboratory-grown diamonds (Diamond Commission), technology and nomenclature (Coloured Stone Commission), compliance and disclosure requirements (Ethics Commission), gemmological laboratory reports (Gemmological Commission), and environmental issues (Pearl and Coral Commissions).

Gem Abstracts from the 2019 GSA Annual Meeting

Abstracts of oral and poster presentations from the 131st annual meeting of the Geological Society of America, held in Phoenix, Arizona, USA, on 22–25 September 2019 are now available online. Oral presentation abstracts can be viewed at https://gsa.confex.com/gsa/2019AM/webprogram/Session47368.html and include topics such as diamond deposits and localities, causes of colour in diamond, inclusions in and chemical composition of sapphire, Oregon sunstone, jet, and the new beryl-group member johnkoivulaite (see What's New entry, above right). Poster session abstracts are available at https://gsa.confex.com/gsa/2019AM/webprogram/Session48617.html and cover the geochemistry of Cr in sapphire, Ni in diamond, inclusions in type II pink diamond, the sapphire auction market in China, and auction pricing of pink and blue diamonds.

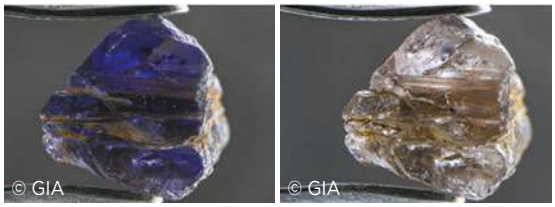

Johnkoivulaite, a New Mineral

A new mineral of the beryl group—johnkoivulaite, $Cs(Be_2B)Mg_2Si_6O_{18}$—has been named after renowned gemmologist John I. Koivula, who is best known for his contributions to photomicrography and research on gem inclusions. The 1.16 ct crystal from Mogok, Myanmar, is strongly pleochroic (deep violet to near-colourless; see photo) and has the following properties: RI—1.608 (birefringence too small to measure accurately), hydrostatic SG—3.01, Mohs hardness—7½, and inert to long- and short-wave UV radiation. News of the discovery was first announced at the September 2019 GSA Conference (see What's New entry, below left) and further information was published in the Gem News International section of *Gems & Gemology* (Vol. 55, No. 3, 2019, pp. 454-455).

Market Research on Responsibly Sourced Diamonds

In September 2019, MVI Marketing released a report titled 'The Need for 3rd Party Verification of Mined and Lab-Grown Diamond Claims of Positive Social and Environmental Impact'. It describes the results of consumer research conducted in July 2019, which found that roughly 40% of consumers make diamond-purchasing decisions based on information about social and environmental responsibility, including country-of-origin claims, especially when supported by third-party verification of such claims. Many will even pay a premium for responsibly sourced diamonds with a known geographic origin. Download the report after filling out an online form at www.mvimarketing.com/download-report.php?report=49.

Santa Fe Symposium Proceedings 2019

Proceedings of the 2019 Santa Fe Symposium (19–22 May) are now available online. While the primary focus of this long-running conference (held annually in New Mexico, USA) is on jewellery manufacturing, some of the presentations are also of interest to gemmologists. These include 'Getting started with blockchain', 'Conflict diamonds and corporate social responsibility in the U.S. jewelry industry' and 'The use of computed tomography in the evaluation and cutting of opaque gemstone material'. Full papers covering the presentations can be downloaded at www.santafesymposium.org/2019-santa-fe-symposium?category=2019. Proceedings from previous symposia are also available back to 2000.

OTHER RESOURCES

2019 SSEF Presentations

Presentations given in 2019 by staff of the Swiss Gemmological Institute SSEF are available online in PDF format, including those titled 'Age dating applied as a testing procedure to gemstones and biogenic materials', 'Multi-element analysis of gemstones for country of origin determination, 'Study of a recut HPHT synthetic diamond', 'A gemmological approach to distinguishing natural from synthetic rubies' and 'Where is the boundary between colour varieties of gems?'. Older presentations (2009–2018) are also available. Visit www.ssef.ch/presentations.

Jewelry Journey Podcasts

The Jewelry Journey Podcast website at https://thejewelryjourney.com/podcasts hosts podcasts dating from October 2018 that feature experts in gems, jewellery and art, from antique to modern. Recent podcasts of potential interest to gemmologists cover the art, jewellery and history of ancient Nubia; a preview of New York City's Jewelry Week 2019; the appraisal of gems, antique and estate jewellery; and much more. Currently, 49 podcasts are available via the website and the Jewelry Journey Podcast app for mobile devices. Podcast host Sharon Berman is a marketing and public relations expert who is also a gemmologist involved in various jewellery organisations, as well as a jewellery collector.

MISCELLANEOUS

Gemewizard Launches Gem Color Academy

In August 2019, Gemewizard Group (Ramat Gan, Israel) introduced its online Gem Color Academy. Two courses are currently offered: grading of fancy-colour diamonds and grading of coloured stones. The courses provide in-depth training with an assigned class and instructor, and are designed to appeal to a broad range of students, from gem and diamond traders to gemmologists and trade professionals to hobbyists. Visit www.gemcoloracademy.com.

What's New provides announcements of new instruments/technology, publications, online resources and more. Inclusion in What's New does not imply recommendation or endorsement by Gem-A. Entries were prepared by Carol M. Stockton unless otherwise noted.

Gem Notes

COLOURED STONES

Amethyst from Zimbabwe

Zimbabwe is known as a source of various gems, including diamond, emerald, aquamarine, chrysoberyl, alexandrite, iolite, garnet, euclase, tourmaline and quartz-family varieties such as amethyst (Ncube 1988). During the February 2019 gem shows in Tucson, Arizona, USA, author BML learned about a new find of amethyst in Zimbabwe from rough stone dealer Sir-Faraz Ahmad (Farooq) Hashmi (Intimate Gems, Glen Cove, New York, USA). He reported that in late 2018, one pocket produced 10–15 kg of good-quality material in pieces weighing up to about 150 g. A significant portion of the rough contained oriented hematite inclusions that were visible in certain directions. Hashmi provided one clean rough sample for faceting to Todd F. Wacks Jr. (Tucson Todd's Gems, Tucson, Arizona). The piece was strongly colour zoned, particularly near the crystal termination, and cutting of its basal portion yielded a 76 ct Portuguese round (Figure 1).

Examination of the faceted stone by author NDR showed that it contained only a few inclusions. A partially healed fracture consisting of two-phase (liquid and gas) fluid inclusions showed thin-film interference colours (Figure 2), and also present were a few elongate brownish needles.

Figure 2: A partially healed fracture in the faceted amethyst consists of fluid inclusions that display thin-film interference colours when viewed with darkfield and oblique fibre-optic illumination. Photomicrograph by N. D. Renfro, © GIA; image width 4.7 mm.

The visual appearance of these slightly curved whiskers indicated they were almost certainly hematite.

The location within Zimbabwe of this amethyst find is not known, and it is not clear if it represents a new mining area or came from an existing deposit such as those in the Karoi District or the Zambezi Valley (cf. www.mindat.org/locentries.php?p=21891&m=198).

Figure 1: The Zimbabwean amethyst on the right (76 ct) was cut from the crystal fragment remaining on the left. Photo by Diego Sanchez, © GIA.

Brendan M. Laurs FGA

Nathan D. Renfro FGA
Gemological Institute of America (GIA)
Carlsbad, California
USA

Reference

Ncube, A.N. 1988. Occurrences of gemstones and ornamental stones in Zimbabwe. *Zeitschrift der Deutschen Gemmologischen Gesellschaft*, **37**(3/4), 139–142.

Apatite from Durango, Mexico

Extensive information is known about the geology of the classic locality for gem-quality fluorapatite at Cerro de Mercado, near Durango, in Durango State, Mexico (e.g. Megaw & Barton 1999, 2013). The use of this apatite as a geochronological and mineralogical standard has also been discussed extensively (e.g. Corona-Esquivel *et al.* 2018). However, less information can be found in the literature on the gemmological properties of this material, so this author was pleased to examine two faceted samples loaned by gem dealer Dudley Blauwet (Dudley Blauwet Gems, Louisville, Colorado, USA). He reported that although faceted Mexican apatite was somewhat available in the trade from approximately 1990 to 2005, the stones were commonly overlooked due to an abundance of new items from previously unobtainable sources that followed the fall of the Soviet Union and Eastern Bloc, along with new finds in Africa and China, which the market considered more exotic than Mexico.

The emerald- and cushion-cut stones measured 14.97 × 9.47 × 7.97 mm (10.00 ct) and 13.88 × 10.51 × 8.69 mm (9.42 ct), respectively. Both were transparent, with a homogeneous greenish yellow colour (Figure 3). The RIs of both samples were 1.631–1.636, yielding a birefringence of 0.005. Their optic character was uniaxial negative. The average hydrostatic SG value for both was 3.21. A calcite dichroscope revealed weak dichroism of light yellow and light greenish yellow. A prism spectroscope revealed a strong doublet at 580 nm, a narrow band at about 525 nm, and other lines visible at about 480, 510 and 600 nm. The gems were inert to long-wave UV radiation, but fluoresced weak yellow to short-wave UV. This differs from the 'lilac pink' fluorescence for yellow apatite indicated by Webster (1994).

Figure 3: These faceted apatites from Durango, Mexico, weigh 9.42 ct (cushion cut) and 10.00 ct (emerald cut). Photo by J. C. Zwaan.

Both stones were relatively clean. Microscopic examination of the cushion revealed straight growth zoning. The emerald cut contained a small liquid feather (Figure 4a) composed of multiphase and necked-down single-phase inclusions (Figure 4b).

A visible-near infrared (Vis-NIR) absorption spectrum collected with a Thermo Scientific Evolution 600 spectrometer gave a more detailed picture of the features observed with the spectroscope, consisting of pronounced peaks at about 514, 526, 578/585 (doublet), 749 (with a shoulder at 740) and 803 nm, accompanied by weaker bands at about 483 and 598 nm (Figure 5). The most pronounced transmission window was at around 545–565 nm, which was responsible for the greenish yellow colour, in conjunction with a gradual absorption in the blue towards an absorption edge in the violet region.

A Raman spectrum obtained with a Thermo Scientific DXR Raman microscope using 532 nm laser excitation showed an excellent match with spectra for fluorapatite in the RRUFF database. Photoluminescence spectra collected with the same green laser showed strong emission peaks in the red region, at about 600 and 645 nm (Figure 6).

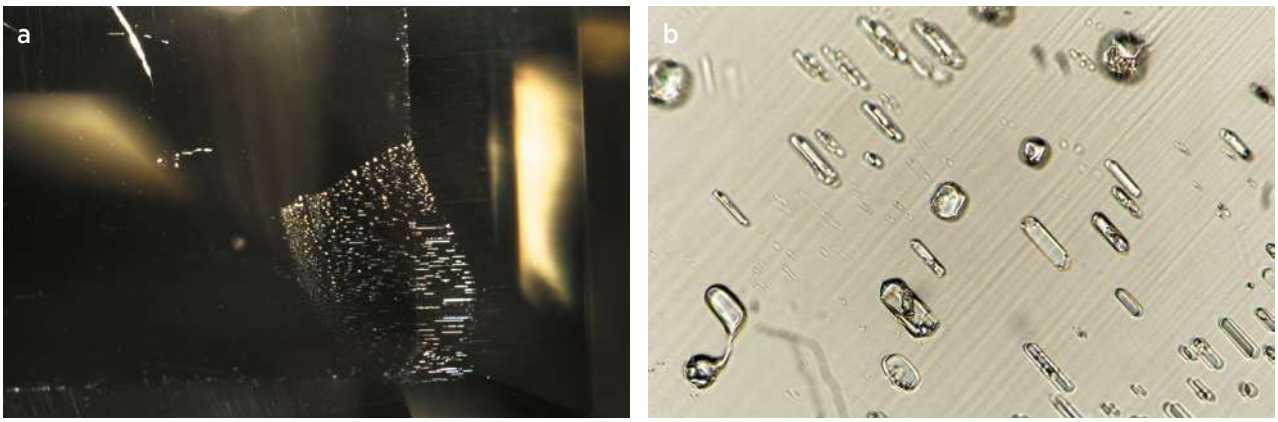

Figure 4: (**a**) A small partially healed fracture is seen in the emerald-cut apatite. (**b**) Closer examination of this feather reveals multi-phase inclusions, with necking-down of some of them (at left) resulting in mono-phase fluid inclusions. Photomicrographs by J. C. Zwaan; (a) darkfield illumination and image width 4.6 mm, and (b) brightfield illumination and image width 0.3 mm.

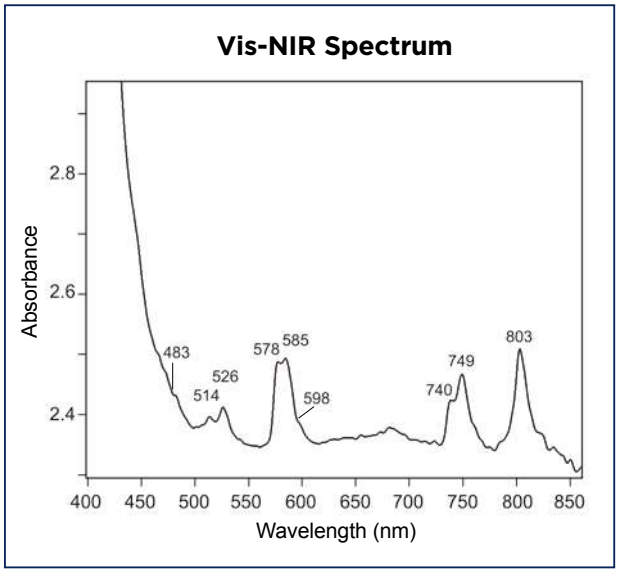

Figure 5: A non-polarised, room-temperature Vis-NIR spectrum of the apatite shows features typically produced by rare-earth elements, in particular Nd^{3+}. The path length of the beam was about 7.5–8.0 mm.

Gemmological textbooks (e.g. Anderson 1980) mention that the characteristic 'didymium' absorption spectrum of apatite is due to the presence of rare-earth elements (REE), in particular neodymium (Nd) and praseodymium (Pr). Although these elements were not detected by energy-dispersive X-ray fluorescence (EDXRF) spectroscopy with an EDAX Orbis Micro-XRF Analyzer, REE can be present at very low concentrations (below 100 ppmw) yet still be detectable with absorption spectroscopy and luminescence techniques. The multiple peaks seen in the Vis-NIR spectrum are typically due to the presence of trivalent rare-earth ions. In particular, the absorption bands centred at around 740 and 800 nm (Figure 5) can be attributed to Nd^{3+}, the intense photoluminescence in the red region (Figure 6) is due to the presence of Pr^{3+}, and the weak fluorescence to short-wave UV might indicate the presence of Ce^{3+} (Cantelar *et al*. 2001).

Dr J. C. (Hanco) Zwaan FGA
(hanco.zwaan@naturalis.nl)
Netherlands Gemmological Laboratory
National Museum of Natural History 'Naturalis'
Leiden, The Netherlands

References

Anderson, B.W. 1980. *Gem Testing*, 9th edn. Butterworth & Co. Inc., London, 434 pp.

Cantelar, E., Lifante, G., Calderón, T., Meléndrez, R., Millán, A., Alvarez, M.A. & Barboza-Flores, M. 2001. Optical characterisation of rare earths in natural fluorapatite. *Journal of Alloys and Compounds*, **323–324**, 851–854, http://doi.org/10.1016/s0925-8388(01)01159-8.

Corona-Esquivel, R., Levresse, G., Solé, J., Henriquez, F. & Pi, T. 2018. New age in the geological evolution of the Cerro de Mercado iron oxide apatite deposit, Mexico: Implication in the Durango apatite standard (DAP) age variability. *Journal of South American Earth Sciences*, **88**, 367–373, http://doi.org/10.1016/j.jsames.2018.09.014.

Megaw, P.K.M. & Barton, M.D. 1999. The geology & minerals of Cerro de Mercado, Durango, Mexico. *Rocks & Minerals*, **74**(1), 20–28, http://doi.org/10.1080/00357529909602510.

Megaw, P.K.M. & Barton, M.D. 2013. Mexican apatite. *In:* Rakovan, J., Dallaire, D.A., Staebler, G.A. & Bunk, D.W. (eds) *Apatite: The Great Pretender*, Lithographie Ltd, Denver, Colorado, USA, 54–66.

Webster, R. 1994. *Gems: Their Sources, Descriptions and Identification*, 5th edn., revised by P.G. Read. Butterworth-Heinemann, Oxford, 1,026 pp.

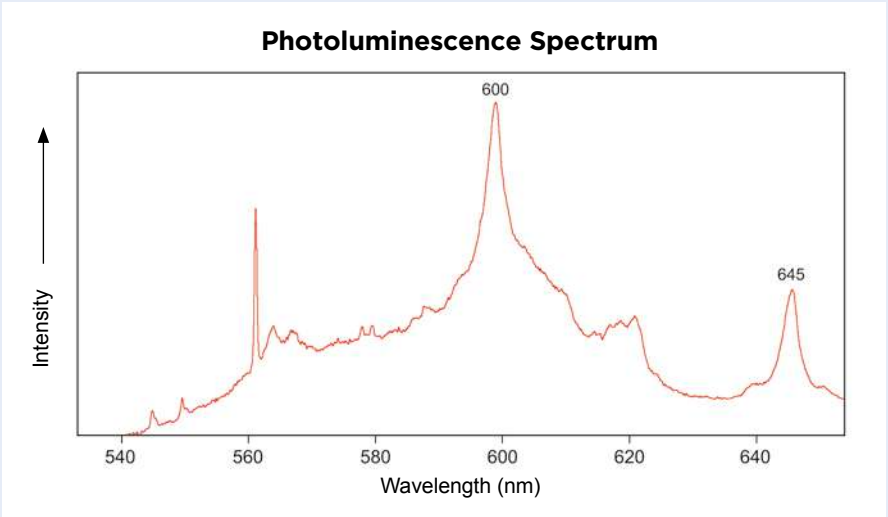

Figure 6: Strong photoluminescence in the red region, excited by a green laser, can be attributed to the presence of Pr^{3+}. Sharp Raman bands of fluorapatite are present in the 540–580 region.

Cobaltocalcite or Cobaltoan Calcite: A Swiss Answer

Switzerland is not known for its gem production, but rather as an important platform for trading, auctioning and certifying gems. However, at the May 2019 GemGenève fair (Geneva International Gem and Jewellery Show), a new Swiss gem material debuted in the designer area. Geneva-based art jeweller Grégoire Maret (Pierre d'Alexis S.A.) presented pink to purplish pink cobaltoan calcite from Switzerland—marketed as 'Rose of Mine'—in his handmade jewellery creations (e.g. Figure 7).

Cobaltoan calcite, $(Ca,Co)CO_3$, is rarely seen in high-end jewellery, and is rather unusual in its nature and geological origin. It is coloured by traces of Co^{2+} in octahedral coordination within the calcite structure (Fritsch & Rossman 1987), and may show variations in saturation and hue. The Swiss rough material, previously described by Meisser (1999), is sporadically extracted from abandoned coal mines situated near the village of Isérables in the canton of Valais in south-west Switzerland. The gemmy material is polished *en cabochon*, and so far approximately 30 stones have been cut, ranging from 5 to 35 ct.

This attractively coloured calcite variety formed under unique conditions. Following the cessation of coal mining in 1943, surface waters interacted with the surrounding rocks, and the cobaltoan calcite crystallised at ambient temperature and pressure through the percolation of fluids enriched with Co, Ni and Zn (Meisser 1999), forming speleothems on black shale host rock (Figure 8) in the moist darkness of the abandoned coal mines.

Figure 7: A free-form cabochon of translucent cobaltoan calcite from Switzerland is set in this pendant (5 cm long) by Grégoire Maret (Pierre d'Alexis S.A.), which is called 'L'Inattendue'. In the background is a piece of the rough speleothem on the host rock. Photo by David Fraga.

Figure 8: A speleothem (3 cm tall) of Swiss cobaltoan calcite is shown on its black shale host rock. (The white material in bottom-centre is a later generation of calcite.) Photo by Alain Pitteloud.

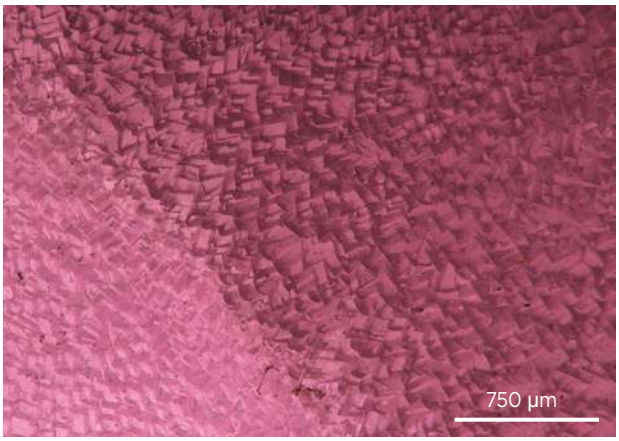

Figure 9: Aggregates of trigonal crystals are seen on the surface of the rough cobaltoan calcite. Photomicrograph by F. Notari.

Standard gemmological testing of this strongly birefringent polycrystalline material revealed RIs of 1.49–1.66 and a hydrostatic SG value of approximately 2.70. Only a very weak purplish luminescence was observed with long-wave UV radiation and the material was inert to short-wave UV. Under magnification, it showed a granular to fibrous appearance and columnar growth with inhomogeneous colour distribution resulting from the presence of remnants of the black shale host rock. The surface of the piece of uncut rough material we examined exhibited trigonal prismatic crystals without preferential orientation (Figure 9), resulting in a generally botryoidal form and making it tougher than monocrystalline calcite.

We identified the material as calcite (rather than aragonite) using infrared specular reflectance. The UV-Vis-NIR

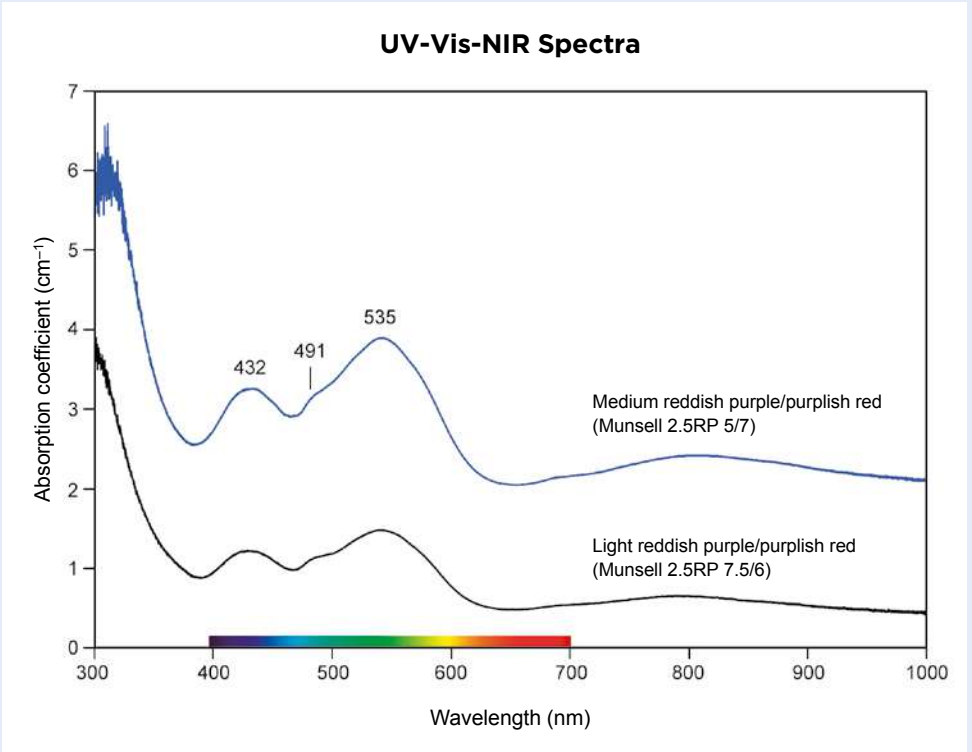

Figure 10: UV-Vis-NIR spectra taken at room temperature of two samples of cobaltoan calcite with different colouration reveal typical absorptions of Co^{2+}, consisting of two broad bands at about 535 and 432 nm and a smaller one at about 491 nm (present as a shoulder; position calculated at 77 K) of unknown attribution.

spectra (Figure 10) exhibited absorptions at about 535 and 432 nm associated with the presence of Co^{2+}. Semi-quantitative analysis of trace elements was measured on zones with different colour saturations using EDXRF spectroscopy (Thermo Fisher Scientific ARL Quant'X), and indicated the presence of about 850–1,400 ppmw Co—with higher amounts corresponding to deeper colouration—and up to about 220 ppmw Ni, as well as detectable levels of Zn. Pink colour in calcite is also known to be due to Mn, but this element was not detected in the Swiss samples by EDXRF analysis, in contrast to the cobaltoan calcite from an unspecified locality that was studied by Siritheerakul and Sangsawong (2015).

There is confusion between the names *cobaltocalcite* and *cobaltoan calcite*. *Cobaltocalcite* was introduced by Palache *et al.* (1951) for $CoCO_3$ (a carbonate of cobalt), but was refused by the International Mineralogical Association and replaced by *spherocobaltite*. The material described here is a variety of calcite in which some Ca is replaced by Co—$(Ca,Co)CO_3$—and therefore should be called cobaltoan calcite since it does not contain cobalt as a main component.

Dr Eric May (eric.may@ggtl-lab.org)
and Franck Notari
GGTL Laboratories
Les Acacias, Switzerland

Dr Nicolas Meisser
Musée Cantonal de Géologie
Lausanne, Switzerland

References

Fritsch, E. & Rossman, G.R. 1987. An update on color in gems. Part 1: Introduction and colors caused by dispersed metal ions. *Gems & Gemology*, **23**(3), 126–139, http://doi.org/10.5741/gems.23.3.126.

Meisser, N. 1999. La calcite cobaltifère d'Isérables, Valais. *Schweizer Strahler*, **12**(11), 594–598.

Palache, C., Berman, H., & Frondel, C. 1951. *The System of Mineralogy of James Dwight Dana and Edward Salisbury Dana, Yale University 1837–1892, Vol. II: Halides, Nitrates, Borates, Carbonates, Sulfates, Phosphates, Arsenates, Tungstates, Molybdates, etc.*, 7th edn. John Wiley and Sons Inc., New York, New York, USA (see pp. 175–176 for cobaltocalcite).

Siritheerakul, P. & Sangsawong, S. 2015. Lab Notes: Pink and reddish purple cobaltocalcite. *Gems & Gemology*, **51**(1), 58–59.

Pyrite and Chromite Inclusion Assemblage in Emerald

Recently, American Gemological Laboratories received a parcel of emeralds for testing. One gemstone (Figure 11), weighing 0.87 ct, stood out from the rest because of its combination of inclusions. Microscopic observation revealed numerous mineral inclusions, some of which appeared to be pyrite (Figure 12a), while others formed black disseminated grains or aggregates (Figure 12b) similar to those commonly encountered in Colombian emeralds.

Raman microspectroscopy confirmed the brassy-coloured crystals were pyrite, whereas the black aggregates proved to be chromite—rather than the bits of black shale that form dark inclusions in Colombian emeralds. Such an association of pyrite and chromite has been published previously on only a few occasions: first in the 1980s (Sauer & Cassedanne 1984; Gübelin & Koivula 1986) and again almost 30 years later (Gübelin & Koivula 2008). Indeed, chromite and pyrite are two of the most distinctive inclusions of emeralds from Santa Terezinha de Goiás in Brazil. Other mineral inclusions common to this locality include amphiboles, carbonates (calcite and dolomite), enstatite, epidote, feldspars, garnet, hematite, ilmenite, phlogopite, talc, quartz and pyrrhotite (Sauer & Cassedanne 1984; Gübelin & Koivula 2008).

Further evidence confirmed the Brazilian origin of this emerald: additional microscopic features such as primary fluid inclusions; UV-Vis-NIR absorption spectra showing the presence of Fe^{2+} (837 nm), Fe^{3+} (372 nm) and Cr^{3+} (435, 607 and 681 nm); and EDXRF chemical analysis indicating considerable Fe content (Sauer & Cassedanne 1984; Schwarz 2002, 2011; Cedeño Ochoa *et al.* 2015; Giuliani *et al.* 2015).

Figure 11: This 0.87 ct emerald attracted our attention due to the presence of abundant black inclusions. Photo by Alex Mercado, AGL.

This emerald is a reminder that pyrite and black aggregates are not exclusive to stones of Colombian origin (e.g. Figure 13). The presence of pyrite, when occurring with other minerals such as chromite, as well as the appearance of the primary fluid inclusions, can help indicate a Brazilian origin.

Lwizahira Vasquez and
Dr Riadh Zellagui (riadh@aglgemlab.com)
American Gemological Laboratories
New York, New York, USA

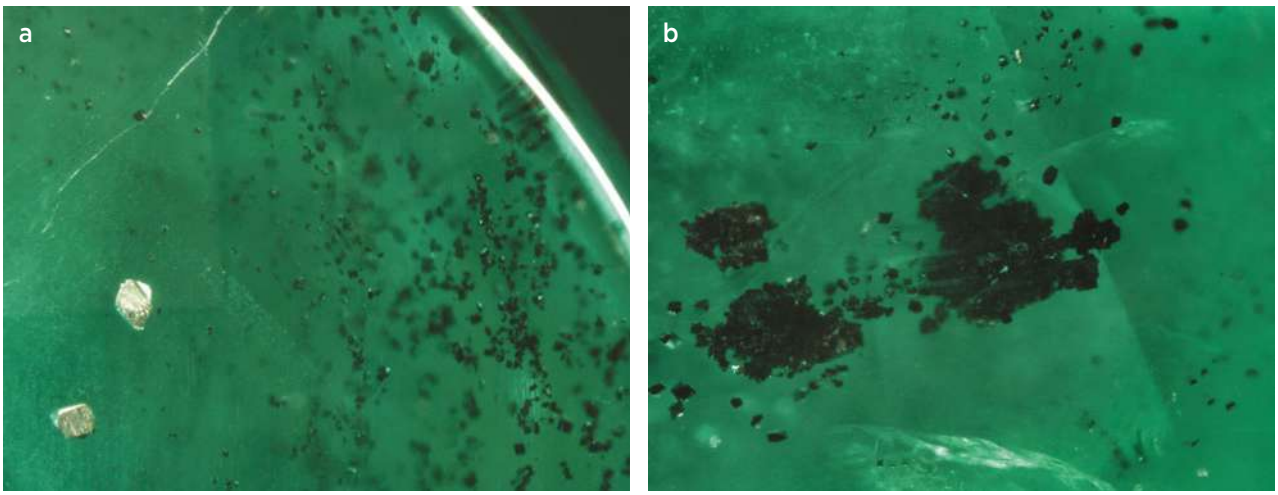

Figure 12: (**a**) Pyrite crystals and abundant chromite grains are prominent in this emerald, consistent with those from Santa Terezinha de Goiás in Brazil. (**b**) The chromite inclusions occur as both isolated grains and clusters in the emerald. Photomicrographs by R. Zellagui in darkfield illumination; magnified 9× (a) and 7× (b).

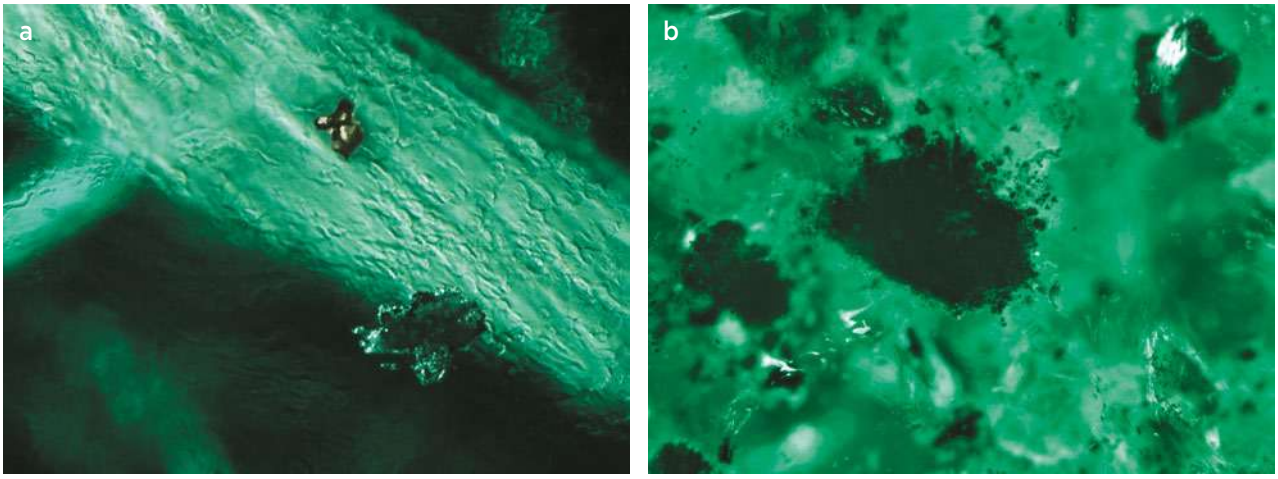

Figure 13: (**a**) Dark inclusions (from the black shale host rock) and pyrite crystals are sometimes encountered together in Colombian emeralds, as shown here. This stone also shows a strong *gota de aceite* effect (graining) that is typical of some emeralds from Colombia. (**b**) At first glance, the bits of black shale in this Colombian emerald strongly resemble the chromite inclusions seen in the Brazilian emerald in Figure 12b. Photomicrographs by R. Zellagui in darkfield illumination; magnified 10× (a) and 6× (b).

References

Cedeño Ochoa, C.J., Herreño Daza, M.J., Fortaleche, D. & Jiménez, J.F. 2015. Progress on the study of parameters related to the origin of Colombian emeralds. *InColor*, special issue, December, 88–97.

Giuliani, G., Branquet, Y., Fallick, A.E., Groat, L.A. & Marshall, D. 2015. Emerald deposits around the world, their similarities and differences. *InColor*, special issue, December, 56–69.

Gübelin, E.J. & Koivula, J.I. 1986. *Photoatlas of Inclusions in Gemstones*. ABC Edition, Zurich, Switzerland, 532 pp.

Gübelin, E.J. & Koivula, J.I. 2008. *Photoatlas of Inclusions in Gemstones*, Vol. 3. Opinio Publishers, Basel, Switzerland, 672 pp.

Sauer, D.A. & Cassedanne, J.P. 1984. The Santa Terezinha de Goiás emerald deposit. *Gems & Gemology*, **20**(1), 4–13, http://doi.org/10.5741/gems.20.1.4.

Schwarz, D. 2002. Gemology of emerald. *In:* Giuliani, G., Jarnot, M., Neumeier, G., Ottaway, T., Sinkankas, J. & Staebler, G. (eds) *Emeralds of the World—extraLapis English No. 2: The Legendary Green Beryl*, Lapis International LLC, East Hampton, Connecticut, USA, 66–71.

Schwarz, D. 2011. Emeralds from South America – Brazil and Colombia. *InColor*, No. 16, 36–46.

Six-Rayed Star Enstatite from Madagascar

Enstatite may display asterism with four, six or eight rays, although it has been documented from only a few localities: southern India (Eppler 1967, 1971), Ratnapura in Sri Lanka (Henn & Bank 1991) and more recently Norway (Schmitz *et al*. 2016). Enstatite is the Mg end member of the enstatite-ferrosilite series, the orthopyroxenes of the enstatite group. Historically, the series has been divided into intermediate members such as 'bronzite', hypersthene, etc. (Dunn 1975; Deer *et al*. 1997), according to Fe content. 'Bronzite' is not recognised by the International Mineralogical Association but occasionally may be encountered in the literature.

Recently, star enstatite was found at a new locality: Madagascar (Figure 14). During the June 2019 Sainte-Marie-aux-Mines Mineral & Gem Show, Renan Deschard,

Figure 14: This 1.24 ct enstatite cabochon from Madagascar shows six-rayed asterism. The strongest rays are parallel to the length of the stone. Some cleavage and parting are also visible. The cabochon measures about 9 × 5 × 3 mm. Photo by T. Cathelineau.

a prospector in Madagascar, donated the 1.24 ct cabochon to the author for characterisation.

The enstatite showed the following properties: colour—light brown; pleochroism—strong, in orangey brown, greyish green and grey; diaphaneity—translucent; RI—1.660–1.670; birefringence—0.010; optic character and sign—biaxial positive; hydrostatic SG—3.25; magnetism—slightly attracted to an N52 (neodymium) magnet; Chelsea Colour Filter reaction—none; fluorescence—inert to long- and short-wave UV radiation; and handheld spectroscope spectrum—continuous absorption in the violet and blue regions with two sharp bands in the green at about 505 and 545 nm. These data are consistent with those reported for enstatite by O'Donoghue (2006).

Light scattering from a dense network of inclusions formed the six-rayed star, with the strongest rays seen parallel to the length of the cabochon. Microscopic examination (Figure 15) revealed parallel acicular (needle-like) inclusions (up to 2 µm wide and 150 µm long) aligned in three directions and intersecting at approximately 57° and 62°. The intersection angles are consistent with the orthorhombic pseudo-hexagonal symmetry of enstatite and published data: 57° and 64° (Eppler 1967, 1971); 57° and 61° (Henn & Bank 1991); and 64° (Schmitz *et al.* 2016). Eppler (1967) suggested rutile as a possible inclusion; Henn & Bank (1991) ascribed the asterism to hollow channels; Gübelin & Koivula (2008) indicated rutile or sillimanite in Sri Lankan enstatite; and Schmitz *et al.* (2016) identified ilmenite in Norwegian enstatite.

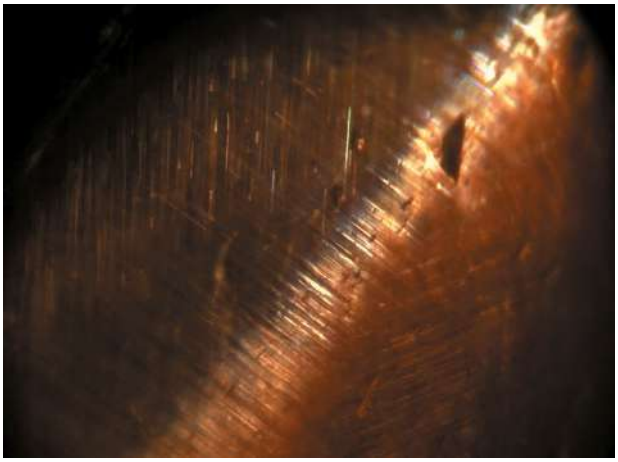

Figure 15: Viewed with oblique illumination, the enstatite shows acicular inclusions that scatter light and intersect at approximately 57° and 62°. Photomicrograph by T. Cathelineau; image width 1.0 mm.

Further investigation such as using Raman microspectroscopy would be necessary to identify the inclusions in the Madagascar enstatite.

Infrared reflectance spectra were collected from several spots on the cabochon, and all yielded the same pattern without any distinct differences (Figure 16). The spectrum is characteristic of enstatite (see spec4gem.info/databases/irs/296; Chihara *et al.* 2002).

Vis-NIR spectra (Figure 17) were collected with the beam entering from the top and oriented nearly perpendicular to the base of the cabochon. Due to the beam's orientation, only two spectra were acquired: one for the orangey brown colour and one for the greyish green

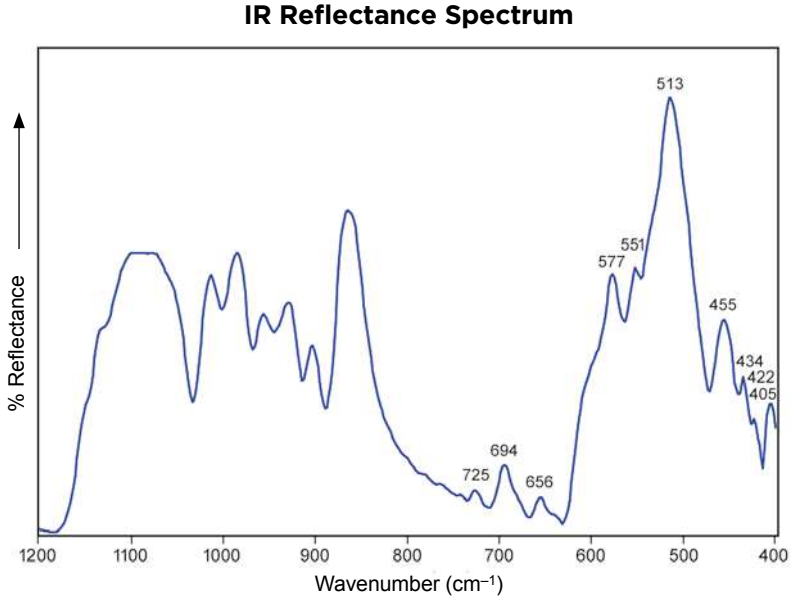

Figure 16: The IR reflectance spectrum for the cabochon in Figure 14 characterises it as enstatite, according to the series of labelled bands.

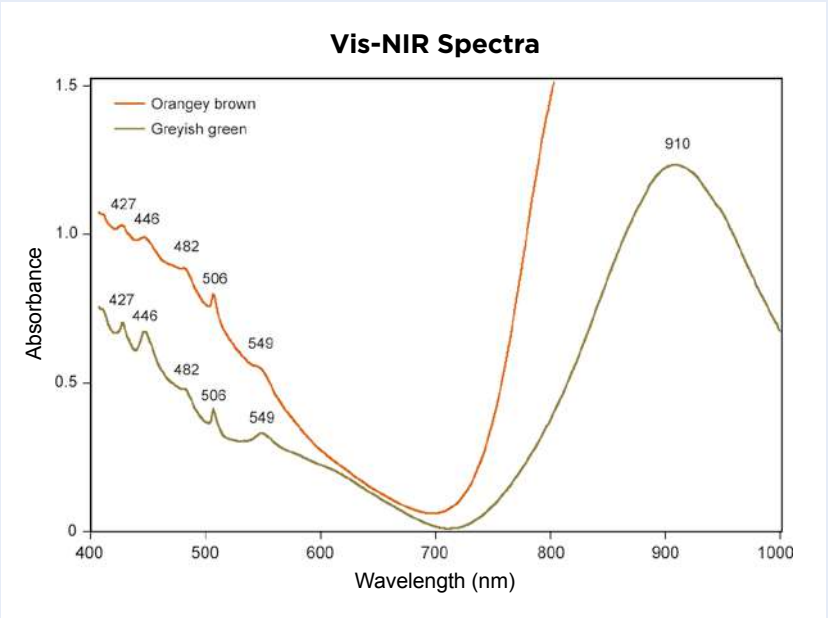

Figure 17: Vis-NIR spectra obtained for two of the enstatite's trichroic colours (orangey brown and greyish green) show iron-related features, including an Fe^{2+} band in the NIR region and characteristic Fe^{2+} spin-forbidden transition features in the 400–600 nm range. The path length of the beam was about 3.1 mm.

colour. The spectra were consistent with reference spectra for enstatite (see, e.g., spec4gem.info/databases/uvvis/297 and minerals.gps.caltech.edu/FILES/Visible/pyroxene). Across the visible range, both spectra showed a continuous absorption increasing towards the UV region (weaker for the greyish green direction), with a superimposed series of narrow bands at 427, 446, 482, 506 and 549 nm; the 506 nm band is characteristic of enstatite. In the near-IR range, both spectra showed a broad, strong absorption band centred at 910 nm (stronger in the orangey brown direction). The continuous absorption in the visible range coupled with the near-IR band creates a transmission window in the orange-to-red region, which is narrower in the orangey brown spectrum than in the greyish green one. The narrower transmission window produced the orangey brown colouration, while the broader one resulted in greyish green colouration since more green was transmitted. The continuum towards the UV and the strong band in the NIR are related to Fe^{2+} substituting for Mg^{2+} in the M1/M2 sites, and the narrow bands between 400 and 600 nm are Fe^{2+} spin-forbidden absorption bands (Hazen *et al.* 1978; Zhao *et al.* 1986). Thus, the stone is coloured by Fe^{2+}.

Thierry Cathelineau
(thierry.cathelineau@spec4gem.info)
Paris, France

References

Chihara, H., Koike, C., Tsuchiyama, A., Tachibana, S. & Sakamoto, D. 2002. Compositional dependence of infrared absorption spectra of crystalline silicates. *Astronomy & Astrophysics*, **391**(1), 267–273, http://doi.org/10.1051/0004-6361:20020791.

Deer, W.A., Howie, R.A. & Zussman, J. 1997. *Rock-Forming Minerals: Single-Chain Silicates*, 2nd edn. The Geological Society Publishing House, Bath, 680 pp.

Dunn, P.J. 1975. On gem orthopyroxenes: Enstatite and bronzite. *Gems & Gemology*, **15**(4), 118–122.

Eppler, W.F. 1967. Star-diopside and star-enstatite. *Journal of Gemmology*, **10**(6), 185–188, http://doi.org/10.15506/JoG.1967.10.6.185.

Eppler, W.F. 1971. Some rare materials. *Journal of Gemmology*, **12**(7), 256–262, http://doi.org/10.15506/JoG.1971.12.7.256.

Gübelin, E.J. & Koivula, J.I. 2008. *Photoatlas of Inclusions in Gemstones*, Vol. 3. Opinio Publishers, Basel, Switzerland, 672 pp.

Hazen, R.M., Bell, P.M. & Mao, H.K. 1978. Effects of compositional variation on absorption spectra of lunar pyroxenes. *9th Lunar and Planetary Science Conference*, Houston, Texas, USA, 13–17 March, 2919–2934.

Henn, U. & Bank, H. 1991. Sternbronzit aus Sri Lanka. *Zeitschrift der Deutschen Gemmologischen Gesellschaft*, **40**(2–3), 145–148.

O'Donoghue, M. (ed) 2006. *Gems*, 6th edn. Butterworth-Heinemann, Oxford, 873 pp.

Schmitz, F., Stephan, T. & Müller, S. 2016. Gem Notes: Polymer-filled star enstatite from Norway. *Journal of Gemmology*, **35**(2), 96–118.

Zhao, S., Wang, H., Zhou, K. & Xiao, T. 1986. The spin-forbidden absorption spectrum of Fe^{2+} in orthopyroxene. *Physics and Chemistry of Minerals*, **13**(2), 96–101, http://doi.org/10.1007/bf00311899.

Yellowish Green Enstatite (and Star Enstatite) from Tanzania

Gem-quality enstatite is typically brown to dark green, and star enstatite was first documented by Eppler (1967) as a dark brown cabochon from southern India showing six-rayed asterism. However, during the February 2019 Tucson gem shows, some attractive yellowish green enstatite entered the market from a new find in Tanzania (e.g. Figure 18). One of the authors (JW) was initially offered the rough material as 'sphene' (titanite). Although the 'chartreuse' colour and overall appearance of the pieces resembled titanite, closer inspection with a loupe did not show the expected high birefringence and dispersion. Suspecting it was peridot, this author purchased a few pieces and took them to Alberto Scarani and Mikko Åström of Magilabs (Rome, Italy and Järvenpää, Finland) for an initial identification with Raman spectroscopy, which indicated enstatite. Upon returning home from Tucson, this author ground away any surface contamination from one of the pieces and confirmed it was enstatite via Raman analysis. In addition, the RIs of 1.66–1.67 and birefringence of 0.01 were consistent with enstatite. According to the supplier, Peter Musomba, the material was mined from the Morogoro area of Tanzania. Musomba was unaware of how much rough was produced, but from a 1 kg parcel he selected approximately 150 g of the cleanest material in pieces ranging from 1 to 3 g.

Although author JW obtained rough specifically for faceting transparent stones, there was also some silky material available in Tucson that could cut cat's-eye and star stones. Gem cutter Thomas A. Trozzo (Trozzo, Culpeper, Virginia, USA) purchased a small parcel from Farooq Hashmi, who obtained it in Tanzania as 'peridot'.

Figure 18: A 2.00 ct enstatite is shown with some rough material from a new find in Tanzania. Photo by J. White.

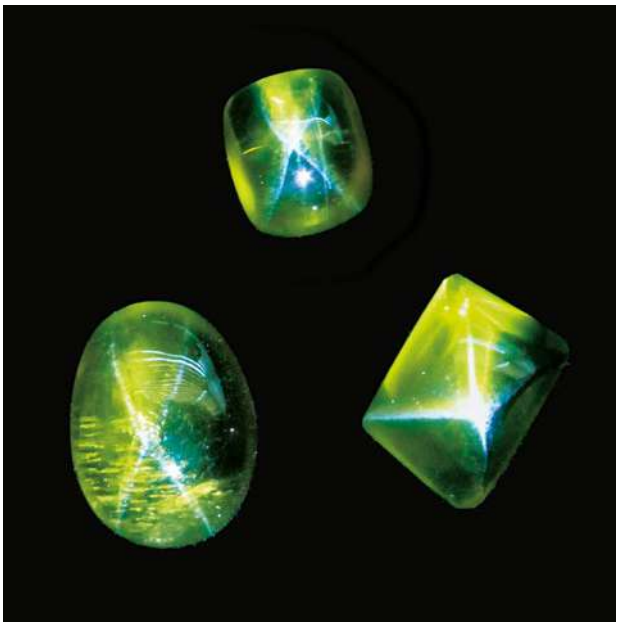

Figure 19: Weighing 3.56–7.32 ct, these star enstatites were cut from the new Tanzanian material. The samples exhibit cross-shaped four-rayed stars, although the orientation and cut of the right-hand stone make it difficult to see the appearance of the asterism. Photo by B. Williams.

Trozzo cut three star enstatites (Figure 19) and reported that although there was a sufficient amount of needle-like inclusions to create asterism, the rough stones were difficult to orient. In addition, author JW notes that enstatite is challenging to facet because of its two distinct cleavage directions, and it is also prone to fraying at the ends of the crystal. These aspects may present difficulties during the preforming and cutting stages. For example, while the stone in Figure 18 was being faceted, a significant crack spontaneously appeared during the early stages of cutting that had to be removed by sawing. To help avoid problems with cracking and fraying, it was necessary to use a fine-grit lap and minimise the pressure applied to the stone. Surprisingly, despite the difficulties encountered during the cutting stage, the enstatite polished very quickly and easily with 50,000 or 100,000 grit diamond paste.

The three star enstatites in Figure 19 along with three pieces of rough were provided by Trozzo to authors CW and BW for characterisation. The RIs were 1.660–1.669 (birefringence 0.009) and SG was measured hydrostatically as 3.25. Both of

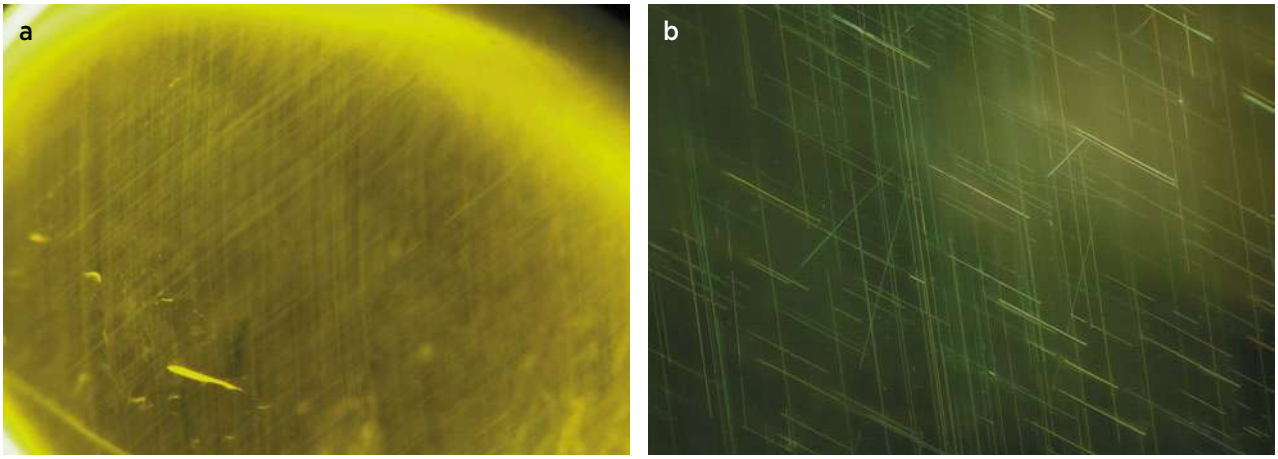

Figure 20: (**a**) Abundant needles are present in two orientations in this star enstatite. Photomicrograph by B. Williams; magnified 10×. (**b**) The faceted enstatite in Figure 18 contains fewer needles, as shown in this image created by stacking 18 photos using Helicon Focus software. The needles running from top to bottom of the photo are nearly parallel to the viewer, while those in the other predominant orientation are steeply inclined into the stone. A few needles are also present in two other orientations. Photomicrograph by J. White; image width 2.5 mm.

these values fall well within the range of enstatite, which was confirmed by Raman analysis and Fourier-transform infrared (FTIR) spectroscopy using GemmoRaman-532SG and PerkinElmer Spectrum100 instruments, respectively. EDXRF spectroscopy with an Amptek X123-SDD spectrometer showed various minor and trace elements, including Ti, V, Cr, Mn and Fe. The stones all contained elongate needles oriented in two directions (Figure 20a), and one of them also had some colour-growth zones bisecting the acicular inclusions, similar to those documented in a brown Tanzanian enstatite by Koivula *et al.* (1988). By comparison, the transparent faceted stone in Figure 18 contained fewer needles (Figure 20b).

A small fragment provided by author JW to GRR was also confirmed as enstatite by infrared reflectance, and EDXRF spectroscopy using an INAM Expert 3L unit showed 1.4% Fe, 0.4% Mn, 0.08% V, 0.07% Ti and 0.01% Cr. Initial attempts to obtain Vis-NIR absorption spectra revealed that the sample was not oriented correctly for polarised spectroscopy along the principal axes, so another piece (supplied by Trozzo) was optically oriented and fabricated into an approximate cube for spectroscopy. Analyses with a combination of a silicon-diode array microspectrometer and an InGaAs FTIR system showed that the spectra were dominated by absorption features of Fe^{2+} in the near-infrared region (Figure 21a). The colour in the visible region, however, was primarily controlled by the weaker V^{3+} absorption bands in the ranges of 420–490 nm and 600–700 nm that defined a window of maximum transmission in the yellow-green region (500–580 nm) of the spectrum (Figure 21b).

Although enstatite with such an attractive bright colour is only rarely encountered, similar material has been documented previously from both Kenya and Tanzania. Schmetzer & Krupp (1982) described transparent yellowish green enstatite from Mairimba Hill, which is located south of the Taita Hills in southern Kenya (RIs = 1.652–1.662, birefringence = 0.010, SG = 3.23), and attributed its attractive colour to small amounts of Fe and Cr replacing Mg. Stockton & Manson (1983) compared transparent yellowish green enstatite and peridot that both reportedly came from the Usambara Mountains in Tanzania (near the border with Kenya), and reported the following properties for the enstatite: n_α = 1.669, n_β = 1.672, n_γ = 1.679 and birefringence = 0.010. Enstatite and peridot can have overlapping colour, RI and SG values, but Stockton & Manson (1983) emphasised that they can be separated by their spectroscope spectra and peridot's higher birefringence (0.036). Coincidentally, both gem varieties can also form four-rayed stars. While star peridot is considered quite rare and highly collectible compared to star enstatite, the Tanzanian enstatite documented here is unusual in showing an attractive bright colouration as well as the possibility of yielding cat's-eye and star stones.

Brendan M. Laurs FGA

Cara Williams FGA and Bear Williams FGA
Stone Group Laboratories
Jefferson City, Missouri, USA

Jeff White
J. L. White Fine Gemstones
Kingsport, Tennessee, USA

Dr George R. Rossman
California Institute of Technology
Pasadena, California, USA

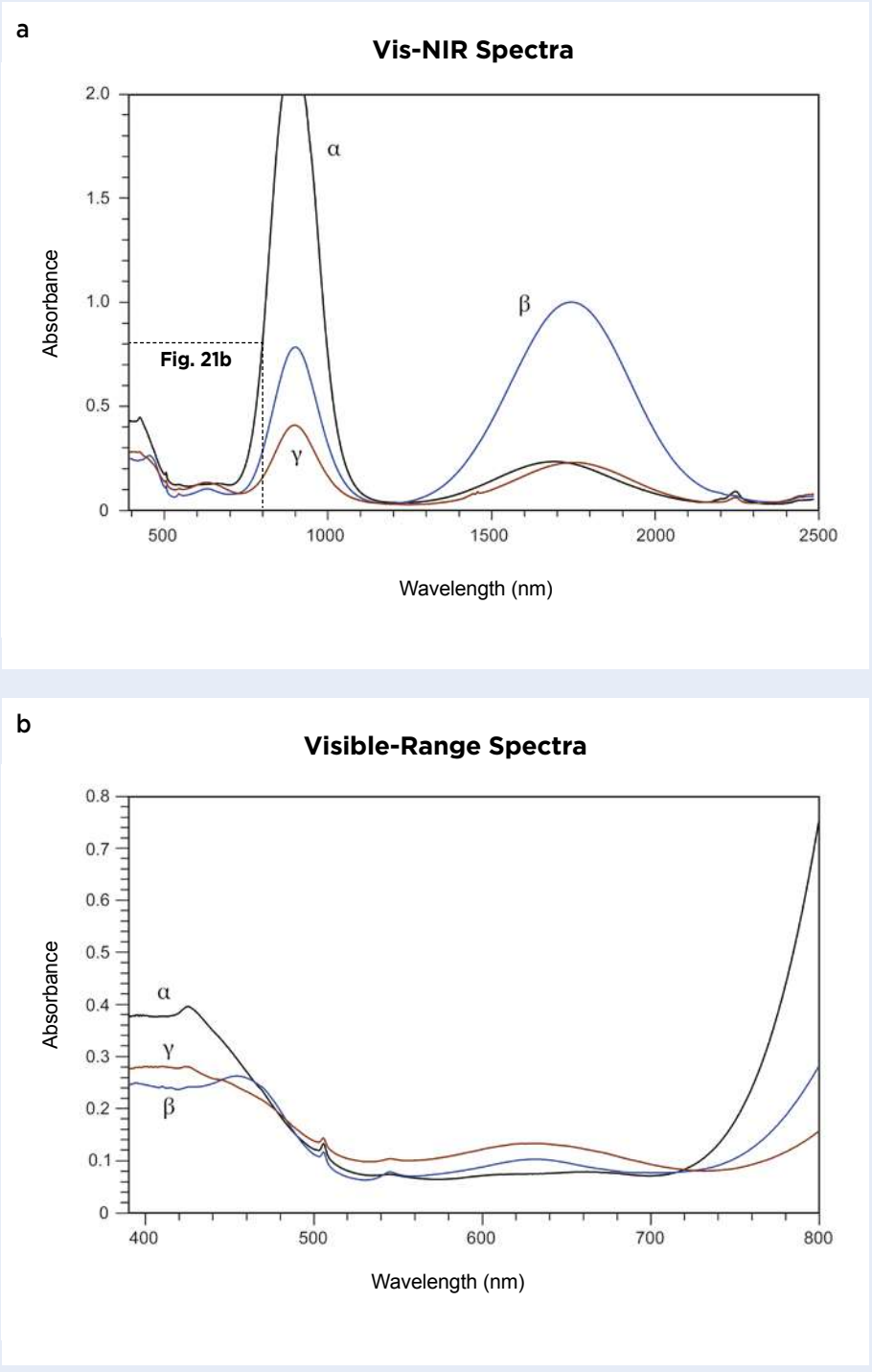

Figure 21: (**a**) Vis-NIR spectra of the Tanzanian enstatite are dominated by strong Fe^{2+} features near 900 and 1750 nm. (**b**) The visible-range spectra show broad V^{3+} features that define an area of maximum transmission in the yellow-green region. The weak, sharp Fe^{2+} peak at 506 nm is a common feature of iron in orthopyroxenes. The spectra are plotted for 2.0 mm thickness.

References

Eppler, W.F. 1967. Star-diopside and star-enstatite. *Journal of Gemmology*, **10**(6), 185–188, http://doi.org/10.15506/jog.1967.10.6.185.

Koivula, J.I., Fryer, C.W. & Shigley, J.E. 1988. Gemmological investigation of a large faceted East African enstatite. *Journal of Gemmology*, **21**(2), 92–94, http://doi.org/10.15506/jog.1988.21.2.92.

Schmetzer, K. & Krupp, H. 1982. Enstatite from Mairimba Hill, Kenya. *Journal of Gemmology*, **18**(2), 118–120, http://doi.org/10.15506/jog.1982.18.2.118.

Stockton, C.M. & Manson, D.V. 1983. Peridot from Tanzania. *Gems & Gemology*, **19**(2), 103–107, http://doi.org/10.5741/gems.19.2.103.

Sunstone Labradorite-Bytownite from Ethiopia

Figure 22: Sunstone has been recovered from surface deposits in the Afar region of Ethiopia. Photo by T. Sintayehu.

In the past several years, Ethiopia has gained attention for a variety of new gem finds. After large deposits of play-of-colour opal were found in 2008, black opal was detected in 2013 (Kiefert *et al*. 2014). In 2016, high-quality emeralds were recovered from southern Ethiopia (Renfro *et al*. 2017; Schollenbruch *et al*. 2017), some of which rivalled those from Colombia. In December of the same year, significant deposits of basaltic blue sapphires were found in the country's north (Bruce-Lockhart 2017).

In 2015, one of the authors (TS) was shown various gem samples—including sunstone—that reportedly came from the Afar region in north-eastern Ethiopia. After further investigation, this author learned the approximate location of the sunstone deposits and later was shown several places where it was found (e.g. Figure 22). These occurrences occupy an area close to 100 km in length and width, and are located south-east of Mek'ele.

The sunstone occurs mostly as loose angular pieces (Figure 23a) but has also been found in coarse-grained rock fragments (Figure 23b) in a basaltic environment. Most of the gem rough recovered so far showed a near-colourless rim with red colour concentrated towards the centre. Occasionally, green zones were also present (again, see Figure 23a). Very few of the stones showed a schiller

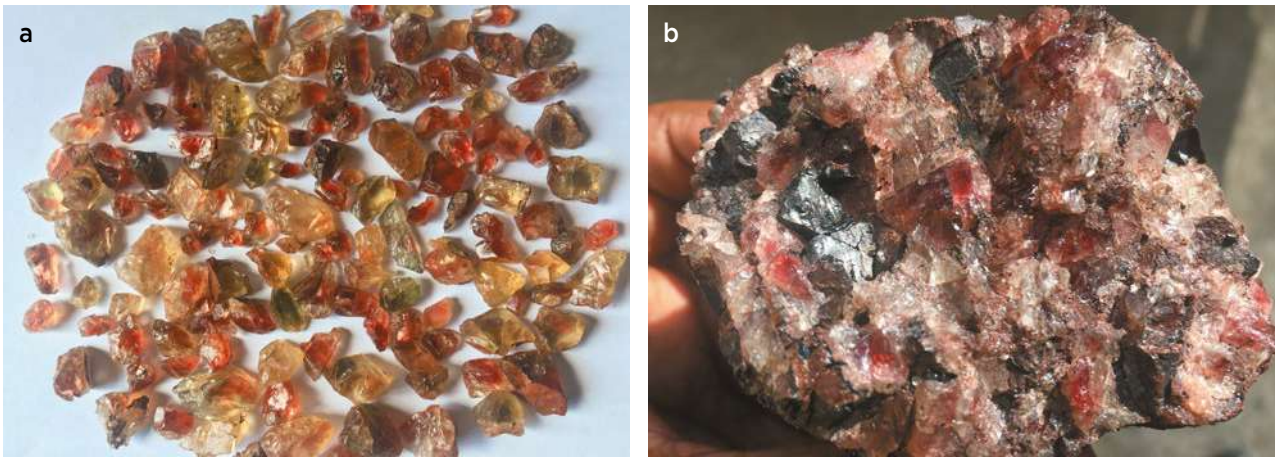

Figure 23: Ethiopian sunstone exhibits various colours (near-colourless, red and green), similar to labradorite from Oregon, USA. The Ethiopian samples shown here include (**a**) broken pieces that are about 5–20 mm long and (**b**) a rock fragment of about 120 mm in maximum dimension that is probably a glomerocryst (crystal cluster of plagioclase and pyroxene). Photos by T. Sintayehu.

Figure 24: These faceted Ethiopian sunstones (0.48–1.91 ct) display various colours. Photo by T. Sintayehu.

effect due to copper-coloured particles large enough to be visible with a gemmological microscope. So far only a few of the Ethiopian sunstones have been faceted, weighing 0.48–1.91 ct (Figure 24).

EDXRF chemical analyses of six rough samples with a Thermo Fisher Quant'X instrument yielded a chemical composition ranging from labradorite to bytownite, with contents of anorthite (An), albite (Ab) and orthoclase (Or) in the range of $An_{66.8–79.7}Ab_{18.6–31.1}Or_{0.1–2.2}$. This composition is more calcic than that of Oregon sunstone documented by Hofmeister & Rossman (1985: $An_{64.7–67.0}$).

UV-Vis microspectroscopy of a colour-zoned sample was performed with a Jasco MSV-5200 spectrophotometer. The near-colourless area showed an overall continuous increase in absorption toward the UV region, while the red portion exhibited a broad absorption band with a maximum at 568 nm (Figure 25). A similar absorption band has been recorded in red Oregon sunstone, but at a lower wavelength (i.e. 561 nm from research done by author CW, and at 560 nm according to Hofmeister & Rossman 1985). Since labradorite is triclinic, differences in sample orientation may cause the variations in the position of the band.

Overall, the colouration and UV-Vis spectral features of this new Ethiopian feldspar are similar to those of Oregon sunstone. Further data will be reported in a future article.

Dr Lore Kiefert FGA
(lore.kiefert@gubelingemlab.com)
Gübelin Gem Lab
Lucerne, Switzerland

Chengsi Wang
Gemmological Institute
China University of Geosciences
Wuhan, Hubei, China

Tewodros Sintayehu
Orbit Ethiopia plc
Addis Ababa, Ethiopia

Klemens Link
Gübelin Gem Lab, Lucerne

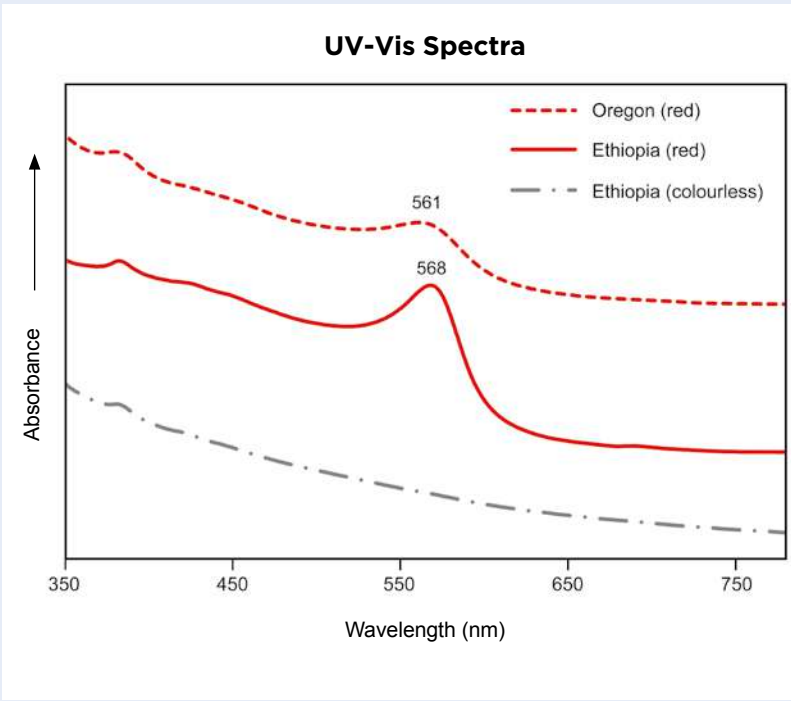

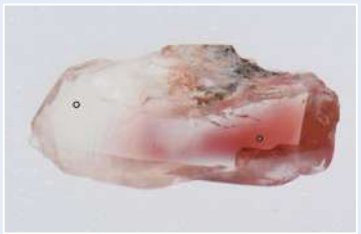

Figure 25: An 11-mm-long sample of bicoloured sunstone from Ethiopia was polished for UV-Vis microspectroscopy. The positions analysed in the near-colourless and red zones are marked with circles. Photo by C. Wang. The spectrum of the near-colourless portion shows a continuous increase in absorption towards the UV region, while the red area exhibits an absorption band centred at about 568 nm. By comparison, the absorption band for a sample of red Oregon sunstone is located at 561 nm. The spectra have been shifted vertically for clarity.

References

Bruce-Lockhart, S. 2017. Gem Notes: Update on sapphires from Tigray, northern Ethiopia. *Journal of Gemmology*, **35**(7), 580–582.

Hofmeister, A.M. & Rossman, G.R. 1985. Exsolution of metallic copper from Lake County labradorite. *Geology*, **13**(9), 644–647, http://doi.org/10.1130/0091-7613(1985)13<644:Eomcfl>2.0.Co;2.

Kiefert, L., Hardy, P., Sintayehu, T., Abate, B. & Woldetinsae, G. 2014. Gem News International: New deposit of black opal from Ethiopia. *Gems & Gemology*, **50**(4), 303–305.

Renfro, N., Sun, Z., Nemeth, M., Vertriest, W., Raynaud, V. & Weeramonkhonlert, V. 2017. Gem News International: A new discovery of emeralds from Ethiopia. *Gems & Gemology*, **53**(1), 114–116.

Schollenbruch, K., Link, K. & Sintayehu, T. 2017. Gem quality emeralds from southern Ethiopia. *InColor*, No. 35, 48–54.

Quartz from Brazil with Gormanite Inclusions

Since approximately 2017–2018, quartz from Brazil containing green epigenetic inclusions has appeared on the market (e.g. Figure 26). It is sometimes referred to as 'hematoid' quartz because of the similar appearance (although different colouration) as the hematite inclusions in quartz that were produced from Minas Gerais at approximately the same time (Laurs 2017). According to Luciana Barbosa (Gemological Center, Weaverville, North Carolina, USA) and Dr Marco Campos-Venuti (Seville, Spain), the quartz containing the green inclusions comes from the same pegmatite in the Galiléia area of Minas Gerais State that recently produced attractive triphylite inclusions in quartz (cf. Costanzo & Laurs 2019). Barbosa reported that some of the quartz contains both the triphylite and green inclusions within the same stone.

Barbosa loaned an 11.45 ct sample of polished quartz containing the 'hematoid' inclusions for examination (Figure 27), and Raman microspectroscopy by author NDR provided a weak signal that showed a close match with gormanite, an iron-aluminium phosphate mineral with the formula $(Fe^{2+},Mg)_3(Al,Fe^{3+})_4(PO_4)_4(OH)_6 \bullet 2H_2O$. Gormanite has been previously documented as a rare secondary mineral in granitic pegmatites (e.g. Antunes *et al*. 2013), consistent with its presence as epigenetic fracture fillings in quartz from Galiléia. The strong pleochroism shown by gormanite was evident when the sample was examined in plane-polarised light (Figure 28).

The inclusions in this quartz range from blue-green to yellow-green to yellow and orange (again, see Figure 26), suggesting that the gormanite is accompanied in places by hematite, which adds to the colour possibilities exhibited by this material.

Brendan M. Laurs FGA and Nathan D. Renfro FGA

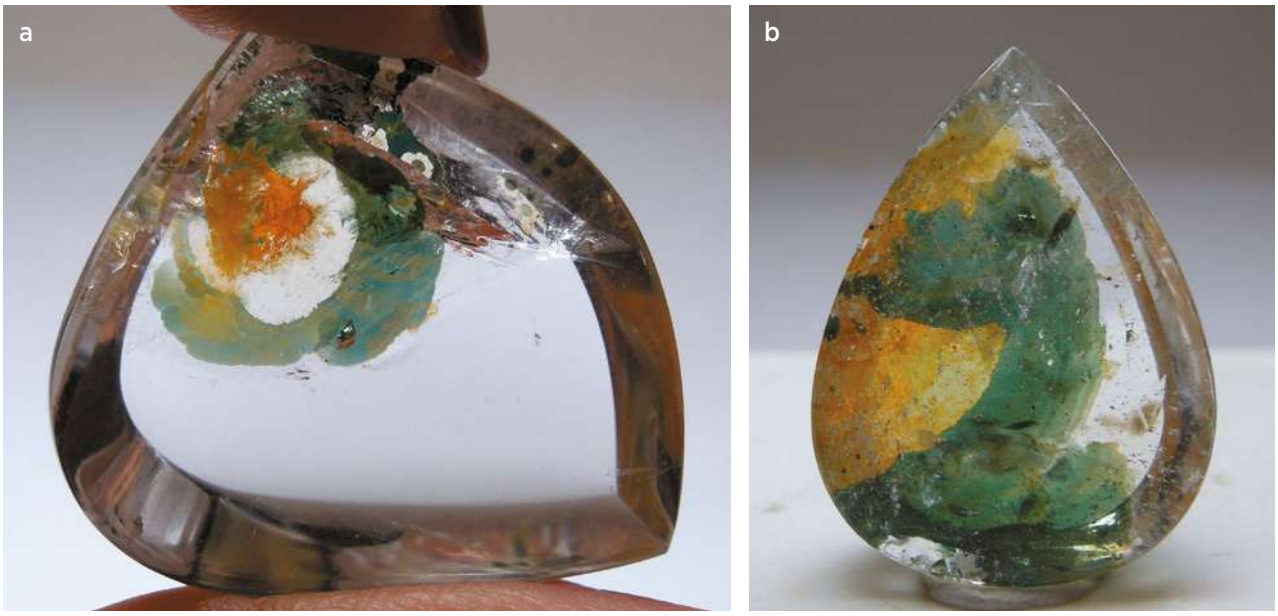

Figure 26: These polished tablets of quartz from the Galiléia area of Brazil contain epigenetic inclusions showing various colours. The samples weigh (**a**) 19.10 ct and (**b**) 20.70 ct. Photos by Luciana Barbosa.

Figure 27: The dark green inclusions in this polished quartz (11.45 ct) were analysed for this report, and proved to be gormanite. Photo by Robison McMurtry, © GIA.

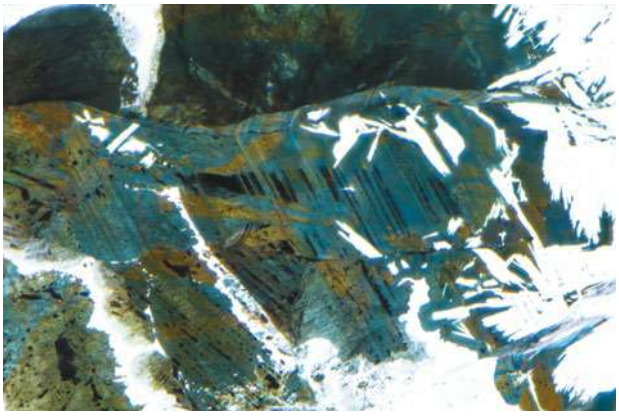

Figure 28: Viewed with plane-polarised light, the gormanite inclusions display strong pleochroism in greenish blue and brownish yellow. The surrounding quartz appears bright white due to the intense lighting needed to bring out the pleochroic colours (a diffuser plate was also placed behind the stone). Sheaf-like white areas within the gormanite appear to be caused by another mineral phase that was formerly present within the same fracture but subsequently leached away. Photomicrograph by N. D. Renfro, © GIA; image width 4.0 mm.

References

Antunes, I.M.H.R., Neiva, A.M.R., Ramos, J.M.F., Silva, P.B., Silva, M.M.V.G. & Corfu, F. 2013. Petrogenetic links between lepidolite-subtype aplite-pegmatite, aplite veins and associated granites at Segura (central Portugal). *Geochemistry*, **73**(3), 323–341, http://doi.org/10.1016/j.chemer.2012.12.003.

Costanzo, A. & Laurs, B.M. 2019. Gem Notes: Quartz with triphylite inclusions from Brazil. *Journal of Gemmology*, **36**(6), 505–507, http://doi.org/10.15506/JoG.2019.36.6.505a.

Laurs, B.M. 2017. Gem Notes: Quartz from Brazil with colourful epigenetic inclusions. *Journal of Gemmology*, **35**(6), 486–487.

Quartz from Chile with Powellite and Molybdenite Inclusions

At one time, molybdenite (MoS_2) was only rarely known as an inclusion in quartz, but this changed dramatically with a large find from the Confianza mine near Tilama, Valparaiso, Chile, in 2004 (Koivula and Tannous 2004; Koivula 2017). In 2011, the author acquired a large quartz crystal from this locality which contained a phantom, measuring 11 cm wide, composed of three planes that were decorated with inclusions. Two of the planes contained molybdenite crystals, while the third one had light brown to white plates with the same morphology as molybdenite. Their strong yellow fluorescence to short-wave UV radiation indicated they were powellite, which formed as pseudomorphs after molybdenite. Powellite is tetragonal $CaMoO_4$ and belongs to the scheelite group.

In April 2019, a new find from the same mine yielded additional quartz with molybdenite inclusions (up to 15 mm diameter; Figure 29), as well as well-formed

Figure 29: Molybdenite crystals up to 15 mm in diameter form prominent inclusions in this quartz, which was recently recovered from the Confianza mine in Chile. The stone weighs 131.35 ct and is 36 mm long. Photo by J. Hyršl.

powellite crystals (Figure 30). The powellite inclusions form transparent light yellow bipyramids up to 4.5 mm long, with a high lustre and typical yellow fluorescence. Some of the powellite crystals are bicoloured, with near-colourless and brownish yellow parts (again, see Figure 30). In addition, the powellite in some specimens forms colourless, sharp hexagonal tablets up to 2 mm across, which appear to be pseudomorphs after molybdenite. Both the powellite and molybdenite crystals are scattered through the quartz, rather than being concentrated along phantoms as in the quartz described above.

Powellite is a relatively common alteration product of molybdenite, but the occurrences mentioned here are the first times the author is aware of it forming inclusions in quartz.

Dr Jaroslav Hyršl (hyrsl@hotmail.com)
Prague, Czech Republic

Figure 30: Inclusions of near-colourless to brownish yellow powellite occur together with dark grey molybdenite in this quartz from the Confianza mine. The stone weighs 62.33 ct and is 27 mm long. Photo by J. Hyršl.

References

Koivula, J.I. 2017. *G&G* Micro-World: Molybdenite phantoms in quartz. *Gems & Gemology*, **53**(2), 245–246.

Koivula, J.I. & Tannous, M. 2004. Gem News International: Quartz in molybdenite. *Gems & Gemology*, **40**(4), 353.

Quartz from Madagascar with Fuchsite Phantom Inclusions

Madagascar has long been known as a source of quartz with interesting inclusions. In early 2015, Michael Puerta (Intimate Gems, Forest Hills, New York, USA) obtained 1–2 kg of quartz crystals from Madagascar that contained conspicuous 'phantoms' decorated by minute green crystalline inclusions. Such quartz is known from Ihovitra (or Anovitra, Iovitra, Ivohitra) in the Ambatofinandrahna area of central Madagascar (www.mindat.org/loc-108282.html). The green inclusions in this quartz have been referred to in the trade as celadonite, fuchsite and chlorite. Renfro (2009) identified the inclusions as fuchsite, together with some brown radial clusters of pumpellyite.

We performed further characterisation of the fuchsite inclusions in this quartz, using rough and cut samples that were loaned by Puerta (Figure 31a). The inclusions in the 2.7-cm-long crystal formed evenly distributed micro-clusters that occurred along a sharp, thin phantom that marked the location of former quartz growth faces (Figure 31b). The 0.35 ct faceted stone incorporated an inclusion-rich area of the quartz to create an overall light green appearance (Figure 31a).

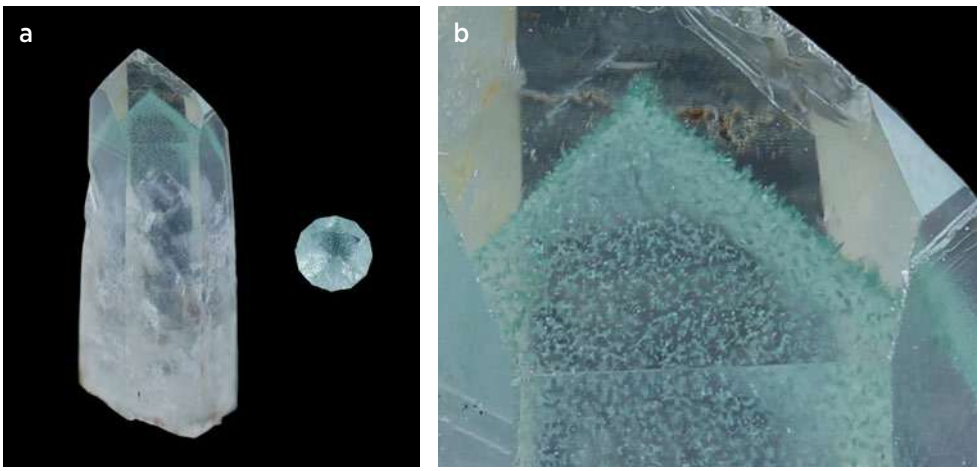

Figure 31: (**a**) These rough and cut samples of quartz from Madagascar containing green phantom inclusions were studied for this report. The crystal measures 2.7 × 1.0 cm and the cut stone weighs 0.35 ct. (**b**) A magnified view of the crystal (image width about 8.3 mm) reveals the even distribution of inclusions along phantom planes in the quartz. Photos by Greg Polley.

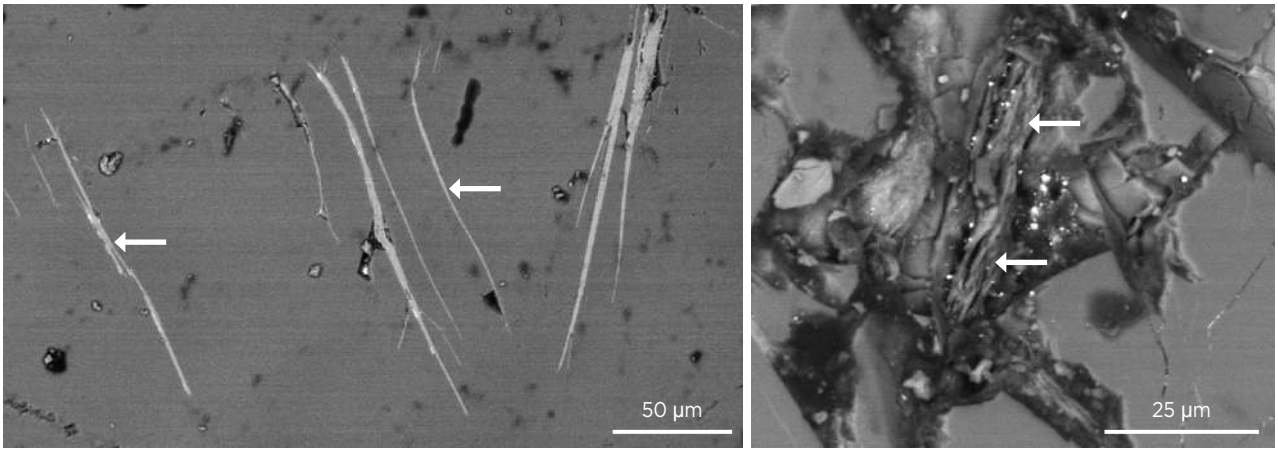

Figure 32: Backscattered electron images show the sheet-like structure of the fuchsite inclusions (see arrows) in the faceted quartz in Figure 31. This morphology is typical for a mica.

The mineralogy of the inclusions was confirmed by X-ray diffraction using a Rigaku D/Max Rapid II micro-X-ray diffractometer, which revealed a clear muscovite-like pattern as a minor phase within the dominant quartz pattern. Similar results were obtained using Raman microspectroscopy (with a Horiba LabRAM Evolution unit) by focusing a 532 nm laser onto a cluster of the inclusions that intersected one of the gem's facets. Finally, scanning electron microscopy using backscattered electron (BSE) mode and energy-dispersive spectroscopy (EDS) was performed on the same inclusion cluster in the faceted sample using an FEI Nova NanoSEM 600 instrument. The BSE images revealed that the inclusions have a sheet-like morphology expected for a micaceous phase (Figure 32). EDS analyses yielded a chemical formula consistent with Cr-rich muscovite (fuchsite) containing traces of Fe and other elements: $(K_{0.87}Na_{0.13})(Si_{3.44}Al_{0.56})(Cr_{1.06}Mg_{0.47}Al_{0.38}Fe_{0.08})O_{10}(OH)_2$.

Our analyses corroborate the previous identification of fuchsite in quartz phantoms from Madagascar. However, we did not observe any pumpellyite inclusions, as reported for the sample examined by Renfro (2009).

Dr Gabriela A. Farfan (farfang@si.edu)
and Dr Jeffrey E. Post
Department of Mineral Sciences
Smithsonian Institution
Washington DC, USA

Reference

Renfro, N. 2009. Lab Notes: Pumpellyite in quartz. *Gems & Gemology*, **45**(3), 211–212.

Tourmaline from Sri Lanka with Transient Tenebrescence?

While on a buying trip to Sri Lanka in November 2017, stone dealer Dudley Blauwet obtained six faceted tourmalines from his supplier in Ratnapura. The stones were reportedly mined in Nivithigala, which is located 18 km by road south-east of Ratnapura. They ranged from 'olive' green to 'golden' brown-orange, and appeared similar to some dravite-uvite from Tanzania and Kenya. Interestingly, Blauwet noticed that two of them (weighing 1.74 and 2.69 ct) appeared to show a reverse colour change—from golden brown in daylight to yellowish green in incandescent light—which is the opposite of most East African tourmaline (cf. Bank & Henn 1988). A third stone (2.72 ct) showed a much weaker colour change, while the others did not show any shift in colour. When checked with a Chelsea Colour Filter (CCF), Blauwet discovered that the two stones showing the noticeable colour change displayed a saturated greenish blue reaction, while the others were inert. The greenish blue CCF reaction was much different than the red appearance typically seen in East African tourmaline showing the typical colour change from 'chrome' green in daylight to greenish yellow in incandescent light.

After returning home, Blauwet decided to check one of the anomalous stones (1.74 ct) for tenebrescence, and he placed it on a south-facing windowsill from 8:30 am to 10:00 am on an overcast day. Surprisingly, this caused it to change from golden brown to slightly greyish olive. He then put the stone in the dark for 1.25 hours, causing it to regain some of its original colour; longer storage in darkness did not return any more of the stone's original

colour. Based on his repeated observations of the stones, Blauwet suspected that the anomalous colour behaviour displayed by the two tourmalines was a short-term transient phenomenon.

Blauwet loaned the tourmalines to authors AUF and WBS to investigate their composition. In July 2018 they performed standard-based scanning electron microscopy energy-dispersive spectroscopy (SEM-EDS) chemical analysis using a JEOL JSM-6400 instrument with the Iridium Ultra software package by IXRF Systems Inc., and found that the tourmalines were mainly uvite with one dravite and one elbaite-liddicoatite series stone. The two stones for which Blauwet noted the anomalous colour behaviour consisted of uvite (1.74 ct) and elbaite (2.69 ct), although authors AUF and WBS did not check them for any usual colour phenomena at that time.

All six tourmalines were then sent to authors AP and ZS for further chemical analysis by laser ablation inductively coupled plasma mass spectrometry (LA-ICP-MS) and thorough documentation of their colour behaviour. The chemical data confirmed the tourmaline compositions obtained by SEM-EDS, and further showed the presence of several trace elements, including variable amounts of V, Cr, Sr, Sn, La, Ce and Pb (Tables I and II).

Table I: Average chemical composition of the Sri Lankan tourmaline samples by LA-ICP-MS.*

Chemical composition	Elbaite	Dravite	Uvite	Uvite	Uvite	Uvite
	2.69 ct	1.63 ct	2.72 ct	1.74 ct	2.23 ct	2.47 ct
Oxides (wt.%)						
SiO_2	36.49	36.52	36.32	36.03	36.40	36.21
Al_2O_3	40.61	34.72	27.64	27.85	27.26	27.12
Na_2O	1.94	2.00	0.08	0.20	0.08	0.08
K_2O	0.01	0.09	nd	nd	nd	nd
MgO	nd	10.23	15.63	15.69	16.04	16.04
CaO	1.37	0.79	5.40	5.23	5.45	5.52
FeO	1.95	0.05	0.18	0.39	0.18	0.32
MnO	0.36	0.04	nd	nd	nd	nd
PbO	0.23	nd	nd	nd	nd	nd
V_2O_3	nd	0.05	0.03	0.01	0.02	0.02
TiO_2	0.01	0.49	0.16	0.20	0.08	0.23
Cr_2O_3	nd	nd	0.03	nd	0.03	0.02
Li_2O (calc.)	2.05	0.28	0.02	nd	nd	nd
B_2O_3 (calc.)	10.96	10.93	10.73	10.72	10.72	10.71
H_2O (calc.)	3.78	3.77	3.70	3.63	3.66	3.65
Atoms per formula unit (27O + 4OH)						
Si	5.788	5.809	5.884	5.844	5.901	5.879
Al	0.212	0.191	0.116	0.156	0.099	0.121
Tet. sum	6.000	6.000	6.000	6.000	6.000	6.000
B	3.000	3.000	3.000	3.000	3.000	3.000
Al (Z)	6.000	6.000	5.161	5.169	5.109	5.068
Mg (Z)	nd	nd	0.831	0.830	0.884	0.927
Z sum	6.000	6.000	5.992	5.999	5.993	5.995
Al (Y)	1.379	0.319	nd	nd	nd	nd
Ti	0.002	0.059	0.020	0.025	0.010	0.028
Fe^{2+}	0.259	0.006	0.024	0.053	0.025	0.044
Mn	0.049	0.005	nd	nd	nd	nd
Mg (Y)	nd	2.426	2.944	2.965	2.992	2.956
Li	1.305	0.178	0.012	nd	nd	nd
Y sum	2.994	2.993	3.000	3.043	3.027	3.028
Ca	0.233	0.134	0.938	0.909	0.947	0.959
Na	0.597	0.616	0.025	0.064	0.025	0.027
K	0.003	0.018	nd	nd	nd	nd
Vacancy	0.158	0.232	0.037	0.027	0.028	0.014
X sum	0.990	1.000	1.000	1.000	1.000	1.000
OH	4.000	4.000	4.000	4.000	4.000	4.000

* Average of three analyses per sample. Data were normalised to a total of 100 wt.% oxides based on the method reported by Sun *et al.* (2019). Some trace elements are not shown here but are reported in Table II. Fluorine was not measured, so the contents of the V and W sites were calculated as OH = 4, and therefore the fluor-species of tourmaline could not be determined. Abbreviation: nd = not detected.

Table II: Average minor- and trace-element composition of the Sri Lankan tourmaline samples by LA-ICP-MS.*

Chemical composition (ppmw)	Elbaite	Dravite	Uvite	Uvite	Uvite	Uvite
	2.69 ct	1.63 ct	2.72 ct	1.74 ct	2.23 ct	2.47 ct
Ti	89.2	2930	962	1220	475	1360
Sc	2.72	242	10.4	3.62	7.17	5.34
P	29.1	35.9	33.8	30.8	30.0	33.4
V	0.3	357	179	66.6	170	166
K	108	717	7.98	17.8	13.6	7.97
Cr	nd*	2.01	220	2.18	210	112
Cu	1.03	0.40	nd	0.043	nd	nd
Ni	nd	nd	5.54	0.86	3.64	0.64
Mn	2810	298	4.50	1.90	2.60	5.40
Be	32.1	1.48	2.28	0.81	0.59	0.21
Sr	467	19.7	322	59.5	366	547
Nb	8.77	0.004	0.10	0.86	0.054	0.12
Sn	165	0.13	6.55	96.4	40.7	17.1
La	56.1	3.22	48.2	1.20	47.2	1.22
Ce	183	7.08	97.6	1.53	65.8	1.46
Pr	22.0	0.65	8.81	0.099	4.20	0.092
Nd	60.7	1.98	24.2	0.20	8.95	0.18
Gd	2.05	0.15	1.04	0.009	0.25	nd
Tb	0.13	0.014	0.068	nd	0.014	0.001
Dy	0.35	0.058	0.18	0.002	0.023	0.004
Tm	0.008	0.012	0.002	nd	nd	0.001
Yb	0.054	0.040	0.016	nd	nd	nd
Lu	0.009	0.008	0.004	nd	nd	nd
Pb	2120	0.66	6.83	1.76	21.2	9.62
Bi	1.57	nd	nd	nd	nd	nd
Th	43.5	nd	0.002	0.022	0.009	0.008
U	0.64	nd	nd	nd	0.003	0.006

* Average of three analyses per sample. Abbreviation: nd = not detected. Detection limits (ppmw): Cr = 0.19, Cu = 0.036, Ni = 0.059, Tb = 0.001, Tm = 0.001, Yb = 0.004, Lu = 0.001, Bi = 0.026, Th = 0.001 and U = 0.002.

None of the trace elements showed any systematic correlation to those tourmalines that displayed the anomalous colour behaviour except Sn, which was present in somewhat greater amounts in those two samples, although this element is not known to influence the colouration of tourmaline. Notably, however, authors AP and ZS were unable to observe any colour change or tenebrescence in any of the samples, even with repeated exposure to various UV excitations and daylight after storage in the dark for up to several weeks. It appears, therefore, that Blauwet's suspicion was indeed correct that the colour phenomena were short-lived. In fact, the two stones appeared to have lost all of their golden brown colouration, appearing greyish to brownish yellowish green (Figure 33) regardless of the light source used to view them.

Figure 33: These six tourmalines were reportedly mined from alluvial deposits in the Nivithigala area near Ratnapura, Sri Lanka. Anomalous colour behaviour was seen in the 1.74 and 2.69 ct samples shortly after their purchase, but subsequently their colouration apparently stabilised. Photo by Robison McMurtry, © GIA.

A literature search did not reveal any previous reports of tenebrescence or transient colour phenomena in tourmaline, although some unusual colour behaviour has been documented, particularly in stones from East Africa. For example, Koivula & Kammerling (1991) documented a pair of dravites from Tanzania or Kenya that appeared slightly brownish yellow in incandescent or fluorescent lighting, but were greenish yellow when illuminated simultaneously with incandescent and fluorescent lighting. In addition, Johnson *et al.* (2000) examined a uvite that had been purchased in Sri Lanka which appeared strongly pleochroic in reddish brown and green in incandescent light, but was uniformly brownish yellowish green in fluorescent light. The chemical composition and gemmological properties of that stone were consistent with the tourmalines from Usambara, Tanzania, which may show dichromatism called the 'Usambara effect': a change of colour from dark green to red when a critical thickness is exceeded (e.g. Taran & Naumenko 2016 and references therein). Nevertheless, these various colour anomalies described in the literature are significantly different from the apparently transient colour behaviour that was exhibited by the two tourmalines described here.

Brendan M. Laurs FGA

Dr Aaron Palke and Ziyin (Nick) Sun
GIA, Carlsbad

Alexander U. Falster and
Dr William 'Skip' B. Simmons
Maine Mineral & Gem Museum
Bethel, Maine, USA

References

Bank, H. & Henn, U. 1988. Colour-changing chromiferous tourmalines from East Africa. *Journal of Gemmology*, **21**(2), 102–103, http://doi.org/10.15506/jog.1988.21.2.102.

Johnson, M.L., Koivula, J.I., McClure, S.F. & DeGhionno, D. (eds) 2000. Gem News: Tourmaline with an apparent change-of-color in one pleochroic direction. *Gems & Gemology*, **36**(3), 270–271.

Koivula, J.I. & Kammerling, R.C. (eds) 1991. Gem News: Tourmaline with unusual "color change". *Gems & Gemology*, **27**(3), 184–185.

Sun, Z., Palke, A.C., Breeding, C.M. & Dutrow, B.L. 2019. A new method for determining gem tourmaline species by LA-ICP-MS. *Gems & Gemology*, **55**(1), 2–17, http://doi.org/10.5741/gems.55.1.2.

Taran, M.N. & Naumenko, I.V. 2016. Usambara effect in tourmaline: Optical spectroscopy and colourimetric studies. *Mineralogical Magazine*, **80**(5), 705–717, http://doi.org/10.1180/minmag.2016.080.016.

PEARLS

Diving for Natural Pearls off Bahrain: A Different Type of Gemmological Sample Collection

Bahrain was (and still is) considered an important centre for the natural pearl trade, and it is one of the few countries where fishing for natural pearls is legal today. Most gem-quality pearls have traditionally been found in waters located 50 km north-north-east of Bahrain (more precisely, at Hayr Shutayah, Hayr Bulthama and Hayr Bu Amamah; *Hayr* means 'oyster bed', see Figure 34). The shoals in these areas contain an average of about 4–30 'oysters' per square metre. To protect these resources, the government has implemented strict laws and regulations on mollusc fishing, and has recognised the three areas mentioned above as part of the Pearling Path project (https://pearlingpath.bh/en) and a UNESCO World Heritage Site. Bahrain is the only country where diving for natural pearls still occurs, and tourists and residents can purchase a pearl-diving pass (http://pearldiving.bh), dive with a licensed diving company, and collect and open up to 60 shells per pass.

The vast majority of pearls fished off Bahrain are found in *Pinctada radiata* (*P. radiata*) and, less commonly, in *P. margaritifera* and Pinnidae (or pen shell) bivalves. The Bahrain Institute for Pearls & Gemstones (DANAT) recently started a project to conduct a full scientific study on these molluscs and their pearls from various locations around Bahrain. For this purpose, several members of DANAT's team have obtained their scuba diving certification and received training in proper collection techniques.

The project's first step is to collect the molluscs from all over Bahrain, starting in the major and well-known

Figure 34: The most important fishing areas for natural pearls in Bahrain—Hayr Shutayah (dark blue), Hayr Bulthama (red) and Hayr Bu Amamah (purple)—are protected by law. These shoals lie about 50 km north-north-east of the main island of the Kingdom of Bahrain. Modified from the map 'Pearl Fishing Banks and Other Named Shoal Areas in the Vicinity of the Kingdom of Bahrain' (scale 1:350,000), first published in 1989 and modified in 2003; © Survey Directorate, Survey & Land Registration Bureau, Kingdom of Bahrain.

diving areas (including the three protected areas mentioned above after obtaining all necessary permissions), most of which are concentrated to the north. The team also plans to dive at 22 additional locations to the east, west and south of Bahrain. The goal is to collect around 1,000 molluscs from each location (principally *P. radiata* and all with a shell size of >6 cm wide), while recording GPS coordinates, ocean depth, water temperature, salinity, pH, etc. At the end of each day's diving, the fished molluscs are carefully opened at DANAT's premises in order to gather accurate data on the location of any pearls inside the animals (Figures 35 and 36). Sometimes multiple pearls are found within the same mollusc (Figure 37).

Figure 35: A photograph of a freshly opened *P. radiata* mollusc (7 cm wide) is overlaid with a diagram showing the various positions where natural pearls may be found. Photo by H. Abdulla, © DANAT.

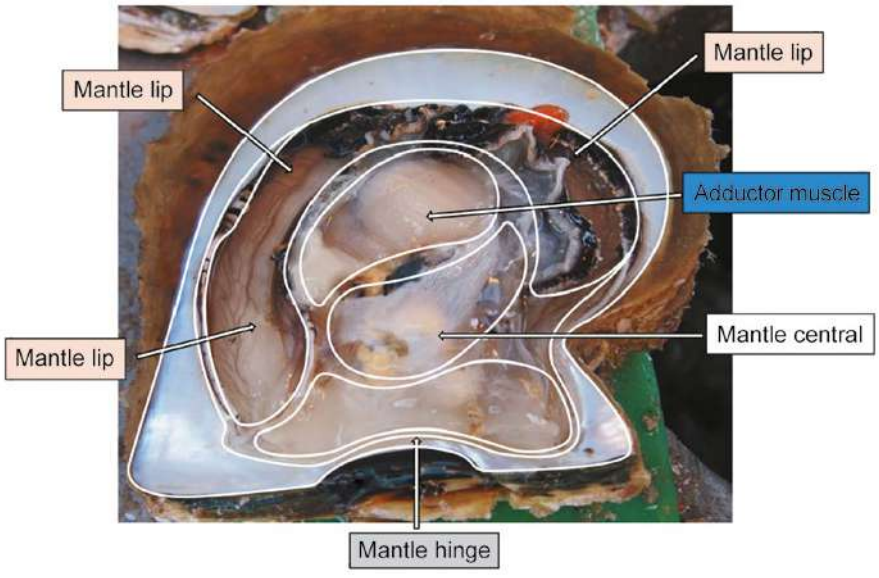

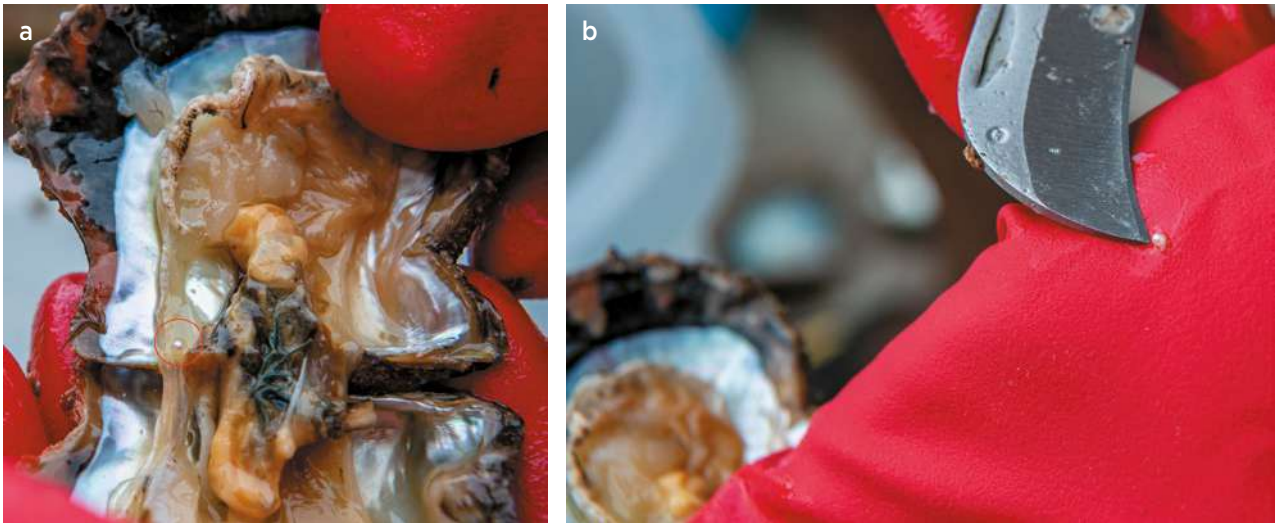

Figure 36: (**a**) Opening this *P. radiata* mollusc revealed a pearl in the mantle lip (lower left). (**b**) The extracted light cream-coloured pearl is oval-shaped and measures 1.60 × 1.49 mm. Photos by H. Abdulla, © DANAT.

Figure 37: Three light cream-coloured pearls of various shapes were found within the same *P. radiata* mollusc. The largest of the three pearls (near the tip of the knife) is 2.60 mm in diameter. Photo by H. Abdulla, © DANAT.

All of the pearls recovered by the team are examined by standard gemmological techniques to document their colour, shape, size, weight, surface features, etc. In addition, all samples are studied with X-ray microradiography and X-ray computed microtomography to look for potential links between their position in the animal and their internal structures. UV-Vis-NIR, Raman, photoluminescence and FTIR spectra are gathered on all samples, and chemical analysis is performed using EDXRF and LA-ICP-MS techniques. All these data are valuable to build a solid database for the accurate determination of a pearl's host mollusc and any treatments. In addition, incorporating the water sampling data will help us better understand the possible link between ocean conditions and chemical characteristics of natural pearls.

After collecting samples from the areas off Bahrain, our goal is to expand the project into the surrounding Arabian Gulf and elsewhere in other important natural pearl-fishing areas worldwide where it is still legal to collect the molluscs.

Ali Alatawi (ali.alatawi@danat.bh),
Dr Stefanos Karampelas, Hasan Abdulla,
Hisham Alsheari, Mohamed Abdulla
and Zakareya Taresh
Bahrain Institute for Pearls & Gemstones (DANAT)
Manama, Bahrain

A Remarkably Large Natural Pearl from *Pinctada radiata*

DANAT recently received a light cream-coloured, undrilled pearl weighing 18.07 ct (13.82 × 13.71 mm) of near-round shape. Viewed with the microscope, it showed nacreous structures. Under long-wave UV radiation (365 nm, 6 watt) the pearl fluoresced light yellow, while in short-wave UV (254 nm, 3 watt) it luminesced light yellowish green-blue. The pearl was inert to X-rays. EDXRF analysis revealed 747 ppmw Sr, with Mn below the detection limit—characteristic of nacreous saltwater pearls (Karampelas & Kiefert 2012).

Digital X-microradiographs of the pearl in three orientations, taken perpendicular to one another, showed only two growth lines (Figure 38). Some additional features were visible in various directions, such as small

Figure 38: This remarkably large (18.07 ct; 13.82 × 13.71 mm), near-round natural pearl from *P. radiata* was recently examined at DANAT. Photo by Ghadeer Abdali, © DANAT.

(i.e. <3 mm) roundish features that looked like seed pearls near the edge of the sample (Figure 39, centre and right). These, as well as the few growth lines, raised suspicions of an atypical beaded cultured pearl, with a natural pearl used as a bead.

DANAT recently upgraded its X-ray computed microtomography (micro-CT) detector and software, which significantly increases the resolution. The resulting micro-CT images of the present sample clearly revealed structures characteristic of natural saltwater pearls (Figure 40). The outer and inner growth lines are clearly visible and followed by natural concentric growth lines toward the centre. Also, natural structures could be observed inside a seed pearl in one of the images (see Figure 40, right). Thus, it became clear that the sample was a natural saltwater pearl.

Chemical analysis using LA-ICP-MS was performed on three spots, yielding an average of 4,695 ppmw ^{23}Na, 326 ppmw ^{24}Mg, 0.70 ppmw ^{55}Mn, 890 ppmw ^{88}Sr and 0.42 ppmw ^{137}Ba. These results are consistent with those previously published for natural pearls from *Pinctada radiata* fished off Bahrain (Karampelas *et al.* 2019b). Raman spectroscopy of the pearl using 514 nm laser excitation showed—apart from the bands characteristic of aragonite vibrations (at about 1086 and 703 cm^{-1})—two additional faint bands (at about 1532 and 1133 cm^{-1}) linked to vibrations of polyenic pigment; natural and cultured products from *P. radiata* and *P. fucata* are the only nacreous saltwater pearls that present such bands

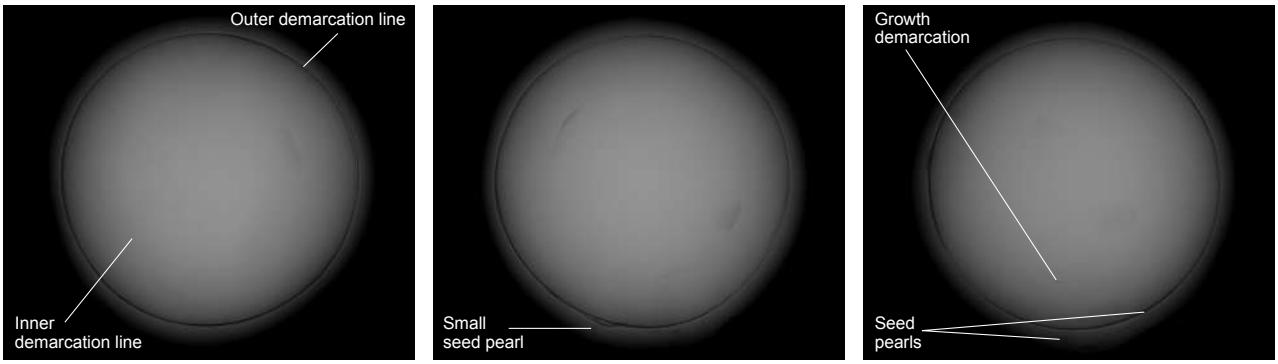

Figure 39: Digital X-microradiographs show the pearl in Figure 38 from three different directions. The contrast was adjusted to reveal features that the authors consider most informative. Depending on the contrast used, the images show some subtle features, although not enough to conclude whether this pearl is natural or cultured.

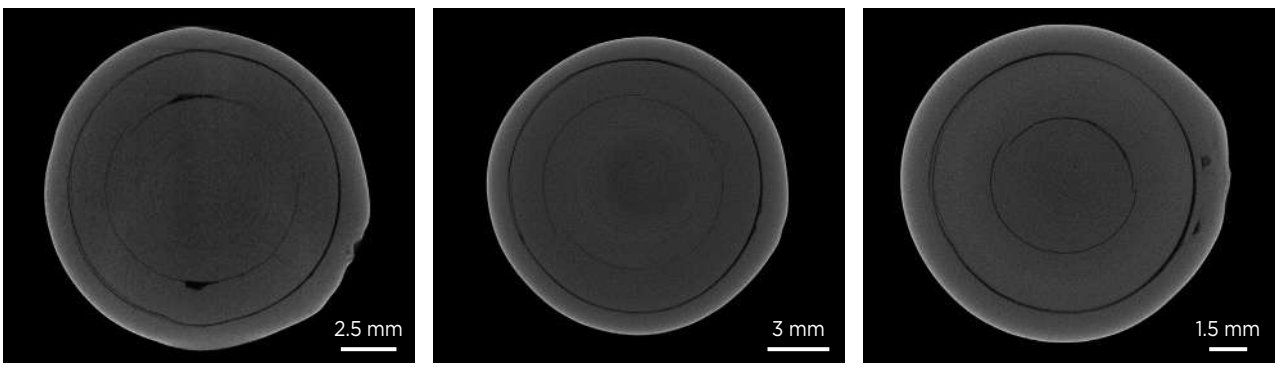

Figure 40: Two-dimensional slices of the micro-CT model of the studied pearl are shown here in three directions. These high-resolution images show natural concentric growth lines near the pearl's centre, as well as natural structures within a seed pearl near the edge of the sample (see right-hand image).

(Karampelas *et al.* 2019a). Thus, all the results are consistent with a natural pearl from *P. radiata*. However, this specimen is remarkably large, as natural pearls from *P. radiata* rarely exceed 8 mm diameter and, very rarely, 10 mm. Therefore, this near-round natural pearl with a diameter of >13.5 mm is an extreme rarity.

The client was a diver who indicated finding this sample himself in waters north of Bahrain. Bahrain is considered one of the most important sources of natural pearls, both in ancient and present times, and strict laws prohibit the trade (import and sale) of cultured pearls there. The government is currently encouraging a revival of the natural pearl fishing heritage by enacting regulations and encouraging people to pursue this profession. As a result, many young people have started pearl fishing during the last couple years.

Acknowledgement: The authors extend their appreciation to Sanad Bin Abdullah Bin Jafan, the diver who found and possesses this remarkable natural pearl, for allowing us to share our findings.

Ali Alatawi, Dr Stefanos Karampelas, Fatema Almahmood, Fatema Albedal and Hisham Alsheari
Bahrain Institute for Pearls & Gemstones (DANAT)
Manama, Bahrain

References

Karampelas, S. & Kiefert, L. 2012. Gemstones and minerals. *In:* Edwards, H.G.M. and Vandenabeele, P. (eds) *Analytical Archaeometry: Selected Topics*, Royal Society of Chemistry, London, 291–317, https://doi.org/10.1039/9781849732741-00291.

Karampelas, S., Fritsch, E., Makhlooq, F., Mohamed, F. & Al-Alawi, A. 2019a. Raman spectroscopy of natural and cultured pearls and pearl producing mollusc shells. *Journal of Raman Spectroscopy* (9 pp.), http://doi.org/10.1002/jrs.5670.

Karampelas, S., Mohamed, F., Abdulla, H., Almahmood, F., Flamarzi, L., Sangsawong, S. & Alalawi, A. 2019b. Chemical characteristics of freshwater and saltwater natural and cultured pearls from different bivalves. *Minerals*, **9**(6), article 357 (20 pp.), http://doi.org/10.3390/min9060357.

Double Grafting in Peanut-Shaped Ming Cultured Pearls

Improved grafting techniques used for Chinese freshwater cultured pearls (FWCPs) during the past few decades (e.g. Scarratt *et al.* 2000; Akamatsu *et al.* 2001; Fiske & Shepherd 2007) have resulted in the production of numerous varieties, including high-quality and large-size round cultured pearls (Hänni 2011) similar to akoya and South Sea products. Observing the roundness and surface texture with the unaided eye can commonly discriminate whitish-coloured Chinese FWCPs from their saltwater counterparts.

The first beaded gonad-grown Chinese FWCPs, marketed under the names 'Ming' and 'Edison' (Laurs 2012), were reported by Hänni (2011) and are characterised by the presence of a drilled nucleus. The grafting technique consists of simultaneously introducing the bead and tissue graft into the gonad of the mussel. In the case of circled Ming cultured pearls, the drill hole is responsible for creating spot defects and circling, as recently reported by Gauthier *et al.* (2018).

Here, we report on a strand consisting of 18 peanut-shaped cultured pearls (Figure 41). Their colours and overtones are typically associated with Chinese FWCPs,

Figure 41: This necklace consists of beaded, gonad-grown baroque Chinese FWCPs. Each peanut-shaped cultured pearl (18.4–25.2 mm long) proved to contain two nuclei. Photo by S. Leblan.

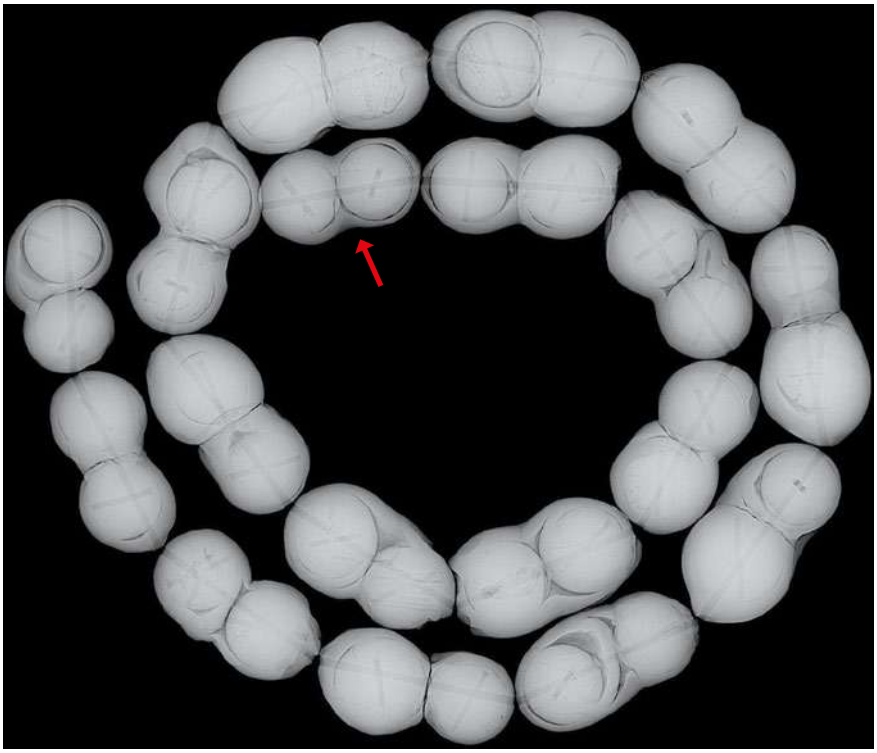

Figure 42: Microradiography of the necklace reveals the presence of two beads in each peanut-shaped cultured pearl, as suggested by external observations of their size, shape and surface texture. One of the FWCPs in the strand contains nuclei of the same size that are in contact without an intervening nacre layer (see arrow), in contrast to the other cultured pearls, which commonly contain nuclei of different sizes (with the smaller bead overgrown by a layer of nacre that appears to contact the adjacent larger bead).

especially gonad-grown products. The appearance, size (10.2–14.1 mm for each 'half') and surface features of the peanut-shaped cultured pearls suggest the presence of two nuclei. They differ from beadless and beaded mantle-grown peanut-shaped Chinese FWCPs, which frequently have a flat side due to their growth against the inner surface of the shell (e.g. Chow 2019: figure 12, left). In the case of beadless peanut-shaped FWCPs, their formation is due to the close proximity of two grafts that are responsible for the growth of the two initially separate cultured pearls, which eventually merge into one. Different colours and qualities are commonly observed in each half of the resulting peanut-shaped FWCPs.

In the strand examined for this report, the presence of nuclei was confirmed by microradiography (Figure 42). Moreover, all of the nuclei contained a randomly oriented drill hole in addition to the one created for each peanut-shaped FWCP to be threaded onto a necklace. This feature is typical of Ming FWCPs (Hänni 2011). In addition, as recently demonstrated by Chow (2019: figure 12), such cultured pearls exhibit a strong green fluorescence to X-rays, typical of FWCPs, and some of them may present a reddish orange reaction in whitish non-nacreous areas. The nuclei may also contain internal linear features that display random patterns (Figure 43), similar to ones illustrated by Chow (2019: figure 13).

In the beaded peanut-shaped FWCPs reported by Chow (2019), the size of the two nuclei were identical, and the absence of a nacre layer between them suggests to the present authors that they were simultaneously inserted into the mantle pocket in a way similar to that explained by Akamatsu *et al.* (2001). However, in the strand described here, the two nuclei in most of the peanut-shaped cultured pearls have different sizes, as seen in Figure 43. The larger nucleus seems to be in contact with a layer of nacre that has been deposited on the smaller nucleus. The difference in diameter between the two nuclei roughly and generally corresponds to the thickness of the nacre layer that was deposited on the smaller nucleus. This suggests that the insertion of each nucleus was probably done at two different times, according to the pearl farmer's understanding

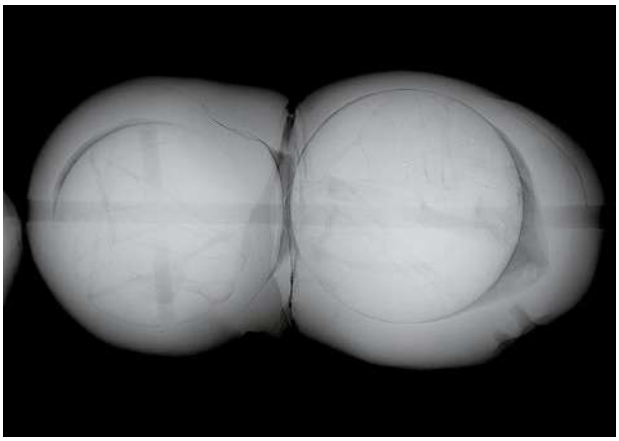

Figure 43: Microradiography of this peanut-shaped cultured pearl shows details that reveal characteristics of the two nuclei and the growth of the nacre layers.

of the growth rate of the nacre layer. By contrast, the nuclei within a FWCP on one end of the necklace (see arrow in Figure 42) seem to have the same size and are in contact without a nacre layer. Those nuclei were probably inserted into the gonad at the same time, as was done for the beaded mantle-grown peanut-shaped Chinese FWCPs described by Chow (2019).

As with gonad-grown cultured pearls in saltwater molluscs, only one Ming FWCP is, in principle, cultivated in the gonad of each mussel. Peanut-shaped cultured pearls are probably an unwanted result of double grafting, and they constitute proof that pearl farmers are tempted to insert more than one nucleus into a gonad, compared to the tens of beads commonly inserted into the mantle of such mussels. The insertion of more than one bead has also been encountered by author TNB in some saltwater cultured pearls (e.g. akoya from Vietnam).

Thanh Nhan Bui (tnhan93@gmail.com)
Université catholique de Louvain
Louvain-la-Neuve, Belgium

Sophie Leblan and Aurélien Delaunay
Laboratoire Français de Gemmologie
Paris, France

References

Akamatsu, S., Zansheng, L.T., Moses, T.M. & Scarratt, K. 2001. The current status of Chinese freshwater cultured pearls. *Gems & Gemology*, **37**(2), 96–113, http://doi.org/10.5741/gems.37.2.96.

Chow, B.H.Y. 2019. Lab Notes: Freshwater bead-cultured pearls with multiple features of interest. *Gems & Gemology*, **55**(1), 94–96.

Fiske, D. & Shepherd, J. 2007. Continuity and change in Chinese freshwater pearl culture. *Gems & Gemology*, **43**(2), 138–145, http://doi.org/10.5741/gems.43.2.138.

Gauthier, J.-P., Fereire, J. & Bui, T.N. 2018. An explanation of a specific type of circling as observed on Ming cultured pearls. *Journal of Gemmology*, **36**(3), 240–250, http://doi.org/10.15506/JoG.2018.36.3.240.

Hänni, H.A. 2011. Ming pearls: A new type of cultured pearl from China. *Journal of the Gemmological Association of Hong Kong*, **32**, 23–25.

Laurs, B.M. 2012. Gem News International: Tucson 2012. *Gems & Gemology*, **48**(1), 54–55.

Scarratt, K., Moses, T.M. & Akamatsu, S. 2000. Characteristics of nuclei in Chinese freshwater cultured pearls. *Gems & Gemology*, **36**(2), 98–109, http://doi.org/10.5741/gems.36.2.98.

TREATMENTS

Dyed Banded Agate from Madagascar

Banded agates from Madagascar are popular on various Internet websites and are commonly represented as 'natural polished' material. They are typically sold for relatively inexpensive prices by dealers based in China. The pieces show banding in various colours such as black, brown, orange, white, etc.

One of the authors (MP) recently purchased one such specimen so he could investigate the cause of its colouration (Figure 44). Slicing of this sample revealed a banded white interior (Figure 45), therefore proving that it had been dyed. The dye penetrated only a short distance into the stone, although some of the more translucent layers of the agate had deeper dye penetration. The banding in this sample only conformed to a portion of its overall external morphology, suggesting that it had previously been broken, had been formed into an attractive shape and then was polished before being dyed.

Some of the stones offered online contain concentric 'eyes' that somewhat resemble those seen in natural orbicular jasper found on Madagascar's north-west coast (cf. Johnson *et al.* 2000). However, that material typically shows an orbicular pattern rather than banded texture, and it also typically has different colouration (e.g. green, blue,

Figure 44: This 'natural' agate was recently purchased from an online auction website to investigate the cause of its colour. It measures 70 × 43 × 33 mm and weighs 128 g. Photo by M. Pantò.

Figure 45: Slicing the specimen in Figure 44 revealed that it consists of dyed white-banded agate. The dye is mostly restricted to a thin layer near the surface. Photo by M. Pantò.

pink and white), as well as areas of fine-grained quartz crystals in the interstices between the jasper orbicules.

White-banded agate from Madagascar that could be used as the starting material for the dyed agates was recently documented by Goldbaum *et al.* (2019), who proposed that the complex forms of the banding were caused by secondary deformation by external forces acting upon the silica gel before it crystallised into agate.

Brendan M. Laurs FGA

Mauro Pantò
The Beauty in the Rocks, Sassari, Italy

References

Goldbaum, J., Howard, C. & Rabinovitch, A. 2019. Spatial chirp of agate bands. *Minerals*, **9**(10), article 634 (9 pp.), http://doi.org/10.3390/min9100634.

Johnson, M.L., Koivula, J.I., McClure, S.F. & DeGhionno, D. (eds) 2000. Gem News: Orbicular jasper from Madagascar. *Gems & Gemology*, **36**(1), 69.

Figure 1: The 11.62 ct Roman sapphire intaglio examined for this study is engraved on the back side with a hippocamp. Photo by E. Butini, IGN.

Gemmological Analysis of a Roman Sapphire Intaglio and Its Possible Origin

Michael S. Krzemnicki, Flavio Butini, Enrico Butini and Ernesto De Carolis

ABSTRACT: The gemmological analysis of a Roman intaglio engraved with a hippocamp (winged 'sea-horse') reveals that it was carved from a sapphire of basaltic origin. Its bluish grey appearance is due to Rayleigh scattering by sub-microscopic inclusions and is not related to an intervalence charge transfer process. In light of historically documented extensive trade relations between ancient Rome and Ethiopia (the kingdom of Aksum), we hypothesise that the recently documented basalt-related sapphire deposits in northern Ethiopia are a possible source of raw material for this Roman intaglio (as well as other basaltic sapphires used in Roman times), in addition to previously held views that ancient sapphires originate from deposits in Sri Lanka, France and perhaps South East Asia. This rare opportunity to characterise in detail one of the very few engraved sapphires from the Roman period permits a better understanding of gem materials used in classical antiquity.

The Journal of Gemmology, **36**(8), 2019, pp. 710–724, http://doi.org/10.15506/JoG.2019.36.8.710

Antique jewels and gems have long fascinated scholars and the public alike, as they offer an intimate insight into human cultural history, unveiling aspects such as adornment, beliefs, social and political status, artistic style, fashion and craftsmanship in ancient cultures (Pinckernelle 2007; Spier 2007; Entwistle & Adams 2011; Papagiannaki 2013). This fascination is further based on their relevance to modern life in design and significance (Unger & Van Leeuwen 2017). Antique jewels are also valuable to archaeological science because they can unveil ancient trade routes (e.g. the Maritime and Central Asian Silk Routes). Gems and jewels were traded extensively in ancient times together with other goods of value over long distances from their (remote) sources to historical marketplaces and political centres (Begley & Puma 1991; Borell *et al.* 2014; Borell 2017; Galli 2017; Sidebotham 2019).

Jewellery and gems of Roman age have been abundantly studied, but only in a few cases has it been possible to carry out a thorough gemmological analysis of such historical items (Giuliani *et al.* 2000; Calligaro 2005; Lüle-Whipp 2006; Entwistle & Adams 2011; Gast *et al.* 2011; Thoresen & Schmetzer 2013; Schmetzer *et al.* 2017; Thoresen 2017b; Gilg *et al.* 2018). This is mainly due to the fact that they are considered cultural heritage and often are not accessible for testing with laboratory analytical methods.

In this article we describe a glyptic masterpiece: a Roman sapphire intaglio (Figure 1) that was found in 1986 in Pompeii. In late 2017, the Museo Archeologico Nazionale di Napoli loaned the engraved sapphire to the authors for detailed examinations at the Istituto Gemmologico Nazionale (IGN; Rome, Italy) and the Swiss Gemmological Institute SSEF (Basel, Switzerland). This article provides a description of the glyptic artwork and gemmological characteristics of the specimen, while also considering possible origins for the sapphire raw material and presenting a new hypothesis that could explain its provenance, as well as that of other historical sapphires of Roman age (e.g. Butini *et al.* 2018).

HISTORICAL BACKGROUND OF POMPEII

Pompeii was an urban settlement with ancient origins (Figure 2), located on the southern slopes of Mount Vesuvius adjacent to the present city of Pompei in southern Italy. Due to its climate and location, Pompeii developed into an important commercial centre, first attracting the Greeks and Etruscans (7th–5th centuries BCE), and later the Samnites (4th century BCE). In the 3rd century BCE, although never conquered by military force, Pompeii became part of the economic

Figure 2: This drone photo of the excavated Roman city of Pompeii includes Mount Vesuvius (on the skyline), which caused the sudden burial of the area during a major volcanic eruption in 79 CE. Photo courtesy of Wikimedia Commons.

and administrative circuit of the Roman Republic, and in 80 BCE it was transformed into a colony under Roman law (Cooley & Cooley 2013 and references therein).

In 62 CE, Pompeii suffered a devastating earthquake, which left it badly damaged and severely weakened economically. The Emperors Nero and Vespasian promoted the reconstruction of the city, which was quickly restored with luxurious governmental and religious buildings and private residences. However, the city had not yet been completely rebuilt when, between August and November 79 CE, an explosive eruption of Mount Vesuvius buried Pompeii under about 6 m of pumice and ash. Approximately 1,500 inhabitants died (the city's population was estimated between 6,000 and 20,000 people), among them the famous naturalist Pliny the Elder—author of the encyclopaedic *Historia Naturalis*, still today a fundamental reference for the ancient use and provenance of gems. Pompeii was not rebuilt again and by 120 CE vegetation began to cover the area that it once occupied until it disappeared completely (De Carolis & Patricelli 2003; Cooley & Cooley 2013).

In 1748, more than 1,600 years later, the first archaeological excavations of Pompeii began at the behest of the Bourbon Dynasty (of Naples, Italy) following the discovery of Herculaneum (another inhabited centre destroyed by the same volcanic eruption). From the beginning of the 19th century the excavations went through various phases until the unification of Italy in 1861. Pompeii was almost entirely unearthed, although some areas later suffered considerable damage due to bombing during World War II. In 1997 the archaeological area was declared a UNESCO World Heritage Site, and in 2012 the Great Pompeii Project was established with the goal to restore and secure the site.

During the excavation of Pompeii a large number of jewels were discovered, consisting of approximately 800 pieces of jewellery and 94 gemstones. Eleven of these were found in 1986 in two wooden boxes at the House of Gemmarius in the south-eastern part of Pompeii (Figure 3), close to the Porta Nocera (Sodo 1988, 1992; Pannuti 1994; D'Ambrosio & De Carolis 1997). The gems in these wooden boxes included the sapphire intaglio described here (Museo Archeologico Nazionale di Napoli, Inventario P 39597; see D'Ambrosio & De Carolis 1997), along with an object identified as a 'stone holder' work tool. In this sector of the ancient city the houses were modest in size, as they were intended for middle-class members of Pompeiian society. The architecture of these buildings reconciled housing with commercial activities, so several workshops were located in this area.

The House of Gemmarius is thought to have been the private home and workshop of a gem cutter and jeweller (D'Ambrosio & De Carolis 1997). This hypothesis is supported by the Latin inscription *Prisco coelator campano gemmario feliciter* ('Prisco from Campania, successful gemstone engraver'; see Toynbee 1951) found on a wall near the house, which supposedly represents an antique billboard. Still, as there is no further written evidence, we cannot fully exclude the possibility that the two boxes just stored the gems of an unknown private owner who lived in the ancient city of Pompeii.

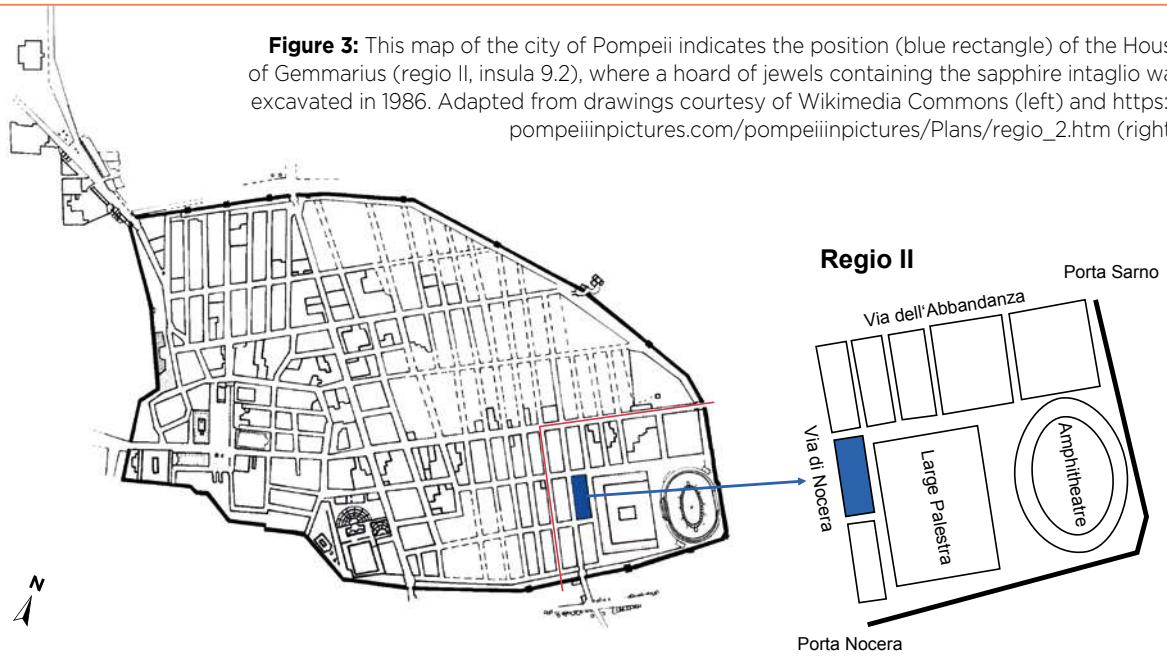

Figure 3: This map of the city of Pompeii indicates the position (blue rectangle) of the House of Gemmarius (regio II, insula 9.2), where a hoard of jewels containing the sapphire intaglio was excavated in 1986. Adapted from drawings courtesy of Wikimedia Commons (left) and https://pompeiiinpictures.com/pompeiiinpictures/Plans/regio_2.htm (right).

MATERIALS AND METHODS

The Roman sapphire intaglio is a flat, oval cabochon measuring 21.78 × 12.27 × 4.31 mm and weighing 11.62 ct.

The intaglio was examined with standard gemmological instruments such as a refractometer (spot method) and a hydrostatic balance (Mettler Toledo), and was also observed under long- and short-wave UV radiation. Detailed microscopic investigation was performed with an Eickhorst Gemmaster trinocular microscope equipped with a Nikon F7000 digital camera.

The intaglio was chemically analysed by energy-dispersive X-ray fluorescence (EDXRF) spectroscopy using a Thermo Scientific ARL Quant'X instrument. Also analysed for comparison were four other Roman sapphire cabochons (one light blue and three dark blue) from the collection of author EB. Raman microspectroscopy of inclusions in the intaglio was performed with a Renishaw inVia unit equipped with an argon-ion laser (514.5 nm). Fourier-transform infrared (FTIR) spectroscopy was accomplished with a Nicolet iS50 instrument. Polarised ultraviolet-visible-near infrared (UV-Vis-NIR) absorption spectra were collected for the o-ray (parallel to the optic axis) in the range of 280–800 nm using a Varian Cary 500 spectrophotometer in transmission mode.

RESULTS AND DISCUSSION

Glyptic and Carving of the Intaglio

The Roman intaglio is a unique piece of cultural heritage, not only because it consists of sapphire—a gem known to the Romans but only rarely used in their jewellery (Spier 2012; Thoresen 2017a, b)—but also because it combines beauty and craftsmanship with a fully documented archaeological provenance. This is very much in contrast to other ancient sapphire intaglios and carvings described in the literature, most of which are from historical gem collections and thus have a more debatable and obscure geographical/historical provenance. Examples of such specimens include the sapphire seal of Alaric II, king of the Visigoths, in the Kunsthistorisches Museum Wien (see Kornbluth 2008; Thoresen 2017b); the Cambridge sapphire cameo depicting Aphrodite (Guy Ladrière Collection; see Ogden 1982; Thoresen 2017b); and other engraved sapphires of Roman age described previously (Spier 2007; Content 2016; Thoresen 2017b).

The sapphire intaglio examined here was masterfully carved (Figure 4) on the back surface. As the sapphire is nearly free of inclusions, the carving is very discernible through the stone, perfectly revealing the fine details of the engraving and craftsmanship of the artist (again, see

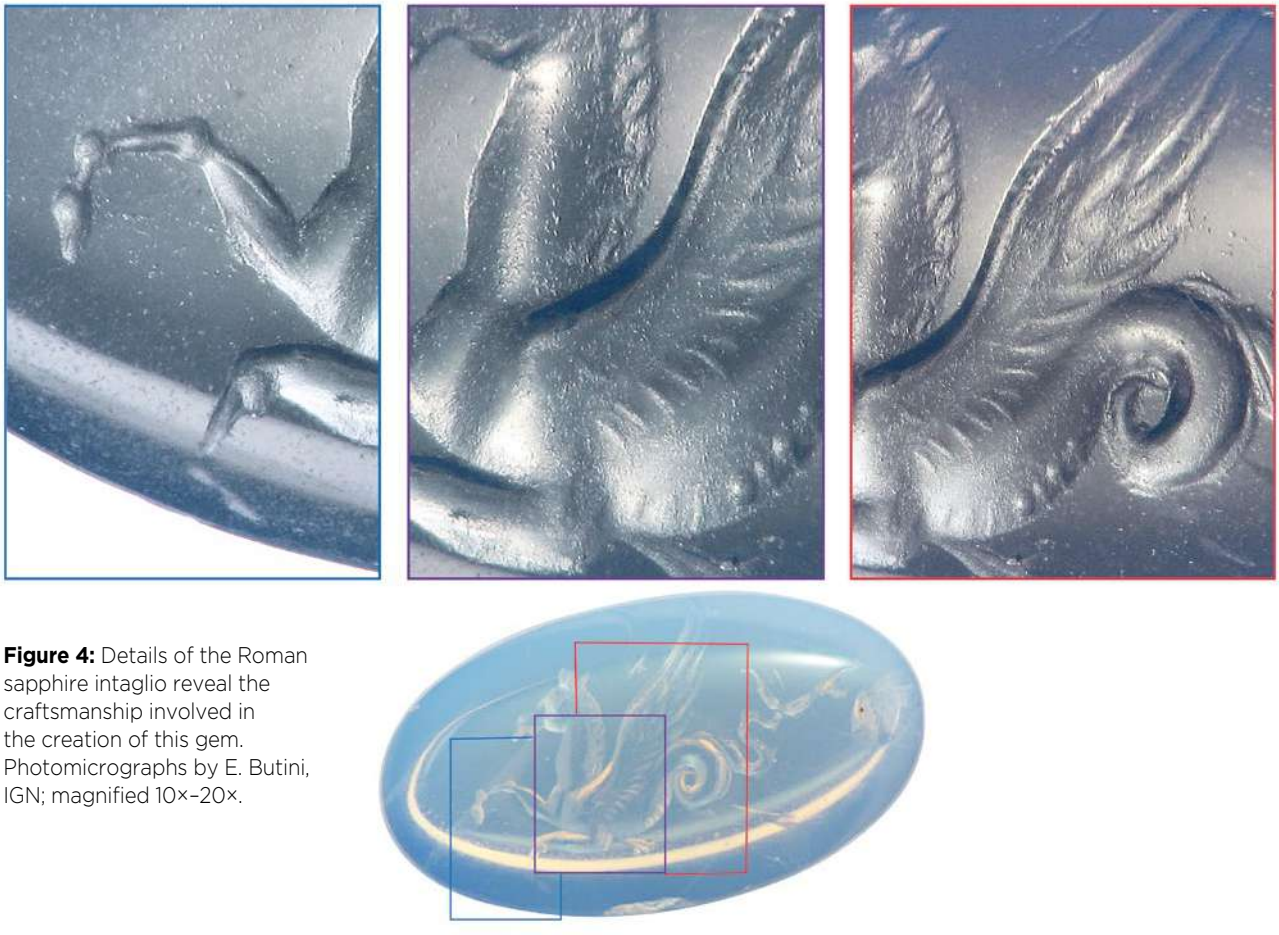

Figure 4: Details of the Roman sapphire intaglio reveal the craftsmanship involved in the creation of this gem. Photomicrographs by E. Butini, IGN; magnified 10×–20×.

Figure 5: This iron tool with a diamond tip for engraving gems was assembled by the authors based on descriptions in the literature. Photo by E. Butini, IGN.

Figure 1). The carving depicts a mythological creature known as a hippocamp—*hippokampoi* or ἱππόκαμπος in Greek, derived from ἵππος (horse) and κάμπος (sea monster)—a winged 'sea-horse' that has the upper body of a horse and the lower body consisting of the tail of a fish. Since ancient times, this motif has been one of the most common emblems of the marine world. Specifically, it appears as one of the symbols of Poseidon/Neptune, and is seen pulling his chariot or being ridden by him (Smith 1849; Charbonneau-Lassey 1994). In addition, the hippocamp is frequently depicted together with Tritons (sons of Poseidon) or Nereids (sea nymphs in Greek mythology), and because of their association with the ocean they are often engraved in 'sea-coloured' gem materials, notably aquamarine (L. Thoresen, pers. comm. 2019; see also Zwierlein-Diehl 2007 and specimen 732 in the Marlborough Gem Collection described in Boardman *et al.* 2009). Hippocamps may be depicted on Hellenistic, Roman and more recent engraved gems (see Richter 1920; Greifenhagen 1970; Zwierlein-Diehl 1991; Spier 1992; Pannuti 1994), as well as on coins (Calciati 1986), sarcophagi (Magni 2009), frescoes (Iacopi 1943) and mosaics in Roman bathing facilities (Di Nunno 2015).

Our study reveals that the hippocamp engraving on this sapphire was carried out with great detail and accuracy (again, see Figure 4). Presumably, this was done using a lathe with pivots and rotating hand-drills of various sizes that were impregnated with oils, grease and abrasives. The engraving may have also been accomplished with the aid of iron tools containing diamond tips (e.g. Figure 5). These tools were well known in Roman times (Maaskant-Kleibrink 1978, 1989; Ogden 1982, 2018; Devoto 1985; Rosenfeld *et al.* 2003), and were used for engravings in stone and gems of high hardness (corundum is 9 on the Mohs scale).

The authors were especially intrigued by small carving traces close to the hippocamp's caudal fin (see arrows in Figure 6) that were visible with the microscope. Although possibly accidental notches caused by a rotating disk, the authors favour another interpretation: at least some of them were made intentionally by the artist to express dynamic movement of the hippocamp, similar to what we recognise today as kinetic markers to express movement and speed in cartoons and comics. The authors incline to this latter hypothesis after having examined numerous other ancient engraved gems that appear to show similar kinetic markers. For example, Figure 7a is a glass 'paste' carving of Roman age reportedly originating from the Middle East (residing in a private collection) that depicts a mythological creature which exhibits five small notches near the end of its tail. These notches are very similar to those of the present sapphire intaglio and, when interpreted as kinetic markers, create a sensation of motion. An even more supportive example is shown by an early Roman green Cr-bearing chalcedony (from author EB's collection) that portrays a man operating a pedal lathe used to produce vases (Figure 7b). Several kinetic markers clearly represent his foot moving up and down on the pedal.

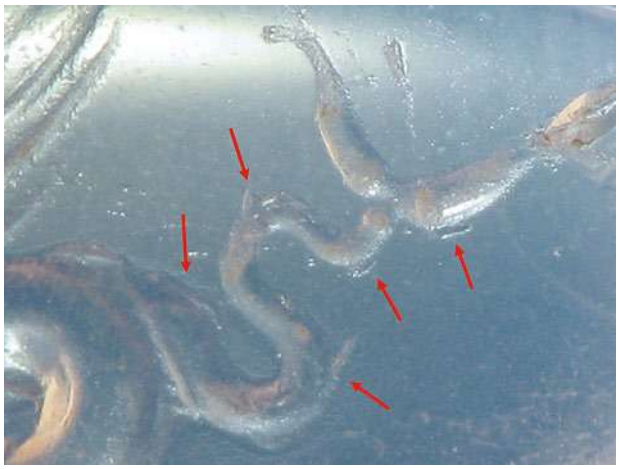

Figure 6: Small notches along the tail of the hippocamp might be kinetic markers added to suggest movement. Photomicrograph by F. Butini, IGN; magnified 15×.

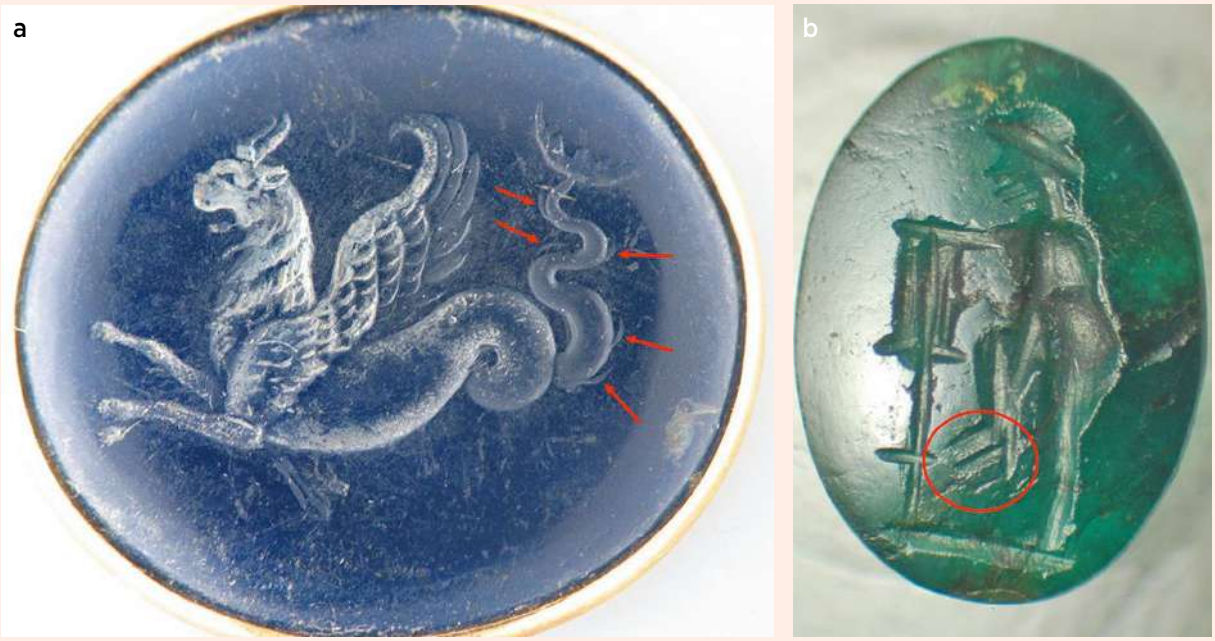

Figure 7: (**a**) This Middle Eastern glass paste intaglio (dating from around the time of the Roman Empire) measures approximately 35.0 × 25.0 mm and depicts a mythological creature. The arrows point to kinetic markers similar to those inferred in Figure 6. (**b**) An early-Roman intaglio of chromium-bearing chalcedony (8.42 × 6.14 mm) depicts a man operating a pedal lathe. Kinetic markers (see red circle) represent the up-and-down movement of his foot. Photos by F. Butini, IGN.

Gemmological Properties

The sapphire intaglio is translucent and appears light bluish grey in most lighting situations, but it is greyish brown when viewed in transmitted light (Figure 8). The bluish grey appearance is the result of light scattering by dispersed sub-microscopic inclusions within the gem, as discussed in more detail below.

The sapphire had an average RI of about 1.77 (spot method) and an SG value of 4.0, both characteristic for corundum. It was inert to long- and short-wave UV radiation. Viewed with the microscope, the sapphire showed a slightly zoned 'velvety' turbidity due to fine sub-microscopic particles (Figure 9). In addition, the specimen contained a few partially healed fissures, characterised by dispersed and randomly structured fluid inclusions. Some of the larger fluid inclusions had expansion discs consisting of a mirror-like internal plane surrounded by a rather thick and structured whitish rim of fluid droplets (Figure 10). Interestingly, these expansion discs locally contained tiny prisms in radial arrangements (see arrow in Figure 10). Based on their visual appearance, they are assumed to be an Al-hydroxide (e.g. diaspore), typical of late-stage precipitates in fissures, partially healed fractures and fluid inclusions

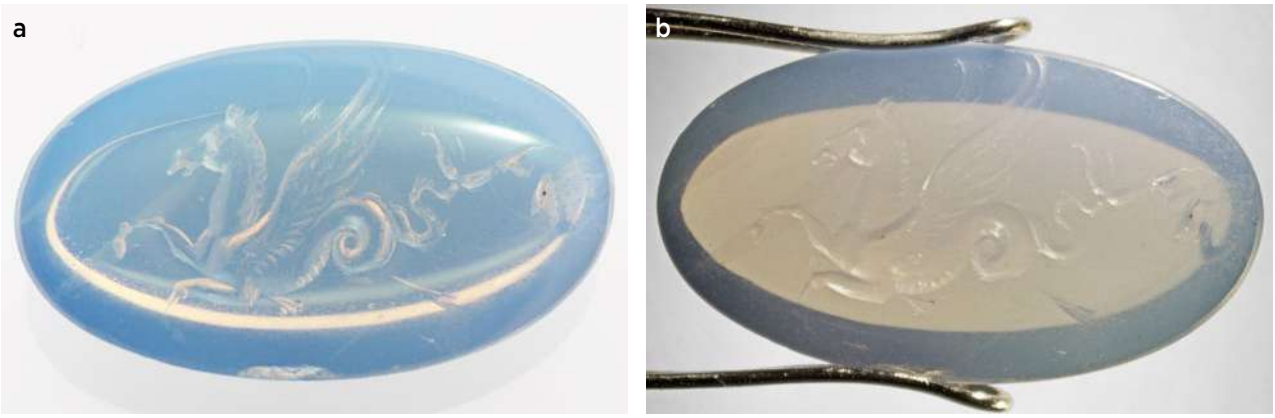

Figure 8: A comparison of the Roman intaglio in (**a**) reflected light and (**b**) transmitted light reveals the different colour appearances of the sapphire (bluish grey and greyish brown, respectively). Photos by M. S. Krzemnicki, SSEF.

Figure 9: Zoned turbidity is present throughout the Roman sapphire intaglio. Photomicrograph by M. S. Krzemnicki, SSEF; image width 10 mm.

Figure 10: Magnification reveals twin planes and a healing fissure with dotted fluid inclusions in the Roman sapphire intaglio. The larger fluid inclusions show structured expansion discs. The main expansion disc contains tiny, radially arranged needles (see arrow) interpreted as Al-hydroxide precipitates. Photomicrograph by M. S. Krzemnicki, SSEF; image width 3 mm.

Figure 11: Small idiomorphic plagioclase (albite) inclusions, identified by Raman microspectroscopy, are also present in the sapphire intaglio. Photomicrograph by M. S. Krzemnicki, SSEF; image width 2 mm.

in unheated sapphires from various locations (e.g. Smith 1995; Hughes 1997). In addition, we found a few small twin planes (again, see Figure 10), as well as colourless idiomorphic inclusions (Figure 11) that were identified by Raman microspectroscopy as Na-rich plagioclase (albite).

The observed microscopic features are consistent with those described in sapphires associated with alkali basalt (Guo *et al.* 1992; Smith *et al.* 1995; Krzemnicki *et al.* 1996; Gübelin & Koivula 2008; Pardieu *et al.* 2014). The specific nature of the mirror-like expansion discs with structured white rims indicates that a natural heating of the sapphire occurred (i.e. associated with its entrainment in alkali basalt). No indications of heat treatment were found in this sapphire, although heating of gemstones was known and practised in antiquity, as documented in ancient literature such as the *Papyrus Graecus Holmiensis* codex (also known as 'The Stockholm Papyrus'; Anonymous ca. 300 CE) that was compiled in the 3rd century CE (see also Caley 1927; Francis 1986; Hackens & Moucharte 1989; Sax 1996), and in Roman times by Pliny the Elder (23–79 CE) who mentioned gem treatments in a more general context in his *Historia Naturalis* (see, e.g., Hughes 1997, p. 103).

Chemical Composition and Spectroscopy

The trace-element analysis by EDXRF revealed that this sapphire of bluish grey appearance contained a relatively high amount of Fe (0.41 wt.% Fe_2O_3), traces of Ti (0.03 wt.% TiO_2) and Ga (0.02 wt.% Ga_2O_3), and almost no Cr (at the detection limit). This composition fits well with basaltic sapphires when plotted according to their trace-element ratios (Figure 12; as proposed by Abduriyim & Kitawaki 2006 and Giuliani *et al.* 2014). Because this Roman sapphire intaglio is an archaeological artefact and considered part of the historical heritage of Italy, it was not possible to analyse its trace-element composition further by laser ablation inductively coupled plasma mass spectrometry (e.g. GemTOF; Wang *et al.* 2016), as this method would have been slightly destructive (leaving a laser ablation spot). We also used EDXRF to analyse four other Roman sapphires, and three of them were found to be of basaltic origin while only one was of metamorphic origin (most probably Sri Lanka; see Figure 12). The above-mentioned analytical limitation may explain why the data obtained by EDXRF on our samples mostly plots outside the indicated distribution fields for basaltic sapphires (which were defined using LA-ICP-MS data).

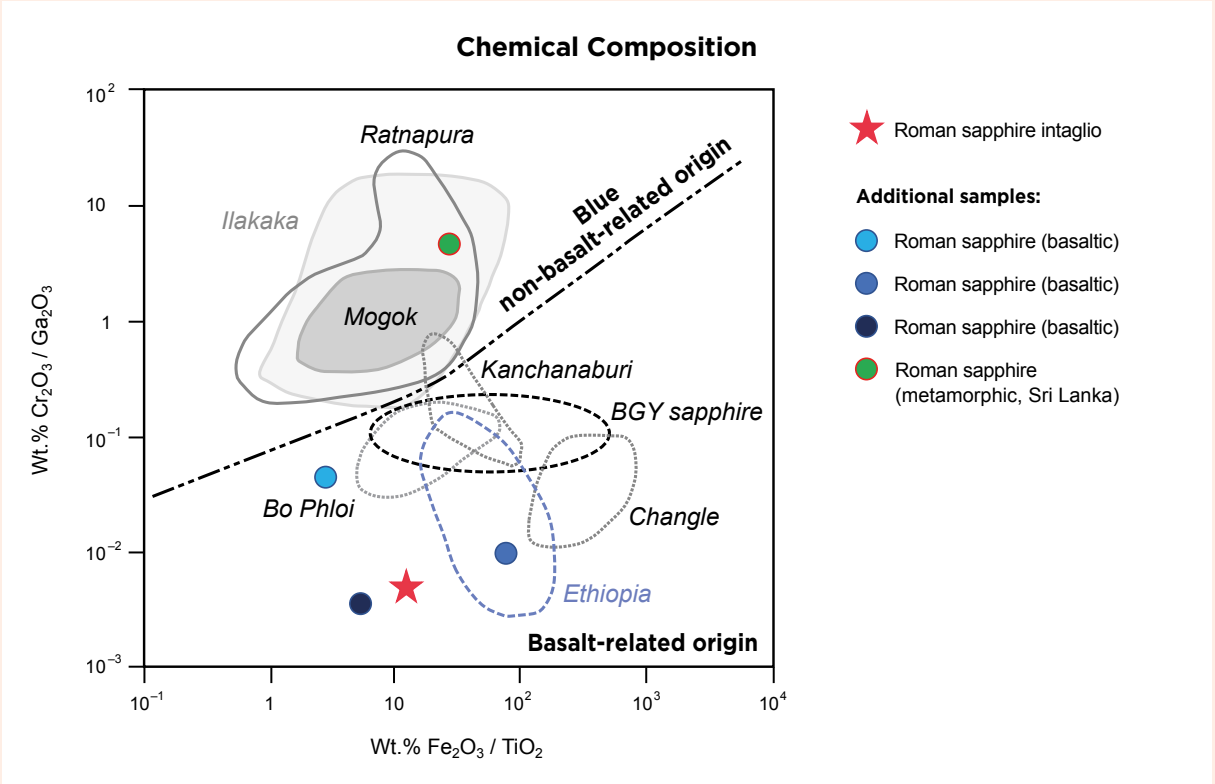

Figure 12: A trace-element ratio diagram reveals that the Roman sapphire intaglio is of basalt-related origin, similar to three other Roman sapphires. An additional Roman sample was found to be of metamorphic origin. The distribution field for Ethiopian sapphires is based on samples in the SSEF research collection. Diagram adapted from Abduriyim & Kitawaki (2006) and Giuliani *et al.* (2014).

FTIR spectroscopy of the sapphire intaglio revealed distinct hydroxide (OH^-) features, with a band at 3309 cm^{-1} dominating a series of lines at 3393, 3377, 3366, 3231 and 3183 cm^{-1} (Figure 13). Such a pattern has been attributed to intrinsic hydrous defects within the sapphire structure (Smith *et al.* 1995; Beran & Rossman 2006), and is commonly found in sapphires from basaltic deposits (unheated and heat treated) and also in metamorphic sapphires that have been heat treated. The features in the range of 2950–2800 cm^{-1} in Figure 13 are due to organic contamination (e.g. skin oils) and are not intrinsic to the sapphire.

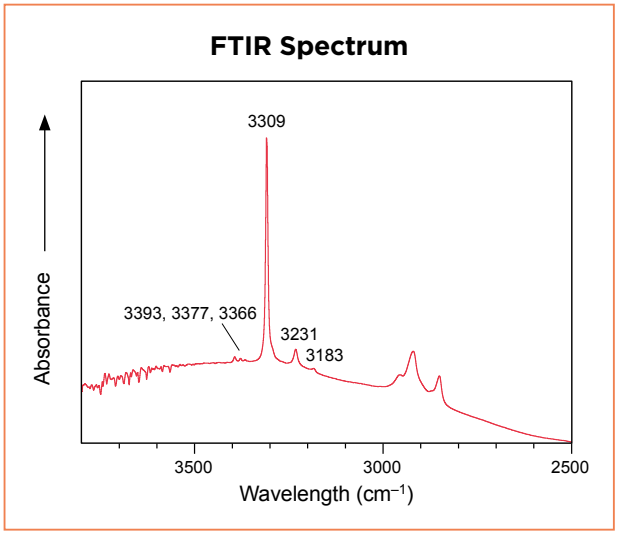

Figure 13: The FTIR spectrum of the Roman sapphire intaglio shows a characteristic pattern—a band at 3309 cm^{-1} accompanied by a series of small features—for the presence of hydroxide (OH^-) in sapphire.

UV-Vis-NIR spectroscopy of the intaglio obtained in transmission mode yielded an absorption curve related to the sapphire's greyish brown body colour (Figure 14). In detail, the spectrum was dominated by a steady increase in absorption from the near infrared towards the ultraviolet region, superposed only by small peaks related to Fe^{3+} at 376, 387 and 450 nm (Figure 14). The general absorption trend in combination with an absorption edge at about 340 nm is mainly due to the presence of numerous sub-microscopic particles that cause the slightly milky appearance of the stone.

The sapphire showed no absorption band centred at 560 nm related to Fe^{2+}–Ti^{4+} intervalence charge transfer (IVCT; Schmetzer & Bank 1981) nor at about 870 nm related to Fe^{2+}–Fe^{3+} IVCT (Ferguson & Fielding 1971;

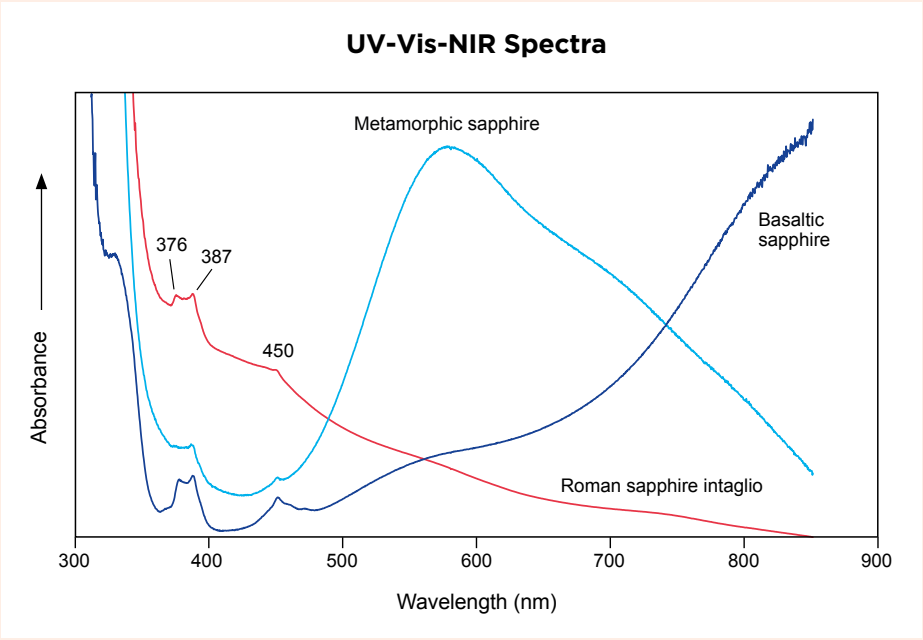

Figure 14: The polarised UV-Vis-NIR absorption spectrum of the Roman sapphire intaglio is very different from those of typical metamorphic and magmatic (basaltic) sapphires, which owe their blue colour to Fe^{2+}–Ti^{4+} and/or Fe^{2+}–Fe^{3+} intervalence charge transfer. The bluish grey appearance of the Roman sapphire is thus not related to absorption, but is the result of Rayleigh scattering by sub-microscopic inclusions. The turbidity caused by these inclusions induces a broad absorption band towards the UV region.

Schmetzer & Bank 1981). These two broad bands (either alone or in combination) are normally the main cause of blue colour in metamorphic and magmatic sapphires (see blue traces in Figure 14; Schmetzer & Bank 1981; Fritsch & Mercer 1993). Therefore, we conclude that the apparent bluish grey colour of this sapphire is not related to absorption but is only the result of Rayleigh scattering by the sub-microscopic particles within the sapphire. Similar scattering effects are well known in sapphires from both metamorphic and basaltic origins (Hänni 1990; Krzemnicki *et al.* 1996; Hughes 1997; Gübelin & Koivula 2008). In such sapphires, the scattering effect supports the blue colour that is mainly caused by IVCT absorption. By contrast, bluish colour caused mainly or only by Rayleigh scattering—as for the sapphire intaglio described here—is rather uncommon and has been described previously for basaltic sapphires from Nigeria (Pardieu *et al.* 2014). Nowadays, such stones are commonly heat treated to enhance their blue colour by creating Fe^{2+}–Fe^{3+} and Fe^{2+}–Ti^{4+} IVCT absorption bands.

POSSIBLE SAPPHIRE ORIGIN

The few sapphires found in jewellery from the Roman period can be divided into two groups: small, dark sapphires of basaltic origin (mostly lenticular beads) and paler sapphires presumably of Sri Lankan origin (Thoresen 2017a, b; J. Ogden, pers. comm. 2019). In the literature, most Roman sapphires have been attributed to Sri Lanka—called Taprobanê in Greek and Roman times—which has been known since antiquity for its gem wealth (see also the ancient text *Periplus Maris Erthraei*; Casson 1989). Stones from this origin are commonly described as being imported into the Roman Empire from the East along the Maritime Silk Route (Ogden 1982; Sevillano-López & Gonzalez 2011; Hughes 2017; Seland 2017). However, since Sri Lanka's secondary gem deposits contain only metamorphic sapphires (and no basaltic ones), it appears that there were other sapphire sources available to the Romans that provided basaltic sapphires for their jewels.

In considering a possible origin of the present intaglio—as well as other basalt-related Roman sapphires—a conclusive determination is presently not possible due to similarities in the characteristics of basaltic sapphires from various deposits. The inclusion features, trace-element concentrations, UV-Vis-NIR absorption and oxygen isotopic signatures of sapphires from alkali basalts are rather uniform, and this is very much in contrast to those from metamorphic deposits such as Ratnapura or Elahera in Sri Lanka, Mogok in Burma and Kashmir in India (Hänni 1994; Abduriyim & Kitawaki 2006; Giuliani *et al.* 2014; Wang *et al.* 2016), for which origin determination is more feasible.

Although sapphire deposits related to alkali basalts are known today from many localities (e.g. Cambodia, Laos, Vietnam, Ethiopia, Rwanda and Nigeria to name a few; see Giuliani *et al.* 2014 and references therein), it is not presently known which of these deposits were productive in the 1st millennium CE. One of the few historical basaltic sapphire deposits is located in the

Massif Central (Puy-en-Velay) in France. Although its initial discovery (first mentioned at the end of the 13th century) is generally assigned to medieval times (Forestier 1993; Gaillou 2003; Médard *et al*. 2012), it is possible that these sapphires had been found much earlier in alluvial sediments of this area. Furthermore, Ogden (2015) suggested the Massif Central as a possible source of dark blue sapphires (typical for iron-rich sapphires from alkali basalts and related volcanic rocks) in the ancient Roman period. However, to our knowledge there are no historical accounts of Roman sapphires from the Massif Central, so this option is possible but remains hypothetical.

Sapphires related to alkali basalts have been known since the 19th century from Scotland (e.g. from Arran, Mull, Ardnamurchan and Aberdeenshire; see Smith *et al*. 2008), but there is no evidence that these localities were known by the mid-1st century CE, when the Roman Empire just started its conquest of northern Britain. In addition, these Scottish sapphires are commonly described as being small and mostly not of gem quality.

Another source of basaltic sapphires in Roman times might be alkali basalt-related deposits in South East Asia, such as those in Thailand (Gunawardene & Sing Chawala 1984; Saeseaw *et al*. 2017), Cambodia (Jobbins & Berrangé 1981), southern Vietnam (Smith *et al*. 1995), Laos (Sutherland *et al*. 2002), or even China (Guo *et al*. 1992; Keller & Keller 1986; Wang 1988). We know that in Roman times the Mediterranean was connected to the Far East along the Maritime Silk Route (Borell *et al*. 2014; Dimucci 2015). This has led authors in the past to attribute antique sapphires of basaltic origin to such South East Asian deposits, although in our opinion the analytical data presented to support such claims (Butini *et al*. 2018) often do not stand up to critical scrutiny.

Most current sources of basaltic sapphire such as Australia (New South Wales and Queensland), Nigeria, Rwanda, northern Madagascar and Colombia, to name a few, can be excluded, as they were beyond reach in Roman times and no historical account has documented their discovery that early.

Although the authors have no scientific proof, we propose a new hypothesis for the origin of (some) basaltic sapphires used by the Romans: that they came from surface deposits in northern Ethiopia which were already known and productive in ancient times, but which were possibly abandoned later, forgotten and only recently rediscovered. This hypothesis is supported by comments made by Pliny the Elder (23–79 CE) and Solinus (early 3rd century CE), both of whom referred to gems from Ethiopia (J. Ogden, pers. comm. 2019) and specifically mentioned *hyacinthos*, which is generally accepted in archaeology to be the ancient name for sapphire (Thoresen 2017a). Specifically, Pliny the Elder stated 'Ethiopia, which produces hyacinthos, produces chrysolithos also, a transparent stone with a refulgence like that of gold' (Eichholz 1962), and Solinus indicated 'Amongst those things of which we have spoken [in Ethiopia] is found the hyacinthos of a shining sky blue colour' (Apps 2011).

Basalt-related sapphire deposits in northern Ethiopia are located near the town of Chila (Tigray region), about 25 km north-west and north of the city of Aksum (Bruce-Lockhart 2017; Vertriest *et al*. 2017). Structurally, this area is located at the northern end of Africa's Great Rift Valley, which is dominated by geologically young extensional tectonics (Tertiary to Quaternary; Corti 2009) similar to sapphire deposits further south of this large-scale structure, such as near Lake Turkana in Kenya (Themelis 1989) and Cyangugu in south-western Rwanda (Krzemnicki *et al*. 1996). This region is characterised by extensive igneous (magmatic and volcanic) rock suites, including alkali basalt and associated secondary gravels containing sapphires in large quantities, often showing some turbidity or milkiness (Lucas *et al*. 2018) similar to the Roman intaglio of this study.

Near the northern border of modern Ethiopia, the city of Aksum and its surroundings were an important trading centre during the Aksumite Empire (early 1st century to 900 CE), which controlled northern Ethiopia and part of present-day Eritrea, including the ancient port of Adulis. This port was an important trading hub between the Roman Empire and the Middle East and India (Figure 15), as described by an anonymous merchant or sailor around the middle of the 1st century in *The Periplus Maris Erythraei* ('Voyage Around the Red Sea'; Casson 1989). Recent archaeological excavations of several ancient graves in Aksum revealed numerous artefacts, including jewellery and glass beads, thus offering evidence of intense trade between the kingdom of Aksum and the Roman Empire (Sidebotham 1986, 1996, 2019; Wendrich *et al*. 2003) since the early 1st century CE (Morrison 1989; Alberge 2015).

Although sapphires have not been found so far in any archaeological excavation at Aksum or its surroundings, the present-day deposits in Ethiopia might have been known in antiquity, as they are located within the realm of the ancient kingdom of Aksum. In addition, the deposits are readily accessible (in mining terms) on the surface and in shallow gravel layers, such that sapphires could be easily gathered from the ground (Vertriest *et al*. 2017; Lucas *et al*. 2018).

Figure 15: This map illustrates ancient trade routes from Aksum towards the Roman Empire and elsewhere. Modified from Addis Herald, www.addisherald.com/aksumite-empire/#gmedia10093.

CONCLUSIONS

This study provides a rare case where a gemstone of archaeological significance and documented provenance (1986 excavation of Pompeii, Italy) could be analysed in a laboratory setting with advanced analytical methods. Based on our analytical data and microscopic observations, we conclude that the studied Roman intaglio was fashioned from an unheated basaltic sapphire. A possible origin from gem gravels of Sri Lanka—known since antiquity as a source of (metamorphic) sapphires and many other gems—can be definitively excluded, although the gem's hazy light bluish grey colour appearance might be considered reminiscent of some Sri Lankan sapphires. Due to its close similarity in trace-element composition to basaltic sapphires from various deposits, a clear geographic origin for this Roman sapphire intaglio cannot be determined based on the currently available data.

In addition to the existing literature, which commonly refers to the origin of ancient sapphires as South East Asia and the Far East, we propose an Ethiopian origin for the studied Roman intaglio as similarly plausible, although we have no direct evidence (by gemmological data, archaeological excavations or historical accounts) to support our hypothesis. Another option for such basalt-related sapphires might be the Massif Central in France. Although first mentioned only in the 13th century (Forestier 1993), sapphires from this area might have been known as early as the 1st century CE.

This study clearly shows that more detailed research on basalt-related ancient (Roman) sapphires is necessary. Especially with the recent progress in gem testing using chemical fingerprinting (e.g. GemTOF; Wang *et al.* 2016), statistical methodology (e.g. non-linear algorithms; see Wang *et al.* 2019) and stable isotopes (e.g. oxygen; see Giuliani *et al.* 2000, 2008, 2014), it might be possible to verify in the future whether the recently documented sapphire deposits near Aksum in northern Ethiopia were known in ancient times as a source of gem-quality basaltic sapphires showing milky bluish or dark blue colouration.

REFERENCES

Abduriyim, A. & Kitawaki, H. 2006. Determination of the origin of blue sapphire using laser ablation inductively coupled plasma mass spectrometry (LA-ICP-MS). *Journal of Gemmology*, **30**(1), 23–36, http://doi.org/10.15506/JoG.2006.30.1.23.

Alberge, D. 2015. Dazzling jewels from an Ethiopian grave reveal 2,000-year-old link to Rome. *The Guardian*, www.theguardian.com/world/2015/jun/07/ancient-ethiopia-gravesite-treasure-rome, posted 6 June 2015, accessed August 2018.

Anonymous ca. 300 CE. *Papyrus Graecus Holmiensis* (The Stockholm Papyrus). National Library of Sweden, Stockholm, manuscript Acc. 2013/75, 15 leaves.

Apps, A.E. 2011. *Gaius Iulius Solinus and his polyhistor.* PhD thesis, Macquarie University, Sydney, Australia, two vols., 386 and 210 pp.

Begley, V. & Puma, R.D.D. 1991. *Rome and India: The Ancient Sea Trade*. University of Wisconsin Press, Madison, Wisconsin, USA, 226 pp.

Beran, A. & Rossman, G.R. 2006. OH in naturally occurring corundum. *European Journal of Mineralogy*, **18**(4), 441–447, http://doi.org/10.1127/0935-1221/2006/0018-0441.

Boardman, J., Scarisbrick, D., Wagner, C. & Zwierlein-Diehl, E. 2009. *The Marlborough Gems: Formerly at Blenheim Palace, Oxfordshire*. Oxford University Press, Oxford, 384 pp.

Borell, B. 2017. Gemstones in Southeast Asia and beyond: Trade along the maritime networks. *In*: Hilgner, A., Greiff, S. & Quast, D. (eds) *Gemstones in the First Millennium AD: Mines, Trade, Workshops and Symbolism*. Römisch-Germanisches Zentralmuseum, Mainz, Germany, 21–44.

Borell, B., Bellina, B. & Chaisuwan, B. 2014. Contacts between the upper Thai-Malay peninsula and the Mediterranean world. *In*: Revire, N. & Murphy, S.A. (eds) *Before Siam Was Born: New Insights on the Art and Archaeology of Pre-Modern Thailand and its Neighbouring Regions*. River Books & The Siam Society, Bangkok, Thailand, 98–117.

Bruce-Lockhart, S. 2017. Gem Notes: Update on sapphires from Tigray, northern Ethiopia. *Journal of Gemmology*, **35**(7), 580–582.

Butini, E., Butini, F., Angle, M., Cerino, P., De Angelis, A., Tomei, N. & Altamura, F. 2018. Archaeometric and gemmological analyses of a Roman imperial gold-and-sapphire jewel from Colonna (Rome, Italy). *Measurement*, **128**, 160–169, http://doi.org/10.1016/j.measurement.2018.06.011.

Calciati, R. 1986. *Corpus nummorum siculorum: la monetazione di bronzo*, Vol. 2. Edizioni G.M., Milan, Italy, 460 pp. (see p. 81).

Caley, E.R. 1927. The Stockholm Papyrus. An English translation with brief notes. *Journal of Chemical Education*, **4**(8), 979–1002, http://doi.org/10.1021/ed004p979.

Calligaro, T. 2005. The origin of ancient gemstones unveiled by PIXE, PIGE and μ-Raman spectrometry. *In*: Uda, M., Demortier, G. & Nakai, I. (eds) *X-rays for Archaeology*. Springer, Dordrech, The Netherlands, 101–112, http://doi.org/10.1007/1-4020-3581-0_5.

Casson, L. 1989. *The Periplus Maris Erythraei*. Princeton University Press, Princeton, New Jersey, USA, 320 pp., http://doi.org/10.1515/9781400843206.

Charbonneau-Lassey, L. 1994. *Il Bestiario del Cristo: La Misteriosa Emblematica di Gesù Cristo*. Edizioni Arkeios, Rome, Italy, 1,400 pp.

Content, D.J. 2016. *Ruby, Sapphire & Spinel: An Archaeological, Textual and Cultural Study*. Brepols Publishers, Turnhout, Belgium, Part I: viii + 452 pp.; Part II: 320 pp.

Cooley, A.E. & Cooley, M.G.L. 2013. *Pompeii and Herculaneum*. Routledge, London, 352 pp., http://doi.org/10.4324/9781315885759.

Corti, G. 2009. Continental rift evolution: From rift initiation to incipient break-up in the Main Ethiopian Rift, East Africa. *Earth-Science Reviews*, **96**(1–2), 1–53, http://doi.org/10.1016/j.earscirev.2009.06.005.

D'Ambrosio, A. & De Carolis, E. 1997. *I Monili dall'area Vesuviana*. L'Erma di Bretschneider, Rome, 162 pp. (see pp. 48–51, 118–119).

De Carolis, E. & Patricelli, G. 2003. *Vesuvius, A.D. 79: The Destruction of Pompeii and Herculaneum*. Getty Publications, Los Angeles, California, USA, 136 pp.

Devoto, G. 1985. *Geologia Applicata all'Archeologia*. La Nuova Italia Scientifica, Rome, Italy, 207 pp.

Di Nunno, P. 2015. Il cavallo marino delle "thermae" di Canosa. www.canosaweb.it/rubriche/giuseppe-di-nunno-stilus-magistri/il-cavalo-marino-delle-thermae-di-canosa, posted 11 March 2015, accessed 16 November 2019.

Dimucci, A.M. 2015. *An ancient iron cargo in the Indian Ocean: The Godavaya shipwreck.* M.A. thesis, Texas A&M University, College Station, Texas, USA, 85 pp.

Eichholz, D.E. (transl.) 1962. *Pliny Natural History, Volume X: Books 36–37*. Harvard University Press, Cambridge, Massachusetts, USA, 368 pp.

Entwistle, C. & Adams, N. (eds) 2011. *'Gems of Heaven': Recent Research on Engraved Gemstones in Late Antiquity,* c. *AD 200–600*. British Museum Research Publication No. 177, London, 274 pp.

Ferguson, J. & Fielding, P.E. 1971. The origins of the colours of yellow, green and blue sapphires. *Chemical Physics Letters*, **10**(3), 262–265, http://doi.org/10.1016/0009-2614(71)80282-8.

Forestier, F.-H. 1993. Histoire de l'un des gisements de gemmes le plus anciennement connu d'Europe occidentale: Saphirs, grenats et hyacinthes du Puy-en-Velay (43). Cahiers de la Haute, Loire, France, 81–152.

Francis, P. 1986. Indian antiquity. *Lapidary Journal*, **39**(12), 45–55.

Fritsch, E. & Mercer, M. 1993. Letters: Blue color in sapphire caused by Fe^{2+}/Fe^{3+} intervalence charge transfer. *Gems & Gemology*, **29**(3), 151, 226.

Gaillou, E. 2003. *Les saphirs du Massif Central: Étude minéralogique des saphirs du Sioulot, du Mont Coupet et du Menoyre.* Master's thesis, Université Blaise Pascal, Clermont-Ferrand; Université Jean Monnet, St Etienne; Université Claude Bernard, Lyon, France, 68 pp., http://doi.org/10.13140/RG.2.2.32416.28163.

Galli, M. 2017. Beyond frontiers: Ancient Rome and the Eurasian trade networks. *Journal of Eurasian Studies*, **8**(1), 3–9, http://doi.org/10.1016/j.euras.2016.12.001.

Gast, N., Gilg, H.A., Weiß, C., Gebhard, R., Schmahl, W. & Stark, R. 2011. Exploring the roots of garnet jewellery: Raman spectroscopic and microscopic analysis of Hellenistic engraved gems. *6th International Congress on the Application of Raman Spectroscopy in Art and Archaeology*, Parma, Italy, 5–8 September, 35–36.

Gilg, H.A., Schmetzer, K. & Schüssler, U. 2018. An early Byzantine engraved almandine from the Garibpet deposit, Telangana State, India: Evidence for garnet trade along the ancient Maritime Silk Road. *Gems & Gemology*, **54**(2), 149–165, http://doi.org/10.5741/gems.54.2.149.

Giuliani, G., Chaussidon, M., Schubnel, H.-J., Piat, D.H., Rollion-Bard, C., France-Lanord, C., Giard, D., de Narvaez, D., *et al.* 2000. Oxygen isotopes and emerald trade routes since antiquity. *Science*, **287**(5453), 631–633, http://doi.org/10.1126/science.287.5453.631.

Giuliani, G., Fallick, A., Ohnenstetter, D. & Pegere, G. 2008. Oxygen isotopes composition of sapphires from the French Massif Central: Implications for the origin of gem corundum in basaltic fields. *Mineralium Deposita*, **44**(2), 221–231, http://doi.org/10.1007/s00126-008-0214-2.

Giuliani, G., Ohnenstetter, D., Fallick, A.E., Groat, L. & Fagan, A.J. 2014. The geology and genesis of gem corundum deposits. *In*: Groat, L.A. (ed) *Geology of Gem Deposits*, 2nd edn. Mineralogical Association of Canada Short Course No. 44, Québec, Québec, Canada, 29–112.

Greifenhagen, A. 1970. *Schmuckarbeiten in Edelmetall*, Vol. 1. Staatliche Museen Preussischer Kulturbesitz, Antikenabteilung, Berlin, Germany (see Inv. Misc.7070 = FG 6756, 77, 79–80, pl. 59.5 and colour pl. VII, 6).

Gübelin, E.J. & Koivula, J.I. 2008. *Photoatlas of Inclusions in Gemstones*, Vol. 3. Opinio Publishers, Basel, Switzerland, 672 pp.

Gunawardene, M. & Chawla, S.S. 1984. Sapphires from Kanchanaburi Province, Thailand. *Journal of Gemmology*, **19**(3), 228–239, http://doi.org/10.15506/JoG.1984.19.3.228.

Guo, J., Wang, F. & Yakoumelos, G. 1992. Sapphires from Changle in Shandong Province, China. *Gems & Gemology*, **28**(4), 255–260, http://doi.org/10.5741/gems.28.4.255.

Hackens, T. & Moucharte, G. (eds) 1989. *Technology and Analysis of Ancient Gemstones: Proceedings of the European Workshop Held at Ravello, European University Centre for Cultural Heritage, November 13–16, 1987*. PACT, Strasbourg, France, 458 pp.

Hänni, H.A. 1990. A contribution to the distinguishing characteristics of sapphire from Kashmir. *Journal of Gemmology*, **22**(2), 67–75, http://doi.org/10.15506/JoG.1990.22.2.67.

Hänni, H.A. 1994. Origin determination for gemstones: Possibilities, restrictions and reliability. *Journal of Gemmology*, **24**(3), 139–148, http://doi.org/10.15506/JoG.1994.24.3.139.

Hughes, R.W. 1997. *Ruby & Sapphire*. RWH Publishing, Bangkok, Thailand, 511 pp.

Hughes, R.W. 2017. *Ruby & Sapphire: A Gemologist's Guide*. RWH Publishing/Lotus Publishing, Bangkok, Thailand, 816 pp.

Iacopi (Jacopi), G.I. 1943. *Scavi in prossimità del porto fluviale di S. Paolo, località Pietra Papa*. Accademia dei Lincei, Milan, Italy, 178 pp.

Jobbins, E.A. & Berrangé, J.P. 1981. The Pailin ruby and sapphire gemfield, Cambodia. *Journal of Gemmology*, **17**(8), 555–567, http://doi.org/10.15506/JoG.1981.17.8.555.

Keller, A.S. & Keller, P.C. 1986. The sapphires of Mingxi, Fujian Province, China. *Gems & Gemology*, **22**(1), 41–45, http://doi.org/10.5741/gems.22.1.41.

Kornbluth, G. 2008. The seal of Alaric, *rex Gothorum*. *Early Medieval Europe*, **16**(3), 299–332, http://doi.org/10.1111/j.1468-0254.2008.00232.x.

Krzemnicki, M.S., Hänni, H.A., Guggenheim, R. & Mathys, D. 1996. Investigations on sapphires from an alkali basalt, south west Rwanda. *Journal of Gemmology*, **25**(2), 90–106, http://doi.org/10.15506/JoG.1996.25.2.90.

Lucas, A., Vertriest, W., Girma, D., Abay, T. & Bekele, B. 2018. Expedition to Ethiopia's sapphire fields. *InColor*, No. 38, 26–34.

Lüle-Whipp, C. 2006. *Mineralogical-petrological and geochemical investigation on some garnets from volcanic rocks of Gorece Village-Cumaovasi, Izmir and metamorphites of Menderes Massif and their possible archaeogemological connections*. Ph.D. thesis, Hacettepe University, Ankara, Turkey.

Maaskant-Kleibrink, M. 1978. *Catalogue of the Engraved Gems in the Royal Coin Cabinet, The Hague: The Greek, Roman, and Etruscan Collections*. Government Publishing Office, The Hague, The Netherlands, 380 pp.

Maaskant-Kleibrink, M. 1989. The microscope and Roman Republican gem engraving. Some preliminary remarks. *In*: Hackens, T. & Moucharte, G. (eds) *Technology and Analysis of Ancient Gemstones: Proceedings of the European Workshop Held at Ravello, European University Centre for Cultural Heritage, November 13–16, 1987*. PACT, Strasbourg, France, 189–215.

Magni, A. 2009. Le gemme di età classica. *In*: Chiesa, G.S., Magni, A. & Tassinari, G. (eds) *Gemme dei Civici Musei d'Arte di Verona*. Giorgio Bretschneider, Rome, Italy, 15–142 (see p. 59).

Médard, E., Paquette, J.L., Devouard, B., Ricci, J., Boivin, P., Gaillou, E., Rochault, J. & Hardiagon, M. 2012. Gem sapphires and zircons from Cenozoic volcanism of the French Massif Central. *1st International Congress on Management and Awareness in Protected Volcanic Landscapes*, Olot, Spain, 21–25 May.

Morrison, H.M. 1989. The beads. *In*: Munro-Hay, S.C. & Phillipson, D.W. (eds) *Excavations at Aksum: An Account of Research at the Ancient Ethiopian Capital Directed in 1972–4 by the Late Dr. Neville Chittick*. British Institute in Eastern Africa, London, 168–178.

Ogden, J. 1982. *Jewellery of the Ancient World*. Trefoil Books, London, 185 pp.

Ogden, J., 2015. Sri Lankan legacy: A history of sapphires. Oral presentation at ICA Congress, Colombo, Sri Lanka, 16–19 May, www.youtube.com/watch?v=DOkxNif8d5U, posted 13 November 2015, accessed May 2017.

Ogden, J. 2018. *Diamonds: An Early History of the King of Gems*. Yale University Press, London, 408 pp.

Pannuti, U. 1994. *La Collezione Glittica del Museo Archeologico Nazionale di Napoli*, Vol. 2. Istituto Poligrafico e Zecca dello Stato, Rome, Italy, 362 pp. (see cat. no. 120, p. 50, pl. XI).

Papagiannaki, A. 2013. Imperial portraiture and the minor arts in the era of Constantine the Great. *In*: Bojović, D. (ed) *Saint Emperor Constantine and Christianity*, Vol. 2. International Conference Commemorating the 1700th Anniversary of the Edict of Milan, Niš, Serbia, 31 May–2 June, 479–491.

Pardieu, V., Sangsawong, S., Muyal, J. & Sturman, N. 2014. *Blue Sapphires from the Mambilla Plateau, Taraba State, Nigeria*. GIA News from Research, 47 pp., www.gia.edu/doc/Nigeria_Mambilla_Sapphire_US.pdf, 16 August 2014, accessed 3 November 2014.

Pinckernelle, K. 2007. *The Iconography of Ancient Greek and Roman Jewellery.* M.Phil. thesis, University of Glasgow, 121 pp.

Richter, G.M.A. 1920. *Catalogue of Engraved Gems of the Classical Style*. The Metropolitan Museum of Art, New York, New York, USA, xxiv + 232 pp.

Rosenfeld, A., Dvorachek, M. & Amorai-Stark, S. 2003. Roman wheel-cut engraving, dyeing and painting microquartz gemstones. *Journal of Archaeological Science*, **30**(2), 227–238, http://doi.org/10.1006/jasc.2002.0829.

Saeseaw, S., Sangsawong, S., Vertriest, W., Atikarnsakul, U., Liliane, V., Raynaud-Flattot, Khowpong, C. & Weeramonkhonlert, V. 2017. *A Study of Sapphire from Chanthaburi, Thailand and its Gemological Characteristics.* GIA News from Research, 42 pp., www.gia.edu/doc/Blue-sapphires-Chantaburi-Thailand-finalfinal.pdf, 12 April 2017, accessed 22 January 2018.

Sax, M. 1996. Recognition and nomenclature of quartz materials with specific reference to engraved gemstones. *Jewellery Studies*, **7**, 63–72.

Schmetzer, K. & Bank, H. 1981. The colour of natural corundum. *Neues Jahrbuch für Mineralogie, Monatshefte*, **1981**(2), 59–68.

Schmetzer, K., Gilg, H.A., Schüssler, U., Panjikar, J., Calligaro, T. & Périn, P. 2017. The linkage between garnets found in India at the Arikamedu archaeological site and their source at the Garibpet deposit. *Journal of Gemmology*, **35**(7), 598–627, http://doi.org/10.15506/JoG.2017.35.7.598.

Seland, E.H. 2017. Gemstones and mineral products in the Red Sea/Indian Ocean trade of the first millennium. *In*: Hilgner, A., Greiff, S. & Quast, D. (eds) *Gemstones in the First Millennium AD: Mines, Trade, Workshops and Symbolism*. Römisch-Germanisches Zentralmuseum, Mainz, Germany, 45–58.

Sevillano-López, D. & González, F.J. 2011. Mining and minerals trade on the Silk Road to the ancient literary sources: 2 BC to 10 AD centuries. *In*: Ortiz, J.E., Puche, O., Rábano, I. & Mazadiego, L.F. (eds) *History of Research in Mineral Resources*. Instituto Geológico y Minero de España, Madrid, Spain, 43–60.

Sidebotham, S.E. 1986. *Roman Economic Policy in the Erythra Thalassa, 30 BC–AD 217*. E.J. Brill, Leiden, The Netherlands, 226 pp.

Sidebotham, S.E. 1996. Romans and Arabs in the Red Sea. *Topoi*, **6**(2), 785–797, http://doi.org/10.3406/topoi.1996.1695.

Sidebotham, S.E. 2019. *Berenike and the Ancient Maritime Spice Route*. University of California Press, Berkeley, California, USA, 456 pp.

Smith, C.G., Faithfull, J.V. & Jackson, B. 2008. Gemstone prospectivity in Scotland. *In*: Walton, G. (ed) *Proceedings of the 14th Extractive Industry Geology Conference*, Edinburgh, Scotland, 14–17 June 2006. EIG Conferences, Oxford, 9–11.

Smith, C.P. 1995. A contribution to understanding the infrared spectra of rubies from Mong Hsu, Myanmar. *Journal of Gemmology*, **24**(5), 321–335, http://doi.org/10.15506/JoG.1995.24.5.321.

Smith, C.P., Kammerling, R.C., Keller, A.S., Peretti, A., Scarratt, K.V., Khoa, N.D. & Repetto, S. 1995. Sapphires from southern Vietnam. *Gems & Gemology*, **31**(3), 168–186, http://doi.org/10.5741/gems.31.3.168.

Smith, W. (ed) 1849. *Dictionary of Greek and Roman Biography and Mythology*, Vol. 2. C.C. Little and J. Brown, Boston, Massachusetts, USA, 480 pp.

Sodo, A.M. 1988. Regio II, insula 9. *Rivista di Studi Pompeiani*, **2**, 195–202.

Sodo, A.M. 1992. Gemme della casa del gemmario di Pompei. *In*: Cappelli, R. (ed) *Bellezza e lusso: Immagini e documenti di piaceri della vita*. Leonardo-De Luca, Rome, Italy, 89–91.

Spier, J. 1992. *Ancient Gems and Finger Rings: Catalogue of the Collections of the J. Paul Getty Museum*. Getty Publications, Los Angeles, California, USA, 200 pp. (see pp. 22, 103, 123).

Spier, J. 2007. *Late Antique and Early Christian Gems*. Reichert Verlag, Wiesbaden, Germany, 374 pp.

Spier, J. 2012. *Byzantium and the West: Jewelry in the First Millennium*. Paul Holberton Publishing, London, 207 pp.

Sutherland, F.L., Bosshart, G., Fanning, C.M., Hoskin, P.W.O. & Coenraads, R.R. 2002. Sapphire crystallization, age and origin, Ban Huai Sai, Laos: Age based on zircon inclusions. *Journal of Asian Earth Sciences*, **20**(7), 841–849, http://doi.org/10.1016/s1367-9120(01)00067-0.

Themelis, T. 1989. A new sapphire deposit: Turkana, Kenya. *Gemological Digest*, **2**(4), 32–34.

Thoresen, L. 2017a. Archaeogemmology and ancient literary sources on gems and their origins. *In*: Hilgner, A., Greiff, S. & Quast, D. (eds) *Gemstones in the First Millennium AD: Mines, Trade, Workshops and Symbolism*. Römisch-Germanisches Zentralmuseum, Mainz, Germany, 155–217.

Thoresen, L. 2017b. Archaeogemology of sapphire. *In*: Overlin, S. (ed) *Fourteenth Annual Sinkankas Symposium – Sapphire*. Pala International, Fallbrook, California, USA, 74–91.

Thoresen, L. & Schmetzer, K. 2013. Greek, Etruscan and Roman garnets in the antiquities collection of the J. Paul Getty Museum. *Journal of Gemmology*, **33**(7), 201–222, http://doi.org/10.15506/JoG.2013.33.7.201.

Toynbee, J.M.C. 1951. *Some Notes on Artists in the Roman World*. Latomus, Brussels, Belgium, 56 pp.

Unger, M. & Van Leeuwen, S. 2017. *Jewellery Matters*. NAI010 publishers, Rotterdam, The Netherlands, 648 pp.

Vertriest, W., Weeramonkhonlert, V., Raynaud, V. & Bruce-Lockhart, S. 2017. Gem News: Sapphires from northern Ethiopia. *Gems & Gemology*, **53**(2), 247–248.

Wang, F. 1988. The sapphires of Penglai, Hainan Island, China. *Gems & Gemology*, **24**(3), 155–159, http://doi.org/10.5741/gems.24.3.155.

Wang, H.A.O., Krzemnicki, M.S., Chalain, J.-P., Lefèvre, P., Zhou, W. & Cartier, L. 2016. Simultaneous high sensitivity trace-element and isotopic analysis of gemstones using laser ablation inductively coupled plasma time-of-flight mass spectrometry. *Journal of Gemmology*, **35**(3), 212–223, http://doi.org/10.15506/JoG.2016.35.3.212.

Wang, H.A.O., Krzemnicki, M.S., Chalain, J.-P., Lefèvre, P., Zhou, W., Hänsel, S., Klumb, A., Dzikowski, T., *et al.* 2019. Multi-element analysis of gemstones for country of origin determination. *36th International Gemmological Conference*, Nantes, France, 27–31 August, 176–178.

Wendrich, W.Z., Tomber, R.S., Sidebotham, S.E., Harrell, J.A., Cappers, R.T.J. & Bagnall, R.S. 2003. Berenike crossroads: The integration of information. *Journal of the Economic and Social History of the Orient*, **46**(1), 46–87, http://doi.org/10.1163/156852003763504339.

Zwierlein-Diehl, E. 1991. *Die Antiken Gemmen des Kunsthistorischen Museums in Wien, Band III*. Prestel, Munich, Germany, 362 pp. (see Inv. XII 24, no. 2537, pp. 236–241, pls. 167, 168).

Zwierlein-Diehl, E. 2007. *Antike Gemmen und ihr Nachleben*. Walter de Gruyter, Berlin, Germany, 567 pp.

The Authors

Dr Michael S. Krzemnicki FGA
Swiss Gemmological Institute SSEF,
Aeschengraben 26, CH-4051 Basel, Switzerland
Email: michael.krzemnicki@ssef.ch

Flavio Butini FGA and Enrico Butini FGA
Istituto Gemmologico Nazionale,
Via di S. Sebastianello 6, 00187 Rome, Italy

Dr Ernesto De Carolis
Archaeologist, formerly at Archaeological Superintendence of Pompei, Italy

Acknowledgements

The authors thank Prof. Dr Massimo Osanna (Parco Archeologico di Pompei), Dr Grete Stefani (Scavi di Pompei), Dr Laura D'Esposito (Parco Archeologico di Pompei) and Dr Anna Civale (Mondadori Electa, Pompei) for their support in our study of the described sapphire intaglio. Further thanks go to Judith Braun and Hannah Amsler, both of SSEF, for their analytical assistance. And finally, we thank the reviewers, namely Dr Jack Ogden and Lisbet Thoresen, and also two anonymous reviewers for their valuable comments and suggestions.

The Fire Within

"For in them you shall see the living fire of the ruby, the glorious purple of the amethyst, the sea-green of the emerald, all glittering together in an incredible mixture of light."

– Roman Elder Pliny, 1st Century AD

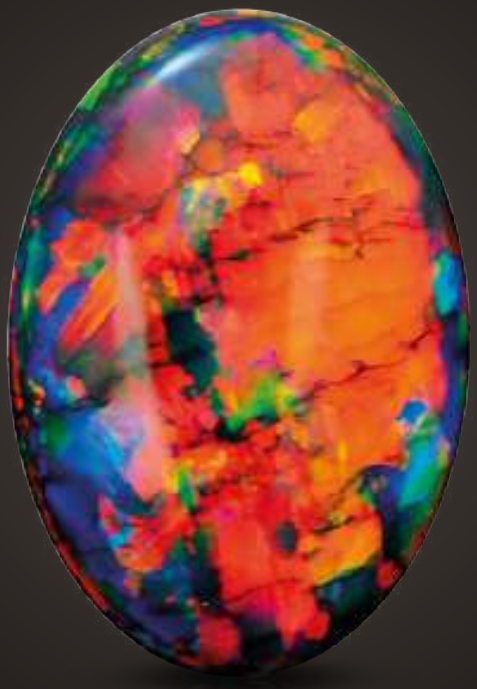

Black Opal 15.7 Carats

Suppliers of Australia's finest opals to the world's gem trade.

CODY OPAL

Level 1 - 119 Swanston Street Melbourne Australia

T. +61 3 9654 5533 E. info@codyopal.com

www.codyopal.com

ICA International Colored Gemstone Association Member

JOG

The Texture and Chemical Composition of Trapiche Ruby from Khoan Thong, Luc Yen Mining District, Northern Vietnam

Isabella Pignatelli, Gaston Giuliani, Christophe Morlot and Pham Van Long

ABSTRACT: The trapiche texture and chemical composition of two rubies from the Khoan Thong placer in northern Vietnam were examined by X-ray computed tomography, scanning electron microscopy and electron microprobe analysis. Their texture is similar to that of some Burmese trapiche rubies, with inclusion-rich sector boundaries intersecting at a small central point and a significant concentration of elongated tube-like voids in growth sectors. The most common inclusions are anorthite and margarite; the latter formed by destabilisation of both ruby and anorthite during retrograde metamorphism. The chemical composition of the samples plots in the field of Vietnamese alluvial and primary marble-hosted deposits, although differences in Fe_2O_3, TiO_2 and Cr_2O_3 contents may distinguish trapiche rubies from various mining areas in Vietnam. Their composition differs from that of Burmese trapiche rubies by a higher Fe_2O_3/TiO_2 ratio and a lower Cr_2O_3 content. Vietnamese trapiche rubies formed in the same geological environment as non-trapiche ones, under metamorphic conditions prevailing for the Himalayan orogenesis. In this geological context, localised fluid pressure variations and hydraulic fracturing caused changes in the driving force of crystallisation, favouring the development of the trapiche texture.

The Journal of Gemmology, **36**(8), 2019, pp. 726–746, http://doi.org/10.15506/JoG.2019.36.8.726

The term *trapiche* was introduced by McKague (1964) to refer to an unusual texture in some Colombian emeralds, which resembles the spokes of a milling wheel that is used to process sugar cane. In the 1990s, trapiche rubies with a similar texture appeared on the gem market from Mong Hsu in Myanmar (Schmetzer *et al.* 1996, 1999; Sunagawa *et al.* 1999). Then, in the 2000s, trapiche tourmalines were reported from Zambia (Hainschwang *et al.* 2007; Schmetzer *et al.* 2011). Recently, a fluid inclusion study of samples from Mong Hsu confirmed that both non-trapiche and trapiche rubies formed from the same parental CO_2-H_2S-rich fluid (Giuliani *et al.* 2018).

In the present article, we describe in detail (and for the first time) trapiche rubies from northern Vietnam (e.g. Figure 1). We examine two samples from the Khoan Thong placer in the Luc Yen mining district of northern Vietnam, and discuss their formation conditions, texture acquisition and growth, as well as their chemical composition, through mineralogical and petrographic studies, X-ray computed tomography and electron probe micro-analysis. The results give a complete overview of the relationships among the three components of the trapiche texture (core, growth sectors and sector boundaries) in Vietnamese rubies, which we compare to those from other localities.

Figure 1: The trapiche texture of this ruby (15 × 15 × 27 mm) is representative of the material from the Luc Yen District of Vietnam described in this article. Photo by Shang-i (Edward) Liu.

TRAPICHE TEXTURE IN RUBY

Trapiche texture is formed of growth sectors separated by more or less sharp boundaries containing abundant mineral and fluid inclusions (Win 2005; Schmetzer *et al.* 2011). These boundaries surround a central portion, generally called the 'core', and extend from its edges to the rim of the crystal. Some trapiche samples lack a distinct core, and the boundaries intersect at a central point. The trapiche texture is best seen in slices cut perpendicular to the *c*-axis, and the presence and size of the core portion depend on the slice's position within the host crystal (Pignatelli *et al.* 2015; see Figure 2).

In the literature, the terminology used to indicate the main components of the trapiche pattern varies with the mineral and the authors (Figure 3). There is consensus only for the 'core'. The growth sectors have been called 'arms' in trapiche emeralds (Nassau & Jackson 1970), and 'ruby sectors' or 'growth sectors' in trapiche rubies (Schmetzer *et al.* 1996, 1999; Sunagawa *et al.* 1999). 'Growth sectors' is also used for trapiche tourmaline (Schmetzer *et al.* 2011). More complex is the nomenclature for the boundaries between the gemmy portions: 'two-phase regions' or 'dendrites' have been used for emeralds (Nassau & Jackson 1970; Pignatelli *et al.* 2015), 'arms' for rubies (Schmetzer *et al.* 1996, 1999; Sunagawa *et al.* 1999) and 'sector boundaries' for tourmalines (Schmetzer *et al.* 2011). To avoid further confusion, in this article we use the terms *core, growth sectors* and *sector boundaries*, consistent with Schmetzer *et al.* (2011).

Trapiche texture in ruby was described for the first time by K. Schmetzer and his co-authors (Schmetzer *et al.* 1996, 1999; Sunagawa *et al.* 1999). According to their data, this texture is characterised by six yellowish or white sector boundaries separating six growth sectors. In some ruby samples the sector boundaries intersect at a central point (a core being absent), giving rise to triangular growth sectors (Figure 2c). In others, a hexagonal core is present, and the growth sectors have a trapezoidal shape (Figure 2b).

The core can appear red, black and, when similar to the sector boundaries, yellowish to white. Zoning in Cr and variable contents of other chromophores such as Ti and V have been reported in different trapiche ruby samples,

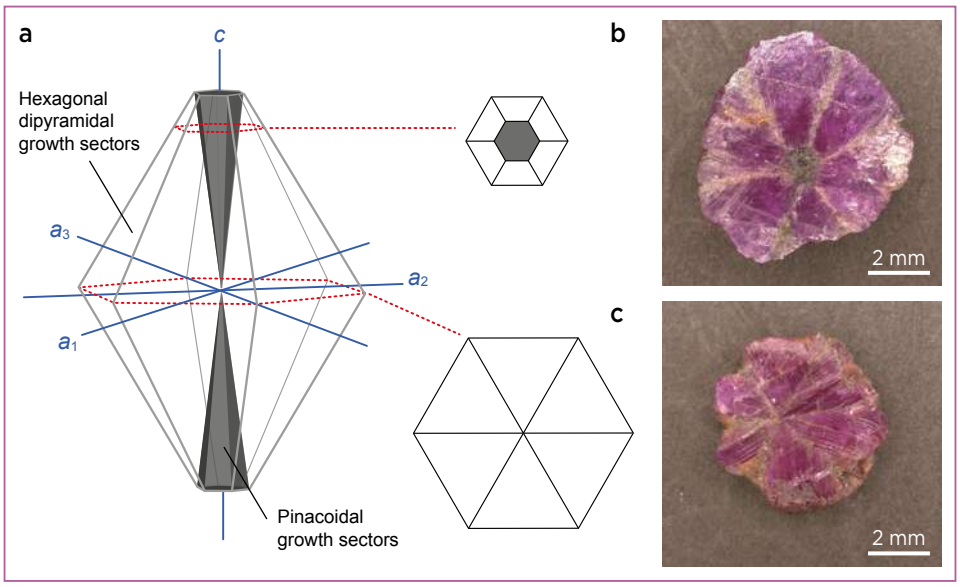

Figure 2: (**a**) Variations in the size of the trapiche core, which corresponds to the pinacoidal growth sectors, can be seen in the areas shown in grey. These sectors have a tapered shape, so the core size varies depending on where a section is cut perpendicular to the *c*-axis. The core is largest near the ends of the crystal (**b**) and decreases towards the centre, where the sector boundaries intersect (**c**). Both slices shown here are from Mong Hsu in Myanmar. Photos by I. Pignatelli and G. Giuliani.

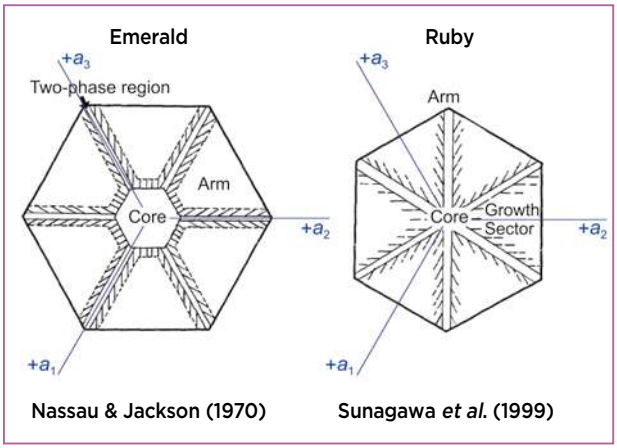

Figure 3: The trapiche texture as seen in sections perpendicular to the *c*-axis is illustrated here for emerald (left) and ruby (right). The *a*-axes are labelled in both drawings, as well as the differing descriptive terminology used in the literature. In the present article, the *arms* referred to by Sunagawa *et al.* (1999) are called *sector boundaries*. Modified from Sunagawa *et al.* (1999).

but also within the same sample (Schmetzer *et al.* 1999; Garnier *et al.* 2002a, b). This explains why the core can be red (Cr>Ti) or bluish to black (Ti>Cr; Peretti *et al.* 1996). The yellowish-to-white colour of both the core and sector boundaries has been attributed to the presence of calcite, dolomite, corundum and K-Al-Fe-Ti silicate inclusions, as well as Fe-rich secondary minerals formed during the weathering process (Schmetzer *et al.* 1999).

Other solid inclusions have also been found within the sector boundaries, including siderite, chlorite, adularia, sillimanite, rutile, titanite, graphite, baryte, mica, amphibole, zircon, diaspore and pyrite (Garnier *et al.* 2002a, b). Tube-like voids filled by solids (i.e. calcite or dolomite), liquid and gas have also been described (Schmetzer *et al.* 1996; Giuliani *et al.* 2018). They originate from the core or sector boundaries and extend into the growth sectors, running perpendicular to the sectors with an inclination of 5° relative to the {0001} faces of the ruby. In some samples, the tube-like voids in the core can also be oriented parallel to the *c*-axis.

Between the tube-like voids and/or their extensions into the sector boundaries, single-phase (liquid), two-phase (liquid + gas) or three-phase (liquid + gas + solid) inclusions have been found (Garnier *et al.* 2002a, b). These inclusions correspond to the trapping of two immiscible fluids during ruby formation: a carbonic fluid in the CO_2-H_2S-COS-S_8-AlO(OH) system and molten salts (Giuliani *et al.* 2015a, 2018).

Trapiche rubies have not been studied *in situ* in their primary deposits; instead, they are typically acquired in Thai and Burmese gem markets. Based on information given by the suppliers, they originated from the Mong Hsu mines in Myanmar, but some of them might have come from Vietnam (Schmetzer *et al.* 1996). Although the geology of Mong Hsu is not well known because of security issues, Hlaing (1991) reported that the trapiche rubies are apparently hosted by marbles similar to those in the Mogok Stone Tract. This was supported by Garnier *et al.* (2002a, b), who underlined that trapiche and non-trapiche rubies from Mong Hsu have similar mineralogical and chemical features because they formed in the same geological environment.

GEOLOGICAL SETTING OF VIETNAMESE TRAPICHE RUBIES

In northern Vietnam, the main ruby and red spinel deposits are located in marble associated with large-scale shear zones that were active during the Tertiary (Leloup *et al.* 1995; Garnier 2003; Garnier *et al.* 2008; see Figure 4). The Red River shear zone is formed by the Day Nui Con Voi metamorphic belt and the Lo Gam tectonic zone (Garnier 2003; Pham *et al.* 2004, 2013, 2018). The Lo Gam zone contains the ruby and spinel deposits, and consists of metasedimentary sequences (i.e. marble units and intercalated gneisses and schists) of Cambrian depositional age, which are situated between two main left-lateral faults in an area about 10–15 km wide within the Red River shear zone, together with granitoid intrusions of Triassic age (Garnier 2003).

Geothermobarometry of the Day Nui Con Voi metamorphic belt revealed that peak metamorphism took place under amphibolite-facies pressure-temperature (P-T) conditions of about 4.5 ± 1.5 kbar and 710 ± 70°C (Leloup and Kienast 1993; Leloup *et al.* 2001), while Nam *et al.* (1998) estimated 6.5 ± 1.5 kbar and about 690 ± 30°C. Gem ruby formed under conditions of about 620–650°C and 2.6–2.9 kbar during a retrograde P-T metamorphic path, mainly by the destabilisation of muscovite or spinel (Garnier *et al.* 2008). The metamorphic fluid system was rich in CO_2 released from the devolatilisation of carbonates, and also contained fluorine, chlorine and boron, as well as salts and sulphates (NaCl, KCl and $CaSO_4$). Evaporites are the key to explaining the formation of these ruby deposits. Molten salts mobilised *in situ* aluminium and metal transition elements contained within phengites hosted by the marbles, leading to the crystallisation of ruby (Giuliani *et al.* 2003, 2018).

Primary ruby occurs as disseminated crystals within marble—associated with phlogopite, dravite, margarite, pyrite, rutile, spinel, pargasite-edenite and graphite

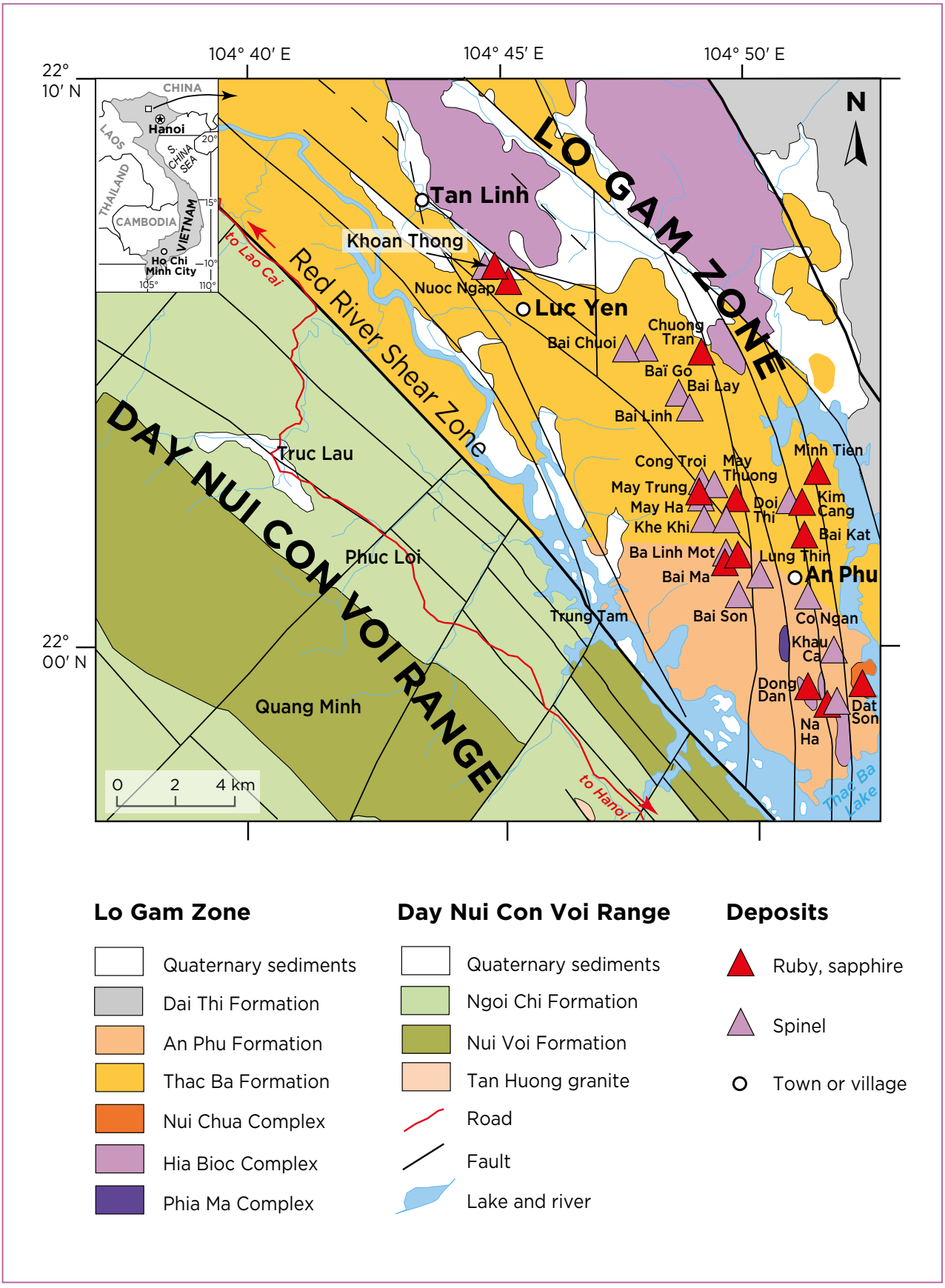

Figure 4: This geological map of the Luc Yen area in northern Vietnam (modified from Garnier 2003) shows the main ruby and red spinel deposits located in marbles associated with large-scale shear zones. The samples studied for this report originated from the Khoan Thong placer north-west of Luc Yen.

(Garnier *et al.* 2008)—in the Luc Yen mining district, which includes the Khoan Thong placer. Ruby also occurs within veinlets and fissures—which crosscut the marbles and are filled by calcite, dravite, pyrite, margarite and phlogopite—at the An Phu, Bai Da Lan and Minh Tien mines.

Placer deposits formed by the concentration of gem-bearing gravels and sands in karst and alluvial fans throughout the Luc Yen mining district. The gem-producing valleys are typically small (i.e. 2–3 km^2). Blue and fancy-colour sapphires, spinel, tourmaline, pargasite, humite and garnet are recovered together with ruby (including rare trapiche ruby). These placers furnish a variety of gem-quality materials to the Luc Yen market, which has been open daily since 1987.

MATERIALS AND METHODS

Seven trapiche rubies were collected by one of the authors (Pham Van Long) in the Luc Yen mining district, from placers related to ruby-bearing marble (i.e. the Cong Troi, May Trung and Khoan Thong mining areas; Figure 4). The crystals were alluvially transported and most of them were transformed into rounded grains. Two of the best-preserved but fractured crystals (samples T1 and T2) found in the Khoan Thong placer were analysed for the present study.

The two samples were analysed by X-ray computed tomography (CT), a non-destructive technique that has previously been used to obtain high-resolution three-dimensional (3D) details of various gem materials, including trapiche emeralds (Karampelas *et al.* 2010; Giuliani *et al.* 2015b; Morlot *et al.* 2016; Pignatelli *et al.* 2017; Richard *et al.* 2019). This technique provides information on the size, distribution and shape of solid inclusions, as well as the geometry and volume of fluid inclusions, and can quantify the volume of porosity. CT scans of the two trapiche rubies were collected with a Phoenix Nanotom S instrument, using resolutions of 6 and 3 µm/voxel and nanofocus X-ray tube tensions of 90 and 110 kV, respectively, for samples T1 and T2. The tomography produces files with voxel (3D pixel) resolutions between 30 and 0.6 µm as a function of sample size. Virtual cross-sections were digitally extracted from the volume of the samples to observe textural details (e.g. porosity) and to visualise the distribution of inclusions with different densities. The volume of porosity and inclusions was calculated using VGStudio and Avizo 9.5 software.

Both samples were sliced perpendicular to the crystallographic *c*-axis, embedded in resin and polished for

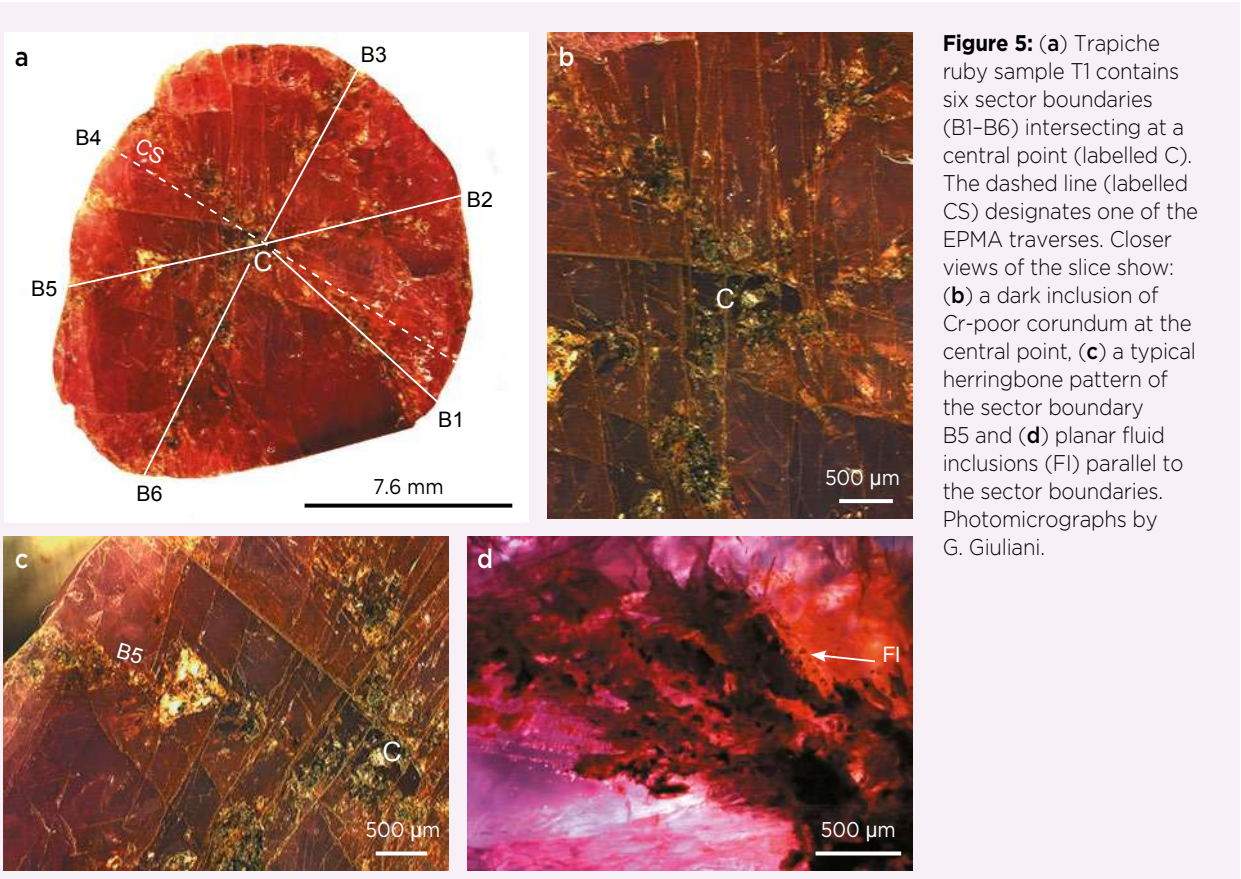

Figure 5: (**a**) Trapiche ruby sample T1 contains six sector boundaries (B1–B6) intersecting at a central point (labelled C). The dashed line (labelled CS) designates one of the EPMA traverses. Closer views of the slice show: (**b**) a dark inclusion of Cr-poor corundum at the central point, (**c**) a typical herringbone pattern of the sector boundary B5 and (**d**) planar fluid inclusions (FI) parallel to the sector boundaries. Photomicrographs by G. Giuliani.

further analysis (Figures 5a and 6a). At the CRPG-CNRS laboratory, they were studied with a JEOL JSM-6510 scanning electron microscope (SEM) equipped with a Genesis energy-dispersive X-ray (EDX) detector, using a 3 nA primary beam accelerated at 15 kV. Backscattered electron (BSE) images and EDX spectra were recorded to analyse the trapiche texture and identify the solid inclusions.

Eighty-seven point analyses of the inclusions and host rubies were performed by electron probe micro-analysis (EPMA) at the Service Commun de Microscopie Electronique et Microanalyse (GeoResources laboratory) with a fully automated Cameca SX100 instrument. The samples were analysed using: an accelerating voltage of 15 kV, a beam current of 12 nA and a raster length of 0.03 µm (focused beam on a surface of 1 µm^2) for Al; and an accelerating voltage of 25 kV, a beam current of 100 nA and a raster length of 0.03 µm for Mg, Ti, V, Cr, Fe and Ga. The collection times were 10 s for Al and 120 s for the other elements. The microprobe was calibrated using mineral and synthetic standards: olivine for Mg, corundum for Al, titanite for Ti, V-SX9 metal for V, chromite for Cr, hematite for Fe and AsGa for Ga. Special care was taken with regard to possible interferences between the chromophores Cr and V: Cr($K\beta_1$) and V($K\alpha_1$) lines were measured using a pentaerythritol (PET) analysing crystal with positive and negative background offsets of 600, large enough to have no interference, respectively, with the V($K\alpha_1$) and Ti($K\beta_1$) lines. The limits of detection were (in ppmw) 48 for Mg, 65 for Ti, 125 for Fe, 154 for Ga, 87 for V and 54 for Cr.

RESULTS

Texture Description

The abraded surfaces of the two trapiche rubies indicate that the crystals had been alluvially transported. They were rounded and fractured, such that little of their original euhedral habit was still recognisable.

Below we describe the features of the trapiche texture in the two Vietnamese samples from the core to the sector boundaries and, finally, the growth sectors.

Core: The trapiche texture in both samples was characterised by sector boundaries that intersected at a central point and the absence of a well-developed hexagonal core. In sample T1, this intersection was underlined by a small inclusion of Cr-poor corundum (Figure 7), which corresponds to the darker area labelled 'C' in Figures 5b and 5c.

Sector Boundaries: The sector boundaries in trapiche rubies develop from the core towards the rim of the crystals and follow <1$\bar{1}$0> directions, whereas they are parallel to

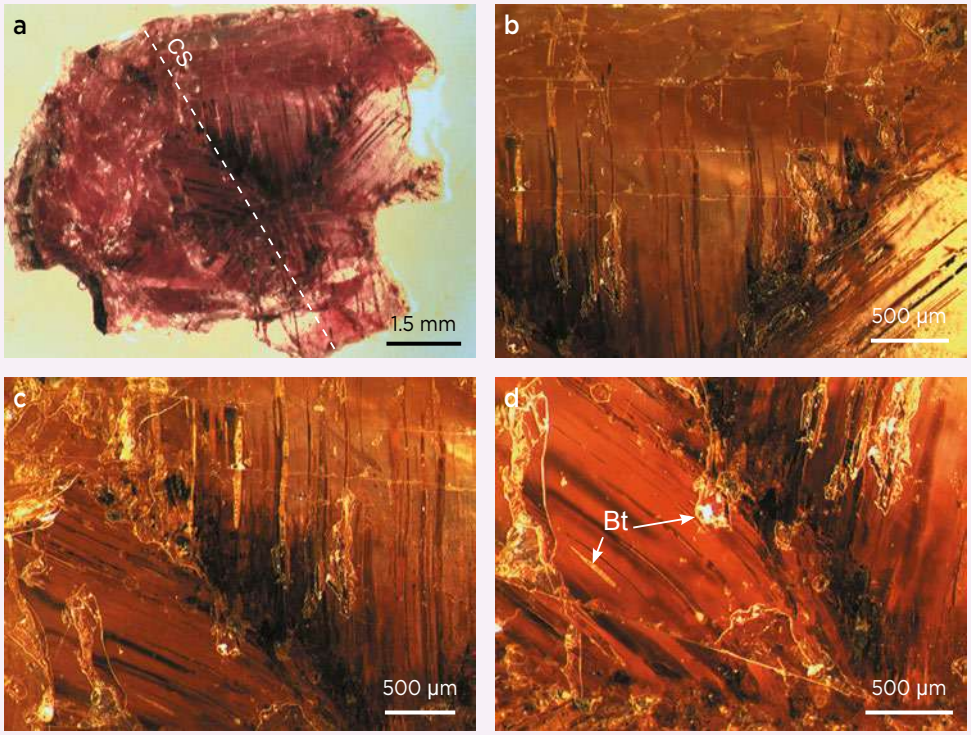

Figure 6: (**a**) Trapiche ruby sample T2 exhibits sector boundaries extending from a central point towards the rim of the crystal. The dashed line (labelled CS) designates one of the EPMA traverses. Closer views of the slice show: (**b**, **c**) tube-like inclusions extending from the sector boundaries into the growth sectors and (**d**) biotite (Bt) inclusions near the sector boundaries. Photomicrographs by G. Giuliani.

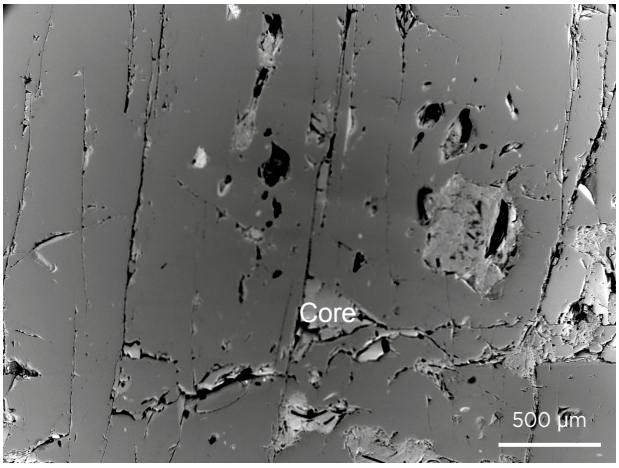

Figure 7: This BSE image of the core of trapiche ruby sample T1 shows an inclusion of Cr-poor corundum (appearing lighter grey) corresponding to the darker-coloured area seen in Figures 5b and 5c.

<100> directions (i.e. *a*-axes) in trapiche emeralds (Figure 3). Their brown colour is due to inclusions of iron oxides/hydroxides (Figures 8d, 8e, 9b and 9d) formed during a late weathering process that affected the trapiche rubies. SEM observations indicate that weathering was favoured by the high porosity of the sector boundaries, which is visible in the CT images (e.g. Figure 10). As calculated from the CT images, the porosity corresponds to a sample volume of 0.6% for T1 (total sample volume 1,720 mm³) and 0.4% for T2 (total volume 267 mm³).

Syngenetic solids were concentrated along the sector boundaries (see Table I); only a few of them were found in the adjacent growth sectors (Figures 11 and 12). There was no correlation between the position and size of inclusions in the rubies, as shown by Figure 12; large and small inclusions were mixed together. The volume occupied by all inclusions, as calculated from CT images, was 0.160 mm³ for sample T1 and 0.246 mm³ for T2 (i.e. about 0.1% and 0.9%).

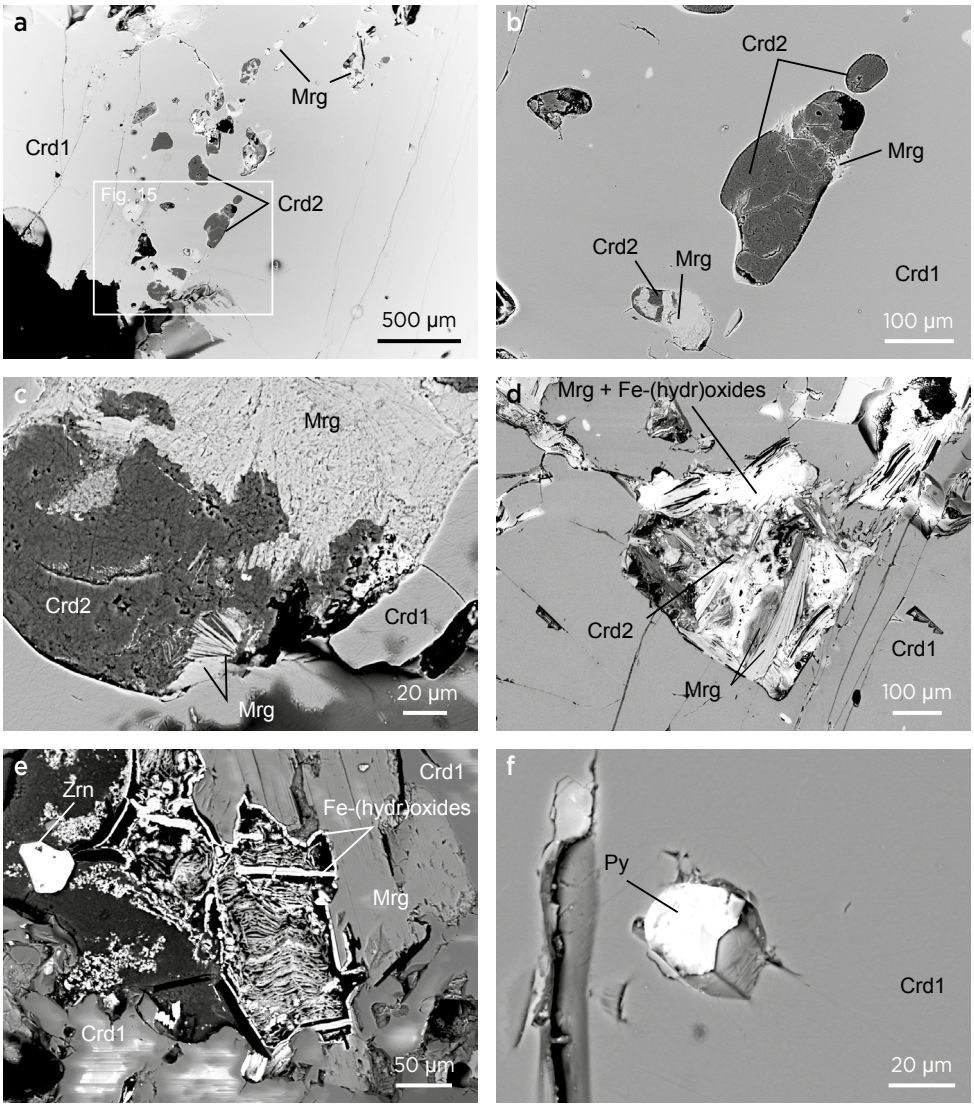

Figure 8: BSE images illustrate the nature of the various solids trapped in trapiche ruby sample T1. (**a**) Inclusions of corundum (Crd2) and margarite (Mrg) are present in the sector boundaries within the ruby (Crd1). The white rectangle corresponds to the location of Figure 15. (**b**) A closer view shows margarite partially replacing a corundum inclusion. (**c**) Margarite is present in the sector boundaries either as porous masses or as flakes developed on corundum inclusions. (**d**) Flakes of margarite are also associated with late Fe-(hydr)oxides in the sector boundaries. Remnants of corundum inclusions are also present. (**e**) Fe-(hydr)oxides are common in the sector boundaries, here associated with margarite and a zircon (Zrn) inclusion. (**f**) A pyrite (Py) inclusion is trapped within a growth sector in the trapiche ruby.

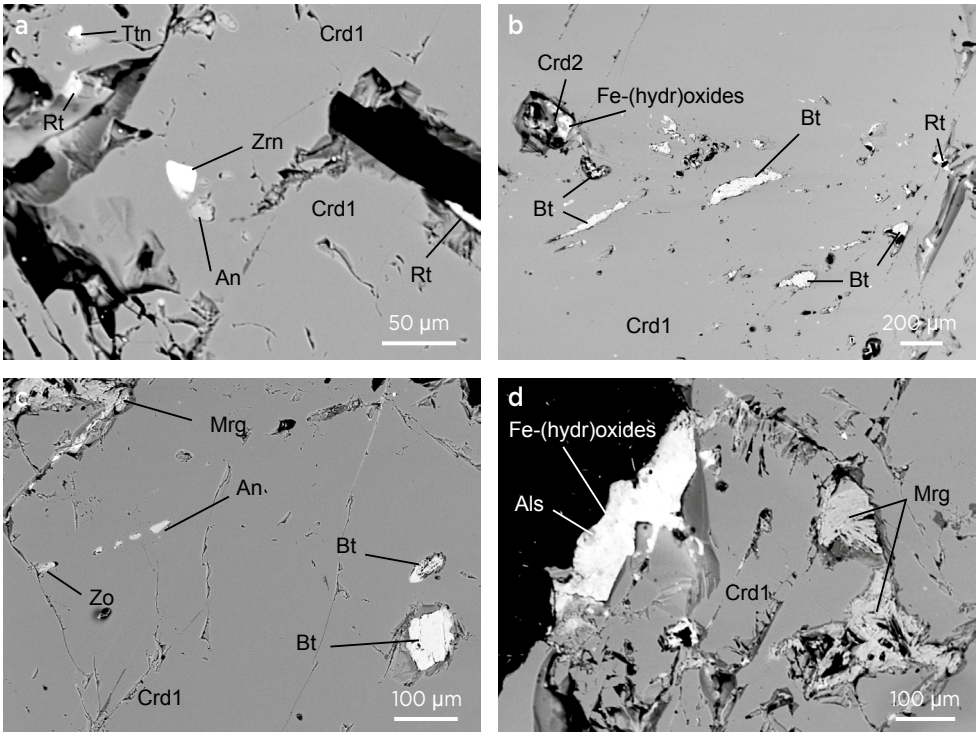

Figure 9: BSE images of sample T2 show a variety of solid inclusions in the sector boundaries of the trapiche ruby, including: (**a**) titanite (Ttn), zircon, anorthite (An) and rutile (Rt); (**b**) biotite (Bt) and corundum (Crd2); (**c**) anorthite, biotite, margarite and zoisite; and (**d**) flakes of margarite associated with Fe-(hydr)oxides and Al-silicates (Als).

The chemical compositions by EPMA of the various solids in samples T1 and T2 are reported in Table II. In sample T1, the most important syngenetic inclusions were anorthite (CaO = 20 wt.%), corundum, margarite, Al-silicates (Al_2SiO_5) and titanite; other minor phases are pyrite, calcite, zircon and rutile. Margarite was present in the sector boundaries either as porous masses (Figure 8c) or as flakes (Figure 8d) developed on corundum inclusions (Crd2—Figure 8b). In sample T2, the main inclusions were biotite and margarite, which were present along with anorthite, corundum, muscovite, rutile, titanite, zircon and zoisite. The biotite had an Fe/Mg ratio of about 1 with a composition between phlogopite and annite. The chemical composition of corundum inclusions (Crd2) is described below.

We found no supported-matrix material from the

Figure 10: This CT image shows the high porosity (here coloured blue) of trapiche ruby sample T1. The porosity corresponds to 0.6% of the sample's volume and is concentrated along the sector boundaries.

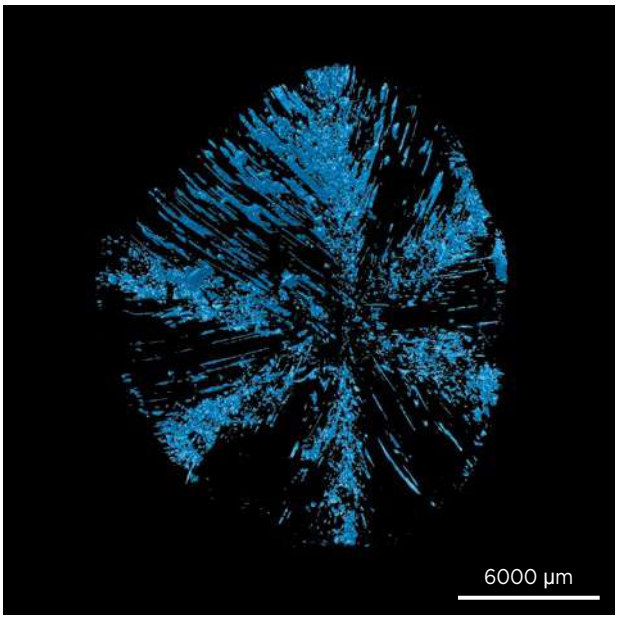

Table I: Solid inclusions observed in trapiche ruby samples T1 and T2.*

Mineral	Sample T1			Sample T2
	Sector boundary B1	Sector boundary B3	Sector boundary B5	
Anorthite	XX	XX	XX	XX
Biotite				XX
Calcite	X		X	
Corundum	XX	X	X	X
Margarite	XXX	XXX	XXX	XX
Muscovite				X
Oxides/ hydroxides of Fe (±Ti±Mn)	XXX	XXX	XXX	XXX
Pyrite	X			
Rutile	X	X		X
Al-silicates	X	X	X	X
Titanite	X	X	X	X
Zircon	X	X		X
Zoisite				X

* Symbols: XXX = main, XX = important and X = occasional phase. All are syngenetic except for the oxides/hydroxides, which are epigenetic (i.e. due to weathering).

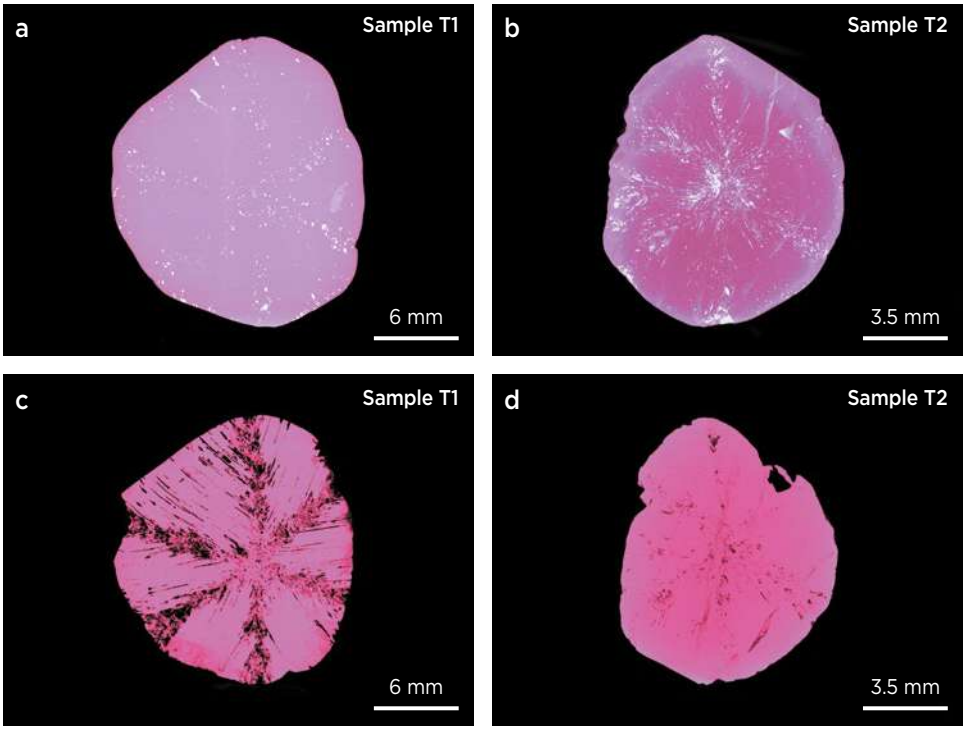

Figure 11: CT images show solid inclusions (white) and fluid inclusions (black) in trapiche ruby samples T1 and T2. (**a**) Solid inclusions in T1 are concentrated along the sector boundaries. (**b**) Tube-like inclusions in T2 are filled by solid phases. (**c**) Tube-like inclusions without solid phases developed in T1 perpendicular to the crystal's faces. (**d**) Fluid inclusions in sample T2 follow the sector boundaries.

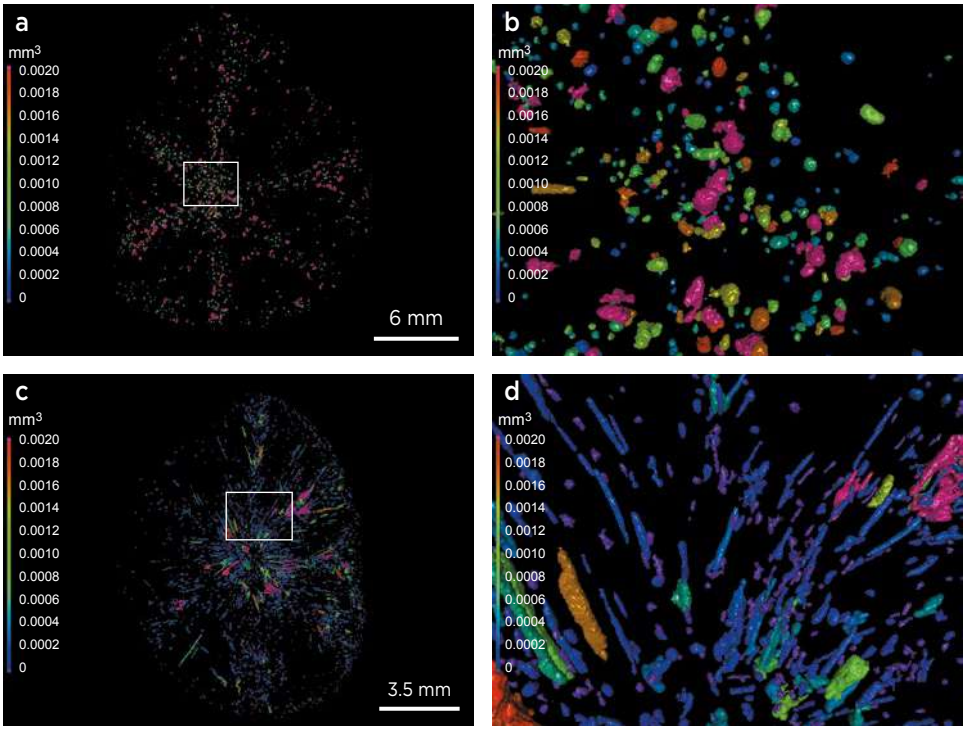

Figure 12: CT images show the spatial distribution of solid inclusions in trapiche ruby samples T1 (**a**, **b**) and T2 (**c**, **d**). The colour of each inclusion corresponds to its volume. Blue-coloured inclusions have the smallest volume and those in pink have the largest volume. The other colours represent intermediate volumes, as indicated by the coloured bar on the left side of each image.

marble host rocks incorporated along the sector boundaries of either sample. The absence of host-rock matrix from these Vietnamese rubies, as also noted previously for trapiche rubies from Mong Hsu (Schmetzer *et al.* 1996), is an important difference from the texture described for Colombian trapiche emeralds (Pignatelli *et al.* 2015).

Growth Sectors: The six growth sectors separated by the sector boundaries were sometimes fractured (e.g. sample T2; see Figure 6). The sectors could not be indexed due to the lack of a well-preserved crystal habit on the water-worn crystals, although they were most likely bounded originally by hexagonal dipyramidal faces.

Table II: Chemical composition by EPMA of solid inclusions in trapiche ruby samples T1 and T2.[a]

Oxides (wt.%)	Anorthite	Titanite	Margarite	Biotite	Muscovite	Zoisite	Corundum (Crd1)[b]	Corundum (Crd2)[b]
	T1-B1-37	T2-28	T1-B1-45	T2-13	T2-3	T2-42	T1-CS	T1-B1
Na_2O	0.90	nd	0.86	0.39	0.18	nd	na	na
MgO	nd	nd	0.38	12.15	0.45	nd	0.005	nd
Al_2O_3	36.61	4.08	52.52	23.71	36.98	33.89	99.64	99.95
SiO_2	42.23	31.81	30.30	33.51	48.25	36.92	na	na
K_2O	nd	nd	nd	10.48	10.18	nd	na	na
CaO	20.25	30.40	12.66	nd	nd	27.94	na	na
TiO_2	nd	33.96	0.03	1.61	0.01	nd	0.040	0.040
V_2O_3	nd	na	na	na	na	na	0.015	nd
Cr_2O_3	na	na	na	na	na	na	0.183	0.110
Ga_2O_3	na	na	na	nd	na	na	0.016	nd
MnO	nd	nd	nd	0.08	nd	nd	na	na
FeO	nd	nd	0.25	14.24	1.45	nd	0.160	0.160
Total	99.99	100.25	97.00	96.17	97.50	98.75	100.06	100.26

[a] Abbreviations: na = not analysed; nd = not detected.
[b] Crd1: Average values for growth sector corundum within the traverse T1-CS (22 points; see Figure 5a). Crd2: Average values for corundum inclusions within a sector boundary of T1 (five points; see Figure 15).

Elongated tube-like voids extended from the sector boundaries into the growth sectors (Figures 6b, 6c and 11d), perpendicular to the crystal faces. The tube-like voids were similar to those observed in trapiche emeralds from Colombia (Touray & Poirot 1968; Pignatelli *et al.* 2015), in trapiche rubies from Myanmar (Schmetzer *et al.* 1996; Sunagawa *et al.* 1999) and in trapiche tourmalines from Zambia (Schmetzer *et al.* 2011). CT images clearly showed that the tube-like voids in sample T2 were often filled by solid phases (Figures 11b, 12c and 12d), while those in T1 were more often fluid-filled (Figure 11c). However, closer analysis of the tomographic contrast (Figure 13) proved that the tube-like voids in sample T2 contained at least two phases: a solid and a less-dense phase (i.e. a liquid and/or a vapour). Viewed with the microscope, isolated primary fluid inclusions occurred along tube-like voids in the sector boundaries and also rarely formed cavities in the growth sectors. They were 15–50 µm wide, and sometimes showed a 'necking-down' phenomenon. At room temperature, the liquid phase occupied 30–90% of the cavity's volume and the remainder was composed of vapour. However, some of these inclusions consisted of a single phase (liquid), while others were multi-phase (liquid + vapour + solid).

Chemical Analysis of Trapiche Rubies

Three cross-sectional traverses of sample T1 and one of sample T2 were analysed by EPMA to evaluate chemical variations in the core, sector boundaries and growth sectors. Two traverses of sample T1 ran along sector

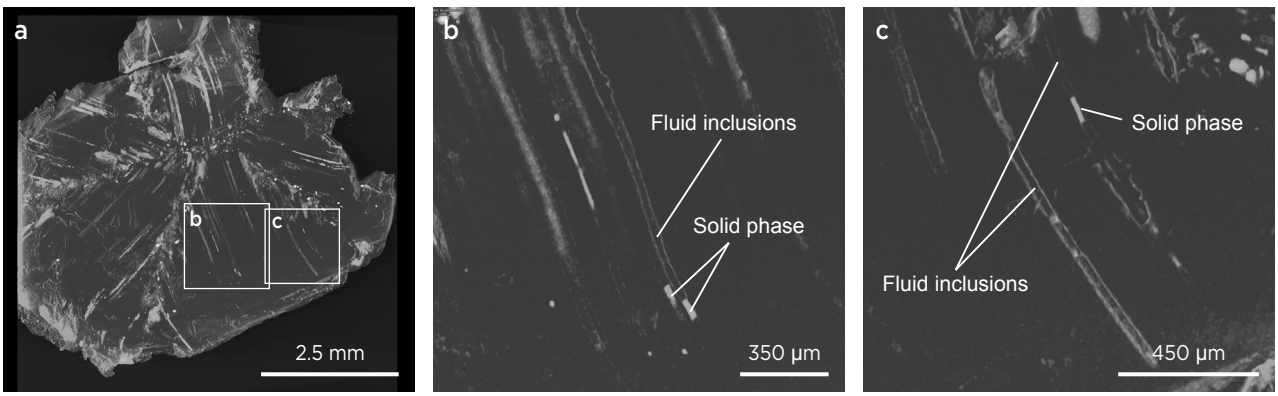

Figure 13: CT contrast images of trapiche ruby sample T2 show tube-like voids that locally contain solid phases (white) or a less-dense phase corresponding to fluid inclusions (dark grey).

boundaries from the rim to the centre (T1-B1 and T1-B3), and the third crossed the sample from rim to rim, passing through its centre (T1-CS; see Figure 5a and Tables III–V). For sample T2, one traverse was analysed between two opposite rims (CS; see Figure 6a and Table VI).

Overall, rubies T1 and T2 had some differences in chemical composition (see Tables V and VI). The Ti concentrations were lower in T2, with TiO_2 contents of 80–1,030 ppmw (vs. 40–1,470 ppmw in T1). The contents of Mg and Ga were more or less the same, with values of 20–70 ppmw for MgO and 70–240 ppmw for Ga_2O_3. Sample T1 had higher concentrations of Fe_2O_3 (1,243–1,698 ppmw) and Cr_2O_3 (1,100–3,340 ppmw). By comparison, sample T2 contained 88–1,500 ppmw Fe_2O_3 and 650–2,190 ppmw Cr_2O_3. Vanadium was much less abundant, and therefore was not the main chromophore; V_2O_3 comprised 80–210 ppmw in T1 and 60–150 ppmw in T2.

The distribution of the various chemical elements in the corundum (Crd1) along sector boundary T1-B1 is recorded in Table III and illustrated in Figure 14. The contents of Fe and V were constant, but those of Cr and Ti behaved differently. Cr_2O_3 decreased from the trapiche ruby rim (point 1—0.39 wt.%) towards the core (point 26—0.11 wt.%). This difference in Cr was not evident in

Table III: Chemical composition (wt.%) by EPMA of corundum in trapiche ruby sample T1, along sector boundary B1 shown in Figures 5a and 14, and as inclusions shown in Figure 15.*

Analysis Point	MgO	Al_2O_3	TiO_2	V_2O_3	Cr_2O_3	Fe_2O_3	Ga_2O_3	Total
Corundum (Crd1) in the Growth Sector and Near the Core								
T1-B1-1	0.007	100.00	0.009	0.011	0.388	0.137	0.018	100.57
T1-B1-2	0.005	98.02	0.009	0.012	0.366	0.139	0.014	99.57
T1-B1-3	0.008	99.41	0.029	0.012	0.326	0.130	0.017	99.93
T1-B1-4	0.002	98.67	0.011	0.016	0.325	0.146	0.019	99.19
T1-B1-5	0.005	99.02	0.015	0.012	0.333	0.139	0.014	99.54
T1-B1-6	0.003	99.78	0.009	0.011	0.312	0.164	0.018	100.30
T1-B1-7	0.006	99.86	0.040	0.017	0.268	0.153	0.017	100.36
T1-B1-8	0.007	98.93	0.048	0.018	0.270	0.100	0.016	99.39
T1-B1-9	0.005	99.65	0.050	0.015	0.268	0.153	0.017	100.16
T1-B1-10	0.002	98.07	0.034	0.014	0.258	0.147	0.021	98.55
T1-B1-11	0.002	98.07	0.034	0.014	0.258	0.147	0.021	98.55
T1-B1-12	0.004	99.20	0.015	0.011	0.222	0.149	0.020	99.62
T1-B1-13	0.010	99.22	0.057	0.019	0.232	0.147	0.020	99.70
T1-B1-14	0.005	99.42	0.054	0.017	0.214	0.148	0.015	99.87
T1-B1-15	0.006	99.00	0.027	0.016	0.210	0.147	0.019	99.42
T1-B1-16	0.006	99.67	0.034	0.014	0.214	0.152	0.028	100.12
T1-B1-17	0.007	99.84	0.050	0.017	0.184	0.157	0.016	100.27
T1-B1-18	0.005	99.08	0.063	0.017	0.199	0.155	0.016	99.54
T1-B1-19	0.004	99.76	0.020	0.016	0.168	0.155	0.020	100.14
T1-B1-20	0.009	99.53	0.024	0.015	0.163	0.160	0.017	99.92
T1-B1-21	0.002	99.60	0.023	0.014	0.141	0.150	0.017	99.95
T1-B1-22	0.004	99.49	0.062	0.017	0.155	0.164	0.015	99.91
T1-B1-23	0.006	99.85	0.050	0.018	0.120	0.155	0.017	100.21
T1-B1-24	0.004	99.95	0.055	0.016	0.124	0.161	0.017	100.33
T1-B1-25	0.005	99.57	0.069	0.018	0.122	0.160	0.016	99.96
T1-B1-26	0.008	99.85	0.020	0.018	0.109	0.184	0.011	100.20
Corundum Inclusions (Crd2) in the Sector Boundary								
1	0.002	99.50	0.020	nd*	0.100	0.200	nd	99.82
2	0.001	99.20	0.060	nd	0.090	0.100	nd	99.45
3	0.001	98.75	0.030	nd	0.150	0.150	nd	99.08
4	0.002	99.80	0.040	nd	0.110	0.160	nd	100.11
5	0.001	98.90	0.040	nd	0.010	0.170	nd	99.12

* Abbreviation: nd = not detected.

Table IV: Chemical composition (wt.%) by EPMA of corundum in sample T1 along sector boundary B3 shown in Figure 5a.

Analysis Point	MgO	Al_2O_3	TiO_2	V_2O_3	Cr_2O_3	Fe_2O_3	Ga_2O_3	Total
T1-B3-1	0.003	99.25	0.010	0.015	0.230	0.152	0.021	99.68
T1-B3-2	0.004	99.25	0.031	0.013	0.240	0.167	0.016	99.72
T1-B3-3	0.001	99.75	0.018	0.016	0.239	0.168	0.020	100.21
T1-B3-4	0.003	99.76	0.009	0.014	0.252	0.160	0.014	100.21
T1-B3-5	0.003	99.52	0.020	0.014	0.226	0.142	0.017	99.94
T1-B3-6	0.003	99.78	0.027	0.016	0.211	0.157	0.014	100.21
T1-B3-7	0.006	99.27	0.058	0.019	0.217	0.157	0.017	99.75
T1-B3-8	0.004	99.01	0.060	0.018	0.199	0.178	0.015	99.49
T1-B3-9	0.004	99.67	0.036	0.016	0.160	0.161	0.016	100.06
T1-B3-10	0.006	99.75	0.050	0.015	0.180	0.157	0.014	100.17
T1-B3-11	0.009	99.85	0.035	0.020	0.166	0.191	0.014	100.28
T1-B3-12	0.007	99.46	0.066	0.025	0.303	0.192	0.014	100.07
T1-B3-13	0.007	99.85	0.060	0.018	0.178	0.168	0.017	100.30
T1-B3-14	0.005	99.26	0.061	0.018	0.154	0.159	0.014	99.67
T1-B3-15	0.004	99.80	0.054	0.018	0.164	0.153	0.017	100.21
T1-B3-16	0.004	99.76	0.066	0.018	0.167	0.171	0.018	100.20

Table V: Chemical composition (wt.%) by EPMA of corundum in sample T1 along cross-section CS shown in Figure 5a.

Analysis Point	MgO	Al_2O_3	TiO_2	V_2O_3	Cr_2O_3	Fe_2O_3	Ga_2O_3	Total
T1-CS-1	0.007	99.82	0.009	0.009	0.334	0.128	0.017	100.33
T1-CS-2	0.003	99.40	0.013	0.016	0.262	0.145	0.019	99.86
T1-CS-3	0.004	99.40	0.037	0.016	0.244	0.158	0.018	99.88
T1-CS-4	0.004	99.68	0.086	0.016	0.207	0.147	0.018	100.16
T1-CS-5	0.004	99.69	0.042	0.015	0.193	0.157	0.016	100.11
T1-CS-6	0.003	99.61	0.021	0.014	0.114	0.141	0.014	99.92
T1-CS-7	0.003	99.51	0.037	0.014	0.149	0.149	0.008	99.87
T1-CS-8	0.007	99.62	0.058	0.018	0.143	0.158	0.021	100.02
T1-CS-9	0.005	99.31	0.147	0.021	0.159	0.169	0.024	99.84
T1-CS-10	0.003	99.53	0.051	0.019	0.150	0.170	0.012	99.93
T1-CS-11	0.004	99.83	0.004	0.012	0.110	0.152	0.012	100.12
T1-CS-12	0.007	99.55	0.072	0.016	0.139	0.162	0.015	99.96
T1-CS-13	0.005	99.49	0.065	0.019	0.136	0.159	0.015	99.89
T1-CS-14	0.005	99.76	0.035	0.017	0.143	0.154	0.016	100.13
T1-CS-15	0.007	99.84	0.038	0.017	0.163	0.161	0.011	100.24
T1-CS-16	0.007	99.87	0.016	0.013	0.111	0.143	0.018	100.18
T1-CS-17	0.007	99.05	0.021	0.013	0.176	0.145	0.016	99.43
T1-CS-18	0.006	99.85	0.020	0.014	0.209	0.151	0.021	100.27
T1-CS-19	0.003	99.97	0.013	0.016	0.205	0.134	0.018	100.36
T1-CS-20	0.006	99.66	0.015	0.014	0.210	0.153	0.018	100.08
T1-CS-21	0.001	99.97	0.009	0.017	0.206	0.131	0.013	100.35
T1-CS-22	0.004	99.74	0.009	0.008	0.253	0.124	0.012	100.15

Table VI: Chemical composition (wt.%) by EPMA of sample T2 along a traverse between opposite rims shown in Figure 6a.

Analysis Point	MgO	Al_2O_3	TiO_2	V_2O_3	Cr_2O_3	Fe_2O_3	Ga_2O_3	Total
T2-1	0.003	99.36	0.091	0.014	0.196	0.107	0.012	99.78
T2-2	0.007	99.63	0.054	0.015	0.190	0.109	0.014	100.01
T2-3	0.002	99.74	0.064	0.012	0.187	0.100	0.013	100.12
T2-4	0.004	99.74	0.076	0.012	0.184	0.143	0.009	100.17
T2-5	0.003	99.89	0.053	0.011	0.065	0.092	0.016	100.13
T2-6	0.007	99.92	0.036	0.010	0.070	0.090	0.009	100.14
T2-7	0.002	99.19	0.086	0.013	0.207	0.150	0.016	99.66
T2-8	0.002	99.23	0.052	0.012	0.155	0.099	0.013	99.56
T2-9	0.003	99.41	0.065	0.012	0.130	0.095	0.012	99.73
T2-10	0.003	99.65	0.058	0.011	0.111	0.092	0.020	99.95
T2-11	0.002	99.75	0.008	0.006	0.067	0.090	0.013	99.94
T2-12	0.005	99.33	0.060	0.012	0.144	0.104	0.017	99.67
T2-13	0.005	99.60	0.011	0.011	0.128	0.088	0.017	99.86
T2-14	0.005	99.47	0.038	0.009	0.147	0.098	0.015	99.78
T2-15	0.002	99.71	0.046	0.011	0.125	0.099	0.016	100.01
T2-16	0.005	99.98	0.059	0.010	0.160	0.097	0.014	100.32
T2-17	0.003	99.77	0.039	0.011	0.128	0.097	0.018	100.06
T2-18	0.005	99.05	0.103	0.014	0.120	0.104	0.015	99.41
T2-19	0.005	99.86	0.064	0.011	0.219	0.098	0.007	100.26

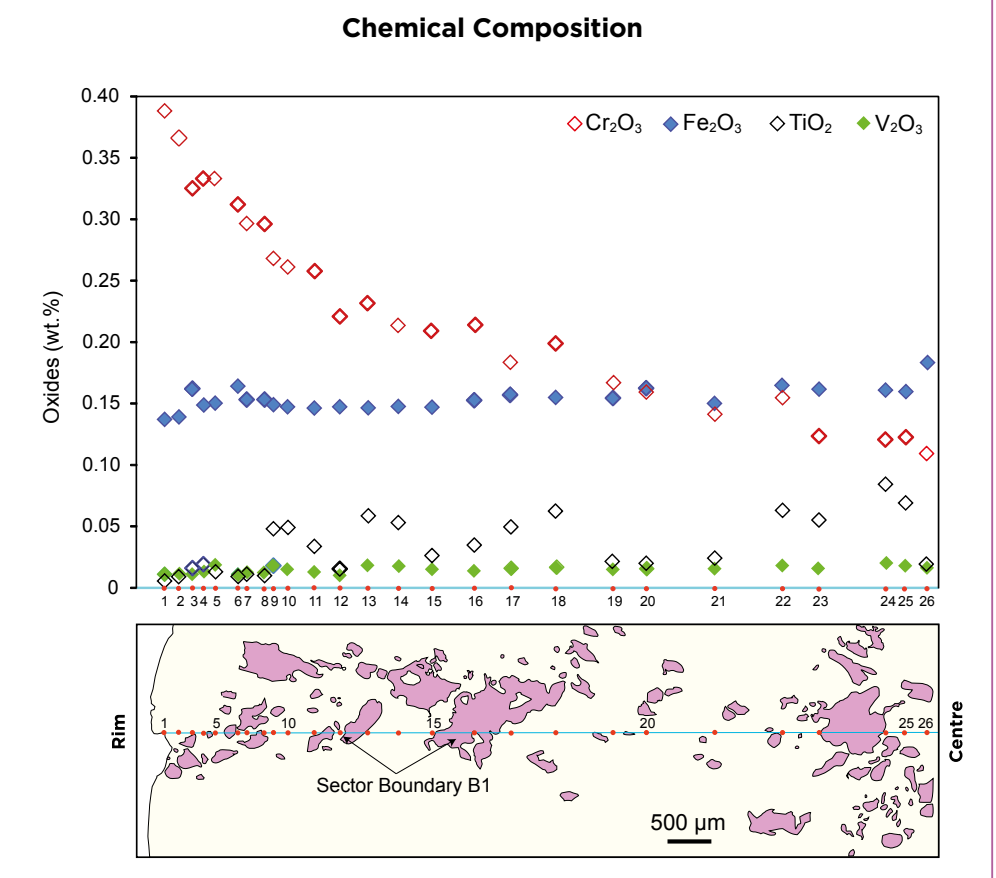

Figure 14: This graph shows variations in Cr_2O_3, Fe_2O_3, TiO_2 and V_2O_3 contents along sector boundary B1 in trapiche ruby sample T1 (see Figure 5a and Table III). The solid inclusions in this sector boundary are shown as pink in the corresponding map below the graph. The red dots in the map correspond to the EPMA point analyses of the corundum (Crd1). The Cr_2O_3 content decreases progressively from the rim towards the centre of the trapiche ruby, from 0.39 to 0.11 wt.%.

the colouration of the sample, but the regular decrease in Cr_2O_3 from the rim (point 1—0.39 wt.%) to point 11 (0.26 wt.%) indicates no sharp chemical discontinuity between the rim and the interior of the crystal. The greater Cr_2O_3 of the rim (points 1–5) corresponded to the outer 1.9 mm of the entire cross-section of the crystal (9.75 mm). The TiO_2 content increased irregularly from the rim to a maximum of 0.07 wt.% near the centre of the crystal. At the centre, the data showed the lowest Cr (and rather low Ti) but the highest Fe of the entire traverse.

The corundum inclusions (Crd2) analysed within the sector boundary (see Figure 15 and Table III) had a very different composition (average Cr_2O_3 = 0.11 wt.%; no detectable Ga_2O_3) compared to corundum Crd1 (average Cr_2O_3 = 0.18 wt.% and maximum = 0.39 wt.%; average Ga_2O_3 = 0.16 wt.%). The average Cr_2O_3 content of the corundum inclusions was similar to the lowest Cr content measured near the centre of sample T1 (see Table III, analysis point T1-B1-26).

The chemical concentrations were plotted in the correlation diagram of Cr_2O_3/Ga_2O_3 versus Fe_2O_3/TiO_2 proposed by Sutherland *et al.* (2003) and applied by Pham *et al.* (2004) to Vietnamese rubies from the Luc Yen and An Phu areas (Figure 16). Overall, the present data plot within the fields of (1) primary non-trapiche ruby-bearing marble deposits and (2) alluvial trapiche rubies from marble-hosted deposits at Luc Yen and An Phu of Pham *et al.* (2004). The chemical compositions of the alluvial trapiche rubies from various localities in Vietnam are presented in Appendix Table A-I.

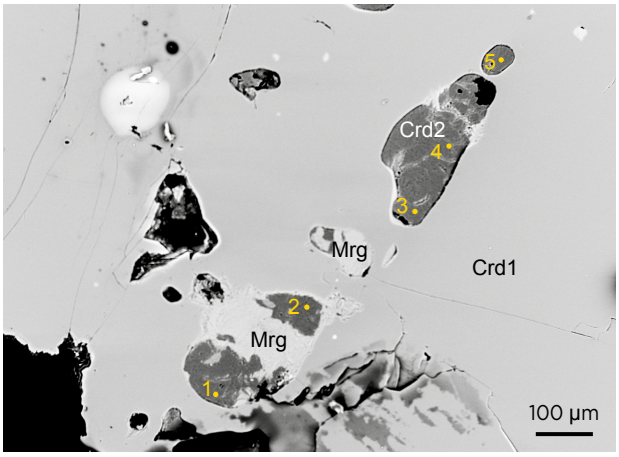

Figure 15: This BSE image (corresponding to the white rectangle in Figure 8a) shows the location of five EPMA analyses of the corundum inclusions (Crd2) in sector boundary B1 of the trapiche ruby (Crd1) sample T1.

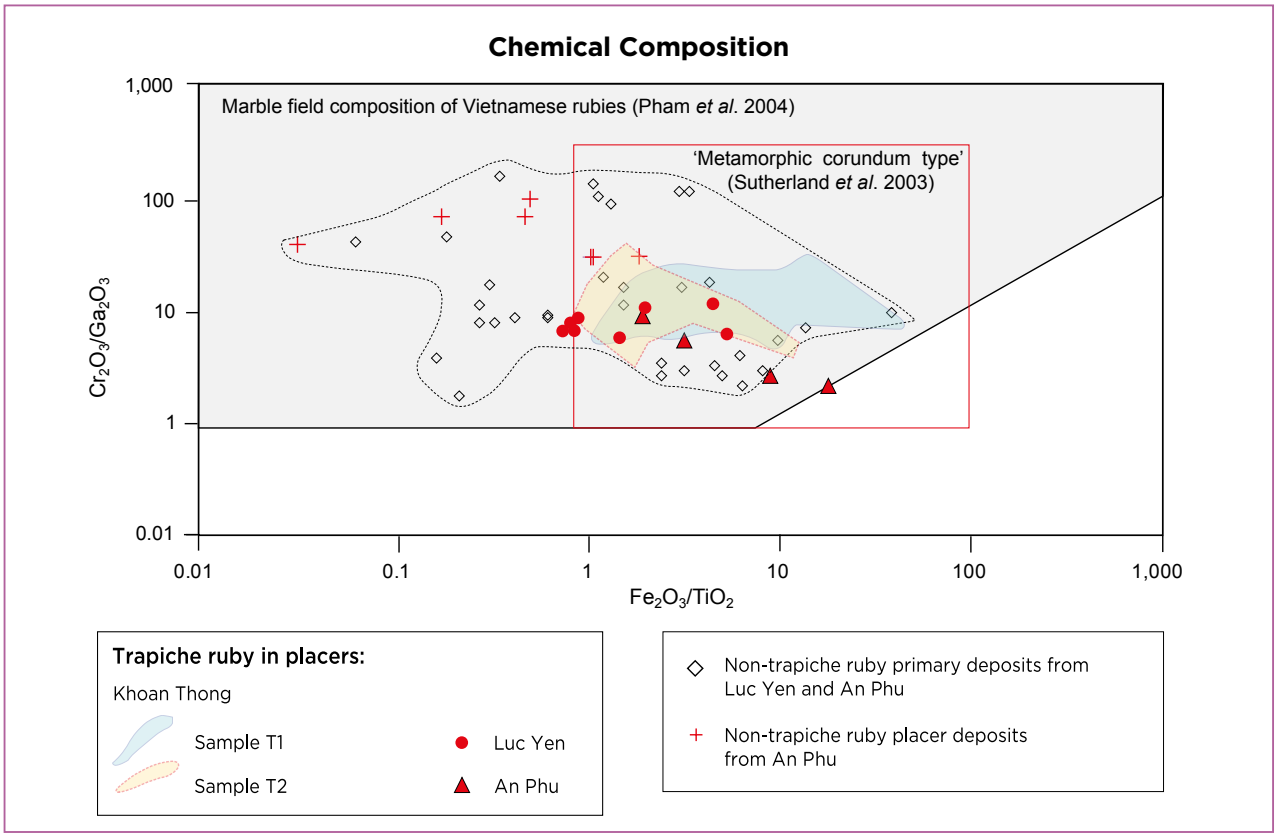

Figure 16: Chemical data for the two trapiche ruby samples (87 point analyses) from Khoan Thong plot within the marble composition field of Vietnamese rubies, as shown in this diagram of Cr_2O_3/Ga_2O_3 versus Fe_2O_3/TiO_2. Shown for comparison are data for trapiche and non-trapiche rubies from different primary and secondary deposits in Vietnam (Pham *et al.* 2004).

DISCUSSION

The solid inclusions observed in the two trapiche rubies from the Khoan Thong placer are dominated by the association anorthite-corundum-margarite. Calcite was found in small amounts and dolomite was absent. The association between coexisting anorthite and margarite with corundum has been documented for Asian ruby-bearing marble deposits (Garnier 2003; Garnier *et al.* 2008). These petrographic relations have shown that ruby and anorthite could form by destabilisation of margarite during prograde metamorphism such as described for the Jegdalek (Afghanistan) and An Phu (Vietnam) deposits (Garnier 2003). Inversely, margarite formed in the presence of water during retrograde metamorphism (Garnier 2003), following reaction 1 (Figure 17):

margarite ↔ anorthite + corundum + water (1)

$CaAl_2(Si_2Al_2)O_{10}(OH)_2 \leftrightarrow CaAl_2Si_2O_8 + Al_2O_3 + H_2O$

Margarite formation at the expense of corundum and anorthite was observed in both samples T1 and T2 (e.g. Figure 8). This retrograde transformation occurred at temperatures between 450 and 500°C (Garnier *et al.* 2008; see Figure 17).

The other chemical reactions involved in the formation of ruby in marbles (Garnier *et al.* 2008) are due to:

- the destabilisation of muscovite, as described at Jegdalek (Afghanistan) and at the Bai Da Lan deposits in the Luc Yen mining area (Garnier 2003):

muscovite ↔ K-feldspar + corundum + water (2)

$KAl_2(Si_3Al)O_{10}(OH)_2 \leftrightarrow KAlSi_3O_8 + Al_2O_3 + H_2O$

- the destabilisation of sapphirine, as evidenced at the deposit in Hunza (Pakistan):

sapphirine + 4 water ↔ 2 spinel + 6 corundum + Mg-chlorite (3)

$Mg_7Al_{18}Si_3O_{40} + 4H_2O \leftrightarrow 2MgAl_2O_4 + 6Al_2O_3 + Mg_5Al(Si_3Al)O_{10}(OH)_8$

- the destabilisation of paragonite, as evidenced at the Hunza and Nangimali (Pakistan) deposits:

paragonite ↔ albite + corundum + water (4)

$NaAl_2(Si_3Al)O_{10}(OH)_2 \leftrightarrow NaAlSi_3O_8 + Al_2O_3 + H_2O$

- the destabilisation of spinel in contact with calcite during retrograde metamorphism (Figure 17), which is the most common reaction, as evidenced at Jegdalek, Hunza and Luc Yen (Garnier *et al.* 2008):

spinel + calcite + CO_2 ↔ corundum + dolomite (5)

$MgAl_2O_4 + CaCO_3 + CO_2 \leftrightarrow Al_2O_3 + CaMg(CO_3)_2$

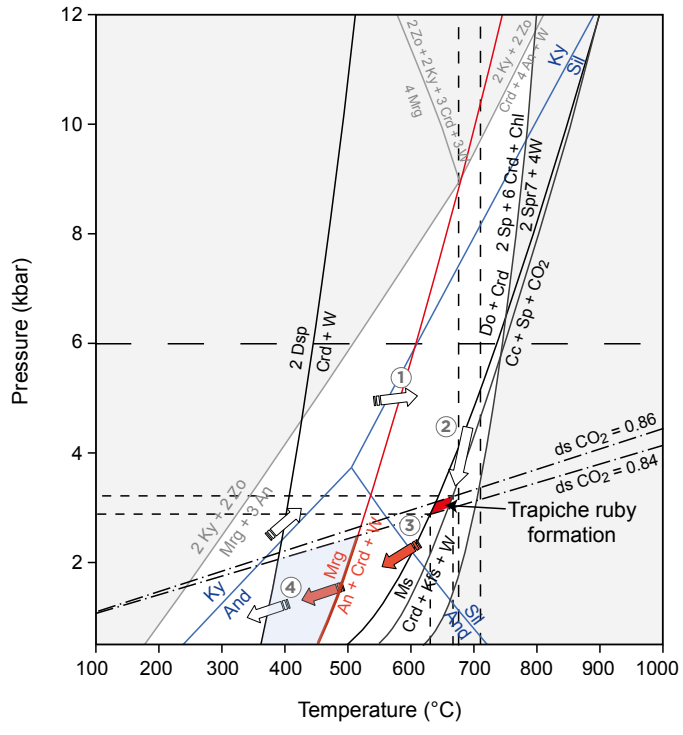

Figure 17: This pressure-temperature diagram shows the conditions of stability for mineral associations in ruby-bearing marbles from Luc Yen (modified from Garnier *et al.* 2008). White arrows 1 and 2 represent different possibilities for forming corundum during prograde metamorphism. The red arrows represent the formation of corundum during retrograde metamorphism (3) and then the transformation of corundum to margarite (4). Abbreviations: An = anorthite, And = andalusite, Cc = calcite, Clin = clinochlore, Crd = corundum, Do = dolomite, Dsp = diaspore, Ksp = K-feldspar, Ky = kyanite, Mrg = margarite, Mu = muscovite, Sil = sillimanite, Spr = sapphirine, Sp = spinel, W = water and Zo = zoisite.

The rubies that form from reaction 5 commonly have calcite and dolomite inclusions trapped either in growth sectors (Peretti *et al.* 1995; Giuliani *et al.* 2018) or in tube-like voids in trapiche rubies (Schmetzer *et al.* 1996, 1999; Giuliani *et al.* 2018). The very low amount of carbonates in trapiche rubies from Khoan Thong cannot exclude their formation in marble. Although the anorthite-corundum-margarite metamorphic assemblage is uncommon for the marble-type deposits, it was already described for the An Phu ruby-bearing marble deposit located south of Khoan Thong (Garnier 2003).

The mineral inclusion assemblage in the Khoan Thong trapiche rubies (Table VII) is completed by micas (biotite and muscovite, in addition to margarite mentioned above), Al-silicates (Al_2SiO_5), anorthite, calcite, pyrite, rutile, titanite, zoisite and zircon, as well as secondary oxide/hydroxides of Fe (±Ti±Mn).

The chemical composition of the trapiche rubies from Khoan Thong plots within the field of Vietnamese marble-hosted rubies (Figure 16). When the data are plotted in a diagram of Fe_2O_3/TiO_2 versus Cr_2O_3 (Figure 18), the Khoan Thong rubies show a similar Fe_2O_3/TiO_2 ratio but somewhat higher Cr_2O_3 contents compared to analyses of trapiche rubies from the An Phu, Luc Yen and Yen Bai mining areas (Pham *et al.* 2004). The diagram also shows that trapiche rubies from northern Vietnam can be distinguished from those of Quy Chau in central Vietnam (Pham *et al.* 2004) and Mong Hsu in Myanmar (Garnier *et al.* 2002a, b). This is due to the higher TiO_2 (up to 0.38 wt.%) and lower Fe_2O_3 (less than 0.01 wt.%) contents of Quy Chau and Mong Hsu rubies.

Table VII: Solid inclusions identified in Khoan Thong samples T1 and T2, compared to those recorded in trapiche rubies from Mong Hsu.

Solid inclusions	Mong Hsu (Myanmar)			Khoan Thong (Vietnam)
	Schmetzer *et al.* (1996, 1999)	Sunagawa *et al.* (1999)	Garnier *et al.* (2002a, b)	This work
Calcite	X	X	X	X
Dolomite	X	X	X	
Silicates (K-Al-Fe±Ti)	X	X	X	X
Corundum		X	X	X
Muscovite				X
Biotite				X
Chlorite			X	
Andularia			X	
Rutile			X	X
Titanite			X	X
Graphite			X	
Baryte			X	
Pyrite			X	X
Mica			X	
Amphibole			X	
Zircon			X	X
Al-hydroxide			X	
Oxides/ hydroxides of Fe (±Ti±Mn)			X	X
Siderite			X	
Bastnaesite			X	
Anorthite				X
Margarite				X
Zoisite				X

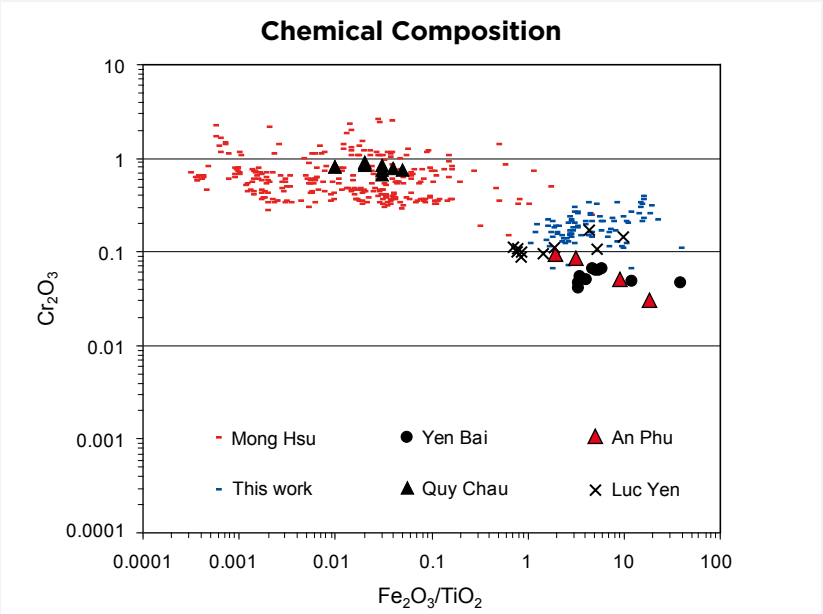

Figure 18: A plot of Cr_2O_3 versus Fe_2O_3/TiO_2 for the trapiche rubies from Khoan Thong analysed in this study is compared to data for trapiche rubies from Mong Hsu (Myanmar; Garnier *et al.* 2002b) and various Vietnamese deposits (Pham *et al.* 2004). Stones from Quy Chau (central Vietnam) and Mong Hsu have overlapping compositions, while those from northern Vietnam contain less Cr_2O_3 and have a greater ratio of Fe_2O_3/TiO_2.

According to the genetic model proposed for marble-hosted ruby deposits in Central and South East Asia by Garnier *et al.* (2008), the Vietnamese rubies formed during Tertiary regional metamorphism and are spatially related to major tectonic structures formed during the Himalayan orogenesis. The sediments of the Paleo-Tethys basin were metamorphosed in the amphibolite facies, transforming carbonates into marbles. The Al, Cr and V necessary for the formation of ruby were mobilised from micas, clay minerals and/or organic matter present in the sedimentary photoliths. Rubies formed during the beginning of the retrograde metamorphic path at 620–670°C and 2.6–3.3 kbar (Garnier 2003). The trapiche rubies formed from the same parental fluids as non-trapiche rubies in the same metamorphic zones within the Luc Yen and An Phu mining areas (Giuliani *et al.* 2015a, 2018). Moreover, the transformation of ruby and anorthite to margarite occurred at lower temperature and pressure conditions (450–500°C and <2 kbar) during retrograde metamorphism.

It is worth noting that the corundum inclusions in the sector boundaries have a similar composition as the small inclusion at the centre of sample T1 (Table III), suggesting that they formed at the same time and under the same conditions. This also means that the trapiche texture formed very quickly, such that the core did not have enough time to develop. According to the formation model proposed by Sunagawa *et al.* (1999), the core seems to be 'frozen' just after the nucleation stage (step 1 in Figure 19). Its development is hindered by the rapid formation of the sector boundaries which enveloped it (step 2). The growth sectors developed at a later stage (step 3), filling the interstices left between the sector boundaries. The rapid formation of the trapiche texture is proven by the elevated number of trapped inclusions and the formation of tube-like voids. When an inclusion is trapped, a channel can develop in the growth direction behind the inclusion, or in front of it if the inclusion moves along the growth direction. This formation mechanism was proposed for similar voids in trapiche tourmalines (Schmetzer *et al.* 2011). However, the fact that the tube-like voids are perpendicular to the faces of the ruby crystals suggests another possible mechanism of formation. They also could form by dissolution along bundles of dislocations after changes in driving-force conditions that occurred during the crystal growth (Scandale & Zarka 1982; Authier & Zarka 1994).

The three growth steps are governed by changes in driving-force conditions (Sunagawa *et al.* 1999). First, a small core can form under low driving-force conditions through layer-by-layer growth (step 1). After driving-force conditions increase, adhesive-type growth takes place, forming the sector boundaries, which constitute the 'skeleton' of the trapiche ruby (step 2). Finally, a decrease in the driving force lets the growth sectors and corresponding crystal faces develop through ordinary layer-by-layer growth (step 3). The morphological stability of the interface is dependent on the driving-force conditions (Sunagawa 2005). At the beginning, a

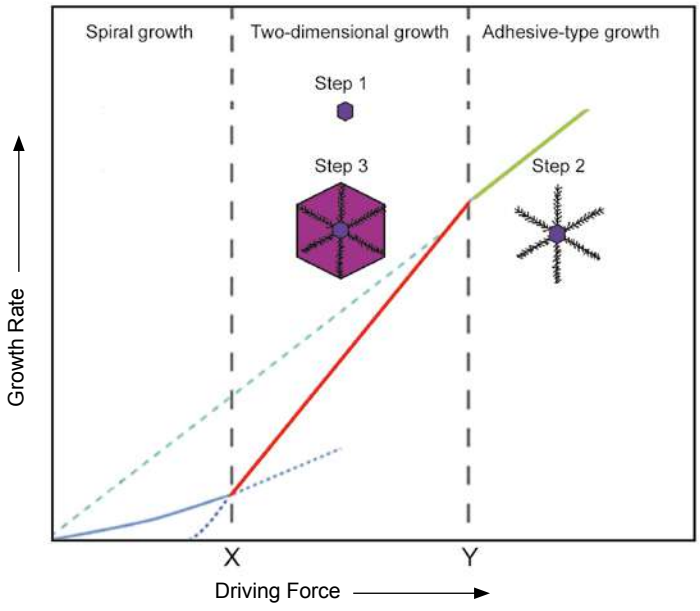

Figure 19: A diagram of growth rate versus driving force of crystallisation (modified from Sunagawa *et al.* 1999) shows the three development steps for trapiche texture in rubies from Khoan Thong. The positions marked by X and Y indicate changes in the predominant growth mechanism according to the driving force of crystallisation. The coloured lines represent growth rate versus driving force relations for spiral, two-dimensional and adhesive-type growth mechanisms. The dashed lines indicate where a particular growth mechanism is not stable.

core with smooth, flat interfaces forms, but when the driving force increases, the interface morphology loses its stability, resulting in one that is rough and dendritic. A further change in driving-force conditions will yield a euhedral ruby bounded by flat faces, with the dendritic 'skeleton' visible inside (Sunagawa 2005).

The changes in the driving-force conditions reflect variations in the growth medium (i.e. fluid composition, temperature and/or pressure). The fluid composition does not change during the rapid development of the trapiche texture, as witnessed by the fact that the corundum in the centre of the trapiche ruby has almost the same chemistry as the corundum inclusions (Crd2) in the sector boundaries. A variation of temperature was hypothesised by Garnier *et al.* (2002a) to explain the formation of Mong Hsu trapiche rubies. They suggested that the layer-by-layer growth became unstable when supercooling occurred and adhesive-type growth took over to form the sector boundaries. The chemical elements not included in the crystal structure of corundum (e.g. Ca and Mg) were pushed towards the sector boundaries and contributed to the formation of solid inclusions there. However, a rapid cooling is in disagreement with the rather stable thermal conditions of the regional metamorphism in Central and South East Asia (Giuliani *et al.* 2018).

A more plausible hypothesis involves variations in fluid pressure. The devolatilisation reactions of carbonate rocks during metamorphism produced a fluid overpressure until hydraulic fracturing occurred and, therefore, provoked an increase in the driving force. At this stage, the core and sector boundaries would have formed quickly and almost at the same time. The opening of fractures and cavities in the marbles led to a decrease of fluid pressure and, therefore, of the driving force (Giuliani *et al.* 2018). This allowed for the formation of the growth sectors that completed the trapiche texture.

CONCLUSIONS

The main conclusions of this study of two trapiche rubies from Khoan Thong can be summarised as follows:

(1) The expected hexagonal core is not well developed, and elongated tube-like voids extend from the sector boundaries into the growth sectors. The voids are filled by solid and fluid inclusions. The sector boundaries contain different syngenetic solid inclusions, in particular margarite that formed at the expense of ruby and anorthite during the retrograde metamorphic path.

Figure 20: This ruby from Tai Dinh near Minh Tien in northern Vietnam exhibits well-developed trapiche texture. Photo by Shang-i (Edward) Liu.

(2) Their chemical composition plots within the field of Vietnamese rubies hosted in marbles. Their Fe_2O_3/TiO_2 ratios (>1) are higher than those of trapiche rubies from Quy Chau (central Vietnam) and Mong Hsu (Myanmar), while their Cr_2O_3 contents are lower (<0.39 wt.%).

(3) The main mineral assemblage of inclusions in equilibrium—anorthite and ruby—has been described for several non-trapiche rubies hosted in marbles from Central and South East Asia, such as at An Phu, Vietnam. The very low amount of calcite and the absence of dolomite in the Khoan Thong trapiche rubies does not mean that these rubies could not have formed from the metamorphism of marble. It signifies that ruby did not form by the main metamorphic reaction involving the formation of corundum and dolomite through the destabilisation of spinel and calcite.

(4) A change of fluid pressure during formation was likely caused by local decompression and fracturing in the marbles. Such pressure variations enhance changes in driving-force conditions, leading to the formation of trapiche texture (e.g. Figure 20). The core forms first, followed by the sector boundaries and then the growth sectors, under high and low driving-force conditions, respectively.

REFERENCES

Authier, A. & Zarka, A. 1994. X-ray topographic study of the real structure of minerals. *In*: Marfunin, A.S. (ed) *Advanced Mineralogy Vol. 1—Composition, Structure, and Properties of Mineral Matter: Concepts, Results, and Problems*, Springer-Verlag, Berlin and Heidelberg, Germany, 221–233.

Garnier, V. 2003. *Les gisements de rubis associés aux marbres de l'Asie Centrale et du Sud-est: Génèse et caractérisation isotopique*. Ph.D. thesis, National Polytechnic Institute of Lorraine, Nancy, France, 390 pp.

Garnier, V., Ohnenstetter, D., Giuliani, G. & Schwarz, D. 2002a. Rubis trapiches de Mong Hsu, Myanmar. *Revue de Gemmologie A.F.G.*, No. 144, 5–12.

Garnier, V., Ohnenstetter, D., Giuliani, G., Blanc, P. & Schwarz, D. 2002b. Trace-element contents and cathodoluminescence of 'trapiche' rubies from Mong Hsu, Myanmar (Burma): Geological significance. *Mineralogy and Petrology*, **76**(3–4), 179–193, http://doi.org/10.1007/s007100200040.

Garnier, V., Giuliani, G., Ohnenstetter, D., Fallick, A.E., Dubessy, J., Banks, D., Vinh, H.Q., Lhomme, T., *et al.* 2008. Marble-hosted ruby deposits from Central and Southeast Asia: Towards a new genetic model. *Ore Geology Reviews*, **34**(1–2), 169–191, http://doi.org/10.1016/j.oregeorev.2008.03.003.

Giuliani, G., Dubessy, J., Banks, D., Hoàng, Q.V., Lhomme, T., Pironon, J., Garnier, V., Phan Trong, T., *et al.* 2003. CO_2–H_2S–COS–S_8–AlO(OH)-bearing fluid inclusions in ruby from marble-hosted deposits in Luc Yen area, North Vietnam. *Chemical Geology*, **194**(1–3), 167–185, http://doi.org/10.1016/s0009-2541(02)00276-0.

Giuliani, G., Dubessy, J., Banks, D.A., Lhomme, T. & Ohnenstetter, D. 2015a. Fluid inclusions in ruby from Asian marble deposits: Genetic implications. *European Journal of Mineralogy*, **27**(3), 393–404, http://doi.org/10.1127/ejm/2015/0027-2442.

Giuliani, G., Boiron, M.-C., Morlot, C., Raoul, J. & Chatagnier, P.-Y. 2015b. Gem News International: Demantoid garnet with giant fluid inclusions. *Gems & Gemology*, **51**(4), 446–448.

Giuliani, G., Dubessy, J., Pignatelli, I. & Schwarz, D. 2018. Fluid inclusions study of trapiche and non-trapiche rubies from the Mong Hsu deposit, Myanmar. *Canadian Mineralogist*, **56**(5), 691–703, http://doi.org/10.3749/canmin.1800013.

Hainschwang, T., Notari, F. & Anckar, B. 2007. Trapiche tourmaline from Zambia. *Gems & Gemology*, **43**(1), 36–46, http://doi.org/10.5741/gems.43.1.36.

Hlaing, T. 1991. A new Myanmar ruby deposit. *Australian Gemmologist*, **17**(2), 509–510.

Karampelas, S., Michel, J., Zheng-Cui, M., Schwarz, J.-O., Enzmann, F., Fritsch, E., Leu, L. & Krzemnicki, M.S. 2010. X-ray computed microtomography applied to pearls: Meth-odology, advantages, and limitations. *Gems & Gemology*, **46**(2), 122–127, http://doi.org/10.5741/gems.46.2.122.

Leloup, P.H. & Kienast, J.-R. 1993. High-temperature metamorphism in a major strike-slip shear zone: The Ailao Shan–Red River, People's Republic of China. *Earth and Planetary Science Letters*, **118**(1–4), 213–234, http://doi.org/10.1016/0012-821x(93)90169-a.

Leloup, P.H., Lacassin, R., Tapponnier, P., Schärer, U., Zhong, D., Liu, X., Zhang, L., Ji, S., *et al.* 1995. The Ailao Shan–Red River shear zone (Yunnan, China), Tertiary transform boundary of Indochina. *Tectonophysics*, **251**(1–4), 3–84, http://doi.org/10.1016/0040-1951(95)00070-4.

Leloup, P.H., Arnaud, N., Lacassin, R., Kienast, J.R., Harrison, T.M., Trong, T.T.P., Replumaz, A. & Tapponnier, P. 2001. New constraints on the structure, thermochronology, and timing of the Ailao Shan-Red River shear zone, SE Asia. *Journal of Geophysical Research: Solid Earth*, **106**(B4), 6683–6732, http://doi.org/10.1029/2000jb900322.

McKague, H.L. 1964. Trapiche emeralds from Colombia, Part I. *Gems & Gemology*, **11**(7), 210–223.

Morlot, C., Pignatelli, I., Giuliani, G., Sterpenich, J., Boiron, M.-C., Ohnenstetter, D., Andriamamonjy, A., Raoul, J., *et al.* 2016. La tomographie à rayons X et ses applications en gemmologie : exemples de l'émeraude trapiche et du grenat démantoïde. *Revue de Gemmologie A.F.G.*, No. 198, 13–18.

Nam, T.N., Toriumi, M. & Itaya, T. 1998. P–T–t paths and post-metamorphic exhumation of the Day Nui Con Voi shear zone in Vietnam. *Tectonophysics*, **290**(3–4), 299–318, http://doi.org/10.1016/s0040-1951(98)00054-7.

Nassau, K. & Jackson, K.A. 1970. Trapiche emeralds from Chivor and Muzo, Colombia. *American Mineralogist*, **55**(3–4), 416–427.

Peretti, A., Schmetzer, K., Bernhardt, H.-J. & Mouawad, F. 1995. Rubies from Mong Hsu. *Gems & Gemology*, **31**(1), 2–26, http://doi.org/10.5741/gems.31.1.2.

Peretti, A., Mullis, J. & Mouawad, F. 1996. The role of fluorine in the formation of colour zoning in rubies from Mong Hsu, Myanmar (Burma). *Journal of Gemmology*, **25**(1), 3–19, http://doi.org/10.15506/JoG.1996.25.1.3.

Pham, V.L., Hoàng, Q.V., Garnier, V., Giuliani, G. & Ohnenstetter, D. 2004. Marble-hosted ruby from Vietnam. *Canadian Gemmologist*, **25**(3), 83–95.

Pham, V.L., Pardieu, V. & Giuliani, G. 2013. Update on gemstone mining in Luc Yen, Vietnam. *Gems & Gemology*, **49**(4), 233–245, http://doi.org/10.5741/gems.49.4.233.

Pham, V.L., Giuliani, G., Fallick, A.E., Boyce, A.J. & Pardieu, V. 2018. Trace elements and oxygen isotopes of gem spinels in marble from the Luc Yen – An Phu areas, Yen Bai Province, North Vietnam. *Vietnam Journal of Earth Sciences*, **40**(2), 165–177, http://doi.org/10.15625/0866-7187/40/2/12241.

Pignatelli, I., Giuliani, G., Ohnenstetter, D., Agrosi, G., Mathieu, S., Morlot, C. & Branquet, Y. 2015. Colombian trapiche emeralds: Recent advances in understanding their formation. *Gems & Gemology*, **51**(3), 222–259, http://doi.org/10.5741/gems.51.3.222.

Pignatelli, I., Giuliani, G., Morlot, C., Rouer, O., Claiser, N., Chatagnier, P.-Y. & Goubert, D. 2017. Recent advances in understanding the similarities and differences of Colombian euclases. *Canadian Mineralogist*, **55**(4), 799–820, http://doi.org/10.3749/canmin.1700011.

Richard, A., Morlot, C., Créon, L., Beaudoin, N., Balitsky, V.S., Pentelei, S., Dyja-Person, V., Giuliani, G., *et al.* 2019. Advances in 3D imaging and volumetric reconstruction of fluid and melt inclusions by high resolution X-ray computed tomography. *Chemical Geology*, **508**, 3–14, http://doi.org/10.1016/j.chemgeo.2018.06.012.

Scandale, E. & Zarka, A. 1982. Sur l'origine des canaux dans les cristaux. *Journal of Applied Crystallography*, **15**(4), 417–422, http://doi.org/10.1107/s0021889882012291 (in French).

Schmetzer, K., Beili, Z., Yan, G., Bernhardt, H.-J. & Hänni, H.A. 1999. Element mapping of trapiche rubies. *Journal of Gemmology*, **26**(5), 289–301, http://doi.org/10.15506/JoG.1999.26.5.289.

Schmetzer, K., Bernhardt, H.-J. & Hainschwang, T. 2011. Chemical and growth zoning in trapiche tourmaline from Zambia — A re-evaluation. *Journal of Gemmology*, **32**(5), 151–173, http://doi.org/10.15506/JoG.2011.32.5.151.

Schwarz, D., Bernhardt, H.-J., Hänni, H.A. & Schmetzer, K. 1996. Trapiche rubies. *Gems & Gemology*, **32**(4), 242–250, http://doi.org/10.5741/gems.32.4.242.

Sunagawa, I. 2005. *Crystals: Growth, Morphology and Perfection*. Cambridge University Press, Cambridge, 295 pp.

Sunagawa, I., Bernhardt, H.-J. & Schmetzer, K. 1999. Texture formation and element partitioning in trapiche ruby. *Journal of Crystal Growth*, **206**(4), 322–330, http://doi.org/10.1016/s0022-0248(99)00331-0.

Sutherland, F.L., Coenraads, R.R., Schwarz, D., Raynor, L.R., Barron, B.J. & Webb, G.B. 2003. Al-rich diopside in alluvial ruby and corundum-bearing xenoliths, Australian and SE Asian basalt fields. *Mineralogical Magazine*, **67**(4), 717–732, http://doi.org/10.1180/0026461036740129.

Touray, J.C. & Poirot, J.P. 1968. Observations sur les inclusions fluides primaires de l'émeraude et leurs relations avec les inclusions solides. *Comptes Rendus de l'Académie des Sciences, Paris*, **266**, Série D, 305–308.

Win, K.K. 2005. Trapiche of Myanmar. *Australian Gemmologist*, **22**(6), 269–270.

The Authors

Dr Isabella Pignatelli
Université de Lorraine, GeoResources UMR 7359 CNRS-UL, BP 70239, 54506 Vandœuvre-lès-Nancy cedex, France
Email: isabella.pignatelli@univ-lorraine.fr

Dr Gaston Giuliani
Université Paul Sabatier, GET/IRD, UMR CNRS-IRD-CNES 5563, 14 avenue Edouard Belin, 31400 Toulouse, France

and

Université de Lorraine, CRPG UMR 7358 CNRS-UL, 15 rue Notre-Dame-des-Pauvres, BP 20, 54501 Vandœuvre-lès-Nancy cedex, France

Christophe Morlot
Université de Lorraine, GeoResources UMR 7359 CNRS-UL, BP 70239, 54506 Vandœuvre-lès-Nancy cedex, France

Dr Pham Van Long
Institute for Gems and Gold Research of Vinagems, 15 Ngoc Hoi, Hoang Liet, Hoang Mai, Hanoi, Vietnam

Acknowledgements

The authors thank Dr Olivier Rouer of the Service Commun de Microscopie Électronique et de Microanalyses laboratory at the University of Lorraine for the EPMA analyses. Corrections and suggestions from three anonymous reviewers helped improve the final version of the manuscript. We also thank Dr Shang-i (Edward) Liu for the photographs in Figures 1 and 20.

APPENDIX

Table A-1: Chemical composition (wt.%) by EPMA of alluvial trapiche rubies from the An Phu, Luc Yen, Yen Bai and Quy Chau mining areas in Vietnam (Pham *et al.* 2004; G. Giuliani unpublished data).

Analysis	MgO	Al_2O_3	TiO_2	V_2O_3	Cr_2O_3	Fe_2O_3	Ga_2O_3	Total
An Phu (Northern Vietnam)								
AP1	nd	98.73	0.080	0.005	0.080	0.255	0.014	99.16
AP2	nd	98.60	0.127	0.006	0.092	0.246	0.009	99.08
AP3	nd	98.75	0.015	0.006	0.029	0.279	0.013	99.09
AP4	nd	99.19	0.023	0.006	0.048	0.297	0.018	99.58
Luc Yen (Northern Vietnam)								
LY1	0.001	99.36	0.196	0.004	0.087	0.173	0.010	99.83
LY2	0.001	99.70	0.216	0.007	0.103	0.174	0.015	100.22
LY3	0.001	99.67	0.228	0.005	0.098	0.178	0.014	100.19
LY4	0.001	99.85	0.275	0.006	0.107	0.200	0.016	100.45
LY5	nd	99.81	0.123	0.004	0.095	0.179	0.015	100.23
LY6	nd	100.06	0.089	0.008	0.107	0.172	0.010	100.45
LY7	0.001	99.73	0.208	0.003	0.096	0.178	0.016	100.23
LY8	nd	99.77	0.031	0.006	0.103	0.166	0.015	100.09
LY9	nd	99.72	0.016	0.006	0.142	0.162	0.013	100.06
LY10	0.001	99.46	0.038	0.015	0.166	0.164	0.015	99.86
Yen Bai (Northern Vietnam)								
YB1	nd	100.88	0.086	0.005	0.044	0.288	0.007	101.31
YB2	0.002	100.04	0.073	0.005	0.047	0.288	0.008	100.46
YB3	nd	100.21	0.093	0.005	0.047	0.319	0.007	100.68
YB4	nd	100.58	0.066	0.003	0.051	0.267	0.004	100.97
YB5	nd	100.38	0.020	0.002	0.049	0.239	0.008	100.70
YB6	0.002	99.89	0.067	0.004	0.054	0.233	0.007	100.26
YB7	nd	98.55	0.051	0.002	0.066	0.308	0.010	98.99
YB8	nd	98.81	0.060	0.003	0.066	0.283	0.010	99.23
YB9	nd	99.94	0.048	0.004	0.063	0.263	0.009	100.33
YB10	nd	98.86	0.050	0.001	0.064	0.259	0.008	99.24
Quy Chau (Central Vietnam)								
QC1	0.001	98.65	0.380	0.029	0.897	0.008	0.011	99.99
QC2	0.011	98.23	0.340	0.028	0.838	0.006	0.012	99.47
QC3	0.012	98.99	0.340	0.032	0.915	0.004	0.011	100.30
QC4	0.007	98.51	0.290	0.029	0.749	0.010	0.005	99.61
QC5	0.003	99.03	0.180	0.031	0.768	0.007	0.013	100.03
QC6	0.004	99.37	0.120	0.037	0.764	0.005	0.012	100.31
QC7	0.009	98.30	0.300	0.047	0.869	0.007	0.010	99.54
QC8	0.009	99.16	0.250	0.040	0.832	0.007	0.009	100.31
QC9	0.011	98.76	0.320	0.045	0.818	0.005	0.010	99.98
QC10	0.006	99.12	0.260	0.048	0.670	0.009	0.009	100.12

An innovator in gemstone reporting

• Identification of colored gemstones • Country of origin determination • Full quality and color grading analysis

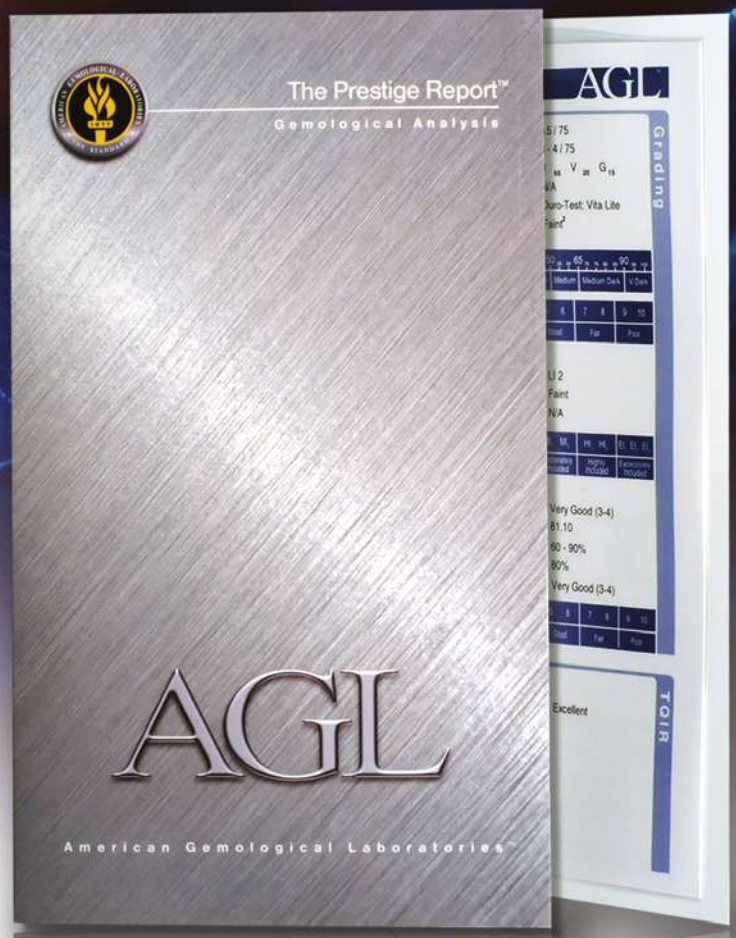

AMERICAN GEMOLOGICAL LABORATORIES AGL

580 5th Ave • Suite 706 • New York, NY 10036, USA
www.aglgemlab.com • +1 (212) 704 - 0727

Figure 1: These synthetic diamonds are typical of near-colourless gem-quality material grown in China. The three on the left are HPHT grown and weigh 0.57–1.0 ct, while the CVD synthetic diamond on the right is 2.0 ct. Photo by Chao Liu.

Current Status of Chinese Synthetic Diamonds

Taijin Lu, Jie Ke, Yan Lan, Zhonghua Song, Jian Zhang, Shi Tang, Jun Su, Huiru Dai and Xuxu Wu

ABSTRACT: China is the world's largest producer of industrial and gem-quality synthetic diamonds, particularly HPHT-grown products. In 2018, production of HPHT synthetic diamonds rose to 18 billion carats of industrial rough and more than 5 million carats of gem-quality rough material. This article summarises the production technology, product quality and output from various companies producing gem-quality HPHT- and CVD-grown synthetic diamonds in China. In recent years, 'hybrid diamonds' (comprised of natural diamond with a CVD overgrowth) have raised identification concerns, and we review differences in the fluorescence, structure and infrared spectrum of the CVD and natural layers. In addition, we briefly discuss diamond-detection devices developed and used in NGTC's laboratories, such as the GV5000. Finally, we compare the gemmological properties of colourless to near-colourless natural and synthetic diamonds.

The Journal of Gemmology, **36**(8), 2019, pp. 748–757, http://doi.org/10.15506/JoG.2019.36.8.748

The first synthetic diamond in China was grown in the 1960s (Qi 1985). Since then, through the support of the Chinese government and joint efforts with the industry, the production of synthetic diamonds in China has seen unprecedented development, and the growth technology has also greatly improved. In the 1990s, cubic presses independently developed in China were successfully promoted and used on a large scale, and subsequently Chinese industrial high-pressure, high-temperature (HPHT) synthetic diamonds entered the world market (Guo *et al.* 2008). In 2014, Zhengzhou Sino-Crystal Diamond Co. Ltd successfully grew colourless to near-colourless melee-size HPHT synthetic diamonds of gem quality (Lan *et al.* 2015). In 2016, Jinan ZhongWu New Materials Co. Ltd grew high-quality, large, colourless HPHT synthetic diamonds, which raised concerns in the trade and were researched by both the National Gemstone Testing Center (NGTC; Song *et al.* 2016c) and the Gemological Institute of America (Wang & Moses 2016).

Compared to HPHT synthetic diamond, the development of chemical vapour deposition (CVD) synthetic diamond growth technology in China has been relatively slow and small scale, without large factories until 2012. In recent years, several companies focused on CVD synthetic diamond have appeared, and their products and growth technology have developed rapidly. These include Ningbo CrysDiam Industrial Technology Co. Ltd and Shanghai Zhenshi Technology Co. Ltd, both of which can produce various colours of gem-quality CVD synthetic diamonds on a large scale.

In the past several years, Chinese synthetic diamonds have become a hot topic for research both in China and abroad (He *et al*. 2019; Kitawaki *et al*. 2019a, b). This article summarises the growth technology, product quality and output from various companies producing gem-quality HPHT- and CVD-grown synthetic diamonds in China. We also report recent research into 'hybrid diamonds' consisting of a natural diamond substrate with a CVD overgrowth, and then review the properties and identification characteristics of colourless to near-colourless natural and synthetic diamonds.

HPHT-GROWN SYNTHETIC DIAMONDS

China is the world's largest producer of industrial synthetic diamonds grown by HPHT techniques. The volume in 2015 was more than 12 billion carats, accounting for 98% of the global supply of industrial diamonds. Chinese production of industrial HPHT synthetic diamond rose to 3,600 tonnes (18 billion carats) in 2018, according to the authors' research.

Since the 1990s, China has independently developed technology for the growth of gem-quality HPHT synthetic diamond, particularly cubic presses for the mass production of colourless type IIa material. Since the beginning of 2015, NGTC's laboratories in Shenzhen and Beijing have identified melee-size colourless HPHT synthetic diamonds submitted by various clients. Therefore, we know that by then such products had already entered the Chinese jewellery market and were being sold as natural diamonds (Lan *et al*. 2015). Currently, Chinese production of melee-size colourless to near-colourless HPHT synthetic diamonds represents about 90% of the global output. According to the authors' research, output of gem-quality HPHT synthetic diamonds in 2018 consisted of more than 5 million carats (Mct) of rough material. Most were faceted in India and distributed to the gem market worldwide (e.g. Figure 1).

Currently, nearly all Chinese producers exclusively use hinge-type cubic-anvil presses (e.g. Figure 2a). This equipment can generate high pressure in six directions. The growth block for producing colourless synthetic diamond consists of pyrophyllite with metallic solvents and catalyst nitrogen-getter materials (Figure 2b).

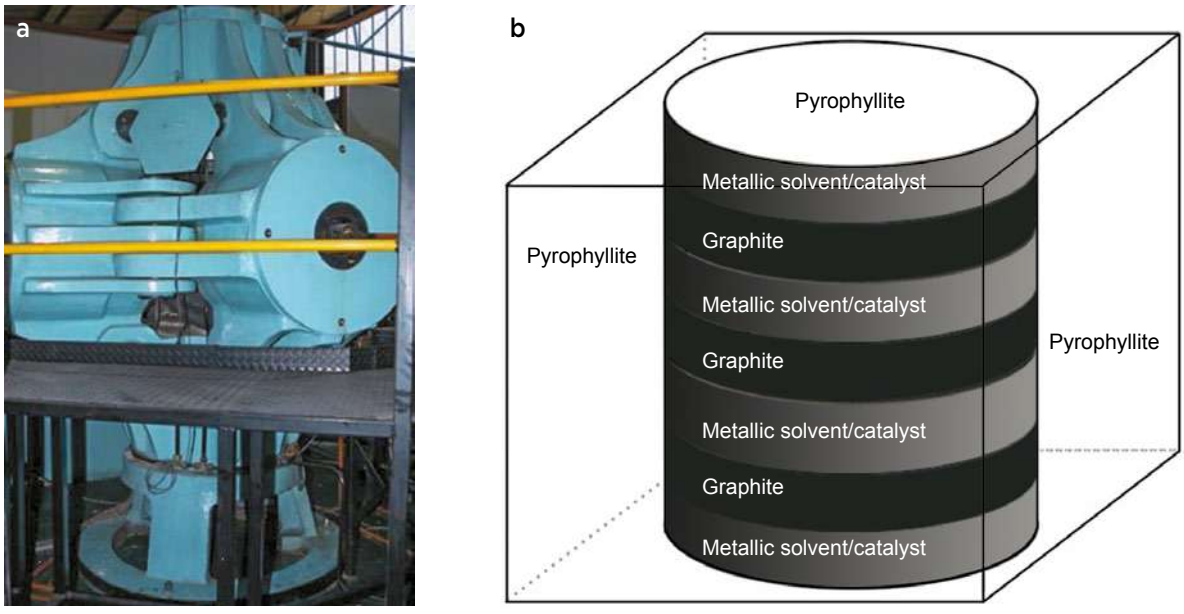

Figure 2: (**a**) A hinge-type cubic-anvil press such as this one is used by most Chinese producers of HPHT synthetic diamond. Photo by T. Lu. (**b**) The structure of the growth block for producing small HPHT synthetic diamonds consists of pyrophyllite with multiple layers of metallic solvent/catalyst and graphite.

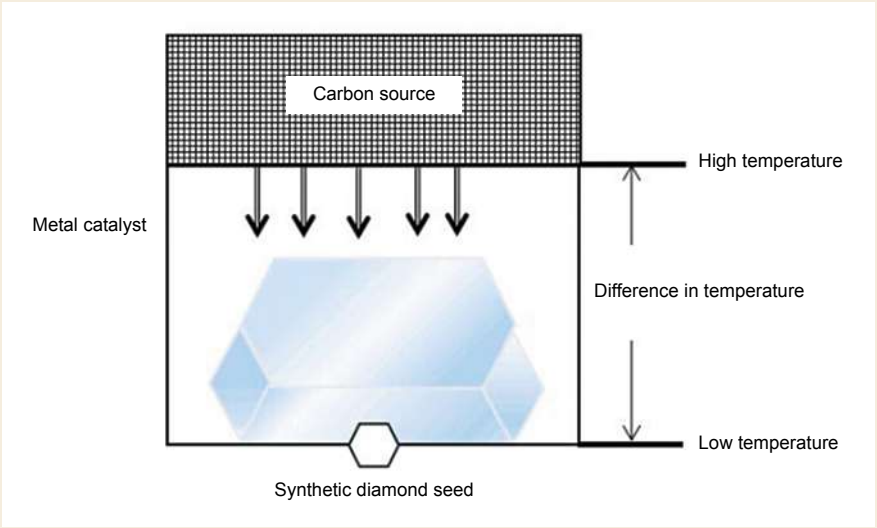

Figure 3: The temperature-gradient technique for growing larger HPHT synthetics involves a high-purity carbon source in the zone of higher temperature. Synthetic diamond crystallises on a seed substrate at the low-temperature end of the gradient.

Depending on the material to be manufactured, the interior structure and combination of these components differ. For example, a mixed powder of graphite and metallic solvent is employed for the growth of abrasive-grade synthetic diamonds. However, the growth of melee-size gem-quality synthetics involves the use of 5–9 layers of graphite and metallic solvent.

Production of larger gem-quality HPHT synthetic diamonds requires the use of a temperature-gradient technique (Figure 3), which can yield type IIa, Ib and IIb products (Eaton-Magaña *et al*. 2017). For example, to grow crystals with a morphology combining {100} and {111} faces, the temperature ranges from about 1,300 to 1,600°C, with a gradient usually around 30°C and a pressure of about 5.4 GPa (Li *et al*. 2007). Carbon from a high-purity (>99.9%) graphite source located at the end of the high-temperature zone diffuses onto seed crystals of synthetic diamond, resulting in the crystallisation of synthetic diamond on the seeds. Depending on the size to be grown, the number of seeds varies from several to several tens.

The gem-quality HPHT synthetic diamonds being produced in China vary from colourless to yellow, blue, pink, orange and brown (e.g. Figure 4). Pink is created through irradiation and annealing of nitrogen-containing material, but other colours can be produced as-grown. According to the authors' research, some companies, such as Zhongnan Diamond, have successfully developed the technology to grow rough material weighing more than 20 ct in the colourless to near-colourless (about D–H colour) range. More than five companies can mass produce colourless to near-colourless crystals weighing <1 ct, and the large-scale production of yellow crystals of up to 3–4 ct is possible.

Over the past 20 years, China has hosted nearly 100 production enterprises for HPHT and CVD synthetic diamonds. The major HPHT synthetic diamond manufacturers are located in Henan and Shandong provinces (Table I). The largest is Zhongnan Diamond, followed by Henan Huanghe Whirlwind, Zhengzhou Sino-Crystal Diamond (Figure 5), and others. Each company has around 1,000–4,000 cubic presses (e.g. Figure 6).

Figure 4: These crystals (0.40–0.80 ct) produced by Jinan ZhongWu New Materials are typical of Chinese HPHT synthetic diamonds that are (**a**) colourless, (**b**) yellow and (**c**) blue. Photo by T. Lu.

Table I: Major companies producing HPHT-grown synthetic diamond in China.

Company	Location	Scale	Products and quality	Growth technology
Zhongnan Diamond	Nanyang, Henan Province	The largest, producing 1,250 tonnes of industrial synthetic diamonds in 2018	Semi-automated production line; yellow and colourless gem-quality crystals up to 20 ct	Cubic press with high-purity graphite that is produced in-house
Henan Huanghe Whirlwind	Zhengzhou, Henan Province	Listed public company in 1998; the second largest, producing 600 tonnes of industrial synthetic diamonds in 2018	Type Ib crystals up to 10 ct possible, and type IIa colourless gem-quality crystals of 0.4–6 ct	Cubic press with temperature control of ±1.5°C
Zhengzhou Sino-Crystal Diamond	Zhengzhou, Henan Province	Listed public company in 2000; the third largest, with 2 Mct gem-quality synthetic diamonds produced in 2018 and 7 Mct projected for 2020	Gem-quality crystals of 0.1–6 ct; marketed under M&C brand name	Cubic press with large chamber (830 mm)
Jinan ZhongWu New Materials	Jinan, Shandong Province	Mainly gem-quality synthetic diamonds	Colourless, blue and yellow; gem-quality crystals of 6.5+ ct and faceted up to 3 ct possible	Cubic press; China-Ukraine joint technology; larger crystals
Henan Hold Diamond Technology	Shangqiu, Henan Province	Mainly industrial synthetic diamonds (300 tonnes per year)	Colourless gem-quality crystals of 1–4 mm (0.4–0.6 ct)	Cubic press; cooperates with State Key Laboratory of Superhard Materials at Jilin University
HeNan LiLiang Diamond	Zhengzhou, Henan Province	Produced gem-quality synthetic diamonds since 2016	Colourless and yellow gem-quality crystals of 1–8 mm	Cubic press
Penglai Bohai Diamond	Penglai, Shandong Province	Earliest manufacturer of synthetic diamonds in Shandong Province, producing mainly melee-size material	Colourless gem-quality crystals of 1–3 mm	Cubic press
Taidiam Technology (Zhengzhou)	Zhengzhou, Henan Province	Produces both HPHT and CVD synthetic diamond, small scale	Colourless, near-colourless, blue and yellow; 1–4 mm colourless gem-quality crystals	Cubic press

Figure 5: The factory of Zhengzhou Sino-Crystal Diamond in China's Henan Province is a major producer of HPHT synthetic diamonds. This facility is scheduled to produce 7 Mct of gem-quality HPHT synthetic diamonds in 2020. Photo by T. Lu.

Figure 6: A typical HPHT synthetic diamond production facility contains numerous cubic presses, some of which are shown here at the factory of Jinan ZhongWu New Materials in China's Shandong Province. Photo by T. Lu.

All of the companies in Table I produce gem-quality material, and according to the authors' research, the top three produced a total of more than 1 Mct in 2018. The company owners indicate that production capacity can be adjusted according to market needs. Zhengzhou Sino-Crystal Diamond reported that they plan to produce 7 Mct of gem-quality HPHT synthetic diamonds in 2020.

CVD-GROWN SYNTHETIC DIAMONDS

Compared to HPHT products, synthetic diamonds grown by CVD techniques have the advantages of high-quality controllability and wide industrial application. Chinese CVD enterprises are characterised by their small scale, rapid development and advanced growth techniques. All of the major CVD synthetic diamond companies in China (Table II) have the capability to produce gem-quality material, and their products first entered the gem market in 2016. However, their production scale is relatively small, and each facility typically has on the order of 10–50 growth reactors.

At present, the most common CVD methods used in China are microwave plasma chemical vapour deposition (MPCVD) for single-crystal synthetic diamonds and direct-current arc plasma jet for polycrystalline synthetics. For MPCVD, high-purity carbon is activated by high-voltage ionisation in a vacuum. The growth substrate consists of a synthetic diamond seed plate with dimensions ranging from 5 × 5 mm to 13 × 13 mm. Carbon atoms crystallise into diamond on the top surface of the seed at low pressure (usually 100–300 torr) and high temperature (typically 800–1,000°C).

The requirements for the growth of single-crystal CVD synthetic diamond by the MPCVD method are as follows (Wu 2019):

1. A carbon source such as methane, other hydrocarbons, CO or CO_2. At present, methane is the main source used.
2. High-purity hydrogen is the gas usually used to inhibit the nucleation, growth and etching of graphite.
3. Suitable C/H content for the gas source, generally less than 10%.
4. Suitable seed substrate temperature, generally limited to about 700–1,200°C, in addition to relatively low-temperature depositional conditions.
5. Low-pressure environment, generally much less than 1 atm.
6. Gas-activation technology (from one to several techniques) to stimulate the carbon sources and hydrogen, and to generate a deposition atmosphere for diamond with active carbon groups and atomic hydrogen.
7. Synthetic diamond seed for the growth of gem-quality material. To obtain high-quality synthetic diamond, it is often necessary to orient the seed crystal—commonly close to a {100} plane—and pre-treat its surface.

In addition, to improve the growth rate and reduce the formation of defects, a certain amount of N_2, O_2 and other gases are introduced into the growth chamber.

Gem-quality CVD synthetic diamonds produced in China are predominantly type IIa and type IIb, and as grown they typically consist of a transparent core surrounded by a rim of carbonaceous material (Figure 7).

Table II: Major companies producing CVD-grown synthetic diamond in China.

Company	Location	Products and quality	Growth technology*
Ningbo CrysDiam Industrial Technology	Ningbo, Zhejiang Province	Mass production of type IIa and IIb; colourless to near-colourless, pink, blue, red and orange; 10 × 10 × 4 mm plates and >1 ct faceted	MPCVD
Hebei Plasma Diamond Technology	Shijiazhuang, Hebei Province	Scientific research and industrial production; colourless to near-colourless; 13 × 13 × 1–3 mm plates	DC arc plasma jet CVD, MPCVD
Shanghai Zhengshi Technology	Shanghai municipality	Mass production of gem-quality type IIa and IIb; D–F colour; 12 × 12 × 3 mm (mainly 1–6 ct) plates	MPCVD
Carbon Star Semiconductor Technology	Xi'an, Shaanxi Province	Scientific and basic research for abrasives and gem-quality material; D–F colour up to 11 × 11 × 3 mm plates	MPCVD
Beijing Worldia Diamond Tools	Langfang, Hebei Province	Predominantly industrial use for tool abrasives, including gem-quality black material	DC arc plasma jet CVD

* Abbreviations: DC = direct current; MP = microwave plasma.

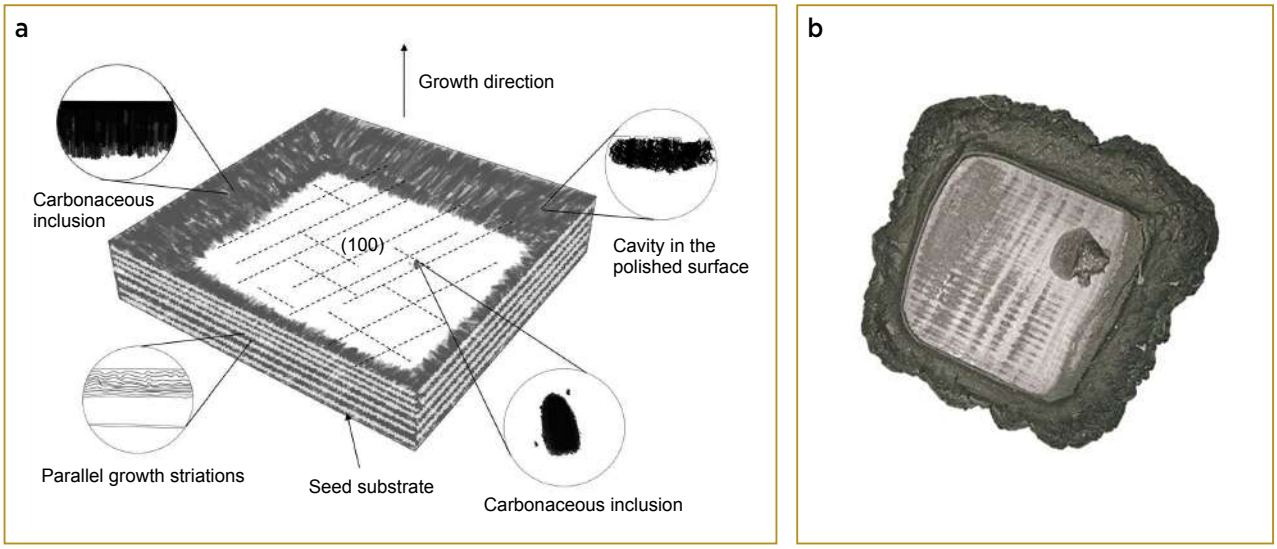

Figure 7: A sketch (**a**) and photo (**b**) of an as-grown plate of CVD synthetic diamond illustrate the typical features of this material. The CVD sample weighs 0.14 g and measures 5.79 × 5.67 × 2.07 mm. Photo by X. Wu.

They range from colourless to near-colourless, brown, blue, green, red, orange, pink and other colours (Figure 8). In some cases, post-growth treatment is needed to produce the desired colour. For example, because CVD synthetic diamonds usually contain non-diamond carbon (i.e. with sp^2 structure), the as-grown crystals are mostly brown, and HPHT treatment is needed to make them colourless to near-colourless (Eaton-Magaña & Shigley 2016). Green colouration presumably requires irradiation, while red, orange and pink are usually created with irradiation and heating (to about 800°C) of nitrogen-containing starting material. Crystals can be grown larger than 10 ct, and faceted CVD synthetic diamonds of about 1–2 ct can be mass produced. It takes about 15 days to grow a crystal weighing 4 ct.

HYBRID CVD SYNTHETIC DIAMOND ON NATURAL DIAMOND

In 2017, the Beijing NGTC laboratory identified a round brilliant-cut sample weighing 0.11 ct that consisted of type Ia natural diamond overgrown by a thick layer of CVD synthetic diamond (Tang *et al*. 2018, 2019). No boundary was visible between the two layers, even with a microscope. It was also very difficult to identify its hybrid nature using standard spectroscopic techniques. However, DiamondView imaging revealed red fluorescence and greenish blue phosphorescence in the CVD layer, separated by a sharp boundary with a layer of natural diamond showing blue fluorescence and no phosphorescence.

Figure 8: Faceted CVD synthetic diamonds from China are available in a range of colours. Shown here are (**a**) near-colourless (2.0 ct, G colour, VS_1 clarity) and (**b**) reddish pink (1.0 ct, VS_1 clarity) samples that were produced by Ningbo CrysDiam Industrial Technology Co. Ltd, and (**c**) a blue specimen (2.52 ct, Fancy Vivid, VVS_1 clarity) produced by Huzhou SinoC Semiconductor Science and Technology Co. Ltd. Photos courtesy of the companies that produced the samples.

Figure 9: Three hybrid samples of CVD synthetic diamond overgrown on natural diamond were created for this study. The samples range from 3.4 to 3.6 mm wide and have CVD overgrowths of 0.92–1.09 mm thickness. Photo by X. Wu.

To further study such material, we prepared three additional samples consisting of CVD synthetic diamond overgrown on natural diamond (Figure 9). A typical octahedral diamond crystal was sawn into three {100} substrates for CVD synthetic diamond growth. The resulting samples were H–K colour and had eye-clean CVD overgrowths of 0.92–1.02 mm in thickness. Viewed with the DiamondView (Figure 10), the substrate of each sample exhibited the typical blue fluorescence of natural type Ia diamond, while the CVD layer displayed orangey red fluorescence. The phosphorescence images also showed the presence of the two layers, with the natural diamond being inert and the CVD layer phosphorescing blue-green. The boundary between the natural diamond and the CVD layer was obvious when each sample was viewed from the side. Fourier-transform infrared (FTIR) spectroscopy with a micro-FTIR unit clearly revealed that the natural diamond substrate was type Ia and the CVD synthetic diamond layer was type IIa (Figure 11).

DIAMOND IDENTIFICATION METHODS AT NGTC

During the past few years, new diamond-identification instruments were developed at NGTC. For example, the GV5000 (Figure 12) combines imaging and spectroscopy (Lan *et al.* 2016). It enables fluorescence and phosphorescence imaging combined with spectral collection, decay-time measurement and growth-pattern observation. Its biggest advantage over similar instruments is its larger field of view and ability to test multiple samples simultaneously. In addition, when diamonds are screened, the phosphorescence spectrum and decay curves can be measured using the same instrument, enabling synthetics to be more conclusively identified based on differences in growth structure, spectroscopic features, etc. (Lu *et al.*

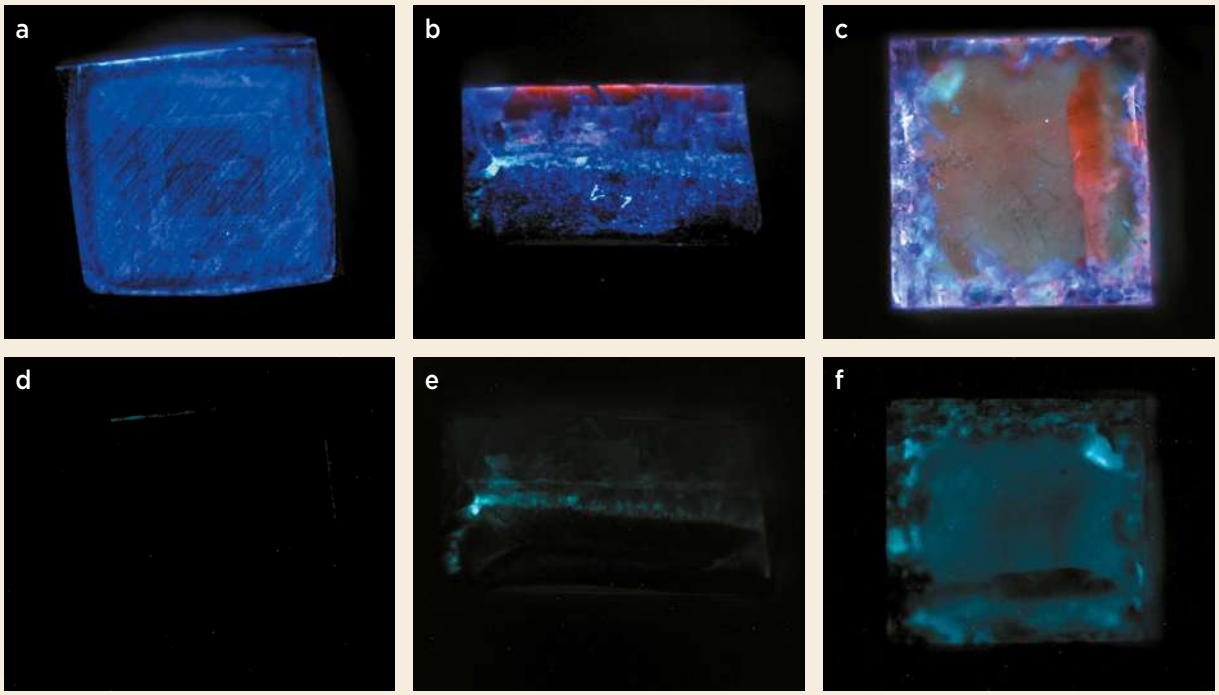

Figure 10: DiamondView images of the hybrid samples (shown here for the centre specimen in Figure 9) display blue fluorescence (**a**–**c**) for the natural diamond substrate and orangey red in the CVD overgrowth. (Views b and c show a mixture of CVD and natural features.) Phosphorescence images (**d**–**f**) show greenish blue for the CVD area while the natural diamond portion is inert. The side views (b and e) clearly show the layering of this hybrid sample. Images by X. Wu.

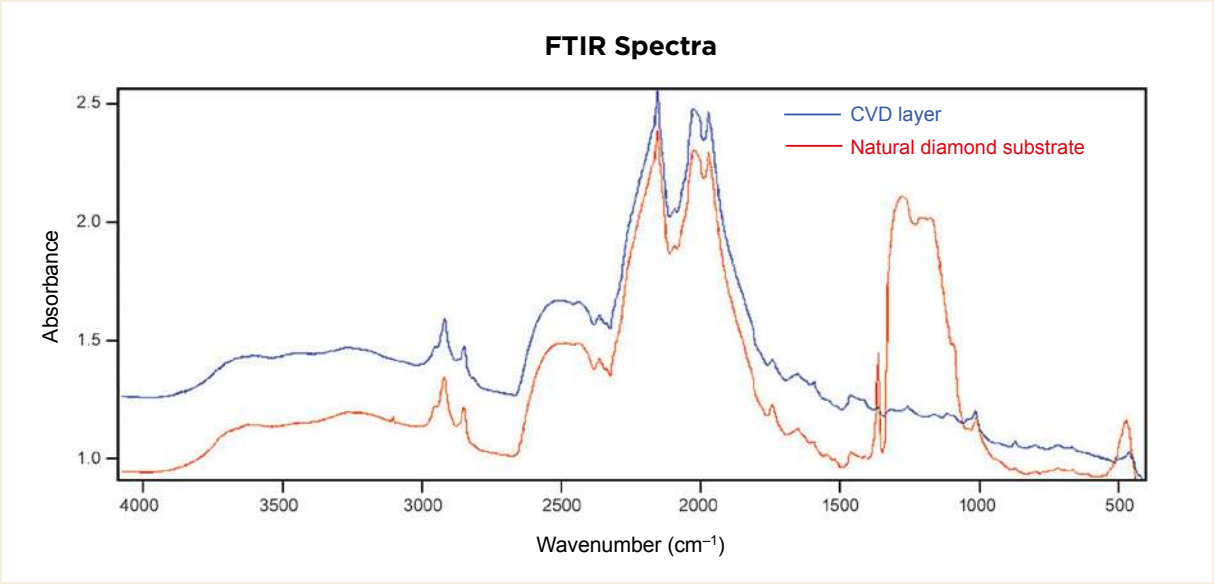

Figure 11: Micro-FTIR spectra of the different layers of the centre hybrid sample in Figure 9 demonstrate that the natural diamond substrate is type Ia and the CVD synthetic layer is type IIa.

Figure 12: The GV5000 diamond-identification instrument was developed at NGTC. It uses fluorescence and phosphorescence imaging and spectral collection, decay-time measurements, and growth-pattern observations to distinguish HPHT and CVD synthetic diamonds from natural ones. Photo by H. Dai.

2015; Lan *et al.* 2016). In China, a large amount of mounted-diamond jewellery is sent to laboratories for testing (e.g. Figure 13), and the GV5000 instrument enables the distinction of HPHT and CVD synthetics from natural diamonds on the basis of fluorescence and phosphorescence images of even numerous tiny mounted stones. The GV5000 has been extensively tested and certified by many diamond-related companies and institutions, including the Diamond Producers Association's (DPA) Assure Program (Dupuy & Phillips 2019).

We have also pioneered new techniques for identification and research using the electrical conductivity and magnetism of HPHT synthetic diamonds. Testing of about 1,000 HPHT synthetic diamonds with an electrical conductivity meter revealed that, regardless of clarity and colour, about 98% of them conducted a small electrical current, ranging from 0.01 to 5,000 µA. From this, we recently developed a highly sensitive device that can detect this conductivity, and it will be put on the market in the near future.

Research on diamond identification is ongoing at Chinese gemmological laboratories and institutions (Song *et al.* 2012, 2016a, b, c; Tang *et al.* 2017). At present, we can accurately detect and identify all natural and synthetic (HPHT- and CVD-grown) diamonds. Table III provides a summary comparison of the gemmological properties to distinguish colourless to near-colourless type II natural and synthetic diamonds manufactured in China.

Figure 13: These rings are mounted with Chinese CVD synthetic diamonds (0.25–0.30 ct). Photo by T. Lu.

Table III: Gemmological properties of colourless to near-colourless type II natural diamonds compared to HPHT synthetic and CVD synthetic diamonds manufactured in China.

Property	Natural	HPHT synthetic	CVD synthetic
Common inclusions	Crystals, clouds, feathers, etc.	Metallic thin rods and irregular shapes	Non-diamond carbon
Birefringence	Higher-order interference colours	Extremely low levels of strain	Higher-order interference colours
DiamondView imaging	Most fluoresce blue, with dislocation networks	Most fluoresce greenish blue, and a few are greenish blue with bluish green; fluorescence pattern follows cuboctahedral growth morphology	Fluorescence appears greenish blue, green, blue, yellowish green, pink with purple mottling, reddish orange, orange, etc.; thin striations or parallel bands
UV-Vis spectra	No absorption band at 270 nm	270 nm band originating from isolated nitrogen	270 nm band originating from isolated nitrogen
Near-IR spectra	Lacks spectral features	Lacks spectral features	Some show absorptions at 8750, 7840, 7354, 6855, 6425 and 5565 cm^{-1}; all these bands become weaker or even disappear with post-growth HPHT treatment
Mid-IR spectra	Type IIa features	Type IIa + IIb features; boron-related feature at 2800 cm^{-1} sometimes can be detected	Type IIa features; some show weak absorptions at 3123, 1344 and 1332 cm^{-1}; with post-growth HPHT treatment, the 3123 cm^{-1} band becomes weaker or even disappears, and a 3107 cm^{-1} band appears
Photoluminescence	GR1 emission at 741 nm present in most type IIa colourless diamonds	883/884 nm doublet related to nickel sometimes present	$Si\text{-}V^-$ doublet at 737.6/737.9 nm is a strong indicator of CVD growth; a 596/597 nm doublet indicates a CVD sample did not undergo HPHT treatment

CONCLUSIONS

China is the world's largest producer of HPHT synthetic diamonds, with an output of more than 5 million carats of gem-quality material in 2018. Currently, the production of melee-size colourless to near-colourless HPHT synthetic diamonds in China represents about 90% of the global output. In addition, Chinese companies can grow large (up to 20+ ct) yellow and colourless HPHT synthetic diamonds.

CVD growth technology in China has been developing rapidly in recent years. Although production volume is still relatively small, the quality of Chinese CVD synthetic diamonds has improved significantly. Compared to early products, current CVD synthetic diamonds grown in China are larger and more pure, and are available in a wider range of colours.

In July 2019, the producers of both HPHT and CVD synthetic diamonds formed a sub-association under the Gems and Jewelry Trade Association of China. NGTC continues to systematically investigate the latest synthetic diamond products and is working to develop new identification techniques to keep up with improvements in growth technology.

REFERENCES

Dupuy, H. & Phillips, J.C. 2019. Selecting a diamond verification instrument based on the results of the Assure Program: An initial analysis. *Journal of Gemmology*, **36**(7), 606–619, http://doi.org/10.15506/JoG.2019.36.7.606.

Eaton-Magaña, S. & Shigley, J.E. 2016. Observations on CVD-grown synthetic diamonds: A review. *Gems & Gemology*, **52**(3), 222–245, http://doi.org/10.5741/gems.52.3.222.

Eaton-Magaña, S., Shigley, J.E. & Breeding, C.M. 2017. Observations on HPHT-grown synthetic diamonds: A review. *Gems & Gemology*, **53**(3), 262–284, http://doi.org/10.5741/gems.53.3.262.

Guo, D., Xu, Z., Lu, Z., Liu, Z. & Hu, Y. 2008. Application status at home and abroad and advantages of cubic hinge press for superhard abrasives. *Superhard Material Engineering*, **20**(6), 33–37 (in Chinese with English abstract).

He, X., Du, M., Zhang, Y., Chu, P.K. & Guo, Q. 2019. Gemologic and spectroscopy properties of Chinese high-pressure high-temperature synthetic diamond. *JOM*, **71**(8), 2531–2540, http://doi.org/10.1007/s11837-019-03592-8.

Kitawaki, H., Emori, K., Hisanaga, M. & Yamamoto, M. 2019a. Current production of synthetic diamond manufacturers in Asia. *36th International Gemmological Conference*, Nantes, France, 27–31 August, 27–29.

Kitawaki, H., Emori, K., Hisanaga, M. & Yamamoto, M. 2019b. Manufacturers of synthetic gem diamonds in China and India and their products. *2019 Annual Meeting of the Gemmological Society of Japan*, abstract 5 (in Japanese).

Lan, Y., Liang, R., Lu, T., Zhang, T., Song, Z., Ma, H. & Ma, Y. 2015. Identification characteristic of near-colourless melee-sized HPHT synthetic diamond in Chinese jewelry market. *Journal of Gems & Gemmology*, **17**(5), 12–17 (in Chinese with English abstract).

Lan, Y., Lu, T., Zhang, C., Liang, R., Ding, T., Chen, H., Ke, J. & Bi, L. 2016. Development of a new multi-spectral induced luminescence imaging system (GV5000) and its application in screening melee-sized near-colorless synthetic diamonds and natural diamonds. *Rock and Mineral Analysis*, **35**(5), 505–512 (in Chinese with English abstract).

Li, S., Zang, C., Ma, H., Tian, Y., Zhang, Y., Xiao, H., Huang, G., Ma, L., *et al*. 2007. Recent progress in the synthesis of type IIa gem class diamond single crystal. *Superhard Material Engineering*, **19**(5), 27–29 (in Chinese with English abstract).

Lu, T., Lan, Y., Liang, R. & Zhang, C. 2015. Testing and screening of melee-sized near-colorless HPHT synthetic diamonds using a multi-spectral induced luminescence imaging system (GV5000) in China. *ICGL Newsletter*, No. 4, 1–3.

Qi, L. 1985. Synthetic diamond in China. *Progress in Crystal Growth and Characterization*, **11**(4), 245–251, http://doi.org/10.1016/0146-3535(85)90006-1.

Song, Z., Lan, Y., Shen, M., Lu, T., Ke, J., Liu, J. & Zhang, Y. 2012. Identification characteristics of undisclosed CVD synthetic diamonds found recently by NGTC. *Journal of Gems & Gemmology*, **14**(4), 30–34 (in Chinese with English abstract).

Song, Z., Lu, T., Su, J., Gao, B., Tang, S. & Hu, N. 2016a. Silicon-doped CVD synthetic diamond with photochromic effect. *Journal of Gems & Gemmology*, **18**(1), 1–5 (in Chinese with English abstract).

Song, Z., Lu, T., Tang, S., Ke, J., Su, J., Gao, B., Hu, N., Zhang, J., *et al*. 2016b. Identification of colourless HPHT-grown synthetic diamonds from Shandong, China. *Journal of Gemmology*, **35**(2), 140–147, http://doi.org/10.15506/JoG.2016.35.2.140.

Song, Z., Lu, T., Su, J., Gao, B., Tang, S., Hu, N., Ke, J. & Zhang, J. 2016c. The spectral characteristics and identification techniques for colorless and near-colorless HPHT synthetic diamonds. *Rock and Mineral Analysis*, **35**(5), 496–504 (in Chinese with English abstract).

Tang, S., Su, J., Lu, T., Song, Z. & Ke, J. 2017. Gem News International: A melee-sized CVD synthetic diamond in pearl and diamond jewelry. *Gems & Gemology*, **53**(3), 382.

Tang, S., Su, J., Ma, Y., Ke, J., Zhang, J., Lu, T., Song, Z. & Liu, H. 2018. A thick overgrowth of CVD synthetic diamond on a natural diamond. *Journal of Gemmology*, **36**(2), 134–141, http://doi.org/10.15506/JoG.2018.36.2.134.

Tang, S., Su, J., Lu, T., Ma, Y., Ke, J., Song, Z., Zhang, J., Zhang, X., *et al*. 2019. Research on laboratory testing features of chemical vapor deposition in overgrowth diamonds. *Rock and Mineral Analysis*, **38**(1), 62–70 (in Chinese with English abstract).

Wang, W. & Moses, T. 2016. Gem News International: Large colorless HPHT synthetic gem diamonds from China. *Gems & Gemology*, **52**(1), 101–102.

Wu, X. 2019. *Gemmological properties of domestic colorless CVD (chemical vapor deposition) synthetic diamonds and hybrid diamonds*. Master of Gemmology thesis, China University of Geosciences, Beijing, 19 pp. (in Chinese).

The Authors

Dr Taijin Lu, Jie Ke, Yan Lan, Zhonghua Song, Jian Zhang, Shi Tang, Jun Su, Huiru Dai and Xuxu Wu
National Gems & Jewelry Technology Administrative Center,
National Gemstone Testing Center,
22 F, Building C, Global Trade Center,
North 3rd Ring East Road,
Beijing 100013, China
Email: taijinlu@hotmail.com

Acknowledgements

This study was supported by the NGTC Research Foundation (grant nos. NGTCBJ17007 and NGTCBJ18002) and partially supported by the National Natural Science Foundation of China (grant nos. 41473030 and 41272086).

Figure 1: Pearls decorate this Byzantine jewelled bracelet (3.8 × 8.2 cm), which was probably made in Constantinople around 500–700 CE. Courtesy of The Met, New York, New York, USA; gift of J. Pierpont Morgan in 1917 (accession no. 17.190.1671).

Renaissance Recipes for Making Artificial Pearls by Leonardo da Vinci and Others

Annibale Mottana

ABSTRACT: A process suggested by a young Leonardo da Vinci in 1480 for reconstituting small pearls into a single large one is here translated into English for the first time. This formula is compared to two other nearly contemporaneous recipes, which are representative of a series of Renaissance processes for making artificial pearls. Leonardo da Vinci also suggested a mechanical method for polishing the reconstituted pearls, and he was aware that mother-of-pearl and pearl behave the same way when attacked with weak acids.

The Journal of Gemmology, **36**(8), 2019, pp. 758–765, http://doi.org/10.15506/JoG.2019.36.8.758

Pearls were among the most popular and precious gems in the Late Medieval period and during the Renaissance (Kunz & Stevenson 1908; Bycroft & Dupré 2019). Their popularity had continued without interruption from antiquity (e.g. Figure 1), and was mainly due to their attractive round shape and natural lustre, thus not requiring any human intervention or improvement such as shaping or polishing. Their colour did not matter, although white was by far the most appreciated. When Christianity became dominant, a religious lore was attached to pearls. Indeed, the most beautiful nacreous pearls occur as single, pure white spheres within their host molluscs, just as Christ was unique in the human consortium (Friess 1980, 144–148).

Unfortunately, pure white pearls were seldom seen during the time of Leonardo da Vinci (1452–1519; usually known as 'Leonardo', and he will be referred to as such in this article). Before the lucky discovery in 1498 of a fishery in the Gulf of Paria in eastern Venezuela (fronting the island of Trinidad) during Christopher Columbus's third journey of exploration along the coast of South America (Oviedo 1526, Chap. LXXXIV), white pearls were rare in Europe and arrived by long-distance trade predominantly from marine fisheries in the Persian Gulf or, to a lesser extent, in the Gulf of Mannar (between India and Sri Lanka: Avial-Chicharro 2019). Although there were numerous scattered findings of freshwater pearls in Europe, they were typically of inferior quality (Landino 1476, Vol. IX, 115–116). Indeed, until recently, pearls were harvested in rivers of northern Europe, provided their waters were cool and oxygenated (Strack 2015), and the most common pearls that could be found in Europe during the Middle Ages were those from Britain. Pliny the Elder stated that Julius Caesar invaded Britain only for its pearl riches, and this conqueror studded his cuirass with them before he dedicated it to Venus Genetrix. Nevertheless, Pliny considered them of little worth in comparison to the marine-origin pearls from the Middle East—such as two of those exhibited by Cleopatra (Landino 1476, Vol. IX, 119)—because the freshwater ones were small, of imperfect form and showed little lustre.

Late Medieval and Renaissance portraits of royalty (e.g. Figure 2) and nobility show that pearls were common constituents of their apparel. However, the origin of these pearls is unknown; they could have come from Venezuela or have been imported from the Orient through Venice. Given the rarity of high-quality pearls at the time, it is no wonder that quite a few alchemists tried simulating them, as they did with other gems (Beretta & Conforti 2014). Many succeeded in making spherical objects with milky colour and some lustre, but no one made them so well that they would be mistaken for true pearls unless viewed from a great distance. Yet, recipes to imitate, counterfeit or simply enhance the quality of pearls are large in number. The first written evidence is believed to be from the 3rd century CE text *Papyrus Graecus Holmiensis* (Halleux 1981, pp. 113–114; Nassau & Hanson 1985), but other recipes can be found in increasing number in various technical manuscripts from the Late Medieval period and the Renaissance (e.g. Berthelot 1887–1888; von Lippmann 1919; Darmstaedter 1925, 1926, 1927a, b, 1928; Venturelli 2001; Silva 2016).

LEONARDO'S RECIPE

Leonardo da Vinci was possibly the most complex combination of artist, thinker and scientist who ever lived in Europe. He died on 2 May 1519, so it was appropriate that in 2019—which marked 500 years since his passing—his work was celebrated through various exhibitions (e.g. www.leonardodavincicelebration.org), most of which highlighted his accomplishments as a painter and scientist. In addition, we might also recall some of Leonardo's accomplishments that are less recognised in the shadow of his masterpieces. Among these lesser works are his experiments in alchemy, a practice that he tested and abandoned, as he did not like it. And within these alchemical works are small investigations pertaining to gems and jewellery materials, such as determining the gold content of metal alloys (Mottana 2018) and trying to make gems from simple materials. His method of assaying gold alloys is quite valid, and it

Figure 2: Pearls adorn Mary Stuart, Queen of Scots, painted by François Clouet in 1558 when she was the fiancée of François II, King of France. Her dress is studded with small pearls, while large white pearls make up her necklace, hair ornament and sash belt. Image courtesy of Wikimedia Commons; supplied by Royal Collection Trust / © H. M. Queen Elizabeth II 2012.

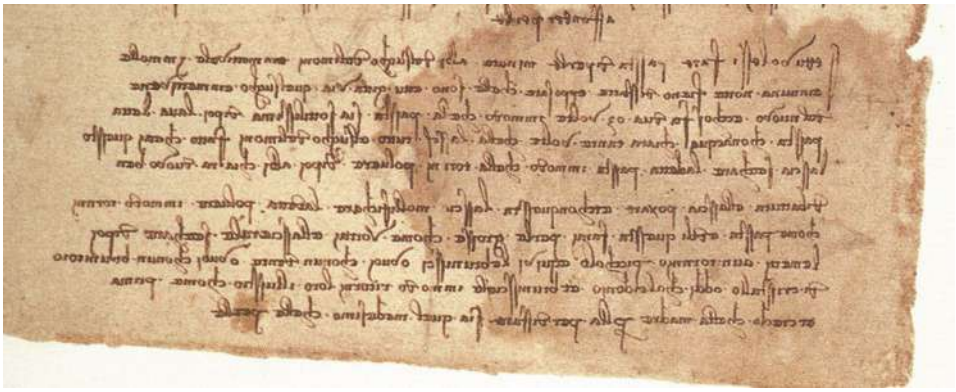

Figure 3: Leonardo da Vinci's recipe for creating artificial pearls was written in 1480 in *Codex Atlanticus* folio 304v (previously f. 109v). The 10 lines under the title 'Affonder perla' describe the method that he proposed to make a big pearl from several small ones. Although the image of the page might appear to be reversed, Leonardo was left-handed and wrote in 'mirror text' from right to left.

is still carried out today. By contrast, the rather crude methods he proposed to make artificial gems have been forgotten. However, such activities deserve to be recalled as demonstrating the variety of Leonardo's technical interests, through which he could—even if involuntarily—have become a forger.

Perhaps to challenge his own experience in alchemy, or else prove to himself that he could do better than others if needed, Leonardo wrote down a recipe to create a large pearl from a handful of small ones while he was still living in Florence. His method was intended to transform minute pearls, useful only to garnish clothing, by reconstituting them into a single large one, which in theory would be very similar in consistency and appearance to a natural pearl. The recipe is recorded in *Codex Atlanticus*, now in the Ambrosian Library of Milan, Italy, which was entirely transcribed twice: by Giovanni Piumati in 1894–1904 (under the responsibility of the Royal Lincei Academy, at that time led by Francesco Brioschi, in which the recipe appeared on f. 109v) and by Augusto Marinoni in 1975–1980 (recipe on f. 304v). It is one of the oldest manuscripts written by Leonardo and has been paleographically and linguistically dated to 1480 (P. C. Marani in Marinoni 2004, p. 75).

The text at the top of the page concerns the making of nut oil for painting, followed by the folio number 148 written alone in the middle, probably in Leonardo's hand (Marinoni 2004, p. 10). The text then continues with five lines in a smaller size (as if they were added at a different time) that describe how rotten nuts should be pressed and distilled. So far, none of this has anything to do with pearls. However, this subject appears towards the bottom of the page with the title 'Affonder perla' (meaning to blend a pearl, or to cast a pearl), in the centre of line 23 (Figure 3). The recipe encompasses 10 lines and displays large, merchant-style, carefully written characters running from right to left typical of the young Leonardo (Calvi 1925, p. 45; Manni 2008, p. 14).

To the present author's knowledge, no one has translated Leonardo's recipe into English before, not even Ladislao Reti (1952), the finest connoisseur of Leonardo's alchemical interests, and the one who first drew people's attention to this recipe by commenting on it briefly (Reti 1952, pp. 734–735). Based on Marinoni's critical transcription (1976, Vol. IV, p. 122)[1], the present author translated the text[2] as follows:

> If you wish to make a paste of very small pearls, take some lemon juice and soak them and within a night they will be dissolved. When they have settled, throw away that juice and add some new, and repeat this [soaking] two or three times until you have a very thin paste. Wash then the said paste with clear water many times, so to let all the lemon juice out. When this is done, let the said paste dry up, so that it turns into powder. Then take egg white, beat it very well and let it stand. Use this to soften the powder, so that it turns again to paste; and from this paste you can make pearls as large as you wish, and then let them dry. Afterwards you put them into a small lathe and smooth them down either with a tooth or with a polisher made of crystal or chalcedony. And polish them so that they re-acquire the same lustre as before. I believe that to dissolve the mother-of-pearl you must follow the same [process] as for pearls.

Pearls consist of calcium carbonate—mostly aragonite (orthorhombic $CaCO_3$), although some contain small amounts of calcite (the rhombohedral polymorph)—as platelets that are locally interlayered with organic matter. Interpreted in modern crystal-chemical terms, the process proposed by Leonardo begins by dissolving the organic matter (a protein similar to keratin) using a weak acid (impure citric acid, $C_6H_8O_7$). The resulting powder is then dried and mixed together with another protein (egg white albumin or ovalbumin), a readily available organic

binder but of different type than the original organic matter. The paste can then be easily manipulated into the spherical shape of a pearl.

Although Leonardo was not aware of the chemical reaction taking place during the process, he certainly knew that the final object would in itself not appear to simulate a genuine pearl unless it was polished. Indeed, pearls have an attractive bright lustre that is appropriately called *pearly*. To obtain this lustre, Leonardo described a mechanical process in which the surface of the object was smoothed down on a 'lathe' (*tornio*), using either the stiff canine tooth of a wild animal (e.g. wolf, bear or wild boar) or polished by an appropriate hard mineral such as quartz or chalcedony. At that time, the tool was likely to be just a rotating wheel driven either by hand, such as the one he later asked his pupil Boltraffio to make (manuscript CII, f. 22v of Institut de France: cf. Marinoni 1987), or by some revolving mechanical apparatus made up of a wheel and coils, similar to that described by Henri Arnaut (see figure 8 of Schmetzer 2019). There were other descriptions of tools designed to cut and polish gem materials at the time (Bol 2019) that could, perhaps, have inspired Leonardo's prototype jeweller's bench shown in Figure 4 (*Codex Atlanticus*, f. 1036v [previously f. 371v]), which he conceived and carefully designed in 1513.

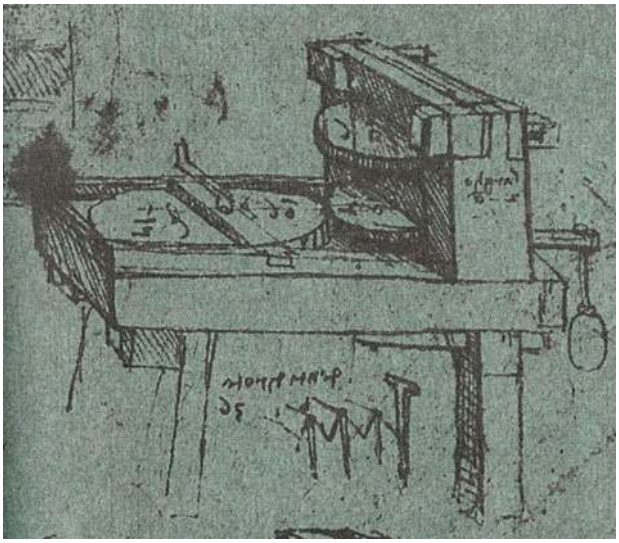

Figure 4: Leonardo da Vinci designed a jeweller's bench with a 'lathe' consisting of a horizontal wheel (left side) driven by hand with a crankshaft to modulate the rotation speed. The rotation also drove a vertical mangle to make flat metal sheets of variable thickness (right side). The surface of the rotating wheel can be smeared with emery paste to polish the gem. Detail from *Codex Atlanticus*, folio 1036v (previously f. 371v).

OTHER LATE MEDIEVAL AND RENAISSANCE RECIPES

There is no evidence whatsoever that Leonardo made use of his process for reconstituting pearls, either in Florence or in Milan—where he moved two years later and where a guild of gem counterfeiters had been established since 1472. By contrast, after moving to Milan, Leonardo conceived and carried out various experiments and wrote down several recipes to simulate coloured gemstones (A. Mottana, in preparation). Most likely, as he always worked alone and wrote for himself, his pearl formula remained largely unknown. Nevertheless, such a concept was not so unusual as not to have predecessors and successors. However, we know little about them because most scientific information at that time was communicated orally.

Ladislao Reti (1952, p. 735) suggested a possible precedent, which was written by an anonymous scientist who authored recipes 13 and 14 in chapter II of codex 164 (153) in the University of Bologna library, Italy, titled *Liber claritatis totius alkimicae artis (Book Clarifying the Entire Alchemical Art)*. This text, dating from the mid-14th century and known long since, was entirely transcribed and published as five separate articles by Ernst Darmstaedter in the 1920s (Darmstaedter 1925, 1926, 1927a, b, 1928). He believed this alchemical book was a translation from Arabic, although he also was certain its author was not the reported 'Geber', because it contained much more advanced alchemy than

[1] There are minimal orthographic differences between Reti's and Marinoni's critical transcriptions. Evidently this discrepancy derives from the fact that Reti used the 1894–1904 edition, in which Giovanni Piumati did the transcription. The present author prefers to use Marinoni's transcription because it is more recent and was performed after the *Codex Atlanticus* had undergone full restoration. The commas sometimes vary but the contents are exactly the same.

[2] *Affonder perle. / Se tu volessi fare pasta di perle minute, abbi del sugo de' limoni e mettivele in molle e in una notte fieno disfatte. E posate ch'elle sono, e tu gitta via quel sugo e mettivene del nuovo, e così fa dua o 3 volte in modo che la pasta sia sottilissima. Di poi lava detta pasta con acqua chiara tante volte, ch'ella lasci tutto el sugo de' limoni. Fatto che hai questo, lascia seccare la detta pasta, in modo ch'ella torni polvere. Di poi abbi chiara d'uovo ben / dibattuta e lascia posare. E con questa lascia mollificare la detta polvere, in modo torni come pasta; e di questa farai perle grosse come vorrai e lascerale seccare. Di poi le metti a un tornio piccolo e quivi le brunisci, o vuoi con un dente, o vuoi con un brunitoio di cristallo o di calcidonio. E bruniscile in modo ritorni loro il lustro come prima. E credo che la madreperla per disfare sia quel medesimo che le perle.*

could have been conceived by that celebrated Arabian alchemist, who had lived some eight centuries before. Darmstaedter's fifth article (1928) contains two recipes on pearls, but Reti considered only the first one, despite being in Latin, to be worth comparing with Leonardo's process. (At that time Leonardo did not know Latin, because he had received only the practical technical training appropriate for his intended career as an artisan.) The recipe, which the present author translated from Reti's reproduction in the note on p.735[3], says:

> Take small pearls and set them in a small vase. And add so much caper juice as to have the pearls covered and let it go for the entire night. Then, drain the juice slowly so as not to touch the pearls. Then wash them with citrus juice and avoid touching them and drain that juice out again. Then filter them through a piece of thick cloth so that no substance of the pearls escapes. Then take a clean slug such as naked snails or red snails and grind as much of them together with the pearls over porphyry until they became a single mass. Then shape them as pearls and pierce them immediately. After that, grease your fingers with fat from fish and set the fish together with the pearls into a warm oven and let all stay until the fish is well cooked. Afterwards, do as you did before.

Reti's suggestion of this being a precedent for Leonardo's recipe was likely too hasty, and thus faulty, owing to the little attention he dedicated to the subject (cf. Reti 1952, p. 735: only two dozen lines of an article comprising 30 dense pages). Leonardo's procedure is much cleaner than the one described above: he suggested egg white rather than the flesh of snails to bind the pearl residues, and he did not measure the time that the reconstituted pearl would take to dry and harden in the same terms that a cook would use. Moreover, there were quite a few other Late Medieval recipes to enhance the size and appearance of pearls that the young Leonardo could have heard about and used as inspiration. Paola Venturelli (2002) listed 25 such processes that span from the 13th to the 16th century, and her list is likely incomplete, as her research was performed only in the public libraries of northern Italy.

Indeed, the most likely predecessor to Leonardo's recipe occurs in another codex at the University of Bologna library (manuscript 2861), bilingual and dated to the late 15th century, possibly 1480—exactly when Leonardo wrote down his recipe in *Codex Atlanticus*. This other codex was highlighted during research aimed at finding various methods used to create the colours available to early Renaissance painters (Guerrini & Ricci 1887), but its section on pearls was neglected and long forgotten. It was never translated into English, possibly because the main subject matter of paint pigments was too well known from other sources, or perhaps because the text has inherent language difficulties. It is a mixture of an imperfectly Latinised northern Italian idiom, full of strange words familiar only to those from that region. The relevant recipe title is in poor Latin: *Ad fatiendum perlas grossas de minutis* (To make big pearls from small ones). Then it continues as follows[4] (translated by the present author):

> Grind finely the small pearls in a mortar of bronze. Afterwards take the juice of lemons and pour it through a filter and add urine and water in the amount of one-third of the lemon juice and mix the powder above with this liquid so that it becomes like a paste and leave it in sunlight for three days. Then lump it carefully and put it over a glass and make up pearls as you wish using tunny [tuna fish] oil. Then pierce them through using a pig bristle, and through that hole put a horse hair and leave them in the sun until they become dry. Afterwards put them in the belly of a very big fish[5] after extracting its entrails, and sew or stitch the belly, and make from it a pie that you shall cook; take it out [of the oven] and you shall find in it hard stones: you must rub them with barley bran in a woollen cloth, very hard. Afterwards, you shall feed them to a pigeon, or to a cock, for one day or more, as you like, and again rub them with bran as before, and they will be perfectly polished.

This recipe describes the process in such a way that some operations are more detailed and have additional steps compared to Leonardo's recipe (e.g. the formed object is made fully dry in an oven after having dried

[3] *Accipe pernas minutas et pone in vasello. Et pone tantum de suco cappari, ut coperiat pernas, et dimitte simul per totam noctem. Postea extrahe sucum desuper suaviter ut non tangas pernas. Postea ablue ipsas cum suco citri, et non tangas eas, et iterum prohice sucum istum. Postea cola ipsas in petia spissa ut non exeat de substantia pernarum. Postea accipe cocavum nudum id est limacas nudas id est marucas, et tere supra porfidum simul com pernis tantum donec efficiantur unum corpus. Postea fac inde pernas et perfora ipsas tunc. Deinde inunge digitos tuos cum pinguedine piscium et pone pisces cum pernis in furno calido et dimitte stare donec pisces sint bene cocti. Postea facias sicut prius fecisti.*

in the sun first to avoid cracking, and a hole is made beforehand to prepare the resulting 'pearls' for stringing), while other steps are simpler and do not require special instruments (e.g. the 'pearls' are placed within the greasy belly of a cooked fish, apparently to absorb additional fat as binder and perhaps acquire some lustre, and are then polished by passing them through the gizzard of a courtyard bird).

Clearly, Leonardo reckons more as an engineer, while the anonymous author of manuscript 2861 attempts to use simple procedures with tools that were readily available. Without a means to measure time, this author used the cooking period of a fish to estimate it. And as the ancient Greeks already knew (Nassau & Hanson 1985, p. 226), the author was familiar with the effectiveness of polishing by rubbing stones together within a bird's gizzard. The results of this recipe are unlikely to be the same as Leonardo's, since polishing such an artificial pearl on a wheel would certainly yield better results than passing it through the gizzard of a chicken. However, the anonymous author was evidently writing for himself, whereas Leonardo may have been preparing to use his recipe for financial gain by applying it towards someone else's pearl harvest or possibly even selling his process to a guild of counterfeiters, who would certainly have had a polishing wheel available.

CONVERTING SHELL INTO ARTIFICIAL PEARLS

The last sentence of Leonardo's artificial pearl recipe rather cryptically introduces an innovative concept: indeed, pearl and mother-of-pearl are such closely similar materials as to behave the same way when attacked by weak acids. Thus they can be manipulated in much the same way to make artificial pearls.

This is an innovation that no alchemist had ever put in writing before, but it was so obvious that soon somebody started using it. Indeed, in the middle of the following century in The Netherlands, it was written[6] (as translated by the present author): 'To counterfeit pearls… to make pearls into something else…take a large clean mussel shell, heat it and put it in wine vinegar, afterwards take the shell and make it into a powder and take crystal glass, also powdered.' Although the name 'P. Koldenbergij' is clearly indicated on the manuscript, and this was interpreted as the name of the author for a long time, it was subsequently identified to be the work of Pieter Van Coudenberghe (1517–1599), an Antwerp apothecary and botanist (Vandamme 1974, pp. 124–125). As usual for apothecaries, he collected an array of recipes, often in Latin, which he could make use of if needed. Two of them describe how to counterfeit pearls, along with a list of alchemical symbols and other miscellaneous subjects, such as a drawing of an oven to bake painted glass, and instructions on how to make or improve upon pigments, discern fake from real stones, gild metal, and make ink, mirrors, enamel and resins. Therefore, taken altogether, this bulky manuscript could be seen as the recipe book of a skilled apothecary. Furthermore, the presence of a pearl recipe fits the locality: in Antwerp, which is well known for its edible oysters, pearls were also (and still are) occasionally encountered. However, they are typically small, of unattractive colour, baroque shaped and non-nacreous—certainly not of the type that could be sold for jewels, although they were used to enhance garments, particularly those of ladies. The owner of such pearls would have understandably felt the need to enhance their appearance, and there would have been an abundance of shell material available for potentially reconstituting the shells into artificial pearls.

CONCLUSION

Bright white, perfectly spherical natural nacreous pearls were popular jewels in Europe during Greek and Roman times and continuing after the Renaissance, although they were exceedingly costly because of their rarity,

[4] *Tere parvas margaritas in mortario bronzi subtiliter. Demum accipe citositatem citrorum et distilla per filtrum et de urina et de aqua tasi quantum est tertia pars aqua citri et impasta dictum pulverem cum hac aqua ita quod deveniat sicut pasta et dimicte per tres dies ad solem. Postea conglutina diligenter et depone super vitrum et forma margaritas ad libitum cum oleo muscellino. Postea perfora cum porcina seta, per quod foramen pone setam equinam et dimite ad solem donec sicentur. Demum pone in ventre piscis bucefalli, eiectis interioribus, et sue, sive cuscias ventrem, et fac inde pastillum et coque et exerge et invenies lapides duros: et frica eas cum furfare ordei in panno, fortiter. Demum da columbo, vel gallo, comedere per diem 1 vel amplius, sicut videtur, et iterum frica cum furfure ut prius et erunt lucidissime.*

[5] The text says *piscis bucefalli,* which this author interprets to mean 'a fish the size of Bucephalus', Alexander the Great's horse, which was the largest animal of this kind in the Greek-Macedonian army.

[6] *Om perlen te conterfeyten…om perlen te maken anders…nempt groote schoon mossel sculpen ende maecktse heet ende doetse in wyn asyn, daer na nempt de sculpen ende poeyertste ende cristalynen gelas ook gepoedert* (manuscript no. 64, Museum Plantin-Moretus, Antwerp, Belgium; reported by Rijks 2014, p. 309).

Figure 5: This close-up of a portrait of Bianca Maria Sforza, painted by Giovanni Ambrogio de Predis (a co-worker of Leonardo da Vinci) in 1493 before her marriage to the future emperor Maximilian of Habsburg, shows magnificent pearls decorating her hair, head and necklace. Image courtesy of the National Gallery of Art, Washington DC, USA (Widener Collection, Accession No. 1942.9.53).

and since most of them came from far away. While the Portuguese imported them from the Gulf of Mannar and the Spaniards obtained them from the newly discovered fisheries in the Caribbean Sea (e.g. Venezuela and Panama), the traditional caravan routes continued supplying these expensive commodities to Europe via Venetian merchants all along the Middle Eastern coast and through Venice. It is no wonder that counterfeiters contemplated how to make use of the typically small, dull, poorly shaped pearls frequently found in the local freshwater fisheries, seeking to develop alchemical methods to improve them. The young Leonardo also considered reconstituting small pearls into a large one, and to make it perfectly round, bright and polished using mechanical methods he adapted from his engineering experience.

No evidence for such artificial pearls is known, although paintings representing high-ranking members of the Milan duke court where Leonardo was employed do show examples of relatively large, round, white pearls. The most magnificent illustration is the portrait of Bianca Maria Sforza, the niece of the acting duke Ludovico Maria 'il Moro'. He was determined to marry her to the emperor-to-be Maximilian of Habsburg in order to have his duke title confirmed. He had her portrayed by Giovanni Ambrogio de Predis, a co-worker of Leonardo (Figure 5), in which her head and hair are covered with perfectly round pearls, and she also wears a pearl necklace with a drop that is mounted with large gemstones and an impressive oval pearl. In addition, a pearl-studded *scopetta* (whisk), the heraldic symbol of the Sforza family, hangs above her left ear, a symbol of her being imbued with Sforza power and cleverness.

Were these beautiful white pearls all natural, or did Leonardo da Vinci, at that time employed as court jewellery designer, besides painter and architect, somehow improve them? We will never know. Certainly, if he did do something more than design the apparel of the empress-to-be, he would not have tried to substitute natural pearls with artificial ones. Ludovico Maria 'il Moro' would not have pardoned such an insult, even from his favourite court painter.

REFERENCES

Avial-Chicharro, L. 2019. Romans prized these jewels more than diamonds. *National Geographic*, 2 April, www.nationalgeographic.com/history/magazine/2019/03-04/roman-republics-captivation-with-pearls.

Beretta, M. & Conforti, M. (eds) 2014. *Fakes!? Hoaxes, Counterfeits and Deception in Early Modern Science.* Science History Publications, Sagamore Beach, Massachusetts, USA, 280 pp.

Berthelot, M. 1887–1888. *Collection des Anciens Alchimistes Grecs.* Georges Steinheil, Paris, France, 536 pp.

Bol, M. 2019. *Polito et claro:* The art and knowledge of polishing, 1100–1500. *In:* Bycroft, M. & Dupré, S. (eds) *Gems in the Early Modern World: Materials, Knowledge and Global Trade, 1450–1800*. Palgrave Macmillan, Cham, Switzerland, 223–257, https://doi.org/10.1007/978-3-319-96379-2_9.

Bycroft, M. & Dupré, S. (eds) 2019. *Gems in the Early Modern World: Materials, Knowledge and Global Trade, 1450–1800.* Palgrave Macmillan, Cham, Switzerland, xvii + 359 pp., http://doi.org/10.1007/978-3-319-96379-2.

Calvi, G. 1925. *I manoscritti di Leonardo da Vinci dal punto di vista cronologico, storico e biografico*. Nicola Zanichelli, Bologna, Italy, ix + 324 pp.

Darmstaedter, E. 1925. Liber claritatis totius alkimicae artis: Bologna Cod. Lat. 164 (153). *Archeion*, **6**(4), 319–330, http://doi.org/10.1484/J.arch.3.194.

Darmstaedter, E. 1926. Liber claritatis totius alkimicae artis als deren Autor "Geber" genannt wird: Bologna Cod. Lat. 164 (153). *Archeion*, **7**(3), 257–266, http://doi.org/10.1484/J.arch.3.228.

Darmstaedter, E. 1927a. Liber claritatis totius alkimicae artis dem arabischen Alchemisten Geber zugeschrieben: Bologna Cod. Lat. 164 (153). *Archeion*, **8**(1), 95–103, http://doi.org/10.1484/J.arch.3.251.

Darmstaedter, E. 1927b. Liber claritatis totius alkimicae artis dem arabischen Alchemisten Geber zugeschrieben: Bologna Cod. Lat. 164 (153). *Archeion*, **8**(2), 214–229, http://doi.org/10.1484/J.arch.3.260.

Darmstaedter, E. 1928. Liber claritatis totius alkimicae artis dem arabischen Alchemisten "Geber" zugeschrieben: Bologna Cod. Lat. 164 (153). *Archeion*, **9**(1), 63–80, http://doi.org/10.1484/J.arch.3.294.

Friess, G. 1980. *Edelsteine im Mittelalter: Wandel und Kontinuität in ihrer Bedeutung durch zwölf Jahrhunderte (in Aberglauben, Medizin, Theologie und Goldschmiede-kunst)*. Gerstenberg-Verlag, Hildesheim, Germany, 206 pp.

Guerrini, O. & Ricci, C. 1887. *Il Libro dei Colori: Segreti del Secolo XV*. Romagnoli Dall'Acqua, Bologna, Italy, 351 pp.

Halleux, R. 1981. *Les Alchimistes Grecs, Tome I. Papyrus de Leyde, Papyrus de Stockholm, Fragments de Recettes.* Les Belles Lettres, Paris, France, xv + 237 pp.

Kunz, G.F. & Stevenson, C.H. 1908. *The Book of the Pearl: Its History, Art, Science and Industry.* The Century Co., New York, New York, USA, 826 pp.

Landino, C. (transl) 1476. *Historia naturale di C. Plinio secondo tradocta di lingua latina in fiorentina per Christophoro Landino fiorentino al serenissimo Ferdinando re di Napoli*. Venetiis, Opus Nicolai Iansonis Gallici impressum.

Manni, P. 2008. *Percorsi nella lingua di Leonardo: grafia, forme, parole* (XLVIII Lettura Vinciana). Giunti Editore, Florence and Milan, Italy, 32 pp.

Marinoni, A. 1975–1980. *Il Codice Atlantico della Biblioteca Ambrosiana di Milano. Trascrizione diplomatica e critica di Augusto Marinoni.* Giunti-Barbèra, Florence, Italy, 12 vols.

Marinoni, A. 1987. La biblioteca di Leonardo. *Raccolta Vinciana*, **22**, 291–342.

Marinoni, A. 2004. *Il Codice Atlantico di Leonardo da Vinci. Indici per materie e alfabetico.* Giunti-Barbèra, Florence, Italy, 128 pp.

Mottana, A. 2018. Separazione chimica e titolo dell'oro nell'Europa premoderna. *La Chimica & L'Industria*, Anno II, No. 5, 10–15.

Nassau, K. & Hanson, A.E. 1985. The pearl in the chicken: Pearl recipes in *Papyrus Holmiensis. Gems & Gemology*, **21**(4), 224–231, http://doi.org/10.5741/gems.21.4.224.

Oviedo (Fernández de Oviedo y Valdés, G.) 1526. *Sumario de la Natural Historia de las Indias*. Ramon Petras, Toledo, Spain, 100 pp.

Piumati, G. & Brioschi, F. 1894–1904. *Il Codice Atlantico di Leonardo da Vinci Nella Biblioteca Ambrosiana di Milano. Riprodotto e pubblicato dalla Regia Accademia dei Lincei sotto gli auspici e col sussidio del Re e del Governo. Trascrizione diplomatica e critica di Giovanni Piumati*. Ulrico Hoepli, Milan, Italy, xiv + 1311 pp. plus atlas.

Reti, L. 1952. Le arti chimiche di Leonardo da Vinci. II. Leonardo e l'alchimia. *La Chimica e L'Industria*, **34**(12), 721–743.

Rijks, M. 2014. Gems and counterfeited gems in early modern Antwerp: From workshops to collections. In: Bycroft, M. & Dupré, S. (eds) *Gems in the Early Modern World: Materials, Knowledge and Global Trade, 1450–1800*. Palgrave Macmillan, Cham, Switzerland, 309–329, https://doi.org/10.1007/978-3-319-96379-2_12.

Schmetzer, K. 2019. A 15th-century polishing machine for gemstones attributed to Henri Arnaut. *Journal of Gemmology,* **36**(6), 544–550, http://doi.org/10.15506/JoG.2019.36.6.544.

Silva, R. 2016. Il colore dell'inganno: Gemme, perle, ambra e corallo artificiali secondo un manoscritto del XIII secolo. *In: Il Colore nel Medioevo. Arte simbolo tecnica, Atti delle Giornate di Studi Lucca, Istituto Storico Lucchese, Lucca*, Italy, 283–296.

Strack, E. 2015. European freshwater pearls: Part 1—Russia. *Journal of Gemmology*, **34**(7), 580–592, http://doi.org/10.15506/JoG.2015.34.7.580.

Vandamme, E. 1974. Een 16e-eeuws Zuidnederlands receptenboek. *Jaarboek van het Koninklijk Museum voor Schone Kunsten Antwerpen*, 101–137.

Venturelli, P. 2001. Segreti di Leonardo da Vinci per ottenere 'perle grosse'. *Arte Lombarda*, **132**(2), 42–47.

Venturelli, P. 2002. Segreti di Leonardo per ottenere «perle grosse». Elenco ricette per realizzare perle false. *Leonardo da Vinci e le Arti Preziose. Milano tra XV e XVI Secolo*, Marsilio Editori, Venice, Italy, 112–122.

von Lippmann, E.O. 1919. *Entstehung und Ausbreitung der Alchemie*. Julius Springer, Berlin, Germany, 772 pp.

The Author

Dr Annibale Mottana
Dipartimento di Scienze, Università Roma Tre, Largo San Leonardo Murialdo 1, 00146 Rome, Italy
Email: annibalemottana86@gmail.com

Conferences

36TH INTERNATIONAL GEMMOLOGICAL CONFERENCE

The 36th biennial IGC took place 27–31 August 2019 at La Cité Nantes Congress Centre in Nantes, France. The conference was organised by **Dr Emmanuel Fritsch**, **Dr Nathalie Barreau** and **Féodor Blumentritt** of the University of Nantes, in collaboration with **Dr Jayshree Panjikar** (Pangemtech and Pangem Testing Laboratory, Pune, India) and the IGC Executive Committee. Approximately 96 delegates, observers and guests from 29 countries gathered for the conference (e.g. Figure 1), and some attended pre- and post-conference field trips. A proceedings volume containing extended abstracts can be downloaded at www.igc-gemmology.org (which now also hosts proceedings volumes from previous IGCs back to 2011).

The first day of the conference was devoted to an 'open colloquium' that was attended by French gemmologists who could not otherwise attend the IGC (a members-only event). **Dr Fritsch** opened the colloquium and introduced the 10 invited presenters (e.g. Figure 2). **John Koivula** (Gemological Institute of America [GIA], Carlsbad, California) reviewed internal features in gems, and showed a variety of solid and fluid inclusions. Some of them inspired the imagination, such as iron oxides in agate that looked like rifle bullets and dendrites in an iron-stained quartz fracture that resembled a cave painting. When inclusions are large and visible enough (e.g. tourmaline 'pinwheels' in quartz, bugs in amber, etc.), they become examples of wearable natural art. **Dr Hanco Zwaan** (National Museum of Natural History 'Naturalis', Leiden, The Netherlands) examined the geochemistry of sapphires for the purpose of studying their geological and geographical origins. Trace elements and their ratios are useful for assessing a magmatic (basalt-related), metamorphic or metasomatic/plumasitic origin, which is particularly helpful for investigating the primary origin of sapphires from secondary deposits such as those in Sri Lanka (which are essentially metasomatic). **Shane McClure** (GIA, Carlsbad) reviewed collaborative research done with several co-authors worldwide on sapphires that are heat-treated under pressure. The gems are treated in Korea and sold by one dealer in Sri Lanka; only a limited amount are produced (about 300–400 stones/month). Although the treatment is accomplished much faster than conventional heating processes, it is restricted to only one or two stones at a time and has a relatively high failure rate (approximately 30%). Their research showed no differences in the durability or brittleness of the treated sapphires compared to those that have undergone conventional heating. **Tom Stephan** (German Gemmological Association, Idar-Oberstein, Germany) gave a presentation for **Dr Claudio Milisenda** and co-authors (DSEF German Gem Lab, Idar-Oberstein) on Mozambique ruby. He described the history of mining at Montepuez and differentiated rubies from two main productive areas that are being mined by Gemfields:

Figure 1: Delegates, observers and guests assemble for the 36th International Gemmological Conference. Photo by Gordon Duan.

Figure 2: The first day of the IGC consisted of an 'open colloquium' that featured presentations from several speakers, including from (left to right): Tom Stephan, Dr Thomas Hainschwang, Peter Lyckberg, Brendan Laurs, John Koivula, Tay Thye Sun, Dr James Shigley, Shane McClure and Dr Hanco Zwaan. (Not shown is Kenneth Scarratt.) Photo by Ahmadjan Abduriyim.

Maninge Nice (a primary occurrence that yields large quantities of flat, light-coloured crystals) and Mugloto (a secondary deposit that produces much smaller amounts of better-quality ruby). At the time of Dr Milisenda's visit to Montepuez, Gemfields was capable of processing 3.5 million tonnes of material per year, and their washing plant was handling 150 tonnes per hour. From August 2012 to December 2015 the mining area yielded a total of 17.2 million carats of mixed-quality ruby and pink sapphire. **Peter Lyckberg** (Museum of Natural History, Luxembourg) reviewed gems and minerals from granitic pegmatites in Afghanistan and Pakistan. He described the production of tourmaline, kunzite, morganite and various rare minerals in Afghanistan since the initial discovery of pegmatites there in 1959 near Kala village in the Pech Valley. In recent times, up to 100,000 miners have been active in Pakistan's Shigar Valley. **This author** described coloured stone and diamond deposits in Namibia (see Gem Notes in Vol. 36, No. 1, 2018, pp. 8–9 and 16–18).

The open colloquium also featured two diamond presentations. **Dr Thomas Hainschwang** (GGTL Laboratories, Balzers, Liechtenstein) reviewed diamond luminescence and its usefulness for distinguishing between natural vs. synthetic material (as well as imitations), natural vs. artificial colour and natural vs. HPHT-treated colourless diamonds. The use of high power and a variety of excitation wavelengths from 210 to 400 nm is helpful for observing diamond fluorescence, even for samples that would not normally show any luminescence under standard UV lamps. **Dr James Shigley** (GIA, Carlsbad) provided an update on synthetic diamonds. While natural diamonds formed over extended periods of time and very long ago, synthetic diamonds crystallise during short periods of time and originated very recently. The key difference between them is the time spent under high-temperature conditions, which influences the type and distribution of their defects as detectable by various spectroscopic techniques, thereby enabling them to be reliably separated by a well-equipped gemmological laboratory.

Biogenic gems were covered in two presentations at the open colloquium. **Kenneth Scarratt** (Bahrain Institute for Pearls & Gemstones [DANAT]) and co-authors described natural pearls from Bahrain. Currently approximately 7 kg of pearls are produced annually from *Pinctada radiata* molluscs, which typically yield one pearl per 100 shells harvested. The pearls are classified at DANAT according to their shape, lustre, surface characteristics, colour and fluorescence, and they can be separated from *P. maxima* pearls by their trace-element composition. **Tay Thye Sun** (Far East Gemmological Laboratory, Singapore) discussed research done with his co-authors on amber from Hti Lin, Myanmar (see article in *The Journal*, Vol. 34, No. 7, 2015, pp. 606–615).

On 28 August, the IGC was opened by Executive Committee secretary **Dr Jayshree Panjikar**, who described the history of IGC activities and also announced the recent passing away of IGC delegates Alan Jobbins, Gerhard Becker and Hermann Bank. Then **Dr Fritsch** (Figure 3) welcomed the attendees to Nantes and mentioned the conference sponsors and logistics.

Diamonds were the subject of the first conference session. **Dr Eloïse Gaillou** (MINES ParisTech, Paris, France) and co-authors examined the genesis of blue diamonds by studying solid and fluid inclusions in four rough samples from the Cullinan mine in South Africa. They found graphite-H_2O assemblages in both primary and secondary inclusions, as well as the presence of a lithospheric mineral assemblage, which shows that type IIb blue diamonds may form at various depths below the deep roots of a craton and do not necessarily have a 'superdeep' origin. **Marie Schoor** (Cartier Joaillerie

Figure 3: Dr Emmanuel Fritsch was one of the organisers of the 36th IGC. Photo by B. M. Laurs.

International, Paris, and University of Nantes) and co-authors characterised growth sectors in asteriated diamonds. They examined 13 samples, most of which showed distinct patterns created by a combination of octahedral sectors that were near-colourless with cuboid sectors that were grey or brown and had 3, 4 or 6 lobes. The colour of the cuboid sectors was due to abundant graphitised discoid micro-inclusions (2–7 µm). Two of the samples contained needle-like inclusions that were interpreted as rose channels (i.e. mechanical twinning created by intense plastic deformation). **Roman Serov** (Octonus Software, Moscow, Russia) and **Sergey Sivovolenko** (Octonus Finland Oy, Tampere) studied the influence of UV fluorescence on the colour appearance of diamonds. The viewing tray is particularly important for colour grading because it is much closer to the diamond than the lamp. While diamonds are graded by laboratories using plastic trays, they are commonly viewed by members of the trade with paper trays. This, and differences in the light sources used, create inconsistencies in assessing the impact of fluorescence on diamond appearance. **Aurélien Delaunay** (Laboratoire Français de Gemmologie, Paris) and co-authors proposed a classification for type IIa diamonds on the basis of their emission colours and patterns seen in the DiamondView. The fluorescence colours reflect the presence of various defects and trace impurities, while the textures can be related to growth (i.e. sectors, banding and layering) or deformation (polygonal dislocations, graining and curved patterns). Nevertheless, growth patterns are rarely seen in type IIa diamonds and are much more easily observed in type Ia stones.

Synthetic and treated diamonds were covered in four presentations. **Dr Hiroshi Kitawaki** and co-authors (Central Gem Laboratory, Tokyo, Japan) reported on the current production of synthetic diamonds in China and India. (*Editor's note*: See the article on pp. 748–757 of this issue for more on Chinese synthetics.) China is the world's largest producer of HPHT-grown synthetic diamonds, and analyses of metallic inclusions in samples from different manufacturers revealed distinct differences in the proportions of Fe, Co and Ni. India is an important source of CVD synthetics (estimated at 125,000 carats/month) and now produces faceted goods up to 5 ct. **Dr Andy Shen** presented research on behalf of his co-authors from the China University of Geosciences (Wuhan, Hubei Province) on the phosphorescence of HPHT-grown type IIb colourless synthetic diamonds from China. Their phosphorescence was long-lived (5 minutes or longer) and was greenish blue and/or yellowish orange. Analysis with a fluorescence spectrometer showed that the phosphorescence was centred at 470 nm and was excited by wavelengths ranging from 215 to 240 nm. **Jean-Pierre Chalain** (Swiss Gemmological Institute SSEF, Basel, Switzerland) and co-authors evaluated the performance of the ASDI diamond verification instrument using different-sized type Ib HPHT synthetic diamonds with identical very low nitrogen concentrations (approximately 1 ppm). A single piece of synthetic rough material was cut into three round brilliants with diameters of 1.5, 2.0 and 3.0 mm so that the correlation between sample size, colour and short-wave UV transmission could be established (the last factor being important for the instrument's 'referral' threshold of specimens for further testing). **Dr Thomas Hainschwang** and **Gianna Pamies** (GGTL Laboratories) examined the effects of HPHT treatment on previously irradiated and annealed diamonds of various types and colours. They were surprised to find that HPHT treatment at 2,500°C of yellow 'cape' diamonds produced brown colouration that probably results from the destruction of the N3 centre, causing an unusual continuum of absorption.

The next session featured presentations on gem and jewellery history and age dating. **Dr H. Albert Gilg** (Technical University of Munich, Germany) and co-authors used the chemical composition of apatite and/or monazite inclusions to evaluate the origin of ancient red garnets of almandine to pyrope composition. Garnets encompassing Hellenistic, Roman and Early Medieval times have been grouped into at least six clusters according to their trace elements and inclusion features, but the original provenance of many of these

archaeological samples has not been well established. The morphology, chemical composition and age data obtained from apatite and/or monazite inclusions yields additional information that can help constrain the source of the garnets. **Dr Karl Schmetzer** (Petershausen, Germany) and **Dr H. Albert Gilg** studied the English crown of Blanche of Lancaster, dated to the 1380s (Late Middle Ages) in the treasury of the Residence Museum in Munich, Germany. The gems adorning the crown consist of diamonds, diamond imitations, blue sapphires, a blue sapphire doublet, pink sapphires, pink spinels, garnets, emeralds and lead glass (green and pink). **Dr Michael Krzemnicki** (Swiss Gemmological Institute SSEF) and co-authors reviewed the age dating of coloured stones and biogenic materials. In support of testing and origin determination, SSEF has successfully performed radiometric age dating (U-Pb and Th-Pb) on corundum and spinel using a variety of inclusions, such as zircon, zirconolite, xenotime, monazite, baddeleyite, rutile, apatite and titanite. For gem corundum, the age dates allow stones to be placed into one of three main global geological frameworks: Pan-African tectono-metamorphic events about 750–450 million years ago (Ma), the Himalayan orogeny about 40–10 Ma and alkali basalts related to extensional tectonics of about 4 Ma and younger. **Elisabeth Strack** (Gemmologisches Institut Hamburg, Germany) and **Bernd Augustin** (Hamburg) performed a gemmological examination of four Mogul jewellery objects dating from the first half of the 17th century. They were found to be set with diamonds (mirror, rose and table cuts, as well as macles), rubies (showing characteristics consistent with a Burmese origin), red spinels, emeralds and pearls.

The next session was devoted to coloured stones. **Carolina Santiago** (University of Bremen, Germany) and **Dr Jurgen Schnellrath** (Mineral Technology Centre, Rio de Janeiro, Brazil) studied cat's-eye opal from Socotó, Bahia, Brazil. Raman microspectroscopy showed that the fibrous mineral responsible for the chatoyancy is chrysotile, while X-ray diffraction analysis confirmed that the host material is opal-CT. The green-to-brown colouration of these opals is due to a combination of mineral inclusions and Rayleigh scattering. **Dr Alessandra Costanzo** (Figure 4) and **Dr Martin Feely** (National University of Ireland Galway, Ireland) reviewed gem and ornamental materials from Connemara, western Ireland. Connemara marble has been widely used in jewellery and souvenir gift items since the 19th century (*Editor's note*: See the article in *The Journal*, Vol. 36, No. 5, 2019, pp. 456–466), and small sapphires are known from two localities (Lough Whelaun and Toombeola). Recently (in 2015), transparent well-formed crystals of fluorite showing various colours were mined from Larkin's Shannapheasteen Granite Quarry.

Figure 4: Dr Alessandra Costanzo discusses colour-zoned crystals of fluorite from Connemara, western Ireland. Photo by B. M. Laurs.

Dr Thet Tin Nyunt (Ministry of Natural Resources and Environmental Conservation, Nay Pyi Taw, Myanmar) and co-authors studied jadeite from the Natmaw deposit in the Khamti (or Hkamti) area of northern Myanmar. Dykes of jadeitite are hosted by serpentinised peridotite associated with 'blackwall' alteration zones. Jadeite has been mined from both primary and secondary deposits, and is categorised into Imperial, commercial and utility grades, as well as into three main texture types (primary, deformed and recrystallised).

Dr Shang-i (Edward) Liu (Gemmological Association of Hong Kong) gave a presentation for **Gamini Zoysa** (Ceylon Gemmological Services, Colombo, Sri Lanka) and co-authors on spinel from Sri Lanka. The most important mining areas for spinel are Ratnapura (which produces all colours, including 'cobalt blue' and star stones), Okkampitiya (green, bluish green, pink and purple), Elahera (pink and purple) and Horana (all colours). The internal features and chemical composition were described for spinel from each of these localities. **Chengsi Wang** (China University of Geosciences, Wuhan) and co-authors characterised copper nanoparticles within Oregon sunstone. They found that red sunstone contains spherical Cu nanoparticles of about 13 nm in diameter, while dichroic green sunstone hosts oriented elongate spheroid Cu-containing nanoparticles with dimensions of about 26 nm in the orientation corresponding to green pleochroism and about 10 nm in the red direction. **Féodor Blumentritt** and co-authors (Institut des Matériaux Jean Rouxel and University of Nantes) investigated mechanisms involved with photochromism (i.e. reversible colour change resulting from exposure to UV radiation, thought to be due to sulphur) in hackmanite—and, by inference, in scapolite and tugtupite. Using synthetic hackmanite powders, they were successful at influencing the degree of the photochromism by changing the amount of sulphate in the starting material.

Peter Lyckberg and co-authors documented giant cavities containing heliodor, topaz and smoky quartz in the Volodarsk-Volinsky granitic pegmatites in Ukraine. Specifically, the Volyn Piezo Quartz deposit was mined for piezoelectric quartz but also contained topaz in 10% of the miarolitic pegmatites and beryl in 2% of them. Rough material is sold as faceting rough and is also processed using automatic cutting machines into finished gemstones (topaz and beryl) and other polished objects (quartz). **Gagan Choudhary** (Gem Testing Laboratory, Jaipur, India) discussed challenges with identifying filled emeralds. He described differences in the process of filling fissures with traditional vs. modern fillers, which typically result in an uneven/reflective vs. smooth appearance of the fractures, respectively. More than one filling substance can be present in a single stone (or fracture), and may result from the application of epoxy during the cutting and polishing process, incomplete cleaning of pre-existing resin-filled fissures, and finally refilling with oil. **Dr Shang-i (Edward) Liu** and co-authors described pezzottaite from Pyi-Gyi-Taung, Myanmar. Pezzottaite was recently produced from a rubellite-bearing pegmatite located 6 km east of Letpanhla village, and occurs mixed with beryl in well-formed pale pink crystals. Only about 1 kg of these 'mixed crystals' has been produced in the past five years. The Burmese pezzottaite contains an average of 14.4 wt.% Cs_2O, which is similar to material from Madagascar. **Tasnara Sripoonjan** and co-authors (Gem and Jewelry Institute of Thailand [GIT], Bangkok, Thailand) examined the gemmological and chemical characteristics of peridot from Yiqisong, Jilin, China. They have similar properties compared to peridot from other localities, and their internal features consist of lily pads, wispy veils, iridescent partially healed fractures and tiny unidentified crystals, as well as protogenetic tabular chromite crystals (brown to brownish red) that appear unique to peridot from this locality. **Dr Isabella Pignatelli** (University of Lorraine, Vandoeuvre-lès-Nancy, France) and co-authors examined trapiche texture in emerald and ruby. This distinctive texture has not been observed in minerals with low symmetry, and appears to be controlled by factors associated with the geological environment of crystallisation, such as the presence of organic material/graphite and evaporites, thermal reduction of sulphates, and variations in the pressure and composition of the parental fluids. (*Editor's note*: For more on this research as it applies to trapiche rubies from Vietnam, see the article on pp. 726–746 of this issue.)

Dr Jaroslav Hyršl (Prague, Czech Republic) reviewed his genetic classification of mineral inclusions in quartz. Of the 10 or more geological environments that produce quartz with inclusions, the vast majority of specimens come from Alpine fissures (hydrothermal veins). About 200 different minerals have been documented in quartz from such veins. Brazil is the largest producer of quartz with inclusions, mostly from veins hosted by quartzites. **Willow Wight** and co-authors (Canadian Museum of Nature, Ottawa, Ontario) described tourmaline from the Leduc mine in Québec, Canada. This small deposit was initially mined for muscovite in 1884, and in 1908 it was explored for gem tourmaline. The largest collection of faceted Leduc tourmaline is owned by Brad Wilson

(Alpine Gems, Kingston, Ontario, Canada) and consists of about two dozen stones that are mostly greenish blue to yellowish green. Selected samples were gemmologically and chemically analysed by the authors and found to consist of fluor-elbaite. **Dr Lutz Nasdala** (University of Vienna, Austria) and co-authors examined ekanite ($Ca_2ThSi_8O_{20}$), a metamict gem material from Sri Lanka. Inclusions consist of an apatite-group mineral, thorium silicate, silica, Ca carbonate, Ca silicate and fluids. Chemical analysis showed impurities of 2.8 wt.% UO_2 and traces of Pb and Fe.

Numerous presentations covered gem corundum. **Dr Rainer Schultz-Güttler** and **Bruno Zampaulo** (University of São Paulo, Brazil) studied unusual ruby-fuchsite rocks from eastern Brazil and western India. The rocks are polished into attractive spheres and other decorative objects, and material from each country contains different mineral assemblages. **Dr Jayshree Panjikar** and **Aatish Panjikar** (Pangemtech and Pangem Testing Laboratory) investigated rubies from Paramathi in the Karur District of Tamil Nadu, India. The material ranges from pinkish red to deep red and is semi-transparent to transparent. It is related to garnet-biotite schist and contains inclusions of zircon, spinel, garnet, ilmenite and rutile. **Supparat Promwongnan** and co-authors (GIT) discussed rubies and sapphires from the Chanthaburi-Trat and Kanchanaburi gem fields in Thailand. The Chanthaburi-Trat area is a source of both ruby and sapphire, which are inferred to have formed under different conditions: ruby from a mafic granulite source at 30–50 km depth and at about 700–1,000°C, and sapphire from a syenite source at a shallower depth and lower temperature. (*Editor's note*: For more on these rubies, see the article in *The Journal*, Vol. 36, No. 7, 2019, pp. 634–645.) Kanchanaburi only produces sapphire, which likewise has a syenite origin. Gem corundum at both localities was brought to surface by alkali basalts that are generally less than 4 Ma. **Stephen Kennedy** (Gem & Pearl Laboratory Ltd, London) discussed the identification of natural vs. synthetic Fe/Ti-diffusion-treated sapphire. Such material may not contain any distinctive inclusions, and therefore it is helpful to check for Plato lines that are characteristic of flame-fusion synthetics, collect UV-Vis spectra (strong peaks at 450 and 375/388 nm indicate a natural origin) and obtain chemical data (very low levels of Ga indicate a synthetic origin). **Kentaro Emori** (Central Gem Laboratory) and co-authors characterised Be-containing nanoinclusions in untreated blue sapphire from northern Madagascar. Analyses by LA-ICP-MS and TEM showed a good correlation of Ti:Be:Nb:Ta = 16:3:1:4 in the nanoinclusions, which may consist of an as-yet unknown mineral. **Dr Pornsawat Wathanakul** (Kasetsart University, Bangkok) delivered a presentation for her co-authors on the Fe and Ti oxidation states in ruby and blue sapphire. Various sample types (natural, synthetic, Be-treated and surface-diffusion-treated sapphires and unheated/heated rubies) were analysed at a synchrotron facility in Thailand by X-ray absorption near-edge spectroscopy. In all of the sapphires, iron was always present as Fe^{3+} and titanium as Ti^{4+}. The authors proposed that blue colour in sapphire is due to Fe^{3+}/Ti^{4+} pairs rather than Fe^{2+}/Ti^{4+} intervalence charge transfer. **Tom Stephan** and co-authors performed low-temperature and flux-assisted heat treatment of rubies and pink sapphires from Mozambique and Greenland. Bluish colour zones were removed from Mozambique rubies by heating to approximately 800°C, and the treatment could be identified by the reddening (oxidation) of secondary iron hydroxides, as well as by spectroscopic evidence for the breakdown of Al-hydroxides and the transformation of Fe-hydroxides to Fe-oxides. The diaphaneity of samples from both localities showing low clarity could only be improved by heating at high temperature with a (borax) flux. Without the use of a flux, Al-hydroxides along twin lamellae dehydrated, leaving white layers of polycrystalline corundum. **Sutas Singbamroong** (Chiang Mai University, Chiang Mai, Thailand and Dubai Central Laboratory, Dubai, United Arab Emirates) and co-authors studied Be-diffused geuda sapphires from Sri Lanka that were treated in Chanthaburi, Thailand, to intensify and even-out their blue colour while also improving their clarity. A three-part process was employed: (1) heating in a traditional furnace to about 1,500°C for two hours in an oxidising atmosphere, (2) Be diffusion in an electric furnace at about 1,700°C for 48 hours in an oxidising atmosphere and (3) reheating in a fuel-type furnace to about 1,700°C for 72 hours in a reducing atmosphere. **Thanapong Lhuaamporn** (GIT) gave a presentation for **Thanong Leelawatanasuk** and his co-authors on the characteristics of blue sapphire enhanced using heat and pressure. During a visit to the treatment facility in Korea, they learned that previously treated material is preferred since the rapid heating causes too much damage to unheated stones. Low-temperature annealing of such treated sapphires may be done to lighten their blue colour, and the authors' experiments showed that the colour faded somewhat at around 1,000°C. However, this also caused partial or complete elimination of distinctive features seen in their inclusions and IR spectra. **Shane McClure** also covered sapphires that are heat-treated under pressure, as reported above

for the open colloquium. **Martial Bonnet** (Centre de Recherches Gemmologiques, Nantes) and **Dr Emmanuel Fritsch** proposed a set of seven absorption bands that are common in the infrared spectra of corundum: a broad band consisting of a group at 3220, 3065, 3025 and 2980 cm^{-1}, and other features at 2625, 2460 and 2415 cm^{-1}.

Presentations on biogenic materials covered pearls, coral and ivory. **Bahareh Shirdam** (China University of Geosciences, Wuhan and University of Tehran, Iran) and co-authors studied rumoured Persian amber samples that were reportedly mined in eastern Azerbaijan, Alborz (north-central Iran) and the Tabas Block (east-central Iran). FTIR spectroscopy was used to classify the Persian amber samples as a type III fossilised resin (perhaps derived from *Liquidambar* or Persian ironwood trees), and their thermal behaviour indicated a high degree of maturation. **Dr Laurent Cartier** (Swiss Gemmological Institute SSEF) and co-authors reviewed the DNA fingerprinting of pearls, precious coral and ivory. DNA has been successfully extracted from cultured pearls obtained from three species (*Pinctada maxima*, *P. margaritifera* and *P. radiata*). Recent research shows that DNA can also be obtained from small samples (2 mg) of precious coral and larger samples of ivory. **Dr Stefanos Karampelas** and co-authors (DANAT) provided new insights on the X-ray luminescence of natural and cultured pearls from freshwater and saltwater bivalves. Although yellow-green luminescence is typical of freshwater cultured pearls due to their appreciable manganese contents, some samples with high Mn exhibit much lower luminescence than expected due to Mn^{2+} self-quenching. In addition, saltwater cultured pearls may also display luminescence due to the presence of a freshwater bead combined with thin nacre. **Abeer Al-Alawi** and co-authors (DANAT) described *P. radiata* cultured pearls from Abu Dhabi in the United Arab Emirates. Pearls from this species are rarely cultured. The samples had a nacre thickness of 0.8–2.0 mm, and most of them displayed green to yellowish green fluorescence to long- and short-wave UV radiation. Compared to natural pearls from *P. radiata*, the cultured products showed higher Mg and lower Ba contents. **Anette Juul-Nielsen** (Ministry of Mineral Resources and Labour, Government of Greenland, Nuuk) and **Hans Lange** (Greenland National Museum & Archives, Nuuk) described the past and present use of ivory from Greenland. The raw material is derived from narwhal and walrus, which are traditionally hunted for their meat and skin. While narwhal ivory typically has cracks along interstitial areas of its spirals, walrus ivory displays an oatmeal-like texture and a central layer of secondary dentine that shows stronger UV fluorescence than the surrounding primary dentine.

Several presentations were given in a session on general gemmology. **Dr Ahmadjan Abduriyim** (Tokyo Gem Science and GSTV Gemological Laboratory, Tokyo, Japan) recounted some gem mining activities that took place after 2000, including sapphires from Sri Lanka (2012 at Kataragama and 2015 at Bogawantalawa), sapphires and rubies from Madagascar (2017 at Bemainty), ruby from Montepuez, Mozambique and emerald from Belmont, Brazil. His presentation also described the simultaneous analyses of multiple spots on a gem sample with LA-ICP-MS using galvanometric optics. **This author** provided insights on writing scholarly gem locality articles, offering advice for the successful preparation and execution of a field expedition, as well as subsequently sharing the research in a peer-reviewed journal. **Dr Hao Wang** and co-authors (Swiss Gemmological Institute SSEF) reviewed developments in the multi-element analysis of gem materials and its application to geographical origin determination. Statistical algorithms for processing multi-element data include t-distributed stochastic neighbour embedding (t-SNE), principal component analysis (PCA) and linear discriminant analysis (LDA). The t-SNE technique was most successful for clustering data obtained for Cu+Mn-bearing tourmalines. **Menahem Sevdermish** (Gemewizard Gemological Laboratory, Ramat Gan, Israel) used colour analysis technology applied to 'big data' obtained from stones offered for sale on the Internet (with and without laboratory reports) to explore commercial gem names. He showed differences in the colour borders for 'pigeon blood' ruby and 'cornflower blue' sapphire (according to consumers from various world regions and gem laboratories), 'vivid green' emerald (according to the trade vs. laboratories) and 'Santa Maria' vs. 'classic' aquamarine. He also gave trade insights on gem varieties that are currently popular in various regions of the world and mentioned that millennials seem to prefer lighter-coloured gems since more saturated stones 'look unreal' to them.

In other presentations on general gemmology, **Lore Kiefert** and **Klaus Schollenbruch** (Gübelin Gem Lab, Lucerne, Switzerland) studied damage in gems that occurs when a jewellery repair laser misses the metal and hits the stone. Using an Nd-YAG laser (1054 nm, 1.45 J, 3+ W), they tested a variety of gems and found that the most damage occurred on the back side of each specimen where the laser beam exited the stones. Laser damage can be avoided by lowering the laser power and hand-holding the gem (or at least putting a finger on it) during the repair procedure. **Tom Stephan** (German

Gemmological Association and Johannes Gutenberg University Mainz, Germany) and co-authors performed UV-Vis-NIR spectral fitting for the quantitative determination of Cr^{3+} and V^{3+} in ruby and emerald. Spectral fitting can be used to assess the colour contribution from each element by mathematically deconvoluting the bands into constituent absorptions, thus permitting an understanding of the influence of each chromophore. In corundum, V^{3+} contributes somewhat to red colouration but is mainly involved with colour-change phenomena, while in emerald V^{3+} and Cr^{3+} both contribute to green colouration. **Dr Emmanuel Fritsch** presented research done with his co-author **Martine Philippe** (Paris) on dissolved dislocations in gems (see Conferences section of *The Journal*, Vol. 36, No. 7, 2019, p. 662).

Poster presentations at the IGC were prepared by **Quanli Chen** and co-authors (turquoise from Zhushan, Hubei Province, China), **Gagan Choudhary** and **Sandeep Vijay** (turquoise imitations), **Claude Drouin** and **Dr Emmanuel Fritsch** (history of cubic zirconia), **Dr Karen Fox** and **K. R. Fox** (gemmological applications of the Arduino open-source electronics platform), **Seung Kwon Lee** and **Randy Luo** (optical properties of hackmanite and sodalite), **Zemin Luo** and co-authors (emerald from Prince Liangzhuang's tomb, Ming dynasty, Hubei, China), **Nalin Narudeesombat** and co-authors (Tairus hydrothermal synthetic ruby and blue sapphire), **Dr Thet Tin Nyunt** and co-authors (amber from Khamti, Myanmar), **Elizabeth Su** (rarity and pricing of different colours of jadeite), **Manuela Zeug** and co-authors (characterisation of parisite), and **Zhiqing Zhang** and **Dr Andy Shen** (amber with violet UV fluorescence from Myanmar).

During the closing ceremony, those who transitioned from IGC observers to delegates were announced (Laurent Cartier, Gagan Choudhary, Stephen Kennedy, Dr Andy Shen, Elizabeth Su and this author). The year 2021 will mark the 70th anniversary of the IGC, which will take place in Tokyo, Japan (Figure 5).

Brendan M. Laurs FGA

Figure 5: The IGC banner is passed to Dr Hiroshi Kitawaki (second from the right), who is a co-host of the 2021 IGC in Tokyo, Japan. Also shown (from left to right) are IGC Executive Committee members Willow Wight, Tay Thye Sun, Dr Emmanuel Fritsch and Dr Jayshree Panjikar. Photo by B. M. Laurs.

GEM-A CONFERENCE

On 2–3 November 2019, approximately 265 attendees from 27 countries gathered for the annual Gem-A Conference at etc.venues County Hall in London. Gem-A CEO **Alan Hart** opened the conference and introduced the speakers during the two-day event.

Charlton August (Namdeb, Oranjemund, Namibia) reviewed the history, geology, mining and production from the Namibian diamond mega-placer. Since diamonds were discovered there in 1908, Namibia has produced nearly 107 million carats (Mct) from a variety of secondary deposits: 63 Mct from littoral (onshore and nearshore) sources, 22 Mct from offshore areas, 16 Mct from aeolian (from wind action) sands, 5 Mct from fluvial deposits along the Orange River and 0.5 Mct from pocket beaches. Namdeb's future activities will focus on further mining of onshore/nearshore areas (through westward beach accretion for up to several hundred metres) and exploration of ancient fluvial sediments that lie under and to the north of the town of Oranjemund.

Dr Barbara Dutrow (Louisiana State University, Baton Rouge, Louisiana, USA) described the history and uses of tourmaline as a gemstone, reviewed its crystal structure and chemical composition, and then explained how it serves as an important recorder of geological information (see also the Conferences section of *The Journal*, Vol. 36, No. 4, 2018, p. 360). As such, it is perhaps the best 'geological storyteller' of any gem material.

Rachel Dery (Gem Legacy, Royal Oak, Michigan, USA) profiled the Gem Legacy initiative, which aims to use coloured gemstones to create tangible, quantifiable change in mining communities in East Africa.

Figure 6: Gem-A CEO Alan Hart takes questions from the audience for conference speaker Prof. Fabrizio Nestola. Photo by Henry Mesa.

Gem Legacy supports education, vocational training and local economies, as demonstrated by activities such as building a school and hiring a teacher in Malawi, improving a gem faceting school in Tanzania, and funding the purchase of beds for a children's home in Kenya. Other important activities include addressing the needs expressed by miners and dealers through training and equipment acquisition.

Prof. Fabrizio Nestola (University of Padua, Italy; Figure 6) provided a connection between diamonds and the origin of the earth's oceans. He differentiated the formation of diamonds in the lithosphere (i.e. at 130–200 km depth) from those of 'superdeep' origin that are thought to have crystallised in the Earth's mantle at depths of up to 800–1,000 km. Recent research has shown that lithospheric diamonds can contain mineral inclusions that are surrounded by thin hydrous films, whereas superdeep diamonds can host inclusions that themselves may contain water (e.g. hydrous ringwoodite), indicating that large amounts of water reside in the mantle. This suggests that the oceans could have an 'internal' origin (e.g. from water initially present in the earth that slowly ascended to the surface), as well as an external origin (e.g. from other sources such as comets).

Nathan Renfro (Gemological Institute of America, Carlsbad, California) took the audience on a microscopic journey through gemstones. He explained how to use diffusers and fibre-optic illumination for optimising the lighting to show internal or external features of gems, and also discussed specialised microscopic techniques such as focus stacking and differential interference contrast. He then displayed numerous engaging photomicrographs, including a looped sequence of images of a diamond containing a mobile diamond inclusion.

Anette Juul-Nielsen (Ministry of Mineral Resources and Labour, Nuuk, Greenland) reviewed the geology and gem materials of Greenland. In addition to deposits of ruby and pink sapphire, Greenland hosts tugtupite, nuummite (aggregates of iridescent amphibole), greenlandite (microcrystalline aventurine quartz), labradorite, chalcedony, garnet, kyanite, amazonite, eudialyte, diamond and biogenic gems (bone, ivory, baleen, horn, etc.). In 2012, legislation was introduced to encourage small-scale gem mining by permanent residents, and ongoing geological mapping is also taking place in support of the gem industry.

Richard Drucker (Gemworld International Inc., Glenview, Illinois, USA) focused on gem market trends, issues and challenges. He discussed the pricing of sapphire, ruby, emerald, tanzanite, fancy-colour zoisite and red spinel, and then covered issues surrounding gem nomenclature such as the distinction between 'Paraíba' and 'cuprian' tourmaline in his pricing guides, the definition of alexandrite by gem laboratories and the use of commercial trade names for describing gem colour. He also reviewed some items that create pricing challenges such as synthetic diamonds (especially when treated), crazed opal and very large faceted stones.

Rui Galopim de Carvalho (Gem Education Consultant, Lisbon, Portugal) recounted the history of Brazilian diamonds. They were first recognised in the 1720s, and eventually the Brazilian deposits produced about 10 times more than those in India. The increased availability of diamonds from Brazil coincided with a change

in jewellery styles from intricate metalwork in the 17th through early 18th centuries to designs in which stones were dominant. Historically Brazilian production came only from alluvial deposits, although recently (in 2016) the first kimberlite pipe mine opened at Braúna in Bahia State, and ongoing exploration projects are targeting other primary deposits.

John Bradshaw (Coast to Coast Rare Stones, Nashua, New Hampshire, USA) described rare gemstones. Of the approximately 200 species that have been faceted, 25 are routinely seen in the trade and the other 175 are considered rare or collector stones. He described the properties, availability and pricing of some of these gems, including taaffeite, sphalerite, fluorite, benitoite, crocoite and haüyne. He also mentioned that recent production of fine-quality rhodonite from Brazil is expected to enter the market in the near future.

Dr Laurent Cartier (Swiss Gemmological Institute SSEF, Basel, Switzerland) covered diamonds from Sierra Leone. Large areas of the country are prospective for alluvial and primary deposits, but relatively little exploration or formal mining has taken place. Artisanal miners account for 80% of the production, mostly from gravel deposits adjacent to rivers. In addition, small teams work in the rivers themselves, diving as deep as 10 m to load diamond-bearing gravel into buckets. Cartier showed a new documentary film on the diamond divers that he produced with a videographer from a recent visit to Sierra Leone in April 2019.

The conference was closed by Gem-A President **Maggie Campbell Pedersen**, who reviewed the diversity of topics presented.

On 4 November, four workshops were held at Gem-A's headquarters: precious coral identification with **Rui Galopim de Carvalho**, new types of cultured pearls with **Dr Laurent Cartier**, visual optics with **Pat Daly** (Gem-A, London), and coloured stone grading and pricing with **Richard Drucker**. That evening marked Gem-A's graduation ceremony and presentation of awards at the Royal Institution of Great Britain in London.

On 5 November, field trips took attendees to private viewings of the British Crown Jewels at the Tower of London, a behind-the-scenes tour of the gem and mineral collection at the Natural History Museum, and a handling session with Indian jewellery objects at the Victoria and Albert Museum.

Brendan M. Laurs FGA

Gem-A Notices

GEM-A CONFERENCE 2019

This year's Gem-A Conference was held at etc.venues County Hall, London, on 2–3 November. Details of the speaker presentations are reported in the Conferences section of this issue of *The Journal*, pages 766–775, and a round-up of all the highlights from the 2019 Conference will be published in *Gems&Jewellery* (Vol. 29, No. 1, 2020). Practical gemmology workshops on precious coral identification, visual optics, new types of cultured pearls, and coloured stone grading and pricing were held at Gem-A HQ on Monday 4 November. On Tuesday 5 November, some delegates attended exclusive private excursions to three of London's best-known museums. At the Victoria and Albert Museum, attendees participated in an Indian jewellery handling session, while visitors to the Tower of London got a tour of the British Crown Jewels, and another group went behind the scenes at the Natural History Museum's gem and mineral gallery.

CONFERENCE SPONSORS

Gold Sponsor

JTV
www.jtv.com

Silver Sponsors

Accredited Gemologists Association
www.accreditedgemologists.org

Canadian Gemmological Association
www.canadiangemmological.com

Marcus McCallum FGA
www.marcusmccallum.com

Bronze Sponsors

Asian Gemmological Institute & Laboratory Ltd.
www.agil.com.hk

Crown of Light
www.crownoflight.com

École de Gemmologie de Montréal
www.ecoledegemmologie.com

Gemworld International Inc.
www.gemguide.com

Ruppenthal UK Ltd.
www.ruppenthal.com

We would also like to thank DG3 Diversified Global Graphics Group (www.dg3.com) for producing the Gem-A Conference materials.

GRADUATION CEREMONY

The 2019 Gem-A Graduation Ceremony was held at the Royal Institution of Great Britain, Albemarle Street, London, on 4 November. Gem-A CEO Alan Hart FGA DGA presented Gemmology and Diamond Diplomas to Gem-A graduates from around the world.

Following the presentation of the Diplomas, Joanna Hardy FGA DGA provided this year's speaker's address, in which she congratulated graduates on achieving such difficult and prestigious qualifications, and spoke of how Gem-A's education helped her develop a successful career in the jewellery industry. Joanna was then joined by Gem-A President Maggie Campbell Pedersen FGA ABIPP to present the Gem-A Medals and Prizes (see pp. 784–785).

Joanna Hardy FGA DGA and Alan Hart FGA DGA with Gem-A's 2019 graduates. Photo by Tempest Photography.

GEMMOLOGY DIPLOMA PASSES

Marianne Pughe, United Kingdom
Lilian Venetia Vildiridi, United Kingdom
Yi-Hong Wu, Taiwan (R.O.C.)
Ahmad Shajaie, Canada
Kay Yee Wong, Hong Kong (S.A.R.)
Emma Barton, United Kingdom
Shan Shan Lai, Hong Kong (S.A.R.)
Chui Ting Lau, Hong Kong (S.A.R.)
Rong Sun, P.R. China
Anuruddha Dharmasiri, Sri Lanka
Edyta Banasiak, United States of America
Elizabeth Bailey, United Kingdom
Meng-Yao Lin, Taiwan (R.O.C.)
Sammantha Maclachlan, United Kingdom
Kenneth Fogelberg, United States of America
Yuk Ting Ng, Hong Kong (S.A.R.)
Alisha Duffy, United Kingdom
Nadia Usman, United Kingdom
Chin Ching Ho, Hong Kong (S.A.R.)
Haibin Huang, P.R. China
Nancy Herdman, United Kingdom
Beverley Warden-Owen, Wales, United Kingdom
Chun Ki Stanley Yu, Hong Kong (S.A.R.)
Tatiana Poliakova, France

Anouck Armand, France
Pok Tso, Hong Kong (S.A.R.)
Mohammedi Siyam, India
Mialy Rakotoarison Amboara, Madagascar
Jemma Beeley, United Kingdom
Jingling Zhao, P.R. China
Yi Ni Li, P.R. China
Bing Yin Lee, Hong Kong (S.A.R.)
Kim Hung Kwee, Hong Kong (S.A.R.)
Shu Hung Wong, Hong Kong (S.A.R.)
Marie Bellard, United States of America
Chun Shan Tang, Hong Kong (S.A.R.)
Charlotte Elmér, Sweden
Lily Reynolds, United Kingdom
Rachel Healy, Republic of Ireland
Augusto Castillo, United States of America
Eleonore De Liedekerke, Germany
Sui-Ying Hsu, Taiwan (R.O.C)
Chor-Man Tang, Hong Kong (S.A.R.)
Suet Ying Ng, Hong Kong (S.A.R.)
Po Yin Leung, Hong Kong (S.A.R.)
Jorge Esteban Alvarado, France
Yanshi Wei, P.R. China
Karine Pollien, France
Shufei Wang, P.R. China
Jiabao Li, P.R. China
Xi Ge, P.R. China
Shuwen Yang, P.R. China
James Evans, United Kingdom
Elizabeth Gass, United States of America
Ank Trumpie-van Eijndhoven, The Netherlands
Sergé Kreher, The Netherlands
Fang Wen, P.R. China
Meng Meng Cui, P.R. China
Lan Wu, P.R. China
Fiona Haines, United Kingdom
Kelly (Jing) Dang, Hong Kong (S.A.R.)
Lezlie Bailey, United Kingdom
Michael Kay, South Korea
Wei-Ting Chang, Taiwan (R.O.C.)
Melissa Allen, United States of America
Yukari Hirashima, Japan
Marian Holt, United States of America
Tsz Fun Lee, Hong Kong (S.A.R.)
Hsuan-Ju Lee, Taiwan (R.O.C.)
Zejun Tian, P.R. China
Yuchen Cheng, P.R. China
Zhelin Zhu, P.R. China
Mingyue Cui, P.R. China
Yan Yang, P.R. China
Miho Murata, Japan
Ayako Takahashi, Japan
Jean-Marie Gaultier, France
Kanjing Liu, P.R. China
Arabella Toler, United Kingdom
Zainab Rajab, Bahrain
Zainab Mohammed, Bahrain
Fatima Albedal, Bahrain
Fatema Almahmood, Bahrain
Bader Alshaybani, Bahrain
Fatema Makhlooq, Bahrain
Tyler Smith, United States of America
Henri Boussin, France
Solofo Emilien Rabenantoanina, Madagascar
Paulette Blot, France
Andrew Culpan, United Kingdom
Carina Hanser, Germany
Sandrine Guymard Viricel, Switzerland
Congyi Yang, P.R. China
Wanqiang Ma, Japan
Sayo Imura, Japan
Rumi Tasaka, Japan
Wan-Yi Lin, Taiwan (R.O.C.)
Yim Yu Cheng, P.R. China
Yuen Wai Hung, P.R. China
Wing Yan Tang, P.R. China
Nicole Flavell-Avery, United Kingdom
Zhehui Huang, P.R. China
Xuefei Quan, P.R. China
Miao-Chan Chang, Taiwan (R.O.C.)

May Tzu Chen, Taiwan (R.O.C.)
Khin Kathy Kyaw, Myanmar
Su Myat Htet, Myanmar
Junjun Shen, P.R. China
Guiyang Ke, P.R. China
Zhiwei Mo, P.R. China
Yao Wang, P.R. China
Yuxi Jing, P.R. China
Siyan Liu, P.R. China
Ruocao Wang, P.R. China
Yijing Yan, P.R. China
Meng Yi, P.R. China
Weiting Zhang, P.R. China
Charlotte Glyde, United Kingdom
Noriko Tsuchiya, Japan
Junpei Yamada, Japan
Tomoe Kawamura, Japan
Qian Shi, P.R. China
Qianyi Zhang, P.R. China
Chuyi Chen, P.R. China
Huaiyu Gong, P.R. China
Jian Qiu, P.R. China
Yue Su, P.R. China
Zhe Fu, P.R. China
Jiahui Pan, P.R. China
Bin Yuan, P.R. China
Qiong Wan, P.R. China
Ziyu Zhou, P.R. China
Rui Zhao, P.R. China
Tingting Wang, P.R. China
Xiaomin Yu, P.R. China
Yanchu Chen, P.R. China
Zikai Zhang, P.R. China
Bokun Hao, P.R. China
Pengyao Feng, P.R. China
Liansai Wang, P.R. China
Dalin Wu, P.R. China
Lu Bai, P.R. China
Shuo Kong, P.R. China
Yuetong Wu, P.R. China
Yuying Chen, P.R. China
Minxuan Song, P.R. China
Dehua Xu, P.R. China
Meng Wang, P.R. China
Qin Chang, P.R. China
Yuxuan Xue, P.R. China
Tin Bo Kwok, Hong Kong (S.A.R.)
Kam Fai Leung, Hong Kong (S.A.R.)
Judy Zhang, United Kingdom
Monique De Klonia, The Netherlands
Anita Matharu, United Kingdom
Rachel Fox, United Kingdom
Fanny Raponi, United Kingdom
Wenshan Chen, P.R. China
Yue Cui, P.R. China
Ruihan Deng, P.R. China
Xue Han, P.R. China
Haoyuan Jia, P.R. China
Jiaxin Liu, P.R. China
Xinyue Liu, P.R. China
Ping Long, P.R. China
Yi Mu, P.R. China
Hongxin Pang, P.R. China
Lanlan Qiao, P.R. China
Lijie Qin, P.R. China
Qianyue Ren, P.R. China
Yu Ren, P.R. China
Hao Ruan, P.R. China
MinLiang Shen, P.R. China
Xiaowei Shi, P.R. China
Yulong Song, P.R. China
Song Song, P.R. China
Rujiao Wang, P.R. China
Qingqing Wu, P.R. China
Yi Xiao, P.R. China
Xing Xing, P.R. China
Mohan Xue, P.R. China
Ju Zeng, P.R. China
Yue Zhang, P.R. China
Yufang Zhang, P.R. China

Jietao Zhu, P.R. China
Jane Kharade, United Kingdom
Rodrice Seva, Madagascar
Chih-Ying Yu, Taiwan (R.O.C.)
Costanza Longanesi Cattani, United Kingdom
Sophie Valzan, France
Louise Teisseire, France
Albane d'Arodes, France
Wei Jiang, P.R. China
Min Zhang, P.R. China
~~Yi Shen, P.R. China~~
Zhe Fan, P.R. China
Li Shen, P.R. China
Zhe Yi Yuan, P.R. China
Yi Fan Lu, P.R. China
Ming Zi Yuan, P.R. China
Yi Qin Xiao, P.R. China
Bei Bei Zhang, P.R. China
Jun Kai Li, P.R. China
Chang Wen, P.R. China
Chenbin Xue, P.R. China
Junqing Zhang, P.R. China
Hui Xu, P.R. China
Hui Shu, P.R. China
Yun Xia, P.R. China
Shengjia Wei, P.R. China
Chen Chen, P.R. China
Xiaodan Li, P.R. China
Yan Wang, P.R. China
Xing Guo, P.R. China
Ying Lin, P.R. China
JiaMing Liu, P.R. China
Qiao Qiao, P.R. China
Jiachen Hou, P.R. China
Chia-Jui Chang, Taiwan (R.O.C.)
Chun-Nan Chen, Taiwan (R.O.C.)
Yen-Hsun Cheng, Taiwan (R.O.C.)
Chih-Yi Chueh, Taiwan (R.O.C.)
Jingwen Li, P.R. China
Deepak Nachankar, India

Note: Yi Shen should have been listed under 'Gemmology Diploma Passes with Distinction'.

Urja Zaveri, India
Kuan-Hsu Chen, Taiwan (R.O.C.)
Yuen Man Kwan, Hong Kong (S.A.R.)
Po Man Leung, Hong Kong (S.A.R.)
Kok Ying Li, Hong Kong (S.A.R.)
Wenting Wang, P.R. China
Xiaohan Ren, P.R. China
Xiao He, P.R. China
Meng-Jou Chiang, Taiwan (R.O.C.)
Louiza Leclercq, United Kingdom
Krista Ptasinskas, Canada
Yixuan Liu, P.R. China
Guidong Ni, P.R. China
Danfeng Yang, P.R. China
Yuxi Huai, P.R. China
Jing Guo, P.R. China
Adèle Gaboriau, France
Véronique Huot, Canada
Maxime Rousselet, France
Fumuyane Gondwe, Malawi
Marwan-Loïc Nsiri, Morocco
Gaëtan Rakotomanana, Madagascar
Wei Chu Chang, Taiwan (R.O.C.)
Hsin-Yu Wang, Taiwan (R.O.C.)
Fang-Yi Teng, Taiwan (R.O.C.)
I-Chia Liang, Taiwan (R.O.C.)
Ssu Ying Chen, Taiwan (R.O.C.)
Jou-Yu Tu, Taiwan (R.O.C.)
Wan-Ting Hsu, Taiwan (R.O.C.)
Hsin-I Liu, Taiwan (R.O.C.)
I Ju Chen, Taiwan (R.O.C.)
Tsai-Jun Yu, Taiwan (R.O.C.)
Tung Han Yeh, Taiwan (R.O.C.)
Jou-Yi Chen, Taiwan
Fouad Amin, France
Anne Dai, France
David Lam, France
Nathalie Leiglon, France
Etienne Du Toit, United Kingdom
Wenjie Gong, P.R. China

Leiyan Lv, P.R China
Sike Cao, P.R. China
Xia Zhang, P.R. China
Mingxiu Li, P.R. China
Ying Zhou, P.R. China
Xinli Gou, P.R. China
Mengjie Ding, P.R. China
Shijia Zhou, P.R. China
Xiaohui Zhong, P.R. China
Miao Jing, P.R. China
Yuting Zheng, P.R. China
Zefeng Li, P.R. China
Tsai-Ti Hung, Taiwan (R.O.C.)
Bo-Xuan Lin, Taiwan (R.O.C.)
Hui-Ming Lai, Taiwan (R.O.C)
Shi-Rong Lan, Taiwan (R.O.C.)
Li Zhang, P.R. China
Yunye Jiang, P.R. China
Xingyue Zheng, P.R. China
Peiru Hu, P.R. China
Wenjuan Xia, P.R. China
Jianren Liao, P.R. China
Bowen Xiao, P.R. China
Juan Li, P.R. China
Zaidong Chen, P.R. China
Xiaoxi Sun, P.R. China
Danya Wang, P.R. China
Fenglin He, P.R. China
Xueting Hu, P.R. China
Xinyi Lu, P.R. China
Chiayen Chang, P.R. China
Jia Sun, P.R. China
Wenwen Lu, P.R. China
Mingfang Xu, P.R. China
Long Fan, P.R. China
Jiani Lu, P.R. China
Yuting Zhou, P.R. China
Li Fan, P.R. China
Ying Zhang, P.R. China
Rong Zhang, P.R. China
Qingqing Deng, P.R. China
Rongrong Shi, P.R. China
Xiang Yu, P.R. China
Weicheng Lin, P.R. China
Yizhou Chen, P.R. China
Bingxin Lin, P.R. China
Rupali Mullick, India
LanTian Wei, P.R. China
Yi Yu, P.R. China
Yue Nian, P.R. China
Ying Li, P.R. China
Baoliang Guo, P.R. China
Zhi Li, P.R. China
Meng Sun, P.R. China
Minyu Jiang, P.R. China
Tianwei Guo, P.R. China
Da Huo, P.R. China
Jinpei Jiang, P.R. China
Ying Qu, P.R. China
Qihang Wang, P.R. China
Shizhu Wang, P.R. China
Yihui Wang, P.R. China
Xueli Wu, P.R. China
Xiaoying Xu, P.R. China
Shuo Yin, P.R. China
Tianyi Zhang, P.R. China
Xiangyu Zhang, P.R. China
Jie Chen, P.R. China
Wenhong Chen, P.R. China
Jinhao Li, P.R. China
Zhikang Hu, P.R. China
Huixuan Huo, P.R. China
Haochan Lei, P.R. China
Jinyuan Li, P.R. China
RunQi Li, P.R. China
JingYi Liu, P.R. China
Xu Miao, P.R. China
Yu Wang, P.R. China
Susu Xia, P.R. China
Na Yan, P.R. China

Rui Yang, P.R. China
Xiaomeng Ma, P.R. China
Tiffany Gombert, Canada
Tzu-Chieh Chen, Taiwan (R.O.C)
Yu Yi Kao, Taiwan (R.O.C)
Rojoniaina François Maurice Sandranirina, Madagascar
Chih-Yu Wu, Taiwan (R.O.C)
Yuyang Zhang, P.R. China
Yuyan Lu, P.R. China
Han Zhou, P.R China
Lu Song, P.R China
Wanyu Yao, P.R. China
Fangqi Cao, P.R. China
Ling Liu, Hong Kong (S.A.R.)
Junxiu Yi, P.R. China
Xuan Fang, P.R. China
Yuanrui Li, P.R. China
Haixin Fu, P.R. China
Mingchen Zhang, P.R. China
Yechengcheng Zheng, P.R. China
Li Wang, P.R. China
Yufu Qiu, P.R. China
Gengzhe Shi, P.R. China
Yubing Chen, P.R. China
Ning Cui, P.R. China
Yiran Du, P.R. China
Yuansheng Jiang, P.R. China
Duan Li, P.R. China
Ningning Li, P.R. China
Ziyuan Liu, P.R. China
Wenfang Liu, P.R. China
Xinyi Qiao, P.R. China
Jianfei Qu, P.R. China
Yujia Shi, P.R. China
Yuxiang Shi, P.R. China
Qi Sun, P.R. China
Xingyang Wang, P.R. China
Yuning Xia, P.R. China
Qi Xie, P.R. China
Hairui Yang, P.R. China
Hua Bai, P.R. China
Xincan Chen, P.R. China
Meihui Gao, P.R. China
PanPan He, P.R. China
Jiawen Li, P.R. China
Ruofei Ma, P.R. China
Xiao Wu, P.R. China
Yifei Yu, P.R. China

GEMMOLOGY DIPLOMA PASSES WITH MERIT

Sarah Bromfield, United Kingdom
Anne Galmiche, United Kingdom
Katrina Hughes, United Kingdom
Catherine Fox, United Kingdom
Kazusa Tachibana, Japan
Connie Bacon, United Kingdom
Liang Zhang, P.R. China
Simone Dunlop, United Kingdom
Kristin Chase, United States of America
Hiromu Kanamori, Japan
Tabitha Downer, United Kingdom
Chi Zhou, P.R. China
Jerome Chi Him Wai, P.R. China
Ayano Kumakiri, Japan
Sophie Caplain, France
Peizhen Nong, P.R. China
Yan-Ling Yeh, Taiwan (R.O.C)
Shih-Ya Cheng, Taiwan (R.O.C)
Maxime Fondi, Canada
Axel Vivant, France
Zhiyong Li, P.R. China
Yu Ren, P.R. China
Cen Bai, P.R. China
Ruyin Jia, P.R. China
Xiaoyao Li, P.R. China
Fangge Liu, P.R. China

Junqi Ma, P.R. China
Ying Yan, P.R. China
Ziyue Yang, P.R. China
Xue Gao, P.R. China
Ying Jiang, P.R. China
Francisca Xiaodan Liu, P.R. China
Siwen Zhou, P.R. China

GEMMOLOGY DIPLOMA PASSES WITH DISTINCTION

Patricia Campion, United Kingdom
Yixuan Zhang, P.R. China
Laury Fondi, France
Lucas Berruyer, France
Wen-Hsin Cheng, Taiwan (R.O.C)
Ziling Liu, P.R. China
Weihua Huang, P.R. China
Siqi Ma, P.R. China
Bo Niu, P.R. China
Lei Zhang, P.R. China
Yining Zhuang, P.R. China
Lizhen Jiang, P.R. China
Yi Shen, P.R. China

DIAMOND DIPLOMA PASSES

Ella Sakura Wolff, The Netherlands
Kwai Fong Maggie Pong, Hong Kong (S.A.R.)
Chi Ho Lau, Hong Kong (S.A.R.)
Aye Aye Khine Ma, Hong Kong (S.A.R.)
Satish Desurkar, United Kingdom
Anna Zorina Konobeevskaya, United Kingdom
Yuan Jung Yeh, Taiwan (R.O.C.)
Holly Ryan, United Kingdom
Shan Jung Ho, Taiwan (R.O.C.)
Kerry Newman, United Kingdom
Chi Ko Tang, Hong Kong (S.A.R.)
Bing Wai Tsui, Hong Kong (S.A.R.)
Lauren Gardner, United Kingdom
Lai Yan Rosanna Fung, Hong Kong (S.A.R.)
Ka Mei Ho, Hong Kong (S.A.R.), China
Chak Hang Jeffrey Kong, Hong Kong (S.A.R.)
Pui Sze Lam, Hong Kong (S.A.R.)
Kwok Ching Wong, Hong Kong (S.A.R.)
Wai Kei Yim, Hong Kong (S.A.R.)
Wing Sing Cho, Hong Kong (S.A.R.)
Alexandra Crossley, United Kingdom
Sherril Dixon, Scotland, United Kingdom
Amanda Mullen, United Kingdom
Wai Kwan Chan, Hong Kong (S.A.R.)
Shuk Wah Suiki Huen, Hong Kong (S.A.R.)
Wing Yan Li, Hong Kong (S.A.R.)
Wai To Poon, Hong Kong (S.A.R.)
Wai Sum Sze, Hong Kong (S.A.R.)
Sunny Pal, United Kingdom
Wen Li Jheng, Taiwan (R.O.C)
Lucy Bedeman, United Kingdom
Samantha Lloyd, United Kingdom
Yang Ting Huang, Taiwan (R.O.C.)
Alexander Davison, United Kingdom
Rachael Jack, Scotland, United Kingdom
Man Kuen Kannus Cheng, Hong Kong (S.A.R.)
Yun-Pin Huang, Taiwan (R.O.C)
Rasika Kirad, India
Wing Yee Fung, Hong Kong (S.A.R.)
Francesca De Watts, Hong Kong (S.A.R.)
Yuen-Li Naa, Malaysia
Chi Wah Chung, Hong Kong (S.A.R.)
Man Sin Yeung, Hong Kong (S.A.R.)
Chiu Kwan Mang, Hong Kong (S.A.R.)
Pui Wah Kate Kiu, Hong Kong (S.A.R.)
Wai Yip Poon, Hong Kong (S.A.R.)
Joanne Maddison, United Kingdom
Catherine Alexander, United Kingdom

Kuan-Hsu Chen, Taiwan (R.O.C)
Po Kei Yeung, Hong Kong (S.A.R.)
Ka Lok Cheng, Hong Kong (S.A.R.)
Kam Fai Chan, Hong Kong (S.A.R.)
Mei Leng Wong, Macau
Pui Fai Lucifer Tam, Hong Kong (S.A.R.)
Sin Yiu Shirley Lam, Hong Kong (S.A.R.)
Yuet Sheung Peggy Leung, Hong Kong (S.A.R.)
Yuk Ling Abey Lai, Hong Kong (S.A.R.)
Man Wai Debbie Leung, Hong Kong (S.A.R.)
Mong Suet Ng, Hong Kong (S.A.R.)
Nicola Whiting, United Kingdom
Pei-Ling Wu, Taiwan (R.O.C)
Pei-Hsien Kevin Chou, Taiwan (R.O.C)
Teng-Yun Chang, Taiwan (R.O.C)

DIAMOND DIPLOMA PASSES WITH MERIT

Beverley Warden-Owen, United Kingdom
Charlotte Williams, United Kingdom
Kit Yi Ho, Hong Kong (S.A.R.)
Samantha Hobson, United Kingdom
Hui-Ming Lai, Taiwan (R.O.C)
Victoria Sparkes, Switzerland
Wai Yiu Wong, Hong Kong (S.A.R.)
Min-Yi Lin, Taiwan (R.O.C)
Sarah Kinsey, United Kingdom
Kim Hung Kwee, Hong Kong (S.A.R.)
Shuai Wu, Hong Kong (S.A.R.)

DIAMOND DIPLOMA PASSES WITH DISTINCTION

Stephane Wainer, Singapore
Jade Watts, United Kingdom
Zoe Lewis, United Kingdom
Lorna McNaught, United Kingdom
Samuel Capstick, United Kingdom
Amber Rose Roberts, United Kingdom
Samantha Homes, United Kingdom
Leonie Armin, United Kingdom
Daisy Welford-Ranson, United Kingdom
Amy Zgraja, United Kingdom
Charles Bexfield, United Kingdom
Michel Phanekham, Thailand
Taffy Schneider, United Kingdom
Wai Kiu Vicky Zee, Hong Kong (S.A.R.)

PRIZE AND MEDAL WINNERS

Awards and prizes are presented to the best candidates of the year, selected from our students worldwide.

GEMMOLOGY FOUNDATION CERTIFICATE

Anderson Medal

Awarded to the candidate submitting best papers of the year in the Gemmology Foundation examination.

This medal was established in 1981 in honour of Basil W. Anderson FGA, former Director of the Gem Testing Laboratory, London.

2019 Winner: Maxime Fondi, a student from École de Gemmologie de Montréal, Canada

GEMMOLOGY DIPLOMA

Christie's Prize for Gemmology

Awarded to the candidate submitting the best papers of the year for the Gemmology Diploma examination.

This prize was established in 1954 as the Rayner Prize, renamed the Diploma Trade Prize in 1991, replaced and sponsored from 2001 by Christie's London.

2019 Winner: Yuying Chen, a student from China University of Geosciences, Wuhan (Beijing Branch)

Anderson Bank Prize

Awarded to the candidates submitting the best theory papers of the year for the Gemmology Diploma examination.

Established in 1981 and named after Basil W. Anderson FGA and Prof. Dr Hermann Bank FGA, former director of the German Gemmological Association in Idar-Oberstein, Germany.

2019 Winners: Sarah Bromfield, an online student from UK and Yuying Chen, a student from China University of Geosciences, Wuhan (Beijing Branch)

The Read Practical Prize

Awarded to the candidate submitting the best practical papers of the year for the Gemmology Diploma examination.

First awarded in 2009 and named in memory of Peter Read FGA, author and former tutor for Gem-A. In 2019 the prize is sponsored by Richard Drucker FGA (Hons) of Gemworld International.

2019 Winner: Ziyu Zhou, a student from China University of Geosciences, Wuhan (Beijing Branch)

Gem-A would like to congratulate all of our students who achieved such fantastic results!

DIAMOND DIPLOMA

The Deeks Diamond Prize

Awarded to the candidates submitting the best theory papers of the year for the Diamond Diploma examination.

First awarded in 2001, the prize is sponsored by Noel W. Deeks FGA DGA, a Vice-President of the Association who taught the diamond course for many years.

2019 Winners: Zoe Lewis, an online student from UK and Stephane Wainer, an online student from Singapore

The Mok Diamond Practical Prize

Awarded to the best practical candidate in the Diamond Practical examination.

First awarded in 2009 and sponsored by Dr Dominic Mok FGA DGA, AGIL, Hong Kong.

2019 Winner: Daisy Welford-Ranson, a student of Gem-A London

The Bruton Medal

Awarded to the overall best candidate of the year in the Diamond Diploma examination.

This silver medal was established in 1996 in honour of Eric Bruton FGA to recognise his work in the field of diamonds.

2019 Winner: Stephane Wainer, an online student from Singapore

GIFTS TO THE ASSOCIATION

Gem-A is most grateful to the following for their generous donations that will support continued research and teaching:

Dr Dominic Mok, Hong Kong, for an ABCD Pro-1 Gem Testing Set.

Brigitte Rust, Bonn, Germany, for six issues of the *GemGuide* dating from Nov.–Dec. 2018 to Sep.–Oct. 2019 for use by Gem-A students.

Alison Summerville, Queensland, Australia, for 14 pieces of boulder opal and matrix opal.

Tay Thye Sun, Far East Gemological Laboratory, Singapore, for a sample of Burmese amber.

Ward Gemstones, Hatton Garden, London, for a lapis lazuli simulant.

GEM-A ANNUAL GENERAL MEETING 2019

The 2019 Gem-A AGM took place at etc.venues Hatton Garden, London, on 31 October and was opened by Chair of the Association's Board of Trustees Justine Carmody FGA. In accordance with the articles of the Association, trustees Kathryn Bonanno FGA and Christopher Smith FGA retired by rotation. Being eligible, each offered themselves for re-election and were reinstated. Following her appointment by trustees in January 2018, Nevin Bayoumi-Stefanovic was also elected to the Council.

In other business, the role of Gem-A trustees and their relationship with Gem-A staff was discussed, as was Gem-A's history and activity in Sri Lanka. The contributions of Evelyne Stern to Gem-A over many years were recognised, following her recent retirement as a Diamond Diploma examiner. In addition, there was a positive discussion about the diversity of the speakers scheduled for the 2019 Gem-A Conference.

Learning Opportunities

CONFERENCES AND SEMINARS

22nd FEEG Symposium
25–27 January 2020
Schoonhoven, The Netherlands
www.feeg-education.com/symposium

NAJA 53rd ACE© IT Annual Winter Conference
2–3 February 2020
Tucson, Arizona, USA
www.najaappraisers.com/html/conferences.html

ASA Fundamentals of Jewelry Appraisal Course
3 February 2020
Tucson, Arizona, USA
www.appraisers.org/Education/View-Class?ClassID=4282

AGTA Gemfair Tucson
4–9 February 2020
Tucson, Arizona, USA
https://agta.org/seminars
Note: Includes a seminar programme

AGA Tucson Conference
5 February 2020
Tucson, Arizona, USA
https://accreditedgemologists.org/currevent.php

Tucson Gem and Mineral Show
13–16 February 2020
Tucson, Arizona, USA
www.tgms.org/show
Note: Includes a seminar programme

Inhorgenta Munich
14–17 February 2020
Munich, Germany
www.inhorgenta.com/en/trendfactory/trendfactory-munich
Note: Includes a seminar programme

Prospectors & Developers Association of Canada
1–4 March 2020
Toronto, Ontario, Canada
www.pdac.ca/convention/programming/technical-program
Theme of interest: The Business of Diamonds: From Rock to Ring

ASA Fundamentals of Jewelry Appraisal Course
2 March 2020
Carlsbad, California, USA
www.appraisers.org/Education/View-Class?ClassID=4304

36th International Geological Congress
2–8 March 2020
Delhi, India
www.36igc.org
Note: Sessions of interest include Geology and Gemstones; Advances in Synthetic Gemstones; Diamonds Today; Gem Species and their Varieties; field trips will visit the diamond fields of southern India and the Indian Institute of Gems & Jewellery's training and educational institute in Jaipur

Hong Kong International Jewellery Show
4–8 March 2020
Hong Kong
https://event.hktdc.com/fair/hkjewellery-en/HKTDC-Hong-Kong-International-Jewellery-Show
Note: Includes a seminar programme

DES-AGIL International Gemmological Conference
8 March 2020
Hong Kong
www.agil.com.hk/en/news.php?newsid=140

MJSA Expo
15–17 March 2020
New York, New York, USA
https://mjsa.org/eventsprograms/mjsa_expo
Note: Includes a seminar programme

Amberif
18–21 March 2020
Gdańsk, Poland
http://amberif.amberexpo.pl/title,Jezyk,lang,2.html
Note: Includes a seminar programme

10th National Opal Symposium
8–9 April 2020
Coober Pedy, Australia
www.opalsymposium.org

47th Rochester Mineralogical Symposium
23–26 April 2020
Rochester, New York, USA
www.rasny.org/minsymp

American Gem Society Conclave
27–29 April 2020
Denver, Colorado, USA
www.americangemsociety.org/mpage/conclave2020-home

Scottish Gemmological Association Conference
1–4 May 2020
Cumbernauld, Scotland
www.scottishgemmology.org/conference

European Geosciences Union (EGU) General Assembly 2020
3–8 May 2020
Vienna, Austria
www.egu2020.eu
Session of interest: Heritage Stones: Global Relevance vis-à-vis Architectonic Heritage

6th Mediterranean Gemmological & Jewellery Conference
15–17 May 2020
Thessaloniki, Greece
https://gemconference.com

34th Annual Santa Fe Symposium
17–20 May 2020
Albuquerque, New Mexico, USA
www.santafesymposium.org

49th Annual Society of North American Goldsmiths Conference
20–23 May 2020
Philadelphia, Pennsylvania, USA
www.snagmetalsmith.org/conferences/grit-to-gold-future-fifty-2020-snag-conference

14th International Conference on New Diamond and Nano Carbons
31 May–4 June 2020
Kanazawa, Japan
www.ndnc2020.org

JCK Las Vegas
2–5 June 2020
Las Vegas, Nevada, USA
https://lasvegas.jckonline.com
Note: Includes a seminar programme

Swiss Gemmological Society Conference
7–9 June 2020
St Gallen, Switzerland
http://gemmologie.ch/en/current

Diamonds – Source to Use 2020
9–11 June 2020
Johannesburg, South Africa
www.saimm.co.za/saimm-events/upcoming-events/diamonds-source-to-use-2020

Goldschmidt Conference
21–26 June 2020
Honolulu, Hawaii, USA
https://goldschmidt.info
Session of interest: Geochemistry of Gem Minerals

Sainte-Marie-aux-Mines Mineral & Gem Show
25–28 June 2020
Sainte-Marie-aux-Mines, France
www.sainte-marie-mineral.com
Note: Includes a seminar programme

9th International Conference Mineralogy and Museums
5–7 July 2020
Sofia, Bulgaria
www.bgminsoc.bg
Note: Gem minerals will be covered in a session titled 'Mineralogical Research and Museums'.

2020 Antique Jewelry & Art Conference
25–26 July 2020
Phillips, New York, USA
www.jewelrycamp.org

Dallas Mineral Collecting Symposium
20–23 August 2020
Dallas, Texas, USA
www.dallassymposium.org

3rd European Mineralogical Conference (emc2020)
6–10 September 2020
Krakow, Poland
https://emc2020.ptmin.eu
Session of interest: Gem Materials

International Jewellery London
13–15 September 2020
London
www.jewellerylondon.com
Note: Includes a seminar programme

31st International Conference on Diamond and Carbon Materials
13–17 September 2020
Palma, Mallorca, Spain
www.elsevier.com/events/conferences/international-conference-on-diamond-and-carbon-materials

2020 American Society of Appraisers International Conference
11–13 October 2020
Chicago, Illinois, USA
www.appraisers.org/Education/conferences/asa-international-conference

Japan Jewellery Fair 2020
14–16 October 2020
Tokyo, Japan
www.japanjewelleryfair.com/en
Note: Includes a seminar programme

Munich Show: Mineralientage München
30 October–1 November 2020
Munich, Germany
https://munichshow.de/?lang=en
Note: Includes a seminar programme

OTHER EDUCATIONAL OPPORTUNITIES

Gem-A Workshops and Courses
Gem-A, London
https://gem-a.com/education

Lectures with Gem-A's Midlands Branch
Fellows Auctioneers, Augusta House, Birmingham
Email Louise Ludlam-Snook at gemamidlands@gmail.com

- Dr Maria MacLennan—Forensic Jewellery
  28 February 2020
- Peter Buckie—The Treasures Seen by an Expert Valuer
  27 March 2020
- Roy Starkey—Minerals of the English Midlands
  24 April 2020

Lectures with The Society of Jewellery Historians
Society of Antiquaries of London,
Burlington House, London
www.societyofjewelleryhistorians.ac.uk/current_lectures

- Thomas Holman—A Box Full of Buttons: The Life and Work of Frederick James Partridge (1877–1945)
  28 January 2020
- Stephen Whittaker—TBA
  25 February 2020
- Carol Michaelson—Chinese Jade Jewellery and Ornaments from the Neolithic to the Present
  24 March 2020
- Ute Decker—TBA
  26 May 2020
- Kirstin Kennedy—TBA
  23 June 2020

Gemstone Safari to Tanzania
8–25 July 2020
www.free-form.ch/tanzania/gemstonesafari.html

Mineralogical Expedition to the Ural Mountains, Russia
13–18 July 2020
www.brankogems.com/shop/tours/july-13-18-2020-ural-mineralogical-expedition

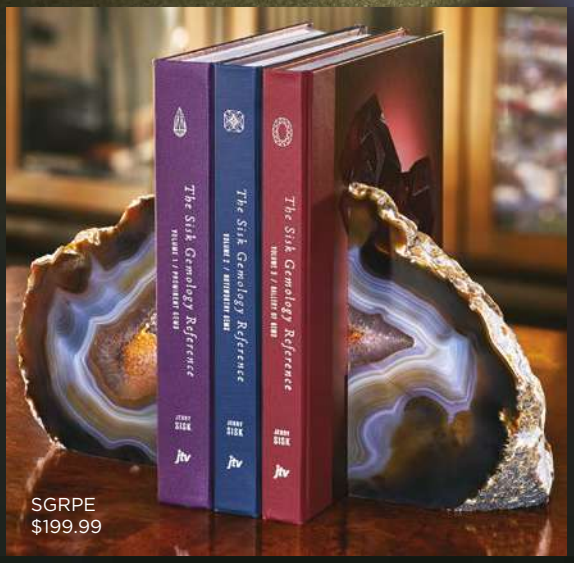

SGRPE
$199.99

The Sisk Gemology Reference

by Jerry Sisk

Professional Edition

A comprehensive and visual gemology resource featuring prominent and noteworthy gemstones.

jtv®
jewelry love

jtv.com/sgr

New Media

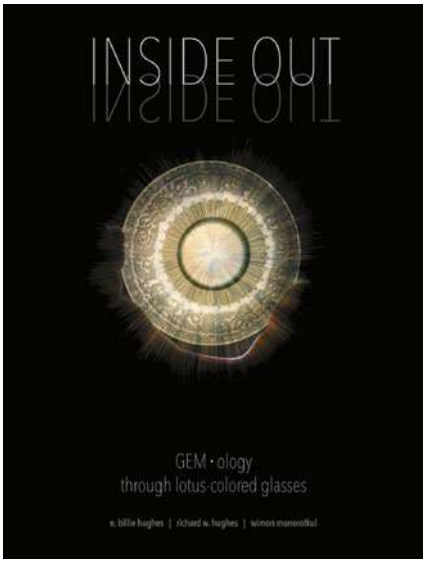

Inside Out: GEM•ology Through Lotus-Colored Glasses

By E. Billie Hughes, Richard W. Hughes and Wimon Manorotkul, 2020. Lotus Publishing, Bangkok, Thailand, and RWH Publishing, Boulder, Colorado, USA, www.lotusgemology.com/index.php/library/books/454-inside-out-gemology-through-lotus-colored-glasses-2020, 152 pages, illus., ISBN 978-0964509733 (in English and Simplified Chinese). USD100.00 (+ shipping) hardcover.

Inside Out: GEM•ology Through Lotus-Colored Glasses is not a book on gemmology or gem deposits in the literal sense. With its large format and masterful photographs, the reader experiences the emotions associated with gemstones. The book reflects in a great way the term *humanistic gemology*, as coined by co-author Richard Hughes. It is primarily about the pictorial representation of the interplay between the inner beauty of gemstones and the people who mine, process and act on them. Thus, the authors have captured the local people and environments in unique moments during their many journeys to important gem-producing regions. These images are juxtaposed with the microscopic world of inclusions in gemstones from these regions, so the aesthetics and emotions associated with the stones emerge equally.

The photographs are of the highest quality, in terms of both selection and technical implementation. The choice of the 'right' moment, which is of decisive importance to capture a mood or emotion, is particularly noticeable in the photos of people. Furthermore, Billie Hughes' micrographs reveal a diverse and incredibly rich world of the inner aesthetics of gemstones. Anyone who has ever photographed gem inclusions knows how difficult it is from a technical point of view. The photomicrographs in this book are excellent from both a technical and artistic point of view. An outstanding example of this is the depiction of a pyrite crystal in quartz on page 20.

This book fills a gap in the literature on gems by pictorially exploring the relationship between humans and gems on an artistic and emotional level. It is a work of art that lives from the quality of the photographs and gets by with minimal textual commentary on the images. The book is aimed at both experts and people who see gems as an important part of culture, as well as decorative objects in jewellery and other merchandise.

Michael Hügi FGA
Swiss Gemmological Society
Bern, Switzerland

Looking at Jewelry: A Guide to Terms, Styles, and Techniques

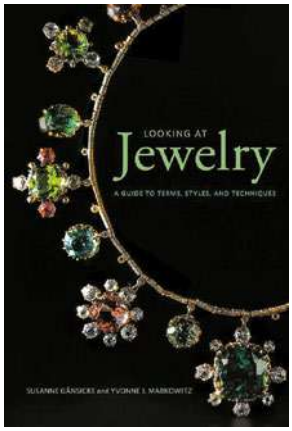

By Susanne Gänsicke and Yvonne J. Markowitz, 2019. Getty Publications, Los Angeles, California, USA, https://shop.getty.edu/products/looking-at-jewelry-br-a-guide-to-terms-styles-and-techniques-978-1606065990, 132 pages, illus., ISBN 978-1606065990. USD19.95 softcover.

This is a nicely produced book with excellent colour illustrations. It has a long introduction that gives an overview of jewellery through the ages. The 'meat' (and indeed the main purpose) of the book is the hundred-page alphabetical glossary. This is essentially a dictionary of jewellery. Surprisingly, it claims to be the first of its kind, although it mentions

the well-regarded *An Illustrated Dictionary of Jewelry* (1987) by Harold Newman in its suggested reading list. No mention is made of the earlier and really excellent *Illustrated Dictionary of Jewellery* (1973) by Anita Mason and Diane Packer.

Many of the entries provide very good comprehensive information, often aided by appropriate illustrations. Some entries are, however, extremely unsatisfactory. For example, imitation and synthetic gems are dealt with under 'Artificial Stone', which only describes Verneuil's method of producing synthetic corundum, in spite of many very long-standing better techniques. Also, 'Assay' is described only as using acid on a touchstone. The more accurate cupellation (fire assay) method has been employed for many centuries, and now XRF instrumentation can analyse metals non-destructively with extraordinary accuracy. It would seem that a wider range of specialist editors would have greatly improved the glossary. A minor irritation for some European readers in using the alphabetical glossary is the American spelling convention (e.g. the purity of gold is listed under 'Karat' rather than 'Carat').

In spite of these drawbacks, this is a useful, wide-ranging dictionary at a relatively modest price.

Nigel Israel FGA DGA
London

Other Book Titles

COLOURED STONES

Rubellite—Tourmaline Rouge
Ed. by William B. Simmons, Gloria A. Staebler, David W. Bunk, Alexander U. Falster, Sarah L. Hanson and Karen W. Webber, 2019. Lithographie, Arvada, Colorado, USA, 148 pages, ISBN 978-0983632399. USD40.00 softcover.

DIAMOND

Diamond Crystals
Ed. by Yuri N. Palyanov, 2019. MDPI, Basel, Switzerland, 174 pages, ISBN 978-3038976301 (print) or ISBN 978-3038976318 (PDF), https://doi.org/10.3390/books978-3-03897-631-8. CHF55.25 softcover or free PDF. *Note:* This book is a printed edition of a special issue on diamond crystals published in the journal *Crystals*.

Hardness 10, 3rd edn.
By Eddy Vleeschdrager, 2018. I. David, Antwerp, Belgium, 1,362 pages, ISBN 978-9090298474. EUR110.00 hardcover.

Novel Aspects of Diamond: From Growth to Applications, 2nd edn.
Ed. by Nianjun Yang, 2019. Topics in Applied Physics Vol. 121, Springer, Cham, Switzerland, 507 pages, ISBN 978-3030124687 (print) or 978-3030124694 (eBook), https://doi.org/10.1007/978-3-030-12469-4. EUR155.99 hardcover or EUR118.99 eBook.

The Origins of Natural Diamonds
By N. O. Sorokhtin, 2019. Scrivener Publishing, Beverly, Massachusetts, USA, 528 pages, ISBN 978-1119593447 (print) or 978-1119593461 (eBook), https://doi.org/10.1002/9781119593461. USD249.00 hardcover or eBook.

GEM LOCALITIES

Minerals of the English Midlands
By Roy E. Starkey, 2018. British Mineralogy Publications, Bromsgrove, Worcestershire, 426 pages, ISBN 978-0993018237. GBP35.00 softcover.

GENERAL REFERENCE

Gemstones: Identifying and Using the World's Most Fabulous Gems
By Judith Crowe, 2019. Bloomsbury Publishing, London, 192 pages, ISBN 978-1912217854. GBP25.00 hardcover.

JEWELLERY HISTORY

The Wyvern Collection: Medieval and Later Ivory Carvings and Small Sculpture
By Paul Williamson, 2019. Thames & Hudson, New York, New York, USA, 448 pages, ISBN 978-0500022832. USD95.00 hardcover.

JEWELLERY AND *OBJETS D'ART*

Be Jeweled
By Patrizia di Carrobio, 2018. Edizioni Polistampa, Florence, Italy, 144 pages, ISBN 978-8859617532. EUR14.00 softcover.

Bulgari: The Story, the Dream
Ed. by Chiara Ottaviano and Lucia Boscaini, 2019. Rizzoli, New York, New York, USA, 328 pages, ISBN 978-8891824325. USD65.00 hardcover.

Contemporary Jewellery in Portugal
By Cristina Filipe, 2019. Arnoldsche Art Publishers, Stuttgart, Germany, 408 pages, ISBN 978-3897905658. EUR54.00 hardcover.

Crystals in Art: Ancient to Today
By Lauren Haynes and Joachim Pissarro, 2019. University of Arkansas Press, Fayetteville, Arkansas, USA, 304 pages, ISBN 978-1682261118, https://doi.org/10.2307/j.ctvqsf33c. USD44.95 softcover.

Diamonds: The Collection of Benjamin Zucker
By Diana Scarisbrick, 2019. Les Enluminures, New York, New York, USA, 340 pages, ISBN 978-0578420189. USD50.00 softcover.

Lacloche Joailliers/Lacloche Jewellers
By Laurence Mouillefarine and Véronique Ristelhueber, 2019. Éditions Norma, Paris, France, 320 pages, ISBN 978-2376660248 (in English and French). EUR60.00 hardcover.

The Power of Love: Jewels, Romance and Eternity
By Beatriz Chadour-Sampson, 2019. Unicorn Publishing Group, London, 144 pages, ISBN 978-191164464. GBP25.00 hardcover.

Rings of the 20th and 21st Centuries: The Alice and Louis Koch Collection
By Beatriz Chadour-Sampson, 2019. Arnoldsche Art Publishers, Stuttgart, Germany, 304 pages, ISBN 978-3897905160 (in English and German). USD115.00 hardcover.

PEARLS

Marchands de Perles: Redécouverte d'une Saga Commerciale entre le Golfe et la France à l'aube du XXe Siècle/Pearl Merchants: A Rediscovered Saga Between the Gulf & France at the Dawn of the 20th Century
By Guillaume Glorieux and Olivier Segura, 2019. L'École des Arts Joailliers/School of Jewelry Arts, Paris, France, and French Institute of the United Arab Emirates, Dubai, 224 pages (in French, English and Arabic). EUR20.00 softcover.

Octopus Crowd: Maritime History and the Business of Australian Pearling in Its Schooner Age
By Steve Mullins, 2019. The University of Alabama Press, Tuscaloosa, Alabama, USA, 336 pages, ISBN 978-0817320249 (print) or 978-0817392383 (eBook). USD54.95 hardcover or eBook.

SOCIAL STUDIES

Opportunities and Pitfalls of Corporate Social Responsibility: The Marange Diamond Mines Case Study
Ed. by Shame Mugova and Paul R. Sachs, 2019. Springer Nature Switzerland AG, Cham, Switzerland, 253 pages, ISBN 978-3030171018 (print) or 978-3030171025 (eBook), https://doi.org/10.1007/978-3-030-17102-5. CHF141.50 hardcover or CHF80.00 eBook.

ERRATUM

In the New Media section of *The Journal* Vol. 36, No. 7, p. 670, the book review of *The Complete Content Cameos* should have indicated that the Ashmolean Museum displayed the collection between 1990 (not 1900, due to an editing error) and 2000. Also, there are 441 (not 425) cameos in the collection because 16 of them are catalogued with 'A' numbers in addition to the 425 items without 'A' numbers. We thank Derek Content for bringing these errors to our attention.

Literature of Interest

COLOURED STONES

Almandine gemstone—A review. N. Sultana and S.P. Podila, *International Journal of Recent Scientific Research*, **9**(10B), 2018, 29204–29209, http://doi.org/10.24327/ijrsr.2018.0910.2812.*

Characteristics of faceted-quality ruby from Longido, Tanzania. T. Leelawatanasuk, N. Susawee and P. Bupparenoo, *Bulletin of Earth Sciences of Thailand*, **9**, 2018, 1–7, http://tinyurl.com/y8pzxf3m.*

The characterization of natural gemstones using non-invasive FT-IR spectroscopy: New data on tourmalines. M. Mercurio, M. Rossi, F. Izzo, P. Cappelletti, C. Germinario, C. Grifa, M. Petrelli, A. Vergara *et al.*, *Talanta*, **178**, 2018, 147–159, http://doi.org/10.1016/j.talanta.2017.09.030.

Color mechanisms in spinel: A multi-analytical investigation of natural crystals with a wide range of coloration. G.B. Andreozzi, V. D'Ippolito, H. Skogby, U. Hålenius and F. Bosi, *Physics and Chemistry of Minerals*, **46**(4), 2018, 343–360, http://doi.org/10.1007/s00269-018-1007-5.

A comparative study of element content and UV–VIS spectroscopy characteristics of rubies from Burma and Mozambique. K. Guo, Z. Zhou, Q. Zhong, M. Lai, H. Wang, Y. Li, X. Qiao and P. Nong, *Acta Petrologica et Mineralogica*, **37**(6), 2018, 1002–1010 (in Chinese with English abstract).

Experimental investigation of the reaction between corundum xenocrysts and alkaline basaltic host magma: Constraints on magma residence times of basalt-hosted sapphires. L.C. Baldwin and C. Ballhaus, *Lithos*, **302–303**, 2018, 447–454, http://doi.org/10.1016/j.lithos.2018.01.020.

Feasibility study on quality evaluation of jadeite-jade color green based on GemDialogue color chip. Y. Guo, X. Zong and M. Qi, *Multimedia Tools and Applications*, **78**(1), 2018, 841–856, http://doi.org/10.1007/s11042-018-5753-7.

Flickering flames over the Libyan Desert [Libyan Desert glass]? J.M. Saul, *International Geology Review*, 2018, **61**(11), 1340–1369, http://doi.org/10.1080/00206814.2018.1512057.

Gemmological characteristic of "crystal opal" from Coober Pedy, Australia. W. Peng and T. Jiang, *Journal of Gems & Gemmology*, **20**(Supp.), 2018, 122–128 (in Chinese with English abstract).

The gemological characteristics of Guatemalan jade. L. Li, Y. Xiong, N. Liu and Y. Cao, *Superhard Material Engineering*, **30**(3), 2018, 55–59 (in Chinese with English abstract).

Genetic significance of the 867 cm^{-1} out-of-plane Raman mode in graphite associated with V-bearing green grossular. R. Thomas, A. Rericha, W.L. Pohl and P. Davidson, *Mineralogy and Petrology*, **112**(5), 2018, 633–645, http://doi.org/10.1007/s00710-018-0563-1.

Geochemical characteristics and Ar-Ar dating of different nephrite deposits in Qinghai Province. H. Yu, Q. Ruan, B. Liao and D. Li, *Acta Mineralogica Sinica*, **38**(4), 2018, 655–668 (in Chinese with English abstract).

Study on mineralogy and spectroscopy of turquoises from Hami, Xinjiang. X. Liu, C. Lin, D. Li, L. Zhu, S. Song, Y. Liu and S. Chong-hui, *Spectroscopy and Spectral Analysis*, **38**(4), 2018, 1231–1239 (in Chinese with English abstract).

Tenebrescence of sapphire. B. Zhao, Y. Zhi, X. Lyu and Y. Wang, *Journal of Gems & Gemmology*, **20**(5), 2018, 1–14 (in Chinese with English abstract).

Unveiling the art of René Lalique with XRF and Raman spectroscopy –Technological innovation in jewellery production. I. Tissot, M. Manso and M.F. Guerra, *Journal of Cultural Heritage*, **33**, 2018, 83–89, http://doi.org/10.1016/j.culher.2018.03.014.

CULTURAL HERITAGE

The antiquity of pearling in the Americas: Pearl modification beginning at least 8,500 years ago in Baja California Sur, México. A.F. Ainis, H. Fujita and R.L. Vellanoweth, *Latin American Antiquity*, **30**(3), 2019, 637–643, http://doi.org/10.1017/laq.2019.49.

The art of glassmaking and the nature of stones. The role of imitation in Anselm De Boodt's classification of stones. S. Dupré, in I. Augart, M. Saß & I. Wenderholm, Eds., *Steinformen: Materialität, Qualität, Imitation*. Walter de Gruyter GmbH, Berlin, Germany, 2018, 207–220, http://doi.org/10.1515/9783110583618-012.

The Chiaravalle Cross: Results of a multidisciplinary study. D.D. Martino, G. Benati, R. Alberti, S. Baroni, C. Bertelli, F. Blumer, L. Caselli, R. Cattaneo, *et al.*, *Heritage*, **2**(3), 2019, 2555–2572, http://doi.org/10.3390/heritage2030157.*

Demystifying jadeite: An underwater Maya discovery at Ek Way Nal, Belize. H. McKillop, G. Harlow, A. Sievert, C.W. Smith and M.C. Wiemann, *Antiquity*, **93**(368), 2019, 502–518, http://doi.org/10.15184/aqy.2019.35.*

The emerald and the eye. On sight and light in the artisan's workshop and the scholar's study. M. Bol, in S. Dupré, Ed., *Perspective as Practice: Renaissance Cultures of Optics*. Brepols Publishers, Turnhout, Belgium, 2019, 71–101, http://doi.org/10.1484/m.Techne.5.117722.

On the way to the New Kingdom. Analytical study of Queen Ahhotep's gold jewellery (17th dynasty of Egypt). M.F. Guerra and S. Pagès-Camagna, *Journal of Cultural Heritage*, **36**, 2019, 143–152, http://doi.org/10.1016/j.culher.2018.09.004.

DIAMONDS

Beaches and bedrock: How geological framework controls coastal morphology and the relative grade of a southern Namibian diamond placer deposit. L.H. Kirkpatrick, J. Jacob and A.N. Green, *Ore Geology Reviews*, **107**, 2019, 853–862, http://doi.org/10.1016/j.oregeorev.2019.03.029.

Carbonatite melt in type Ia gem diamond. A.M. Logvinova, A. Shatskiy, R. Wirth, A.A. Tomilenko, S.S. Ugap'eva and N.V. Sobolev, *Lithos*, **342–343**, 2019, 463–467, http://doi.org/10.1016/j.lithos.2019.06.010.

A common parentage-low abundance trace element data of *gem* diamonds reveals similar fluids to fibrous diamonds. M.Y. Krebs, D.G. Pearson, T. Stachel, F. Laiginhas, S. Woodland, I. Chinn and J. Kong, *Lithos*, **324–325**, 2019, 356–370, http://doi.org/10.1016/j.lithos.2018.11.025.*

Diamond destruction and growth during mantle metasomatism: An experimental study of diamond resorption features. Y. Fedortchouk, C. Liebske and C. McCammon, *Earth and Planetary Science Letters*, **506**, 2019, 493–506, http://doi.org/10.1016/j.epsl.2018.11.025.

Diamond exploration and mining in southern Africa: Some thoughts on past, current and possible future trends. W.F. McKechnie, *Journal of the Southern African Institute of Mining and Metallurgy*, **119**(2), 2019, 123–131, http://doi.org/10.17159/2411-9717/2019/v119n2a4.*

Diamonds and the mantle geodynamics of carbon. S.B. Shirey, K.V. Smit, D.G. Pearson, M.J. Walter, S. Aulbach, F.E. Brenker, H. Bureau, A.D. Burnham, *et al.*, in B.N. Orcutt, I. Daniel & R. Dasgupta, Eds., *Deep Carbon: Past to Present*. Cambridge University Press, Cambridge, 89–128, 2019, http://doi.org/10.1017/9781108677950.005.*

Diamonds from the Deep—Kimberlites: Earth's diamond delivery system. K.V. Smit and S.B. Shirey, *Gems & Gemology*, **55**(2), 2019, 270–276, www.gia.edu/gems-gemology/summer-2019-kimberlites-earths-diamond-delivery-system.*

Fluorescence of natural and synthetic gem diamond: Mechanism and applications. C.M. Breeding and S. Eaton-Magaña, *Encyclopedia of Analytical Chemistry: Applications, Theory and Instrumentation*, 26 pp., 2019, http://doi.org/10.1002/9780470027318.a9670.

Jwaneng – The untold story of the discovery of the world's richest diamond mine. N. Lock, *Journal of the Southern African Institute of Mining and Metallurgy*, **119**(2), 2019, 155–164, http://doi.org/10.17159/2411-9717/2019/v119n2a8.*

Operational changes enable Namdeb's Southern Coastal Mining team to reduce risk and increase productivity as we advance deeper into the Atlantic Ocean. S. Kirkpatrick and J. Mukendwa, *Journal of the Southern African Institute of Mining and Metallurgy*, **119**(2), 2019, 104–112, http://doi.org/10.17159/2411-9717/2019/v119n2a2.*

Prospecting for diamonds in South Africa. M.R. Cullinan, *Journal of the Gemmological Association of Hong Kong*, **40**, 2019, 28–33, www.gahk.org/journal/GAHK_Journal_2019_v6.pdf.*

A quantitative testing method for the evaluation of diamond color. Y. Cheng, C. Fan, Y. Wang, C. Zhang, H. Zhu and S. Chen, *Spectroscopy and Spectral Analysis*, **39**(5), 2019, 1643–1647 (in Chinese with English abstract).

A record-breaking jewel [cutting the 1,109 ct Lesedi La Rona rough diamond]. Anonymous, *Gems&Jewellery*, **28**(2), 2019, 39–41.

FAIR TRADE

Corporate social and environmental responsibility in the diamond supply chain. N. Cucari, E. Wankowicz and M. Calabrese, in S. Mugova and P.R. Sachs, Eds., *Opportunities and Pitfalls of Corporate Social Responsibility: The Marange Diamond Mines Case Study*. Springer, Cham, Switzerland, 73–99, 2019, http://doi.org/10.1007/978-3-030-17102-5_5.

Could sustainability improve the promotion of luxury products? S. Dekhili, M.A. Achabou and F. Alharbi, *European Business Review*, **31**(4), 2019, 488–511, http://doi.org/10.1108/ebr-04-2018-0083.

Gemstone supply chains and development in Pakistan: Analyzing the post-Taliban emerald economy in the Swat Valley. M. Makki and S.H. Ali, *Geoforum*, **100**, 2019, 166–175, http://doi.org/10.1016/j.geoforum.2019.01.005.

Strategies for enhancing the contribution of gemstone mining in developing countries. S. Kambani, *International Journal of Advanced Research and Publications*, **3**(6), 2019, 61–66, www.ijarp.org/published-research-papers/june2019/Strategies-For-Enhancing-The-Contribution-Of-Gemstone-Mining-In-Developing-Countries.pdf.*

GEM LOCALITIES

Amethyst occurrences in Tertiary volcanic rocks of Greece: Mineralogical, fluid inclusion and oxygen isotope constraints on their genesis. P. Voudouris, V. Melfos, C. Mavrogonatos, A. Tarantola, J. Götze, D. Alfieris, V. Maneta and I. Psimis, *Minerals*, **8**(8), 2018, article 324 (26 pp.), http://doi.org/10.3390/min8080324.*

Collector's Note: The reemergence of two important emeralds from Alexander County, North Carolina. M.I. Jacobson, *Rocks & Minerals*, **94**(6), 2019, 560–563, https://doi.org/10.1080/00357529.2019.1641027.

Connoisseur's Choice: Tanzanite, gem variety of zoisite, Merelani Hills, Simanjiro District, Manyara region, Tanzania. B. Cairncross, *Rocks & Minerals*, **94**(6), 2019, 530–539, https://doi.org/10.1080/00357529.2019.1641023.

Corundum formation by metasomatic reactions in Archean metapelite, SW Greenland: Exploration vectors for ruby deposits within high-grade greenstone belts. C. Yakymchuk and K. Szilas, *Geoscience Frontiers*, **9**(3), 2018, 727–749, http://doi.org/10.1016/j.gsf.2017.07.008.*

A decade of ruby from Mozambique: A review. W. Vertriest and S. Saeseaw, *Gems & Gemology*, **55**(2), 2019, 162–183, http://doi.org/10.5741/GEMS.55.2.162.*

The Emmons pegmatite, Greenwood, Oxford County, Maine. A.U. Falster, W.B. Simmons, K.L. Webber, D.A. Dallaire, J.W. Nizamoff and R.A. Sprague, *Rocks & Minerals*, **94**(6), 2019, 498–519, https://doi.org/10.1080/00357529.2019.1641021.

Gem corundum deposits of Greece: Geology, mineralogy and genesis. P. Voudouris, C. Mavrogonatos, I. Graham, G. Giuliani, V. Melfos, S. Karampelas, V. Karantoni, K. Wang, *et al.*, *Minerals*, **9**(1), 2019, article 49 (42 pp.), http://doi.org/10.3390/min9010049.*

Gems & collection stones of the Krasnoyarsk territory (Russia). S.A. Ananyev, Yu.A. Zadisensky, T.A. Ananyeva and S.S. Bondina, *Journal of the Gemmological Association of Hong Kong*, **40**, 2019, 13–17, www.gahk.org/journal/GAHK_Journal_2019_v6.pdf.*

Gems of Italy [prehnite to dendritic spessartine]. E. Amore, R. Appiani, V. Bordoni, M. Campos Venuti, G. Cattaneo, F. Caucia, G. Conti-Vecchi, E. Costa, *et al.*, *Rivista Italiana di Gemmologia/Italian Gemological Review*, No. 7, 2019, 22–33.

Genesis of dolomite-related nephrite from Hetian and color-forming factors of typical nephrite in Hetian, Xinjiang. D. Han, X. Liu, Y. Liu, Y. Zhang, F. Zheng, M. Abuduwayiti, H. Zhang and Z. Wen, *Acta Petrologica et Mineralogica*, **37**(6), 2018, 1011–1026 (in Chinese with English abstract).

The Golconda District, Minas Gerais, Brazil. C. Cornejo, A. Bartorelli and W.E. Wilson, *Mineralogical Record*, **50**(5), 2019, 519–627.

Greenland ruby. S.M. Robertson. *GemGuide*, **38**(6), 2019, 12–13.

Metacarbonate-hosted spinel on Baffin Island, Nunavut, Canada: Insights into the origin of gem spinel and cobalt-blue spinel. P.M. Belley and L.A. Groat, *Canadian Mineralogist*, **57**(2), 2019, 147–200, http://doi.org/10.3749/canmin.1800060.

Mighty Montepuez [ruby mine in Mozambique]. M. Dettmer, *Gems&Jewellery*, **28**(2), 2019, 22–25.

Mineralogy of the amethyst mines in the Thunder Bay area, Thunder Bay, Ontario, Canada. D.E. Kile, *Rocks & Minerals*, **94**(4), 2019, 306–343, http://doi.org/10.1080/00357529.2019.1595939.

Modern discovery of Aappaluttoq [ruby mine in Greenland]. D. Turner, W. Rohtert, M. Ritchie and B. Wilson, *Gems&Jewellery*, **28**(2), 2019, 14–17.

A new Russian sapphire discovery in the Naryn-Gol Creek placer deposits (Dzhida flood basalt, Baikal rift system). A.V. Aseeva, E.V. Kislov, S.V. Vysotskiy, O.Y. Korshunov, T.A. Velivetskaya, R.R. Coenraads, V.V. Vanteev, A.A. Karabtsov et al., *Australian Gemmologist*, **27**(1), 2019, 20–26.

Pedogenic origin of precious opals from Wegel Tena (Ethiopia): Evidence from trace elements and oxygen isotopes. B. Chauviré, B. Rondeau, A. Alexandre, S. Chamard-Bois, C. La and F. Mazzero, *Applied Geochemistry*, **101**, 2019, 127–139, http://doi.org/10.1016/j.apgeochem.2018.12.028.

Remarkably uniform oxygen isotope systematics for co-existing pairs of gem-spinel and calcite in marble, with special reference to Vietnamese deposits. A.E. Fallick, G. Giuliani, T. Rigaudier, A.J. Boyce, V.L. Pham and V. Pardieu, *Comptes Rendus Geoscience*, **351**(1), 2019, 27–36, http://doi.org/10.1016/j.crte.2018.11.008.*

The Tashisayi nephrite deposit from south Altyn Tagh, Xinjiang, northwest China. K. Gao, G. Shi, M. Wang, G. Xie, J. Wang, X. Zhang, T. Fang, W. Lei *et al.*, *Geoscience Frontiers*, **10**(4), 1597–1612, 2018, http://doi.org/10.1016/j.gsf.2018.10.008.

Trace elements and U-Pb ages of zircons from Myanmar jadeite-jade by LA-ICP-MS: Constraints for its genesis. S. Cai and E. Zhang, *Spectroscopy and Spectral Analysis*, **38**(6), 2018, 1896–1903 (in Chinese with English abstract).

INSTRUMENTATION

Advances in 3D imaging and volumetric reconstruction of fluid and melt inclusions by high resolution X-ray computed tomography. A. Richard, C. Morlot, L. Créon, N. Beaudoin, V.S. Balistky [*sic*], S. Pentelei, V. Dyja-Person, G. Giuliani, *et al.*, *Chemical Geology*, **508**, 2019, 3–14, http://doi.org/10.1016/j.chemgeo.2018.06.012.

Application of hyperspectral imaging technique in identification of polymer-impregnated gemstone: Taking jadeite and turquoise as example. X. Liu, M. Chen and Z. Liu, *Journal of Gems & Gemmology*, **21**(1), 2019, 1–11 (in Chinese with English abstract).

The art of photomicrography. D. Pregun, *Gems&Jewellery*, **28**(2), 2019, 34–37.

The digital microscope and multi-scale observation in the study of lapidary manufacturing techniques: A methodological approach for the preliminary phase of analysis in situ. E. Morero, H. Procopiou, J. Johns, R. Vargiolu and H. Zahouani, in K. Kelley and R. K. L. Wood, Eds., *Digital Imaging of Artefacts: Developments in Methods and Aims*. Archaeopress Publishing Ltd, Summertown, Oxford, 2018, 75–100, https://eprints.soton.ac.uk/426431/1/seals2018.pdf#page=89.*

MISCELLANEOUS

The 709 carat diamond, Rapaport, ethics and auctions in Sierra Leone. D. Angelino, *Rivista Italiana di Gemmologia/Italian Gemological Review*, No. 7, 2019, 41–44.

Jewellery: From material to affection. A. Passos, *Journal of Jewellery Research*, **2**, 2019, 16 pp., www.journalofjewelleryresearch.org/download/ana-passos.*

The local translation of global norms: The Sierra Leonean diamond market. N. Engwicht, *Conflict, Security & Development*, **18**(6), 2018, 463–492, http://doi.org/10.1080/14678802.2018.1532639.*

Making history [Christie's sale of Mughal treasures from the Al Thani Collection]. J. Ogden, *Gems&Jewellery*, **28**(3), 2019, 22–25.

Man-made diamonds are diamonds too. This new extended definition isolates the FTC from European standards. P. Minieri, *Rivista Italiana di Gemmologia/Italian Gemological Review*, No. 7, 2019, 34–38.

The siren's call [422.66 ct Siren of Serendip blue sapphire necklace]. R. Galopim de Carvalho, *Gems&Jewellery*, **28**(3), 2019, 36–37.

NEWS PRESS

Amulets of deities, skulls and phalluses found in ancient Pompeii. L. Geggel, LiveScience, www.livescience.com/amulets-discovered-in-pompeii.html.*

Bizarre 'nesting doll' diamond found inside another diamond. M. Wei-Haas, *National Geographic*, 10 October 2019, www.nationalgeographic.com/science/2019/10/rare-diamond-diamond-found-siberia/#close.*

Blue diamond affair: The mystery of the stolen Saudi jewels. R. Hughes and C. Yongcharoenchai, BBC News, 28 September 2019, www.bbc.com/news/world-asia-49824325.*

Misidentified Roman 'pendants' were actually women's makeup tools. B. Katz, *Smithsonian*, 19 September 2019, www.smithsonianmag.com/smart-news/these-misidentified-roman-pendants-were-actually-womens-makeup-tools-180973184.*

Romans prized these jewels [pearls] more than diamonds. L. Avial-Chicharro, *National Geographic*, 2 April 2019, www.nationalgeographic.com/history/magazine/2019/03-04/roman-republics-captivation-with-pearls.*

Russian farmer unearths the remains of a 2,000-year-old nomadic 'royal' buried alongside a 'laughing' man with an egg-shaped head and a haul of jewellery, weapons and animal sacrifices. W. Stewart, *Daily Mail*, 15 May 2019, www.dailymail.co.uk/sciencetech/article-7031613/Treasure-trove-Russia-includes-remains-2-000-year-old-nomadic-royal.html.*

ORGANIC/BIOGENIC GEMS

Can DNA be extracted from amber? K. Szawaryn, *Bursztynisko (The Amber Magazine)*, No. 43, 2019, 96–97, https://issuu.com/internationalamberassociation/docs/bursztynisko_43/98 (in English and Polish).*

Development and application of a method for ivory dating by analyzing radioisotopes to distinguish legal from illegal ivory. A. Schmidberger, B. Durner, D. Gehrmeyer and R. Schupfner, *Forensic Science International*, **289**, 2018, 363–367, http://doi.org/10.1016/j.forsciint.2018.06.016.

Elephant ivory and rhino horn. B. Martin, in *Survival or Extinction?* Springer, Cham, Switzerland, 2019, 37–46, http://doi.org/10.1007/978-3-030-13293-4_5.

Inclusions [in amber]: Imagination vs. reality. A.K.-K.E. Sontag, *Bursztynisko (The Amber Magazine)*, No. 43, 2019, 92–94, https://issuu.com/internationalamberassociation/docs/bursztynisko_43/94 (in English and Polish).*

Infrared spectroscopic characteristics of Borneo and Madagascar copal resins and rapid identification between them and ambers with similar appearances. L. Dai, G. Shi, Y. Yuan, M. Wang and Y. Wang, *Spectroscopy and Spectral Analysis*, **38**(7), 2018, 2123–2131 (in Chinese with English abstract).

Ivory identification. A. Rodriguez, in E. Simpson, Ed., *The Adventure of the Illustrious Scholar*. Brill, Leiden, The Netherlands, 2018, 645–661, http://doi.org/10.1163/9789004361713_033.

Jumping to more knowledge – Remarks about fleas in Baltic amber. C. Hoffeins, *Bursztynisko (The Amber Magazine)*, No. 43, 2019, 84–85, 87–89, 91, https://issuu.com/internationalamberassociation/docs/bursztynisko_43/86 (in English and Polish).*

The three-dimensional arrangement of the mineralized collagen fibers in elephant ivory and its relation to mechanical and optical properties. M. Albéric, A. Gourrier, W. Wagermaier, P. Fratzl and I. Reiche, *Acta Biomaterialia*, **72**, 2018, 342–351, http://doi.org/10.1016/j.actbio.2018.02.016.

PEARLS

Component analysis and identification of black Tahitian cultured pearls from the oyster *Pinctada margaritifera* using spectroscopic techniques. L. Shi, Y. Wang, X. Liu and J. Mao, *Journal of Applied Spectroscopy*, **85**(1), 2018, 98–102, http://doi.org/10.1007/s10812-018-0618-4.

Effects of nucleus position, profile and arrangement on the quality of mabé pearls produced by the winged pearl oyster, *Pteria penguin*. S.E. Gordon, S. Malimali, M. Wingfield, D.I. Kurtböke and P.C. Southgate, *Aquaculture*, **498**, 2019, 109–115, http://doi.org/10.1016/j.aquaculture.2018.08.055.*

Evidence of rotation in flame-structure pearls from bivalves of the Tridacnidae family. J.-P. Gauthier, J. Fereire and T.N. Bui, *Gems & Gemology*, **55**(2), 2019, 216–228, http://doi.org/10.5741/GEMS.55.2.216.*

Freshwater pearl culture. J. Li, X. Wu and Z. Bai, in J.-F. Gui, Q. Tang, Z. Li, J. Liu and S.S.D. Silva, Eds., *Aquaculture in China*. John Wiley & Sons Ltd, Hoboken, New Jersey, USA, 2018, 185–196, http://doi.org/10.1002/9781119120759.ch3_1.

The optical characteristics of cultured akoya pearl are influenced by both donor and recipient oysters. T. Iwai, M. Takahashi, C. Miura and T. Miura, in K. Endo, T. Kogure & H. Nagasawa, Eds., *Biomineralization*. Springer, Singapore, 2018, 113–119, http://doi.org/10.1007/978-981-13-1002-7_12.*

A pearl identification challenge. N. Sturman, L.M. Otter, A. Homkrajae, A. Manustrong, N. Nilpetploy, K. Lawanwong, P. Kessrapong, K.P. Jochum, *et al.*, *Gems & Gemology*, **55**(2), 2019, 229–243, http://doi.org/10.5741/GEMS.55.2.229.*

SIMULANTS

Gemological identification of tanzanite imitation. P. Wang and S. Yue, *Journal of Gems & Gemmology*, **21**(2), 2019, 34–38 (in Chinese with English abstract).

Study on the vibration spectra of turquoise imitation and natural turquoise from Zhushan County, Hubei Province. X. Zeng, Z. Yang, X. Li, X. Lei, S. Huang and Y. Chen, *Spectroscopy and Spectral Analysis*, **39**(3), 2019, 834–839.

SYNTHETICS

10x – From the analyst's notebook. An investigation on a red faceted stone [flux-treated Verneuil synthetic ruby]. C. Cumo, *Rivista Italiana di Gemmologia/Italian Gemological Review*, No. 7, 2019, 7–13.

Crystallography 101 – A seven-sided emerald crystal [hydrothermal synthetic emerald]? J.-M. Arlabosse, *Gemmology Today*, June 2019, 5–8, www.worldgemfoundation.com/GTJUNE2019DV.*

Laboratory-grown diamonds – An update and a new exchange and price list. R.B. Drucker, *GemGuide*, **38**(6), 2019, 4–8.

Gemologic and spectroscopy properties of Chinese high-pressure high-temperature synthetic diamond. X. He, M. Du, Y. Zhang, P.K. Chu and Q. Guo, *JOM*, **71**(8), 2019, 2531–2540, http://doi.org/10.1007/s11837-019-03592-8.

Synthesis of large diamond crystals with $C_3H_8N_4O_2$ as organic additive under HPHT conditions. L. Guo, H. Ma, L. Chen, N. Chen, X. Miao, Y. Wang, Z. Wang, Z. Yang *et al.*, *International Journal of Refractory Metals and Hard Materials*, **79**, 2019, 47–52, http://doi.org/10.1016/j.ijrmhm.2018.11.001.

Synthesis of large diamond single crystals under high pressure and high temperature through effective utilization of the synthesis cavity. Y. Li, Y. Li, Y. Wang, J. Zhang, M. Song, Y. She and X. Chen, *CrystEngComm*, **20**(29), 2018, 4127–4132, http://doi.org/10.1039/c8ce00786a.

TREATMENTS

Aesthetic improvement of transparent natural quartz by heat treatment at different temperature. R.K. Sahoo, B. Dhal, S.K. Singh and B.K. Mishra, *International Journal of Nano and Biomaterials*, **7**(3), 2018, 231–241, http://doi.org/10.1504/ijnbm.2018.094251.

Blue diffusion-treated natural & synthetic sapphires recently available in the market. V. Pisutha-Arnond, S. Promwongnan, N. Narudeesombat, P. Ounorn, T. Leelawatanasuk, T. Sripoonjan, N. Nilhud and W. Atichat, *Journal of the Gemmological Association of Hong Kong*, **40**, 2019, 87–95, www.gahk.org/journal/GAHK_Journal_2019_v6.pdf.*

Characterization of various centers in synthetic type Ib diamond under HPHT annealing. N. Chen, H. Ma, B. Yan, L. Chen, L. Chen, L. Guo, X. Miao, C. Fang *et al.*, *Crystal Growth & Design*, **18**(7), 2018, 3870–3876, http://doi.org/10.1021/acs.cgd.8b00145.

Comparison of HPHT and LPHT annealing of Ib synthetic diamond. N.M. Kazuchits, M.S. Rusetsky, V.N. Kazuchits, O.V. Korolik, V. Kumar, K.S. Moe, W. Wang and A.M. Zaitsev, *Diamond and Related Materials*, **91**, 2019, 156–164, http://doi.org/10.1016/j.diamond.2018.11.018.

Effect of heat treatment on the luminescence properties of natural apatite. P. Chindudsadeegul and M. Jamkratoke, *Spectrochimica Acta Part A: Molecular and Biomolecular Spectroscopy*, **204**, 2018, 276–280, http://doi.org/10.1016/j.saa.2018.06.056.

Importance of emerald clarity enhancement: Gübelin Gem Lab standards. H.-P. Kan-Nyunt and B. Kwok, *Journal of the Gemmological Association of Hong Kong*, **40**, 2019, 47–51, www.gahk.org/journal/GAHK_Journal_2019_v6.pdf.*

Madagascar sapphire: Low-temperature heat treatment experiments. E.B. Hughes and R. Perkins, *Gems & Gemology*, **55**(2), 2019, 184–197, http://doi.org/10.5741/GEMS.55.2.184.*

Titanium – Heating rutile is never futile. G. Dominy, *Gemmology Today*, March 2019, 22–26, www.worldgemfoundation.com/GTMARCH2019DV.*

COMPILATIONS

***G&G* Micro-World.** Emerald inclusion within an emerald crystal from Chivor • Purple fluorite in Russian emerald • Helical inclusion in Colombian emerald • Mexican opal with large fluid inclusion • Pyrope-almandine in sapphire host • Euhedral phantom sapphire in sapphire • Curved banding in flame-fusion synthetic sapphires • Iridescent geode from Tabasco, Mexico • Inclusion-rich black topaz from Utah, USA • Dioptase in and on quartz. *Gems & Gemology*, **55**(2), 2019, 260–269, www.gia.edu/gg-issue-search?ggissueid=1495287212844&articlesubtype=microworld.*

Gem News International. Plume agate from Iran • Jadeite from the Polar Urals • Pearls from the Mississippi River system, USA • Trapiche quartz from Inner Mongolia • Rubies from Rock Creek, Montana, USA • Glass-filled *polki*-cut CVD synthetic diamonds • Low-temperature heat treatment of pink sapphire • Tagua nut as a sustainable replacement for ivory. *Gems & Gemology*, **55**(2), 2019, 278–292, www.gia.edu/gg-issue-search?ggissueid=1495287212844&articlesubtype=gni.*

Lab Notes. Resin-coated and clarity-enhanced aquamarine pendant • Rough diamond with fake green 'radiation stains' • Separation of kornerupine and prismatine • Faceted milarite • 'Hollow' pearl filled with foreign materials • Dyed serpentine imitating sugilite • Color-change spessartine • Spurrite cabochon • Natural-looking exsolved particles in flux-grown pink synthetic sapphire. *Gems & Gemology*, **55**(2), 2019, 246–259, www.gia.edu/gg-issue-search?ggissueid=1495287212844&articlesubtype=labnotes.*

CONFERENCE PROCEEDINGS

International Gemmological Conference. M. Krzemnicki & L. Cartier (Eds.), Nantes, France, 27–31 August 2019, 234 pp., www.igc-gemmology.org/s/IGC2019-web.pdf.*

**Article freely available for download, as of press time*

Thank You, Guest Reviewers

The following individuals served as guest reviewers during the past publication year. A special thanks is extended to each one of them for lending their expertise to reviewing manuscripts submitted to *The Journal*. Together with the Associate Editors, these individuals have enhanced the quality of *The Journal* through their knowledge and professionalism.

Dr Ilaria Adamo
University of Milan, Italy

Shigeru Akamatsu
Japan Pearl Promotion Society, Toba, Japan

Dr James Butler
Huntingtown, Maryland, USA

Dr Alessandra Costanzo
Birmingham City University, Birmingham

Dr David Fisher
De Beers Technologies, Maidenhead, Berkshire

Dr Gaston Giuliani
Paul Sabatier University, Toulouse, France, and University of Lorraine, Vandœuvre-lès-Nancy, France

Dr Edward Grew
University of Maine, Orono, Maine, USA

Dr Le Thi Thu Huong
~~University of Graz, Austria~~

Note: The correct affiliation is Staatliche Zeichenakademie Hanau, Germany.

Dr A. J. A. (Bram) Janse
Archon Exploration Pty Ltd, Carine, Western Australia

Guy Lalous
Egenhoven, Belgium

Dr Shang-i (Edward) Liu
Hong Kong Institute of Gemmology

Anna Malecka
Warsaw, Poland

Dr Annibale Mottana
Roma Tre University, Rome, Italy

Justin Prim
Institute of Gem Trading, Bangkok, Thailand

William R. Rohtert
William Rohtert Consulting LLC, Phoenix, Arizona, USA

Dr Gabi Schneider
Namibian Uranium Institute, Swakopmund, Namibia

Note: The correct affiliation is L'École des Arts Joailliers/ School of Jewelry Arts.

Olivier Segura
~~Laboratoire Français de Gemmologie~~, Paris, France

Jeremy Shepherd
Pearl Paradise, Los Angeles, California, USA

Dr William B. 'Skip' Simmons
Maine Mineral & Gem Museum, Bethel, Maine, USA

Dr Frederick Sutherland
Port Macquarie, New South Wales, Australia

Dr Rolf Tatje
Duisburg, Germany

Lisbet Thoresen
Temecula, California, USA

Dr Zuowei Yin
China University of Geosciences, Wuhan, Hubei, China

Dr Joe Yuan
Taidiam Technology Co. Ltd, Zhengzhou, Henan, China

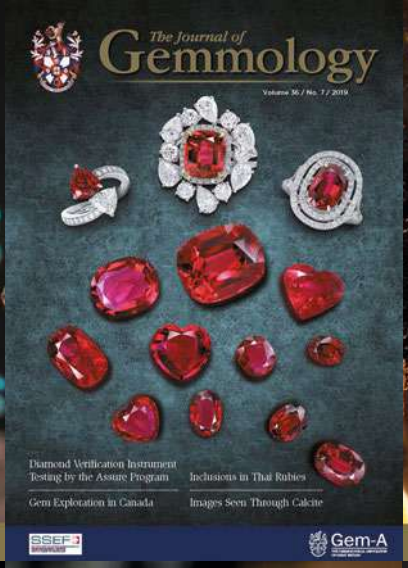

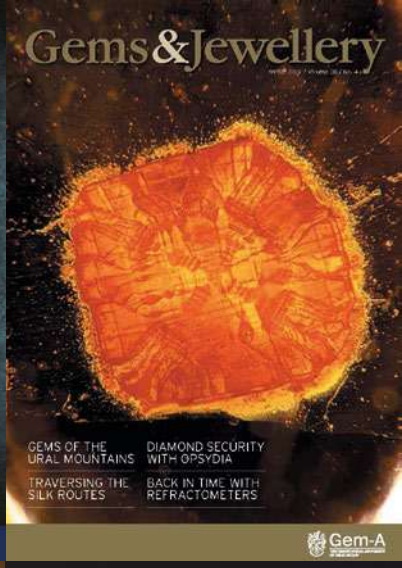

Don't forget to renew your Gem-A Membership!

If you renew before 31st December 2019 you only pay £110*

*(£135 thereafter)

We've made it **easier** for you to **renew** your **membership** with us.

Live in the UK?
Pay using
GoCardless

Live elsewhere?
Pay using
Paypal Subscription

By paying with **GoCardless** or **PayPal Subscription**, payment is taken automatically every year so you no longer have to worry about not renewing on time and missing your issues.

To renew, simply log in to the Gem-A website: **https://gem-a.com/log-in** and choose the payment method you wish to use.
Don't want to subscribe? You can still log in and make a one-off payment.

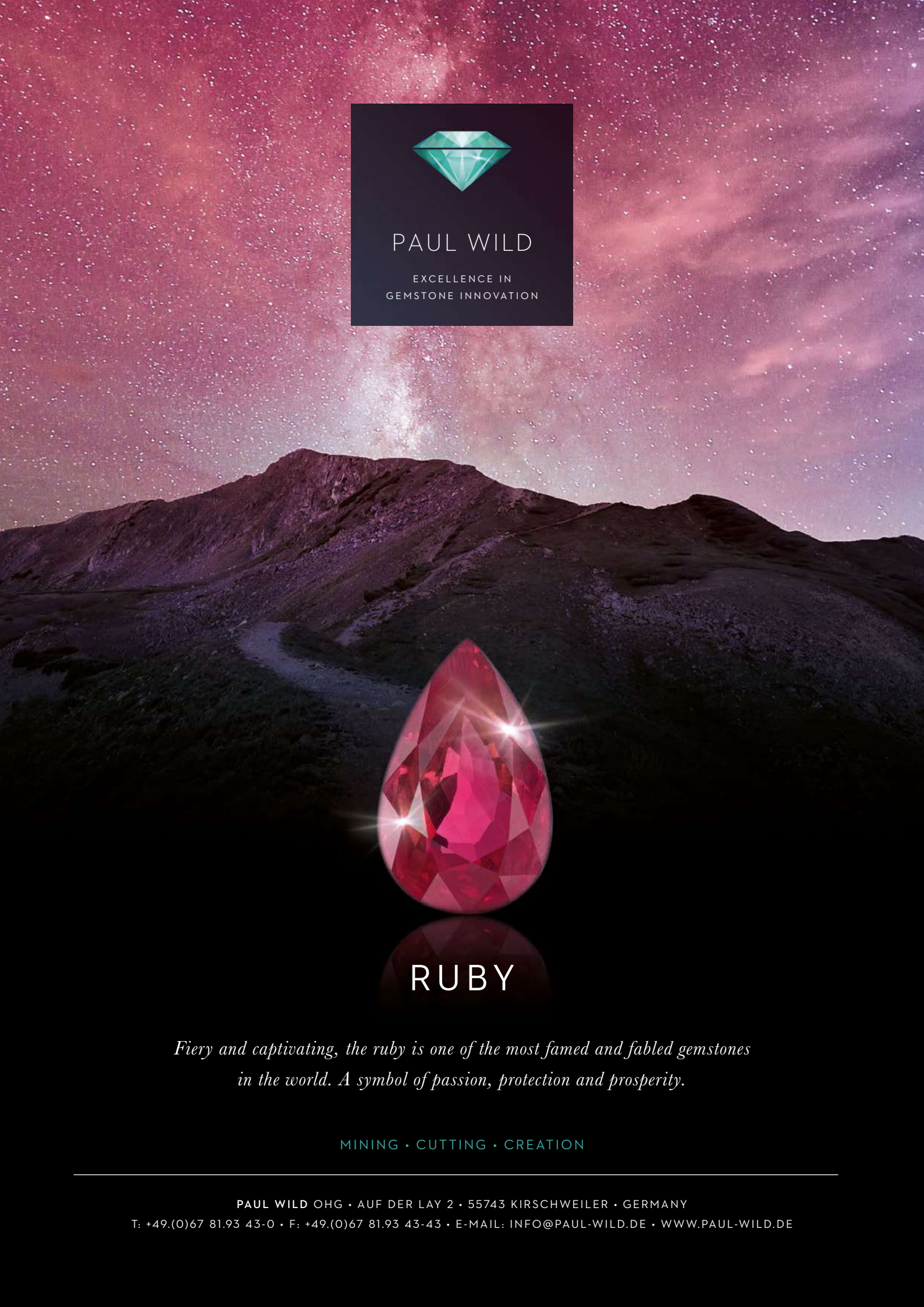

Fiery and captivating, the ruby is one of the most famed and fabled gemstones in the world. A symbol of passion, protection and prosperity.

MINING • CUTTING • CREATION

PAUL WILD OHG • AUF DER LAY 2 • 55743 KIRSCHWEILER • GERMANY
T: +49.(0)67 81.93 43-0 • F: +49.(0)67 81.93 43-43 • E-MAIL: INFO@PAUL-WILD.DE • WWW.PAUL-WILD.DE